Technical Report Documentation Page

1. Report No.	2. Government Accession No.	3. Recipient's Catalog No.
FHWA/TX-98/1360-2F		

4. Title and Subtitle	5. Report Date
CROSS FRAME DIAPHRAGM FATIGUE AND LOAD DISTRIBUTION BEHAVIOR IN STEEL HIGHWAY BRIDGES	September 1997
	6. Performing Organization Code

7. Author(s)	8. Performing Organization Report No.
Peter B. Keating, Kenneth C. Saindon, and Scott D. Wilson	Research Report 1360-2F

9. Performing Organization Name and Address	10. Work Unit No. (TRAIS)
Texas Transportation Institute The Texas A&M University System College Station, Texas 77843-3135	11. Contract or Grant No. Study No. 0-1360

12. Sponsoring Agency Name and Address	13. Type of Report and Period Covered
Texas Department of Transportation Research and Technology Transfer Office P. O. Box 5080 Austin, Texas 78763-5080	Final Report: September 1992-August 1994
	14. Sponsoring Agency Code

15. Supplementary Notes

Research performed in cooperation with the Texas Department of Transportation and the U. S. Department of Transportation, Federal Highway Administration.
Research Study Title: Repair Procedures for Fatigue Damage in Steel Highway Bridges

16. Abstract

An investigation into the behavior of cross frame diaphragms in steel highway bridges was conducted. The investigation involved both field testing of three bridges as well as analytical studies using finite element analysis. Diaphragms were removed from the structure and less than half replaced by a new diaphragm design. The remaining diaphragms were permanently removed from the structure. The removal of the diaphragms provided a unique opportunity to study the effects of diaphragms on the load distribution characteristics of the structure. Strain measurements, under controlled loading conditions, were obtained with diaphragms and with the new diaphragm arrangement in place. Combined with the previous measurements for the as-built condition, a direct comparison was made. The research team found that the girder flange stresses doubled when the diaphragms were removed. With the new diaphragm pattern, the increase in stresses was limited to 20 percent. The increase without the diaphragms was still significant below the stress levels predicted by the American Association of State Highway and Transportation Officials (AASHTO) design methods.

Two additional bridges were instrumented in their as-built condition and the data were compared with the results obtained from the finite element analysis. This allowed for the prediction in the change of load distribution due to diaphragm removal or modification. Researchers developed a method to predict diaphragm member forces under vehicle live load for both the strength and fatigue limit states. Other types of fatigue damage in steel highway bridges were studied and generalized repair procedures are provided.

17. Key Words	18. Distribution Statement
Fatigue, Diaphragm, Web Gap, Cracking, Repair, Retrofit	No restrictions. This document is available to the public through NTIS: National Technical Information Service 5285 Port Royal Road Springfield, Virginia 22161

19. Security Classif.(of this report)	20. Security Classif.(of this page)	21. No. of Pages	22. Price
Unclassified	Unclassified	298	

Form DOT F 1700.7 (8-72) **Reproduction of completed page authorized**

CROSS FRAME DIAPHRAGM FATIGUE AND LOAD DISTRIBUTION BEHAVIOR IN STEEL HIGHWAY BRIDGES

by

Peter B. Keating, Ph.D.
Engineering Research Associate
Texas Transportation Institute

Kenneth C. Saindon
Graduate Research Assistant
Texas Transportation Institute

and

Scott D. Wilson
Graduate Research Assistant
Texas Transportation Institute

Research Report 1360-2F
Research Study Number 0-1360
Research Study Title: Repair Procedures for Fatigue Damage
in Steel Highway Bridges

Sponsored by the
Texas Department of Transportation
In Cooperation with
U.S. Department of Transportation
Federal Highway Administration

September 1997

TEXAS TRANSPORTATION INSTITUTE
The Texas A&M University System
College Station, Texas 77843-3136

IMPLEMENTATION STATEMENT

The results of this study provide competent recommendations to the district engineers for the evaluation and repair of fatigue damage at cross frame diaphragms in steel highway girders. This type of fatigue cracking is common to steel highway bridges where no rigid attachment of the diaphragm connection plate has been provided to the tension flange. A viable repair option is the partial removal of diaphragms from the structure. Up to 50 percent of the diaphragms can be removed without altering the load distribution characteristics of the bridge. With the permanent removal of the driving source of the web gap out-of-plane distortion (by cross frame removal or rigid attachment of the connection plate) these repairs will result in an acceptable performance of the bridge when combined with continued inspection and sound engineering judgment.

DISCLAIMER

The contents of this report reflect the views of the authors who are responsible for the facts and accuracy of the data presented herein. The contents do not necessarily reflect the official view or policies of the Texas Department of Transportation (TxDOT) or the Federal Highway Administration (FHWA). This report does not constitute a standard, specification, or regulation. It is not intended for construction, bidding, or permit purposes.

ACKNOWLEDGMENT

The research results described herein were part of a study cooperatively sponsored by the Texas Department of Transportation and the Federal Highway Administration under research project 1360 titled *Fatigue Repair Procedures for Fatigue Damage in Steel Highway Bridges*. The research project was coordinated for TxDOT by Gregg Freeby, P.E. under the supervision of Mark Bloshcock, P.E.

TABLE OF CONTENTS

TABLE OF CONTENTS (continued)

LIST OF FIGURES

LIST OF FIGURES (continued)

LIST OF FIGURES (continued)

LIST OF FIGURES (continued)

LIST OF TABLES

LIST OF ABBREVIATIONS AND SYMBOLS

A_{LS}	Cross sectional area of diaphragm lower strut, mm^2 (in^2)
b	One-half of the bridge width, m (ft)
D	Measure of load distribution, m (ft)
D_x	Longitudinal flexural rigidity per unit width
D_y	Transverse flexural rigidity per unit length
D_{xy}	Longitudinal torsional rigidity per unit width
D_{yx}	Transverse torsional rigidity per unit length
D_1	Longitudinal coupling rigidity per unit width
D_2	Transverse coupling rigidity per unit length
D.F.	Distribution factor
d	Overall depth of longitudinal girder, mm (in)
E_s	Modulus of elasticity of steel, MPa (ksi)
E_c	Modulus of elasticity of concrete, MPa (ksi)
G_c	Shear modulus of concrete, MPa (ksi)
H	Dimensionless ratio of longitudinal girder stiffness to transverse slab stiffness
I_g	Composite moment of inertia of steel girder and associated portion of bridge deck, mm^4 (in^4)
K_D	Stiffness of the slab and diaphragm in the transverse direction, kN-mm (k-in.^{2})
K_S	Stiffness of the slab in the transverse direction, kN-mm (k-in.^{2})
L	Span length, m (ft)
P	Concentrated load, kN (kips)
S	Girder spacing, m (ft)
t	Slab thickness, mm (in)
α	Dimensionless ratio of torsional rigidity to flexural rigidity
Δ	Vertical deflection of diaphragm cross-frame, mm (in)
θ	Ratio of deflection stiffness in longitudinal and transverse directions
ν_c	Poisson's ratio of concrete
φ	Skew angle, degrees

SUMMARY

An investigation into the behavior of cross frame diaphragms in steel highway bridges was conducted. The investigation involved both field testing of three bridges as well as analytical studies using finite element analysis.

The investigation was prompted by the reoccurrence of fatigue damage in a West Texas highway bridge near the city of Midland. Cracks developed at unstiffened web gaps where diaphragm connection plates were not rigidly attached to the girder tension flanges. In addition, due to the high levels of distortion in the cross frame diaphragms, fatigue cracks developed in individual diaphragm members, as well as in the weld between the diaphragm and the connection plate. As recommended by a previous study, all the diaphragms were removed from the structure and less than half replaced by a new diaphragm design. The remaining diaphragms were permanently removed from the structure.

The removal of the diaphragms provided a unique opportunity to study the effects of diaphragms on the load distribution characteristics of the structure. Strain measurements, under controlled loading conditions, were obtained with diaphragms and with the new diaphragm arrangement in place. Combined with the previous measurements for the as-built condition, a direct comparison was made. The research team found that the girder flange stresses doubled when the diaphragms were removed. With the new diaphragm pattern, the increase in stresses was limited to 20 percent. The increase without the diaphragms was still significant below the stress levels predicted by the American Association of State Highway and Transportation Officials (AASHTO) design methods.

Two additional bridges were instrumented in their as-built condition and the data were compared with the results obtained from the finite element analysis. This allowed for the prediction in the change of load distribution due to diaphragm removal or modification. Researchers developed a method to predict diaphragm member forces under vehicle live load for

both the strength and fatigue limit states. These forces were shown to vary significantly among bridges with different diaphragm-deck stiffness ratios. These forces also increase for bridges with high skewness, and a correction factor for this was included in the method. The field data was used to confirm that the diaphragm forces predicted by the developed method came close to actual diaphragm forces measured on three different bridges.

While the primary focus of the research study was the behavior of cross frame diaphragms and associated fatigue damage, other types of fatigue damage in steel highway bridges were studied. The investigation included the review of bridge inspection records to indicate potential problem connection details. While other types of fatigue damage have occurred in the State's steel bridges, no other type of cracking is a prevalent as the distortion-induced cracking at the unstiffened web gap of cross frame diaphragms. Nevertheless, generalized repair procedures are provided as part of this study.

1. INTRODUCTION

Numerous concrete slab-on-steel girder bridges were constructed on rural and interstate highways throughout Texas during the late 1950s through the early 1970s. This type of bridge, consisting of four or more longitudinal girders, was economical and easy to construct. Figure 1-1 shows a typical cross section of a concrete slab on a steel girder highway bridge.

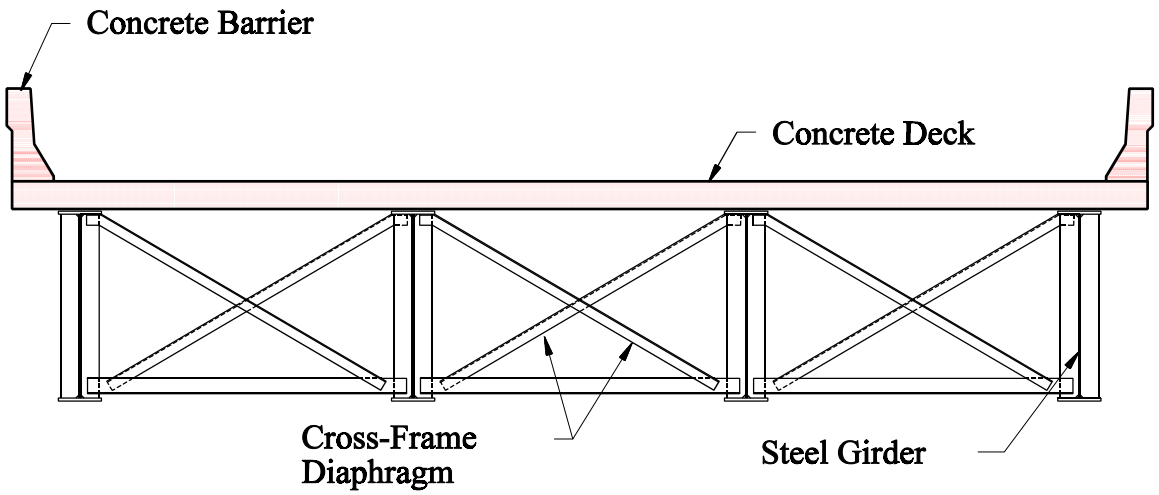

Figure 1-1: Typical cross section of slab-on-girder bridge.

Cross frame (or solid) diaphragms are used transversely between girders to provide lateral stability to the girders and aid in the distribution of the truck loading between the girders. Diaphragms can also be used to help resist the horizontal wind loading; however, it is more efficient to use the weak axis bending strength of the girders and provide lateral bracing in a plane at or near the girders' bottom flange.

By far the most important function of cross frame diaphragms is during construction where they stabilize the compression flange and help resist lateral torsional buckling. This is

particularly true in the positive moment regions of bending where the girder's design moment capacity is based on the assumption that the concrete deck slab will provide the flange support along its entire length. However, the slab support comes only after the concrete has cured. While stay-in-place metal deck forms may be used in the construction of the concrete deck slab, their ability to laterally support the flange is highly dependent on the adequacy of the connection between the forms and flange. In the negative moment region of bending, the compression flange is supported by the lateral resistance of the support bearing and the possibility of lateral torsional buckling is reduced. Cross frame diaphragms also allow a pair of adjacent girders to be lifted and placed on the bridge supports as a unit. The girders, with the diaphragms in between, form a torsionally stiff system unlike a single I-shaped girder.

Historically, the AASHTO bridge design specifications have never quantified the load distribution characteristics of diaphragms in non-horizontally curved girder bridges but AASHTO has required their use nevertheless. Current AASHTO bridge design provisions (AASHTO 1992) required the use of intermediate diaphragms at a maximum spacing of 7600 mm (25 ft) when the span length is 38,000 mm (125 ft) or greater. However, no guidance is given to their component design. As a consequence, diaphragms have been used liberally without full knowledge of their load distribution effect between girders nor the magnitude of force they transmit to the girder.

AASHTO has relaxed the requirements for intermediate diaphragms, as seen in the Load and Resistance Factor Design (LRFD) bridge design provisions (AASHTO 1994), by allowing for a rational analysis that may lead to the elimination of diaphragms. (This is an attempt to remove fatigue-prone details from the structure.) To date, the rational analysis will mean performing a finite element analysis of the structure. The need for the use of diaphragms is now an engineering design decision. When intermediate diaphragms are needed, they must be designed to carry the forces indicated in the analysis, as well as other forces that they intend to transmit.

Note that even if the elimination of diaphragms can be justified through engineering calculations, their use is required at the end of the bridge and at intermediate points (supports) where the concrete slab is discontinuous. This requirement is to prevent the lateral motion of the concrete slab relative to the girders and supports. In addition, diaphragms will be required at end and intermediate supports to transverse the wind loading resisted by the weak axis bending of the girders to the support bearings. The seismic resistance of a bridge may be increased through the use of diaphragms. Intermediate diaphragms will always be needed in horizontally curved girder bridges where the diaphragms form an integral part of the bridge cross section. The torsional deformation that occurs in this type of structure is far greater than in a horizontally straight girder bridge.

The cross frame diaphragms are normally attached to the girder by either welding or bolting them to a vertical connection plate. Typically, the connection plate is of the same design as an intermediate transverse shear stiffener and serves as one also. A typical cross frame diaphragm and connection plate detail is shown in Fig. 1-2.

Figure 1-2: Typical cross frame diaphragm and connection plate detail.

During the late 1940s a series of bridge collapses occurred in Europe. These failures were attributed to the brittle fracture of weldments on tensions flanges. As a consequence, a prohibition against welding to tension flanges found its way into the bridge design provisions both in Europe and in the United States. This prohibition had a direct impact on the diaphragm connection plate detail. Specifically, bridges were fabricated without rigid attachments between the end of the connection plate and the tension flange.

Two different details were used for the termination of the connection plate at the tension flange: cut-short and tight-fit. The cut-short detail, one of which is shown in Fig. 1-3, terminates the connection plate short of the tension flange by 25 to 100 mm (1 to 4 in). Application of the web crippling criteria for intermediate shear stiffeners has led to a recommended gap of four to six times the web thickness. The tight-fit detail, on the other hand, is cut to the full depth of the girder web but is only welded to the web and compression flange. An example of a tight-fit detail is given in Fig. 1-4.

Figure 1-3: View of typical cut-short stiffener detail.

Figure 1-4: View of typical tight-fit stiffener detail.

Without a rigid attachment between the end of the connection plate and tension flange, the resistance of the girder cross section to torsional deformation is reduced. The torsional stiffness of an I-shaped cross section is developed primarily from the warping of the flanges. The imposed torsional force, coming from the diaphragm, enters the girder cross section at the connection plate and must be transmitted to the flanges. Without the rigid attachment, the torsional deformation is concentrated in the unstiffened web gap, as shown schematically in Fig. 1-5. The distortion results in the out-of-plane bending of the web plate. The bending stress can easily exceed the specified yield stress of the steel for relatively high levels of distortion. High levels of distortion have been measured in the field and laboratory as 0.08 mm (0.003 in) when measuring the relative displacement of the ends of the web gap.

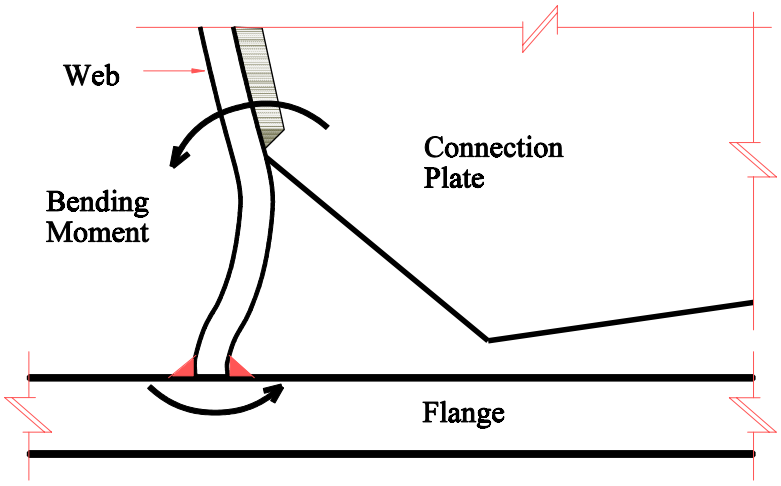

Figure 1-5: Scheme of web gap bending distortion.

The web gap bending stresses are caused by truckling loading and are therefore cyclic in nature. Consequently, fatigue cracks will develop in the web plate around the web gap region if the distortion level is high enough. With both termination details, a crack will develop in the toe of the web-to-flange fillet weld. An example of this type of fatigue cracking is given in Fig. 1-6 for the cut-short detail. In addition, fatigue cracks can also develop in the toe at the termination of the connection plate fillet weld, also shown in Fig. 1-6. The vertical weld toe crack is more critical since it is driven not only by the out-of-plane distortion stresses but also by the in-plane bending stress. Fortunately, this crack is shielded from the flange by the web-to-flange crack.

The tight-fit detail will also experience web gap fatigue cracking but is usually limited to the web-to-flange fillet weld unless unusually high levels of distortion exist. Figure 1-7 shows an example of a fatigue cracked cut-short detail. The connection plate detail causing the distortion is actually on the opposite side of the web plate from the view shown. The diaphragms on this bridge were offset slightly at this location.

Figure 1-6: Fatigue crack at end of unstiffened web gap of cut-short termination detail.

Figure 1-7: Fatigue crack at unstiffened web gap with tight-fit connection detail.

In addition to the web gap cracking, the diaphragm members and their connections can be susceptible to fatigue damage. Figure 1-8 shows an example of a fatigue crack that developed in the toe of the fillet weld between the cross frame lower strut angle section and the connection plate. This cracking was caused by the eccentric loading between the diagonal and lower strut members resulting in bending stress in the weld to the connection plate. This crack separated the diaphragm from the connection plate and helped minimized fatigue damage to the tight-fit web gap detail. Figures 1-9 and 1-10 show examples where the cross frame members themselves have developed fatigue cracks. Again, this type of cracking can be attributed to poor detailing of the member connections that result in bending stresses from eccentric loading.

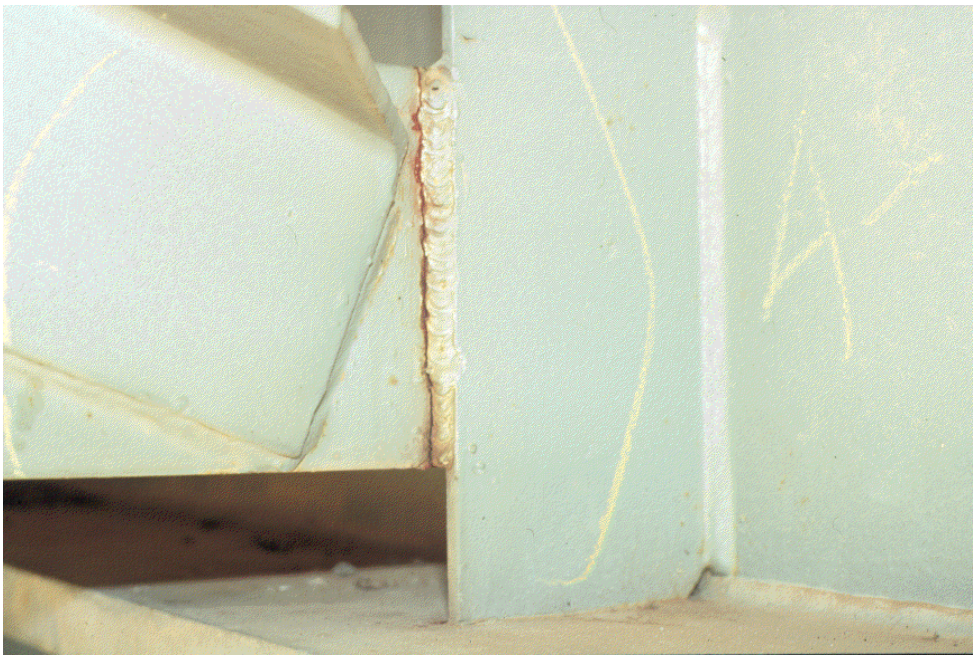

Figure 1-8: Fatigue crack in fillet weld between cross frame diaphragm lower strut and connection plate.

Figure 1-9: Fatigue crack in cross frame upper strut at diagonal connection.

Figure 1-10: Fatigue crack in cross frame lower strut at diagonal connection.

The level of distortion and, hence, the degree of fatigue damage that will occur in a given steel multi-girder bridge is a function of many parameters. A few of the important parameters are listed below:

- Frequency of loading,
- Diaphragm stiffness,
- Diaphragm member connection,
- Girder spacing,
- Concrete deck stiffness,
- Bridge skew, and
- Girder stiffness.

Due to the number of parameters, prediction or estimation of diaphragm forces is difficult without an exhaustive finite element analysis. Consequently, the repair of this type of fatigue damage is made difficult without a reasonable estimate of the driving force(s) behind the damage.

The intent of the current study is to investigate the effect of diaphragms on the load carrying capacities of girders and to develop a means of predicting diaphragm forces. The study involves the field investigation of three bridges where stress measurements were taken under controlled live load conditions. Finite element models of these bridges were developed so that the load distribution contribution of the diaphragms could be studied. Additionally, a finite element parametric study was undertaken to develop guidelines for the prediction of diaphragm forces. The objectives of the study can be summarized as:

- Determining the effective diaphragm removal on the load carrying characteristics of the longitudinal girder, and

- Evaluating and predicting diaphragm member forces.

In order to better understand the effect cross frame diaphragms have on the fatigue behavior or steel, multi-girder highway bridges, several bridges in the state of Texas were selected for field investigations. This included the measurement of stress/strain under controlled live load conditions. The repair of the Midland County bridges presented a unique opportunity to the study. As part of the recommended repair procedures for fatigue damage at unstiffened web gaps, all cross frame diaphragms required either permanent removal or replacement. Consequently, measurements were obtained for one three-span continuous structure without any cross frame diaphragms. Measurements were then taken with the new, staggered diaphragm arrangement. This allowed for the comparison of live load stresses under different diaphragm arrangements. In addition to the Midland bridges, two other bridges were investigated to augment the study.

2. BACKGROUND

2.1 AASHTO Distribution Factors

The design of concrete slab-on-steel girder highway bridges is governed by the AASHTO Standard Specifications for Highway Bridges. Of key concern in the design of concrete slab-on-steel girder bridges is the lateral distribution of live loading from a girder with a truck wheel line directly above it to an adjacent girder. AASHTO uses wheel load distribution factors to account for this effect. Use of the distribution factor reduces the flexural design of a concrete slab-on-steel girder bridge to that of a single beam, or line girder. The distribution factor, abbreviated *D.F.*, describes the maximum load effect occurring in any one girder under highway loading relative to the effect for a single line of wheels acting on one girder, and is expressed as a fraction shown in Eq. (2-1).

$$D.F. = \frac{S}{D} \tag{2-1}$$

S is the girder spacing in meters (feet), and *D* is a quantity with units of length which gives a measure of the load distribution characteristics of a bridge. For a given girder spacing, a higher *D* value means loads are more evenly distributed from one girder to the next (Newmark 1948).

To understand the concept of the *D.F.*, one must first visualize the deck as being simply supported between each of the longitudinal girders. Using this idealization, it is possible to calculate the load that a girder must carry using statics. However, since the deck is continuous over all girders, this approach is conservative. The AASHTO distribution factors take into account the beneficial effect of the continuous deck, in the transverse direction, in distributing the loads to adjacent girders. Figure 2-1 shows a single truck with a 1830 mm (6 ft) gauge positioned with one wheel directly over a girder. The girder spacing in this instance is 1830 mm (6 ft), and static distribution would give a value of 1.0 for the distribution factor. The AASHTO value for a single truck is expressed as *S*/2.13 (*S*/7), which for this case gives 0.85 as the distribution factor. This value is lower than that obtained using static distribution. Figure 2-2

shows how the static distribution factor compares with the AASHTO value for girder spacings between 1830 mm and 3050 mm (6 ft and 10 ft).

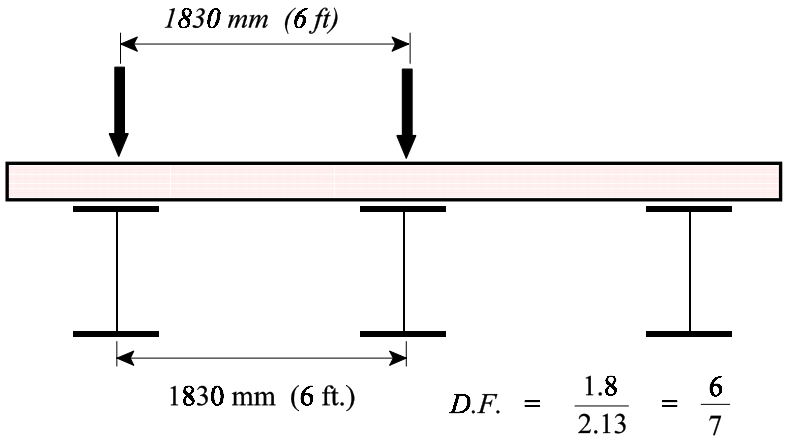

Figure 2-1: AASHTO Distribution Factor for single lane loaded.

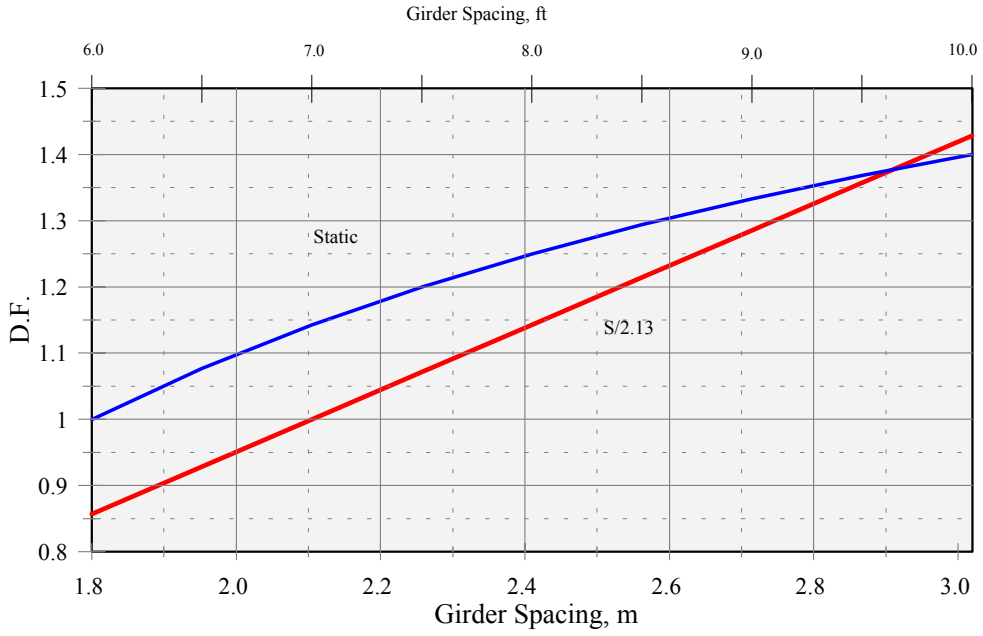

Figure 2-2: Comparison of AASHTO and static *D.F.*s for one lane loading.

Figure 2-3 shows two trucks positioned side by side on a bridge with a space of 1220 mm (4 ft) between them. This loading arrangement is required by the AASHTO Specifications, and the distribution factor is given as S/5.5, or 1.09. The static distribution factor for this arrangement is 1.33. The AASHTO distribution factor is much less than the static factor, as it should be. As the loading across a bridge becomes more uniform, the distribution factor would approach the case where all girders deflect equally and therefore share the total load equally. Figure 2-4 shows a comparison between the AASHTO and static *D.F.*s for two lanes loaded.

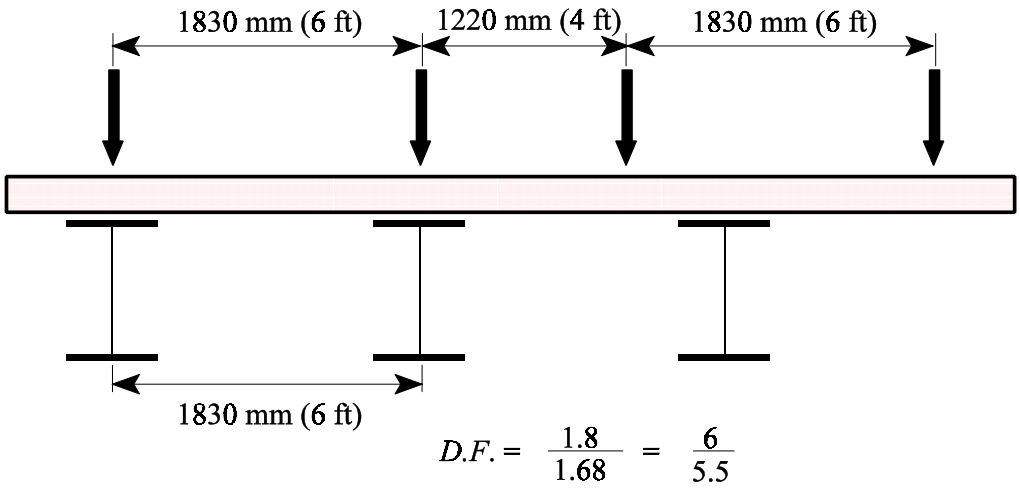

Figure 2-3: AASHTO Distribution Factor for two lanes loaded.

Cross frame diaphragms, as seen in Figs. 1-2 and 1-3 for example, have been used in all concrete slab-on-steel girder highway bridges for several reasons. During construction, the longitudinal girders are erected and the diaphragm cross-bracing is installed to provide stability, keeping the longitudinal girders from failing in lateral-torsional buckling. This is especially crucial during placement of the concrete for the deck, since the newly poured concrete heavily loads the girders but contributes no strength until curing progresses.

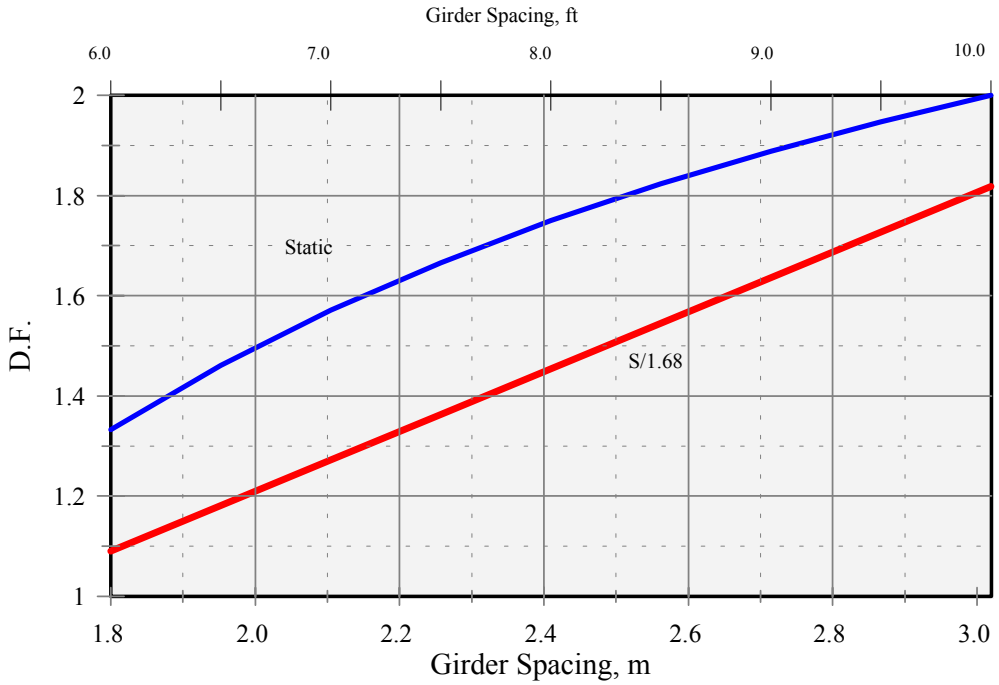

Figure 2-4: Comparison of AASHTO and static *D.F.*s, two lanes loaded.

Diaphragms also help to distribute lateral forces acting on the deck and girders to the girder bearings at the abutments. These forces include horizontal effects from the vehicle live load, wind load, and earthquake effects. It is also assumed that cross frame diaphragms contribute to the lateral distribution of the vehicle live loading. Such cross frame bracing is required by the AASHTO specifications at the bearings and at not greater than 7620 mm (25 ft) intervals along the length of the bridge. It is important to have cross frame diaphragms at the girder bearings since all horizontal forces from the deck must pass from the deck through the girders to the bearings. Diaphragms provide the needed strength to prevent the deck from sliding transversely relative to the longitudinal girders. Though cross frame diaphragms are required along the span of the bridge by the AASHTO specifications, no rationale is given for their design, and their effect in the lateral distribution of live loading has never been quantified.

The AASHTO LRFD specifications do not require the use of diaphragms in bridges. The specifications state that they may, at the discretion of the designer, be placed at the ends of the structure, across intermediate supports, and intermittently along the span. The commentary for

this section of the specification states that eliminating the arbitrary spacing requirements in the previous edition of the specification and replacing it with a requirement for rational analysis of the need for diaphragms will often result in the elimination of fatigue-prone attachment details. However, the specifications still do not give any simplified analysis methods for determining diaphragm forces under vehicle live load. Thus, any bridge designer is required to resort to a refined analysis to predict these forces.

2.2 Previous Research

Newmark (1948) developed the first procedure for the lateral distribution of wheel loads on I-girder highway bridges. His work recognized the fact that lateral distribution is affected by the span length, girder spacing, and ratio of the girder stiffness in the longitudinal direction to that of the slab in the transverse direction. The procedure, as previously mentioned, consists of assigning a portion of a line of wheels to each beam. This portion is less than the fraction obtained by assuming the slab to be simply supported between longitudinal girders and using static distribution.

The H parameter is basic to Newmark's method, and is defined as follows:

$$H = \frac{E_s I_g}{L E_c I} \tag{2-2}$$

The H parameter is the dimensionless ratio of the longitudinal girder stiffness to the transverse slab stiffness. In Eq. (2-2), E_s refers to the modulus of elasticity of the steel girders, I_g is the moment of inertia of a girder, L is the span length, E_c is the modulus of elasticity of the slab, and I is the moment of inertia of the slab per unit width. Newmark (1948) developed an empirical equation to describe the proportion of a wheel load to be assigned to each beam based upon live load moments obtained from a field of tests of more than 50 bridges under standard truck loading. Knowing the values of the live load moments and the girder spacings, he solved for the D value of each bridge, and used a curve fit to describe the variation in D based upon L and H. His equation is:

$$D = 1.4 + 0.012\frac{L}{\sqrt{H}} \quad \left(D = 4.6 + 0.04\frac{L}{\sqrt{H}}\right) \tag{2-3}$$

Newmark (1948) later recommends a conservative D value of 1.67 m (5.5 ft) for non-composite bridges and 1.58 m (5.2 ft) for composite bridges. These values were given to simplify the procedure for designers, and no consideration is given to having only a single lane loaded. He states that the relationship given by Eq. (2-3) will remain valid for any design case considered, assuming two lanes loaded, but this relationship was not included in any specifications and seems to have been lost from current practice.

Newmark (1948) mentions using diaphragm cross-bracing for construction purposes or if the slab is made thin, but does not attempt to quantify any contribution that the diaphragms could make in distributing the vehicle live load. He does point out that cross frame diaphragms are only effective when the live loads occur at or near the critical section. It should be noted that diaphragms were never assumed in the development of Newmark's method and therefore have never been taken into account in developing distribution factors.

Finite element studies were performed to determine the effect of diaphragms in concrete slab-on-prestressed girder bridges (Kostem and deCastro 1977). The study focused on prestressed girder bridges with rectangular concrete diaphragms poured monolithically with the slab. However, these diaphragms are not continuous across the supporting girders. Studied were two bridge configurations, a six beam and a five beam bridge with span lengths of 21,800 mm and 20,900 mm (71.5 ft and 68.5 ft) respectively, with one, two, or three loaded lanes. The results given in the study indicate that as the number of loaded lanes increases, the contribution of the diaphragms decreases. They also show that an increase in the number of lines of evenly spaced diaphragms does not lead to a more even distribution of the live load at maximum moment sections.

These results led the researchers to conclude that diaphragms only give a small contribution to the lateral distribution of vehicle live load, regardless of the loading pattern. However, the diaphragms they describe are very different from full depth X-type cross-bracing diaphragms used with steel girder bridges, which are fully continuous across the transverse section of a bridge, forming a truss system. It should also be noted that diaphragms work by decreasing the differential deflections of adjacent girders in a bridge, and because a concrete girder bridge has a much higher dead load to live load ratio, it will not experience as much differential deflection in adjacent girders under live loading. Kostem and deCastro (1977) state that diaphragms are believed to contribute to a more uniform distribution of load when a bridge is subjected to a vehicle overload.

$$\left(D.F. = 0.0014L^2 - 0.69L + 0.7\sqrt{S} - \frac{(S + 2.13)}{3.05} \right) \quad \left(D.F. = 0.00013L^2 - 0.021L + 1.25\sqrt{S} - \frac{(S + 7)}{10} \right) \tag{2-4}$$

Tarhini and Frederick (1992) used the finite element method to develop a load distribution factor formula in terms of girder spacing and span length, given in Eq. (2-4). In their analysis, they did consider the effect on the distribution factor in bridges with and without diaphragms. However, they simply state that the effect of diaphragms on the distribution factor was negligible. They do not state what type of diaphragm configuration was used, or the size or spacing of the diaphragms. The load model used in their study consisted of a train of HS-20 trucks, with additional trucks placed on the bridge for larger span lengths. This procedure is quite conservative, and does not accurately represent a realistic loading condition. Additionally, the transverse positioning of the train of trucks used in their load model assumes that the line of wheels nearest the edge occurs two feet from the centerline of the outermost girder. This load condition is not as conservative as required by the AASHTO specifications, and led them to conclude that the interior girders of a multi-girder bridge would be the most critical design case.

Bishara et al. (1993) used the finite element method to develop distribution factor formulas for interior and exterior girders of skewed multi-girder bridges. Separate equations were developed for interior and exterior girders, with correction factors for skew angles larger

than 30 degrees. In their study, the size and spacing of diaphragm members for various bridges were varied, but not systematically.

Keating and Crozier (1992) studied the interaction between the diaphragms and the longitudinal girders and possible removal of the diaphragms in connection with a study on repair of distortion-induced fatigue damage in a single, skewed concrete slab-on-steel girder continuous span bridge. Skewed bridge geometry results when the bridge is not perpendicular to the stream or highway it crosses. The bridge geometry is changed so that the shortest possible span can be constructed over the obstruction. This results when the supporting piers are aligned parallel with the obstruction to be crossed. The planform of the bridge becomes like a parallelogram instead of a rectangle.

Keating and Crozier concluded that the complete removal of diaphragms would increase the stresses in the longitudinal girders by 25 percent. They also indicated that the transverse slab stresses would be increased if diaphragms were removed from the structure. Their recommendation for the study bridge was to provide a staggered diaphragm arrangement, with approximately half of the original diaphragms removed. This new diaphragm pattern consisted of partial lines of diaphragms near the interior supports, and two complete lines of diaphragms in the positive moment regions. They also provided a new design for the diaphragm members and their connections to the longitudinal girders since those used in the original design were inadequate.

A study sponsored by the Oklahoma Department of Transportation (ODOT) investigated load carrying characteristics of cross frame diaphragms as part of an overall investigation of a bridge widening project that resulted in poorly welded connection details (Zwerneman et al. 1995). The structure under investigation carries U.S. Highway 69 over the South Canadian River. The bridge was widened by closing the gap between the north- and southbound spans and extending the road deck outward on both spans (similar to Town Lake Bridge, Chapter Four). Due to fit up errors in the field, the cross frame diaphragms were welded instead of bolted to the girder connection plates (stiffeners). In addition, the ends of the connection plates were field

welded to the girder tension flange where the design called for no such welding. Compounding the situation was the fact that the field welding was conducted under normal traffic conditions. It was reported that movement of the girders made it difficult to maintain the welding electrode arc. As a result of this and other procedural errors (lack of preheat and incorrect electrodes), poor weld quality resulted. A schematic drawing of the cross frame diaphragm is given in Fig. 2-5.

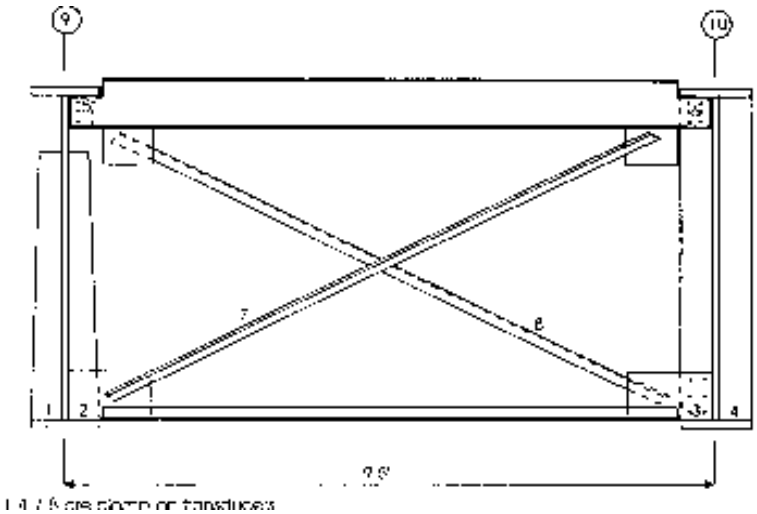

Figure 2-5: Example of cross frame diaphragm detail for ODOT study.

Because of the low quality field welds, the fatigue strength of the connection plate girder flange detail was assumed to be lowered from AASHTO Category C to Category D. This reduction in fatigue strength would result in the calculated stress range exceeding the allowable stress range (based on Category D) at 136 locations along the bridge. The result is an overall reduction in the service life of the bridge. The objective of the study was to determine more accurate stress ranges than the calculated stress ranges to effects of load distribution, composite action, and support conditions. The investigation involved strain measurements (similar to that reported in TxDOT Report 1313) coupled with laboratory fatigue tests and computer-aided analyses.

Results of the investigation indicated that measured stress ranges were significantly lower than those calculated using design procedures and assumptions. In addition, the cross frame diaphragms played an important roll in distributing the load between the directly loaded girder and adjacent girders. The investigation did not consider diaphragm removal.

The Nebraska Department of Transportation (NDOT) sponsored a research program that specifically addressed the influence of cross frame diaphragms on the load carrying capacity of steel girder bridges (Azizinamini et al. 1995). This investigation was accomplished through a combination of analytical and experimental analyses.

A full-scale bridge was constructed and tested in a laboratory setting. The bridge was a 21.34 m (70 ft) long simple span structure with a total deck width of 7.92 m (26 ft). Three 1372 mm (54 in.) deep plated girders were spaced at 3.05 m (10 ft) centers. A 90 mm (7.5 in) thick composite concrete slab was used. Different cross frame diaphragm scenarios were investigated. These included K-type cross frames (similar to Fig. 6-12 but with an upper strut member) spaced at either 3.41 m (11.2 ft) or 6.83 m (22.4 ft) intervals, X-type cross frames spaced at 6.83 m (22.4 ft) intervals, or no cross frame diaphragms.

The bridge was tested using different simulated truck load conditions. This included a truck in either lane, both lanes, or straddling the lanes. Load applications via six or 12 hydraulic rams were configured to simulate an AASHTO HS-20 design truck at midspan. The maximum applied load was 801 kN (180 kips) for a single truck which resulted in a 250 percent overload.

Based on the analysis of the experimental data, a comparison of distribution factors was made with both the current AASHTO bridge design provisions (discussed in Sec. 2.1) and the AASHTO LRFD design provision, shown in Table 2-1. As indicated by the values in Table 2-1, the distribution factors obtained experimentally were lower than those given in either of the AASHTO design provisions. This indicates that actual load distribution between girders is higher than that assumed for design purposes. Specifically, the following conclusions were reached:

- The distribution factors for exterior girders were smaller than those for interior girders.
- Distribution factors were similar for the X- and K-type cross frames when spaced at 6.83 m (22.4 ft) intervals.
- The distribution factors for both the exterior and interior girders with no cross frame diaphragms were not significantly different from those obtained with either the X- and K-type cross frame diaphragms.

Table 2-1: Load distribution factors (Azizinamini et al. 1995).

Cross Frame Type	Cross Frame Spacing		Experimental		Current AASHTO		AASHTO LRFD Provisions	
	m	ft	Interior	Exterior	Interior	Exterior	Interior	Exterior
K	3.41	11.2	1.21	1.03	1.82	1.82	1.62	1.62
K	6.83	22.4	1.34	1.05	1.82	1.82	1.62	1.62
X	6.83	22.4	1.38	1.06	1.82	1.82	1.62	1.62
None	--	--	1.42	1.01	1.82	1.82	1.62	1.62

3. MIDLAND COUNTY BRIDGE INVESTIGATION

3.1 Background

An inspection of the IH-20 Midland County (Texas) bridge that was performed in 1989 indicated that the structure had experienced fatigue related problems due to the unintended interaction between the longitudinal girders and the cross frame diaphragms (Diaz and Andrews 1990, Keating and Crozier 1992). The original construction of the bridge did not specify a rigid attachment between the ends of the connection plate and the flanges. Figure 3-1 provides a view of the twin structure.

Figure 3-1: View of IH-20 Midland County Bridge.

A partial solution to the fatigue cracking was to remove the source of the distortion by either permanently removing diaphragms or using a connection plate welded to the flanges. By removing the diaphragm, the driving force behind the crack growth would also be removed. Providing a rigid attachment between the connection flange and tension would also prevent the driving force behind the crack. While these methods prevented further fatigue crack growth, it was still necessary to remove or arrest the existing fatigue cracks since they could propagate

when subjected to the primary stresses. TxDOT Report 1360-1 (Keating et al. 1996) discusses the recommendations and procedures for the repair of web gap fatigue cracking.

The repair of the Midland County bridges presents a unique opportunity to the TxDOT Project 1360 study. As part of the recommended repair procedures for fatigue damage at unstiffened web gaps (Keating and Crozier 1992), all cross frame diaphragms required either permanent removal or replacement. Consequently, measurements were obtained for one three-span continuous structure without any cross frame diaphragms. Measurements were then taken with the new, staggered diaphragm arrangement. This allowed for the comparison of live load stresses under different diaphragm arrangements since measurements were also obtained for the original diaphragm configuration, as reported in TxDOT Report 1313-1F. Therefore, three sets of field data were obtained and are summarized, along with the date of testing, as follows:

1) Original diaphragm configuration, prior to 1992 repair (July 10-11, 1991),
2) No diaphragms (October 6, 1992), and
3) New diaphragm configuration (November 11-12, 1992).

3.2 Load Testing

The methodology used to obtain field measures was similar to that used in TxDOT Project 1313. Strain measurements were recorded at various locations under both controlled trucking loading and normal traffic conditions. Different strain gage groups of eight gages each were again utilized due to the limitations of the data acquisition equipment. While it would have been desirable to use the same gage groups for all three field data sets, this was not possible. Diaphragm lines were eliminated and accessibility problems occurred. Table 3-1 and Fig. 3-2 provide the gage group locations for the first set of field measures.

Table 3-1: Summary of gage group locations, Field Test No. 1.

Gage Group Number	Description of Gage Group Location
1	Type C' diaphragm members, Diaphragm Number 40, Bay D, Positive Moment Region.
2	Type B diaphragm members, Diaphragm Number 40, Bay C, Positive Moment Region.
3	Type C diaphragm members, Diaphragm Number 43, Bay C, Negative Moment Region.
4	Type C' diaphragm members, Diaphragm Number 43, Bay D, Negative Moment Region.
5	Bottom flanges and diaphragm lower struts at Diaphragm Line 40.
6	Type C diaphragm members, Diaphragm Number 39, Bay C.

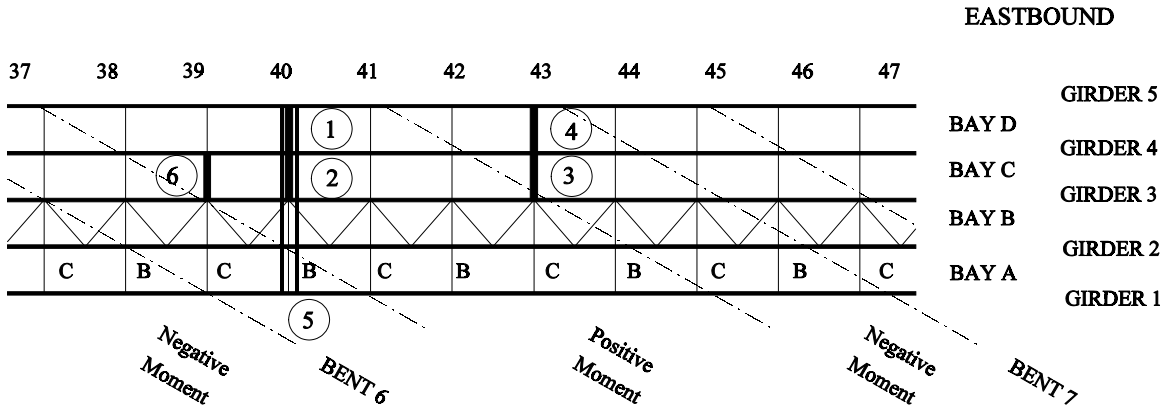

Figure 3-2: Gage group locations on Eastbound structure, Field Test No. 1.

3.2.1 Field Data Set 2

The acquisition of Field Data Set 2 was obtained by passing a TxDOT vehicle of known weight, as shown in Fig. 3-3, over the bridge and recording the strains at various locations. The gross vehicle weight was measured at 205 kN (46.1 kips). Axle loads and configurations are given in Appendix A.

Figure 3-3: View of TxDOT vehicle used as test vehicle for Field Test No. 2.

Figure 3-3 shows the gage groups used for Field Test No. 2 and are summarized in Table 3-2. Note that only four gage groups where used for this field test since no diaphragm lines existed. Two gage groups were in a line perpendicular to the longitudinal axis of the structure while the other two were located in a line parallel with the skew of the structure. Only Gage Group 5 corresponds to a Gage Group (5) for Field Test No. 1 with the exception of three gages located on the girder web plates near the top flange instead of diaphragm bottom struts. Field Test No. 1 did not used gage groups that were skewed to the longitudinal axis of the structure.

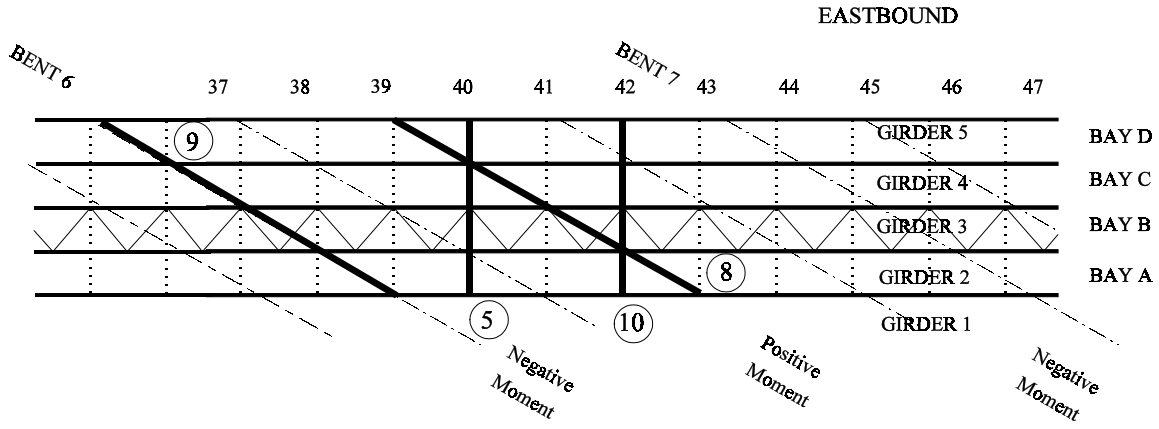

Figure 3-4: Gage group locations on Eastbound structure, Field Test No. 2.

Table 3-2: Summary of gage group locations, Field Test No. 2.

Gage Group Number	Description of Gage Group Location
5	Bottom flanges and web plates at Diaphragm Line 40.
8	Bottom flanges and web plates along skew in Positive Moment Region.
9	Bottom flanges and web plates along skew at Bent 6, Negative Moment. Region.
10	Bottom flanges and web plates at Diaphragm Line 42.

Strains were continuously recorded during the passage of the test vehicle. Three lane positions were used: centered in the passing lane, centered in the driving lane, and centered in the right shoulder lane. The truck driver was instructed to maintain a constant speed of 80 km/hr (50 mph) while traversing the bridge and to remain in the designated lane position as best as possible. The truck driver was successful in isolating the test vehicle from all other traffic for all truck passages. Therefore, no superposition with normal traffic occurred during the recording of the test truck passage.

A typical measured stress history is given in Fig. 3-5. These stresses are for five of the gages of Gage Group 5 with the test truck positioned in the center of the driving lane, as shown in Fig. 3-6. These five gages were located on the bottom flanges of each of the five girders, directly below Diaphragm Line 40. Maximum recorded stress ranges for each gage are given in Table 3-3. Note that the maximum stress range of 17 MPa (2.4 ksi) tension occurs in Girder No. 3, which is below the left side set of wheels. Girder No. 4 measured 14 MPa (2.1 ksi), the next highest stress range, since the test vehicle was located above Girder Nos. 3 and 4. Girder No. 1, the furthest girder from the test vehicle recorded primarily vibrational stresses. No non-zero stresses in four of the five girder flanges were indicative of the load distribution between girders in a cross section.

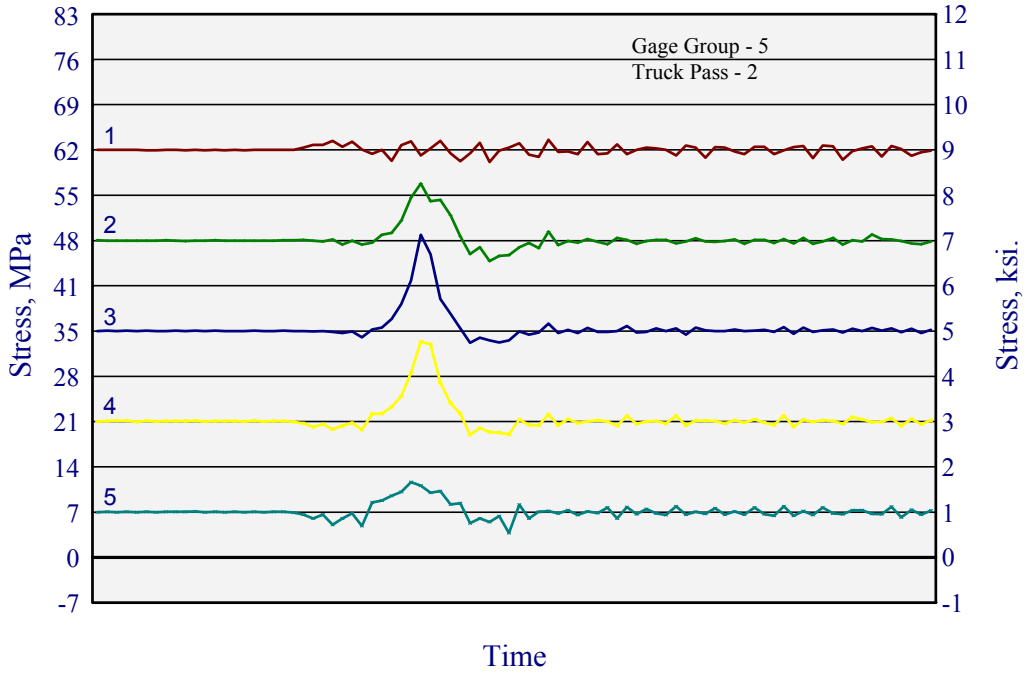

Figure 3-5: Bottom flange stress histories for Gage Group 5 (test truck in center lane).

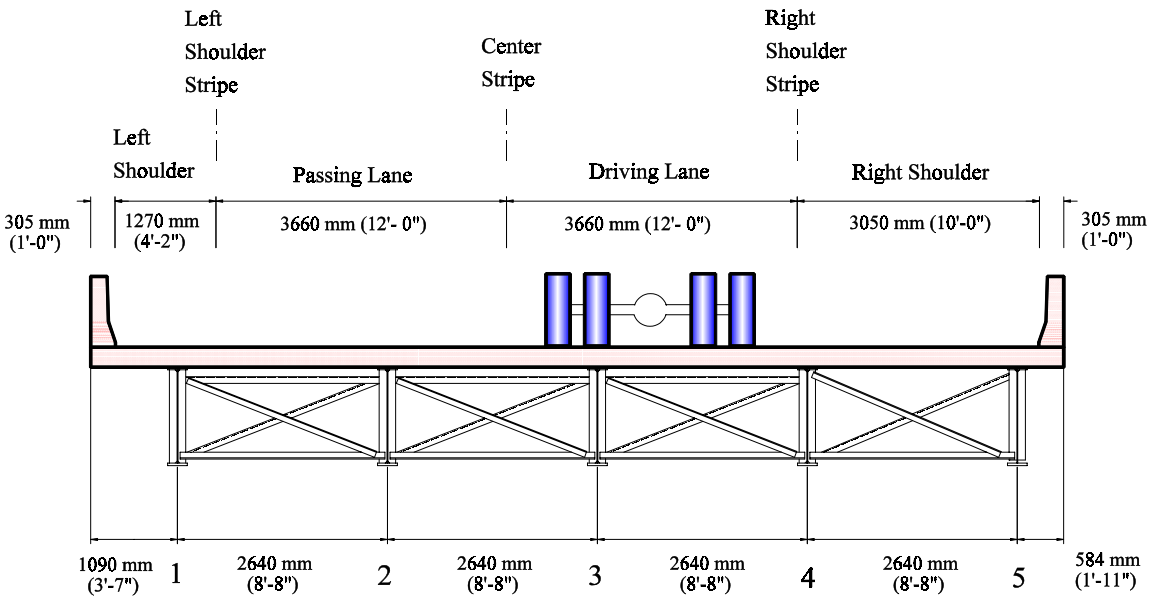

Figure 3-6: Location of test truck positioned in center of driving lane.

Table 3-3: Maximum measured stress ranges and direction for Gage Group 5 (test truck centered in driving lane).

Gage Number	Location	Max. Stress Range, MPa	Max. Stress Range, ksi
1	Bottom flange, Girder No. 1	3.5 (C)	0.5 (C)
2	Bottom flange, Girder No. 2	12 (T)	1.7 (T)
3	Bottom flange, Girder No. 3	17 (T)	2.4 (T)
4	Bottom flange, Girder No. 4	14 (T)	2.1 (T)
5	Bottom flange, Girder No. 5	7.6 (T)	1.1 (T)
6	Web, Girder No. 2	0.7 (T)	0.1 (T)
7	Web, Girder No. 3	2.1 (T)	0.3 (T)
8	Web, Girder No. 4	0.7 (C)	0.1 (C)

3.2.2 Field Data Set 3

The acquisition of Field Data Set 3 was obtained in a similar fashion. A different test vehicle was used due to the unavailability of the previous one. The gross vehicle weight was measured at 197 kN (44.2 kips), which is 96 percent of the gross weight for Field Test No. 2. Axle loads and configurations are given in Appendix B.

Figure 3-7 shows the gage groups used for Field Test No. 3 and are summarized in Table 3-4. Eight gage groups were used for this field test. In addition to the four gage groups used in Field Test No. 2, diaphragm members were gaged for the four other gage groups. The new diaphragm lines were offset from the old diaphragm lines so that the new connection plates were not installed over web gap cracking repairs. Figures 3-8 and 3-9 are views of the old diaphragm configuration and the new reduced configuration, respectively.

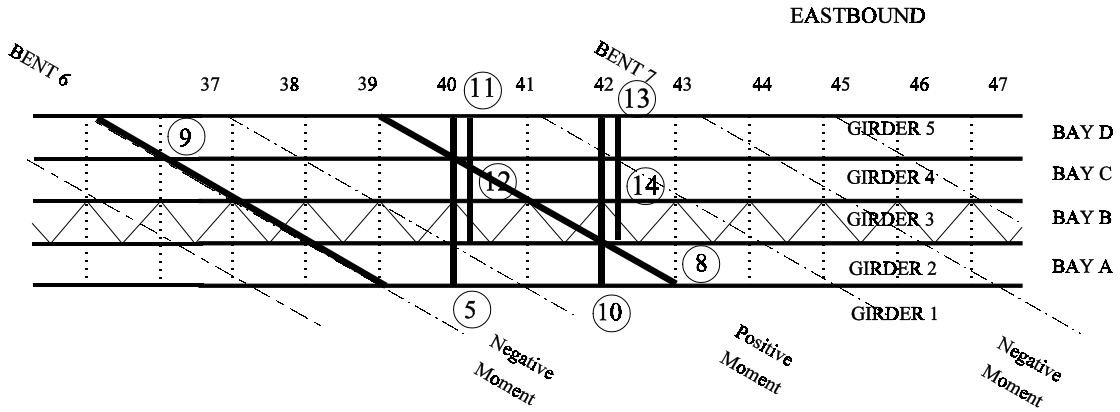

Figure 3-7: Gage group locations on Eastbound structure, Field Test No. 3.

Table 3-4: Summary of gage group locations, Field Test No. 3.

Gage Group Number	Description of Gage Group Location
5	Bottom flanges and web plates at Diaphragm Line 40.
8	Bottom flanges and web plates along skew in Positive Moment Region.
9	Bottom flanges and web plates along skew at Bent 6, Negative Moment Region.
10	Bottom flanges and web plates at Diaphragm Line 42.
11	Bottom flanges and new diaphragm members, Bay C, between diaphragm Lines 40 and 41.
12	New diaphragm members, Bay C, between Diaphragm Lines 40 and 41.
13	Bottom flanges and new diaphragm members, Bay C, between Diaphragm Lines 42 and 43.
14	New diaphragm members, Bay C, between Diaphragm Line 42 and 43.

Figure 3-8: View of old (pre-1992) diaphragm configuration.

Figure 3-9: View of new diaphragm configuration.

A typical measure stress history for Field Test No. 3 is given in Fig. 3-10. These stresses are for the same five of the gages of Gage Group 5 and the same test truck position as for those stresses shown in Fig. 3-6. Maximum recorded stress ranges for each gage are given in Table 3-5. The magnitudes of the measured stress ranges have decreased when compared to the Field Test Set No. 2 due to the addition of the diaphragms. The maximum stress range in Girder No. 3 is now 9.6 MPa (1.4 ksi) tension versus 17 MPa (2.4 ksi) tension with no diaphragms, a 43 percent decrease. The stress range in Girder No. 4 decreased to 11 MPa (1.6 ksi) tension from 14 MPa (2.1 ksi), a 21 percent decrease, but is higher in magnitude than that measured in Girder No. 3. This is due primarily from the higher moment reversal in Girder No. 4 when compared to Girder No. 3. An increase in load distribution between girders is evidenced by comparing the stress histories in Figs. 3-5 and 3-10. The peak tension stress levels in Fig. 3-10 are closer in magnitudes than in Fig. 3-5.

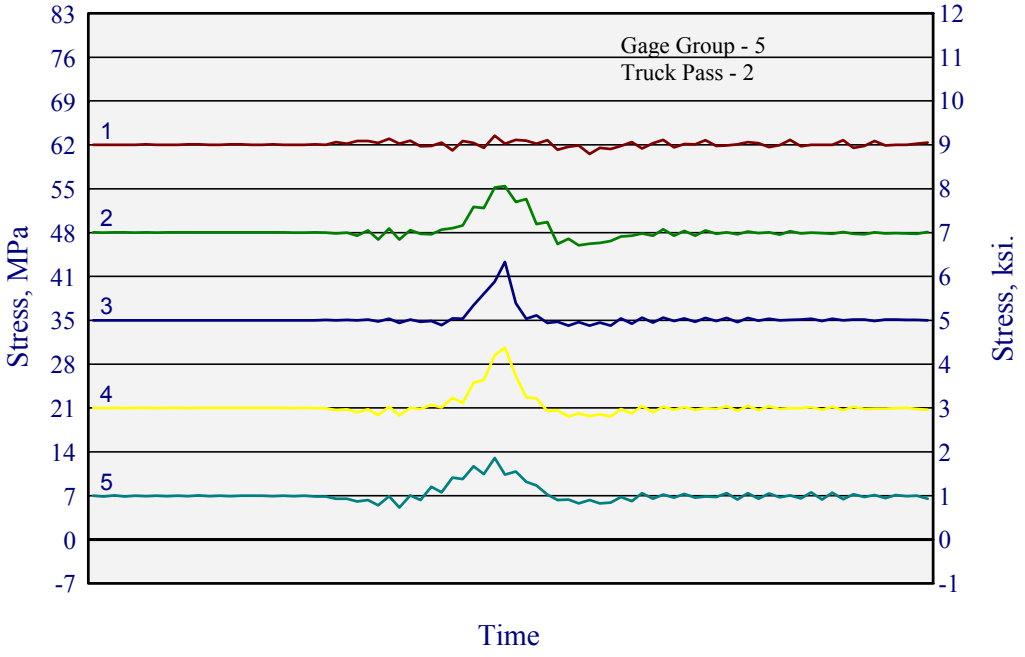

Figure 3-10: Bottom flange stress histories for Gage Group 5 (test truck centered in driving lane).

Table 3-5: Maximum measured stress ranges and direction for Gage Group 5 (test truck centered in driving lane).

Gage Number	Location	Max. Stress Range, MPa	Max. Stress Range, ksi
1	Bottom flange, Girder No. 1	2.8 (C)	0.4 (C)
2	Bottom flange, Girder No. 2	9.0 (T)	1.3 (T)
3	Bottom flange, Girder No. 3	9.6 (T)	1.4 (T)
4	Bottom flange, Girder No. 4	11 (T)	1.6 (T)
5	Bottom flange, Girder No. 5	7.6 (T)	1.1 (T)
6	Web, Girder No. 2	0.7 (T)	0.1 (T)
7	Web, Girder No. 3	2.8 (T)	0.4 (T)
8	Web, Girder No. 4	0.7 (T)	0.1 (T)

3.3 Comparison of Diaphragm Configurations

To investigate the influence of the diaphragms on the load distribution behavior of the structure, stress histories for a given location for the three field tests are compared. Figure 3-11 shows the stress histories for the different diaphragm configurations (all diaphragms (original), no diaphragms, and staggered diaphragm (1992 repair)) for Gage Group 5 (positive bending moment region). As indicated by the peak stress (test vehicle located over the diaphragm (see Fig. 3-6)), there was a marginal increase in stress between the original diaphragm configuration (diaphragms spaced every 4.6 m (15 ft)) and the new staggered diaphragm configuration. The peak stress was approximately 7.6 MPa (1.1 ksi) for the original configuration and 8.9 MPa (1.3 ksi) for the new configuration, an 18 percent increase. This increase is consistent with the predicted increases reported in TxDOT Research Report 1313. A significant increase in stress occurred when all the diaphragms were removed from the structure. The peak stress increased to 15 MPa (2.2 ksi) when the diaphragms were removed, an increase of approximately 100 percent, again, consistent with the previous research findings.

Figure 3-12 provides a similar comparison of stress histories for the bottom flange of Girder No. 3 in Gage Group 9). Again, the test vehicle is located in the center of the driving lane.

The measured increases in the peak stresses for the different diaphragm configurations are consistent with the finding of TxDOT Research Report 1313. A 100 percent increase in girder flange stresses with all diaphragms removed was found to be intolerable and was the governing factor behind the staggered diaphragms pattern recommended for the repair. It was observed by the construction crew performing the repairs, that there was a noticeable increase in the vibration and deflection of the structure when all diaphragms were completely removed. Even though the recommendation required the reinstallation of diaphragms, the total number of diaphragms was decreased from 488 diaphragms used in the original configuration to 156 for the staggered configuration, a decrease of 68 percent.

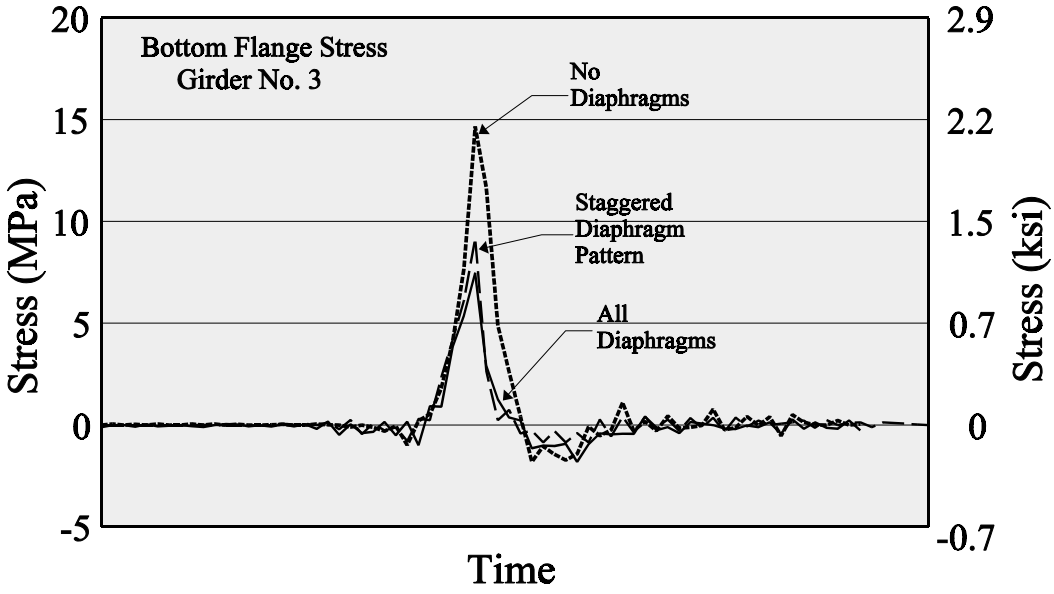

Figure 3-11: Comparison of stress histories for different diaphragm configurations, Girder No. 3 bottom flange, test vehicle centered in driving lane.

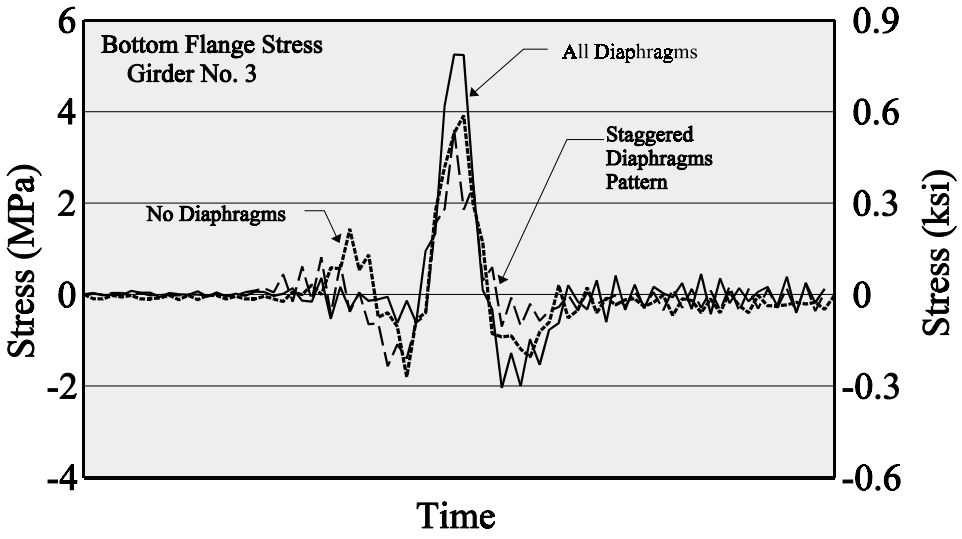

Figure 3-12: Comparison of stress histories for different diaphragm configurations, Girder No. 3, test vehicle in driving lane.

3.4 Comparison with Line Girder Computed Stresses

Even a 20 percent increase in tension flange stresses can be considered intolerable from a fatigue standpoint. An increase in the stress range can exceed the allowable stress range for a particular connection detail. In an effort to investigate this possibility, stress ranges were computed using the same assumptions that would be used in the design process; the use of AASHTO distribution factors. The analysis was performed using the distribution factors for a truck in a single lane and with the same weight and wheel configuration as the test vehicle. Figure 3-13 compares measured stress and computed stress for the bottom flange stress of a girder in Gage Group 5 (positive moment region of bending). It is evident that the AASHTO line girder analysis overestimates the stress history. A peak stress of 85.7 MPa (12.3 ksi) was computed while only a peak stress of 14.5 MPa (2.1 ksi) was measured. Based on these values, the AASHTO line girder analysis overestimated the maximum stress by 490 percent. Therefore, the 20 percent increase observed between the original diaphragm configuration and the staggered diaphragm configuration would be acceptable in terms of fatigue.

Since the portion of the bridge investigated is a three-span continuous structure, negative bending occurs at the location of Gage Group 5 when the truck occupies an adjacent span. This behavior is evident in the stress history for the AASHTO line girder analysis shown in Fig. 3-13. The maximum compressive stress is -20 MPa (-2.9 ksi). However, the measured stress history shows very little reversal of stress. The maximum measured compressive stress was -1.4 MPa (-0.2 ksi). This further discrepancy between the AASHTO line girder analysis and measured stresses is due to the skewness of the structure.

A similar comparison of stress histories in the positive moment region of bending is given in Fig. 3-14 for the bottom flange stress at Gage Group 8. The stress history for the AASHTO line girder analysis is identical to that given in Fig. 3-13 since the gage location is the same distance from the support. Here, the maximum measured stress is 13.7 MPa (2.0 ksi).

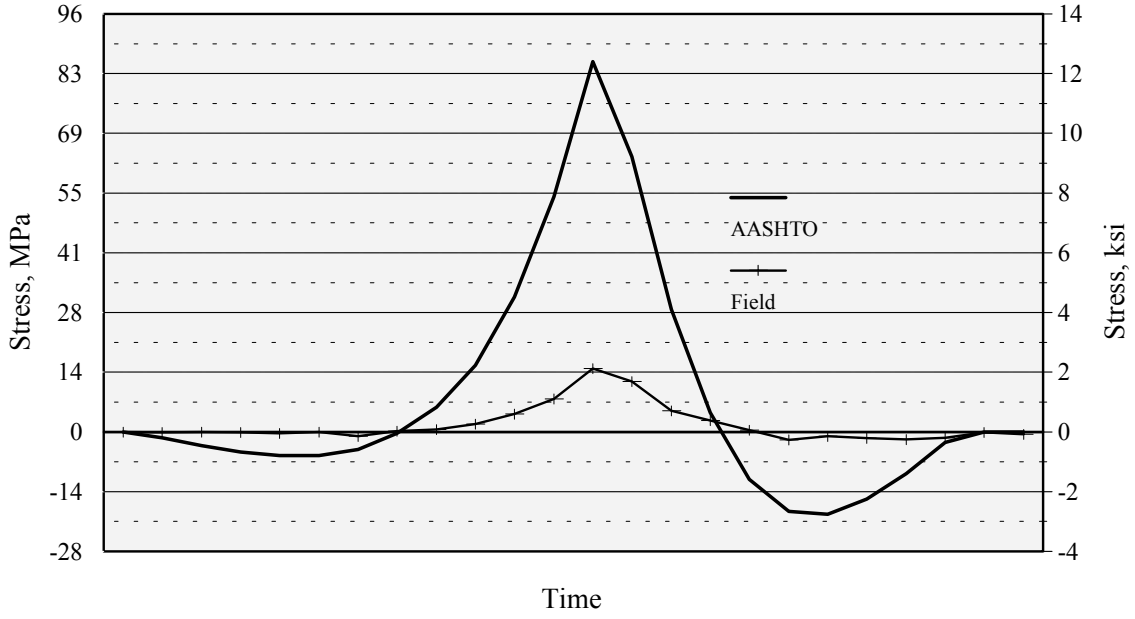

Figure 3-13: Comparison of measured stress and line girder predicted stress for bottom flange, Gage Group 5 - No Diaphragms.

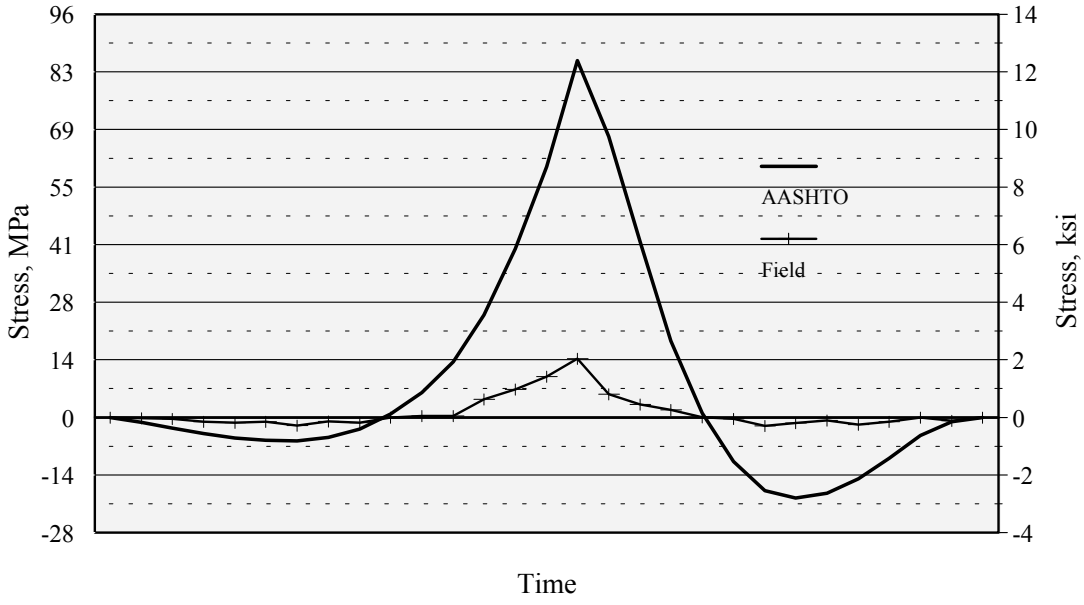

Figure 3-14: Comparison of measured stress and line girder predicted stress for bottom flange, Gage Group 8 - No Diaphragms.

Figure 3-15 provides a similar comparison of stress histories for Gage Group 9, except that this gage group is located in the negative moment region of bending. The maximum compressive stress predicted by the AASHTO line girder analysis is -57.2 MPa (-8.3 ksi) while the maximum measured compressive stress was 7.6 MPa (-1.1 ksi). The AASHTO line girder analysis overestimates the peak compressive stress by 650 percent. As with the positive moment regions of bending, actual stress reversal is reduced to negligible levels.

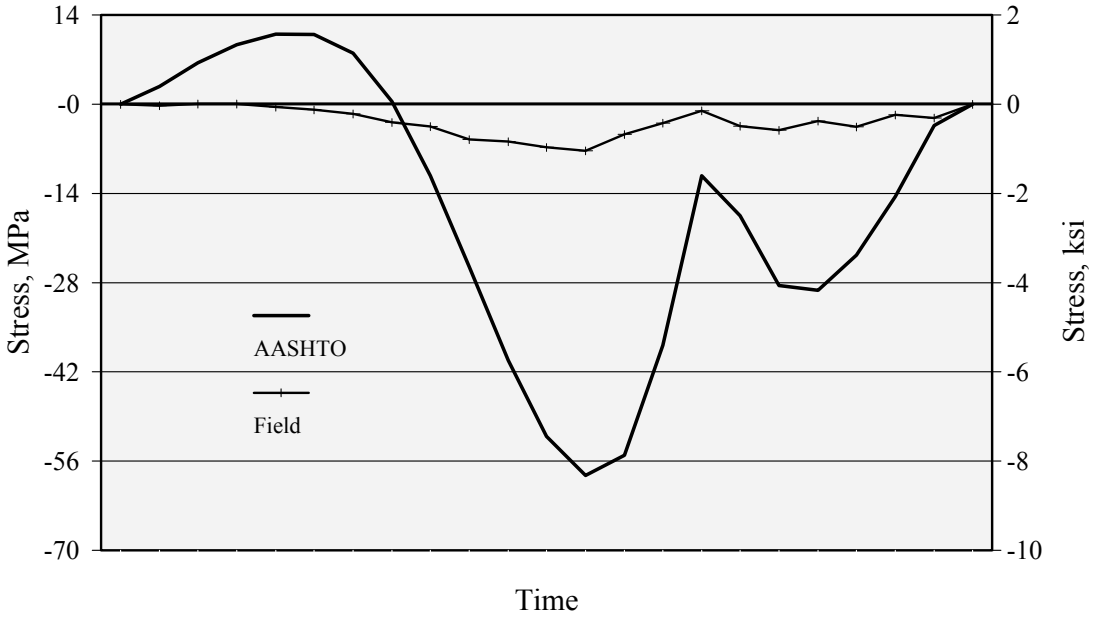

Figure 3-15: Comparison of measured stress and line girder predicted stress for bottom flange, Gage Group 9 - No Diaphragms

4. TOWN LAKE BRIDGE INVESTIGATION

4.1 Background

It was determined through discussions with TxDOT personnel that the Town Lake Bridge carrying IH-35 over the Colorado River in Austin, Texas, would be an ideal candidate for field testing because it is a moderately skewed bridge with recently detected fatigue cracking. This bridge was originally composed of two identical structures, one carrying three lanes northbound, and the other carrying three lanes southbound. A view of the bridge roadway is given in Fig. 4-1, looking in the southbound direction.

Figure 4-1: View of Town Lake bridge, looking in the southbound direction.

The original structure was composed of two continuous plate girder units of 134 m (440 ft) and 186 m (610 ft). The 134 m (440 ft) unit has four equal spans of 33.6 m (110 ft), while the 186 m (610 ft) unit has spans of 33.6, 39.6, 39.6, 39.6, and 33.6 m (110, 130, 130, 130, and 110 ft). The bridge was built on a 30 degree skew (measured with respect to the transverse

direction). The original cross section consisted of five 1520 mm (60 in) deep plate girders on a 2.74 m (9 ft) spacing, with a 172 mm (6.75 in) thick concrete deck.

In 1979, the northbound and southbound structures were each widened by the addition of a sixth girder. A new slab was poured and cross frames added between the two structures, effectively joining the northbound and southbound structures into one. A Jersey type guardrail was placed in the center of this new slab to separate the northbound and southbound traffic. The right shoulders were widened in each direction and traffic lanes were shifted, but no additional traffic lanes were provided. Figure 4-2 shows the cross section of the widened bridge. Note that a 2.13 m (7 ft) spacing was used for the additional girder, as opposed to the 2.74 m (9 ft) spacing used in the original construction.

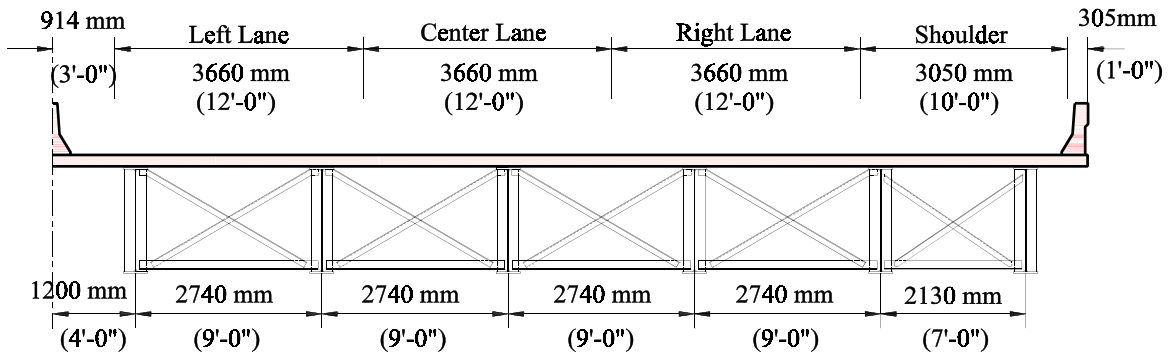

Figure 4-2: Town Lake Bridge cross section.

The framing plan for the 134 m (440 ft) unit is shown in Fig. 4-3. Diaphragm lines are spaced at 3.81 m (12.5 ft) or 4.57 m (15 ft), with some additional lines of diaphragms added at the interior supports. Two types of diaphragms, shown in Figs. 4-4 and 4-5, were used in the original construction, designated as types D2 and D3 on the original drawings. The diaphragm types were alternated longitudinally throughout the length of the bridge. At each diaphragm line, the same type was used between the original five girders. The transverse stiffeners that the diaphragms connect to had a tight-fit detail at the girder flanges, but were not welded. When the bridge was widened, additional diaphragm types were used, designated as D4 and D5. Except for the width of the diaphragm, as determined by the girder spacing, diaphragms D4 and D5 are identical. Figure 4-6 shows the configuration of this diaphragm type. The connection plates for this diaphragm type utilize a 25 mm (1 in) web gap at the girder tension flange. (The D1 diaphragm configuration was used at the end supports.) Figure 4-7 provides a view of the diaphragm framing from beneath the bridge.

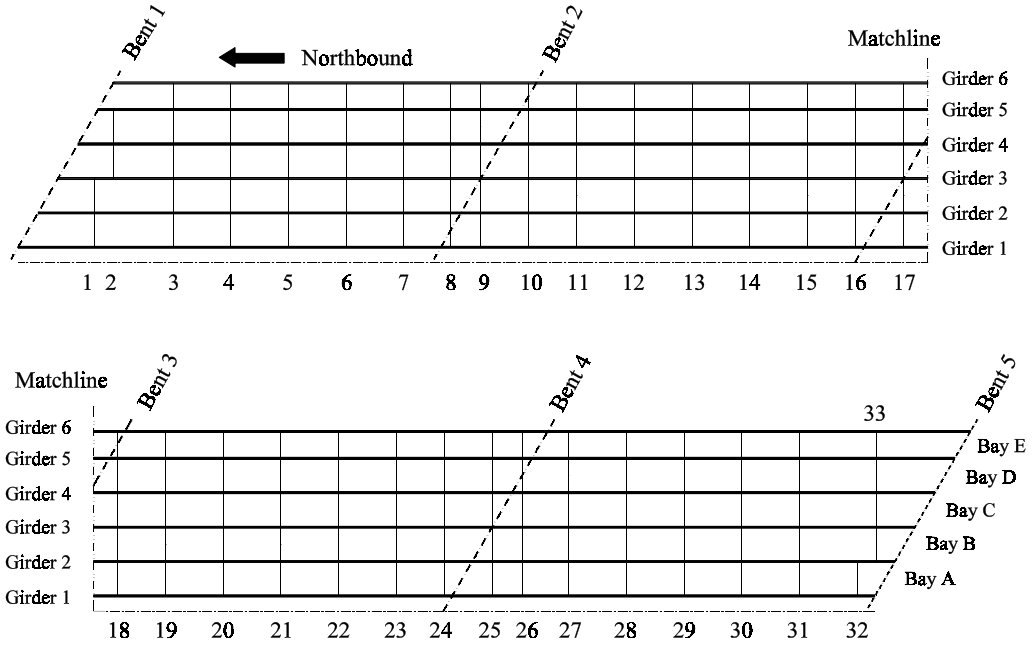

Figure 4-3: Framing plan of 134.2 m (440 ft) unit.

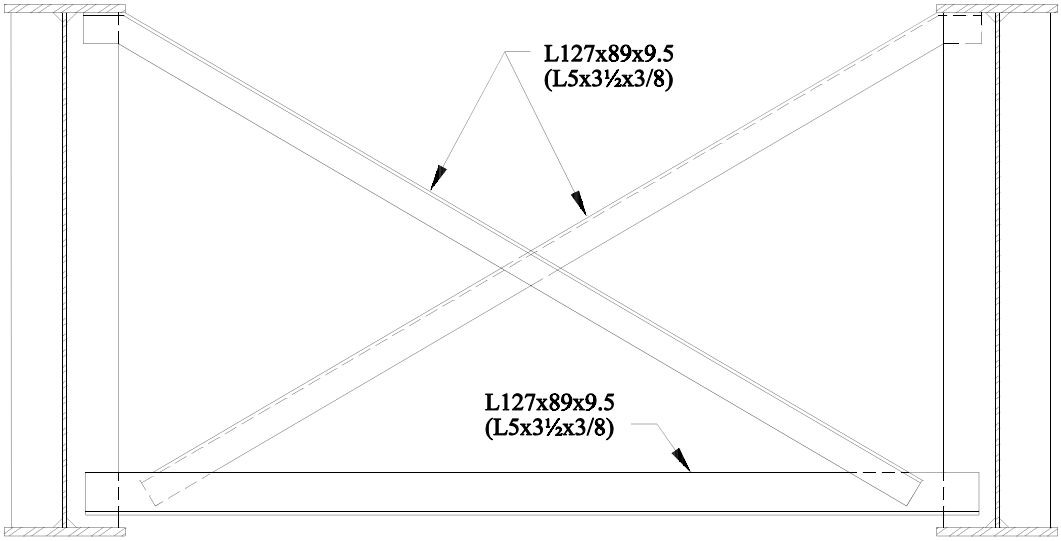

Figure 4-4: Type D2 diaphragm configuration, Town Lake Bridge.

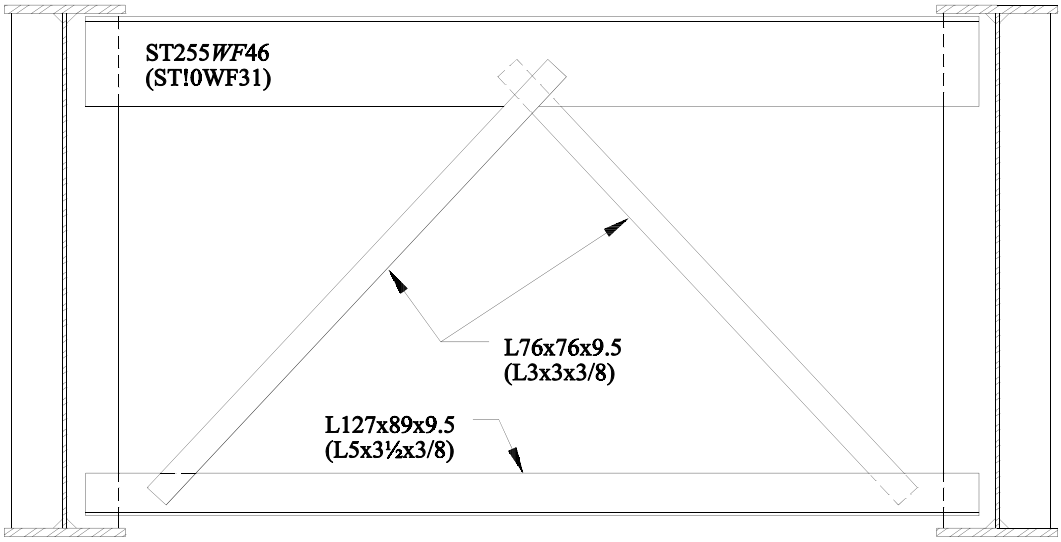

Figure 4-5: Type D3 diaphragm configuration, Town Lake Bridge.

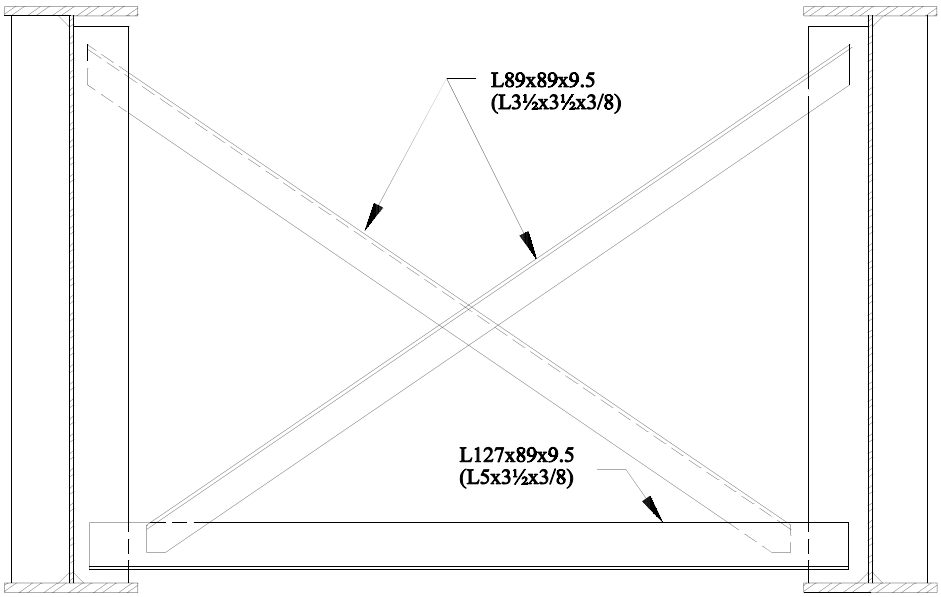

Figure 4-6: Type D4 and D5 diaphragm configurations, Town Lake Bridge.

Figure 4-7: View of diaphragm framing of northbound structure looking south from the north shore of Town Lake.

The tight-fit detail used on the Town Lake Bridge is different than the tight-fit detail used on the Midland County bridges. The corner cope of the connection plate provides little clearance for the web-to-flange fillet weld. Consequently, the fillet weld between the connection plate and web extends into the web-to-flange weld, as shown in Fig. 4-8. This weld configuration increases the stiffness of the detail to the cross frame diaphragm out-of-plane distortion. However, the resulting intersecting welds increase restraint stresses and the possibility of weld defects and should therefore be avoided. Again, with the tight-fit detail, the end of the connection plate is not welded to the tension flange.

Figure 4-8: Example of tight-fit detail with intersecting welds, Town Lake Bridge.

4.2 Summary of Fatigue Damage

An inspection of the Town Lake Bridge in 1978 revealed that the structure had been experiencing continuing fatigue damage. It was observed that several diaphragms had broken welds where the diaphragm lower strut connects to the connection plate, and consequently the diaphragm had broken free of the connection plate. The connection was rewelded, but again broke free due to continued fatigue cracking. Figure 4-9 shows an example of a cracked lower strut to connection plate weld. The 1978 inspection indicated that this type of fatigue damage occurred exclusively to diaphragms connected to Girder 3 and was, in most cases, confined to the positive moment region. Figure 4-10 shows the location of the fatigue damage on the framing plan for the Town Lake Bridge. Types D2 and D3 diaphragms both experienced this separation of lower strut from the connection plate. Other fatigue damage has occurred but has not be documented.

Figure 4-9: View of cracked fillet weld at diaphragm connection, Town Lake Bridge.

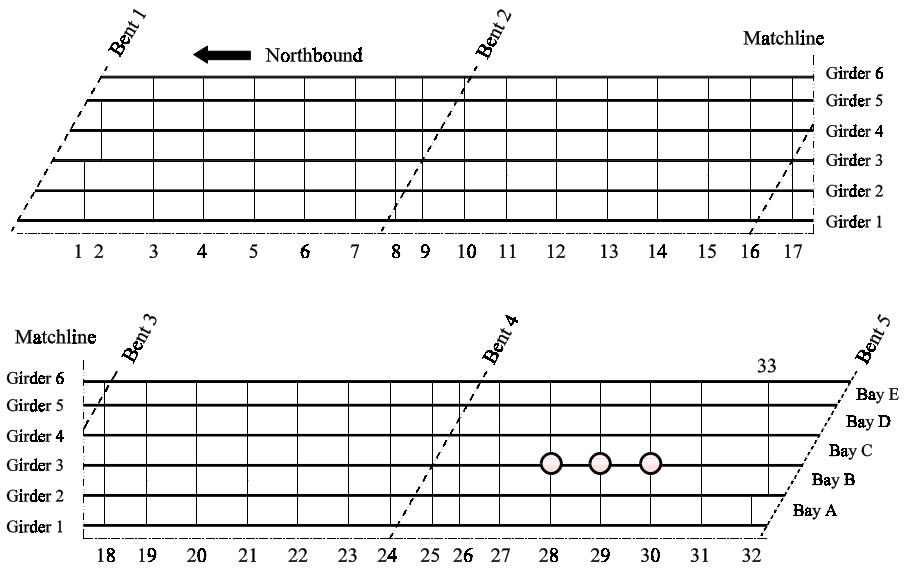

Figure 4-10: Framing plan with locations of repaired fatigue damage.

4.3 Load Testing

Field tests were performed to determine the load distribution between the girders, the forces in the diaphragms, and to provide data to correlate with finite element modeling. These tests were performed on July 10 and 11, 1993, in conjunction with the Texas Department of Transportation.

The tests were conducted by passing a TxDOT vehicle of known weight, as shown in Fig. 4-11, over the bridge and recording the strains at various locations. The gross vehicle weight of the test truck was 117.4 kN (26.4 kips). A vehicle speed of approximately 80.5 kph (50 mph) was used for all tests. An attempt was made to isolate the test vehicle from other traffic while it traversed the bridge. Since this bridge carries Interstate 35, there was always some other vehicle in the vicinity of the test vehicle and lane closures were precluded by safety concerns. The driver was instructed to isolate the test vehicle from other trucks. Testing was performed on a

weekend starting at approximately 6:30 am and continuing until the traffic volume increased to the point where superposition of stress histories was occurring.

Figure 4-11: View of test vehicle used for Town Lake Bridge.

An eight channel digital data acquisition system was used to record strains at various locations in the northbound structure. Figure 4-12 shows the gage group locations where strain data were taken along the bridge. Since only eight channels of data could be simultaneously recorded, multiple passes of the truck are required in order to obtain data for all gage groups. Table 4-1 describes each of the five gage groups. Figure 4-13 shows the details of each gage group for Gage Group 2 and Fig. 4-14 is a view of the actual gage wiring. A complete set of stress histories for all gage groups and test truck positions can be found in Appendix C.

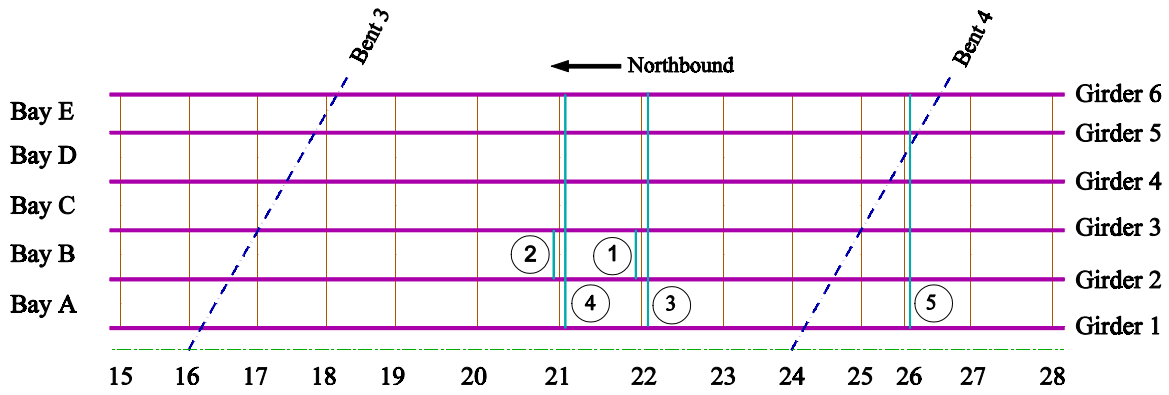

Figure 4-12: Locations of strain gage groups for Town Lake Bridge.

Table 4-1: Summary of gage group locations, Town Lake Bridge.

Gage Group Number	Description of Gage Group Location
1	Type D2 diaphragm members, Diaphragm Line 22, Bay B, Positive Moment Region.
2	Type D3 diaphragm members, Diaphragm Line 21, Bay B, Positive Moment Region.
3	Bottom Flanges and Bay B diaphragm members, Diaphragm Line 22, Positive Moment Region.
4	Bottom Flanges and Bay B diaphragm members, Diaphragm Line 21, Positive Moment Region.
5	Bottom Flanges and Bay B diaphragm members, Diaphragm Line 26, Negative Moment Region.

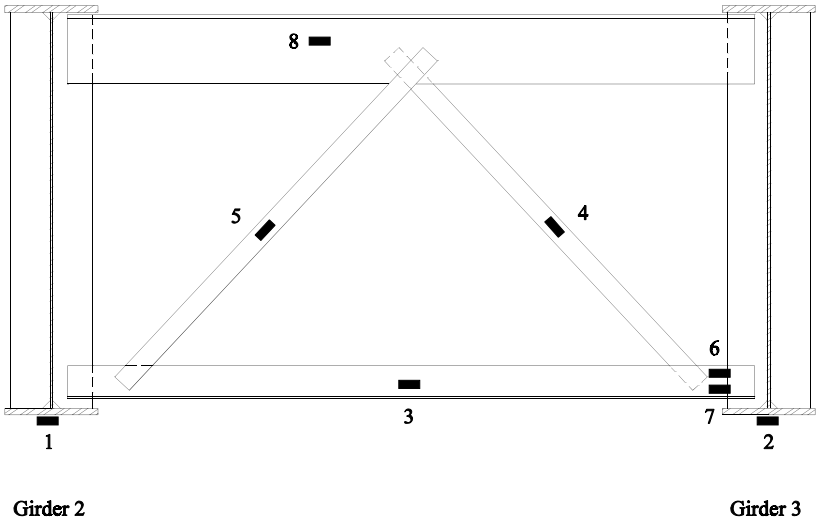

Figure 4-13: Strain gage locations for Gage Group 2.

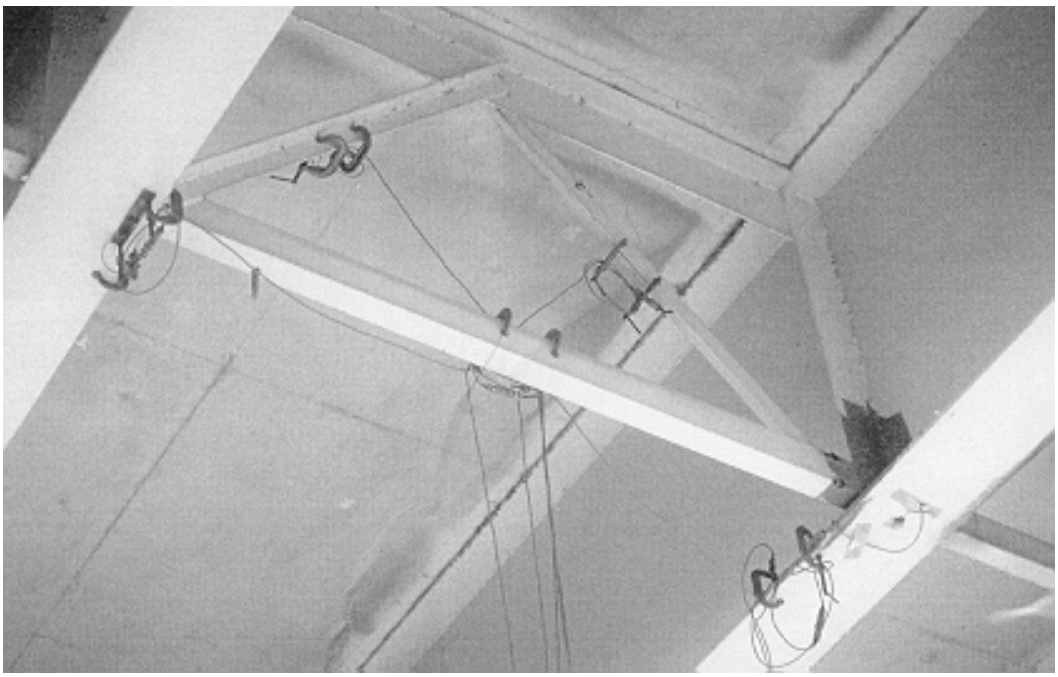

Figure 4-14: View of strain gage wiring for Gage Group 2.

Typical measured stress histories are given in Figs. 4-15 and 4-16 for Gage Group 2 with the test vehicle centered in the center lane as shown in Fig. 4-17. Table 4-2 provides the

maximum recorded stress range for each of the eight gages in the group. Of interest is the bending stress that is occurring in the bottom diaphragm strut, as indicated by the stress levels in Gage Nos. 6 and 7. These stresses are indicative of the forces that are causing the separation of the lower strut from the connection plate. Simply rewelding this connection as a repair will not prevent a reoccurrence of the cracking. Note that the stress levels in the other gages are relatively low.

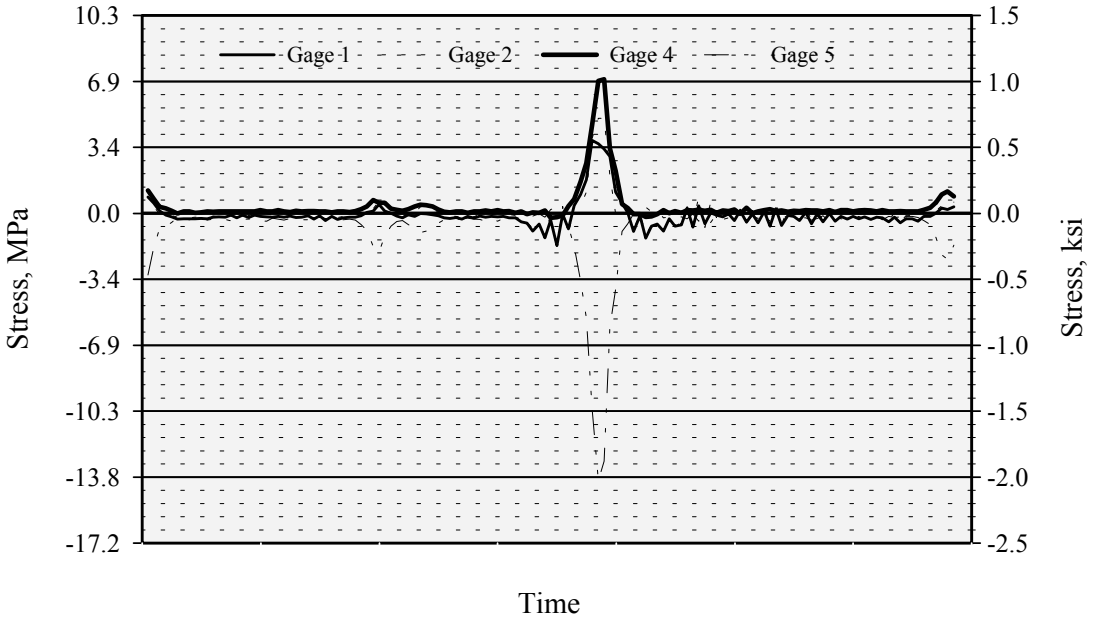

Figure 4-15: Stress histories for Gage Group 2A, Truck Pass 2 (test truck centered in center lane).

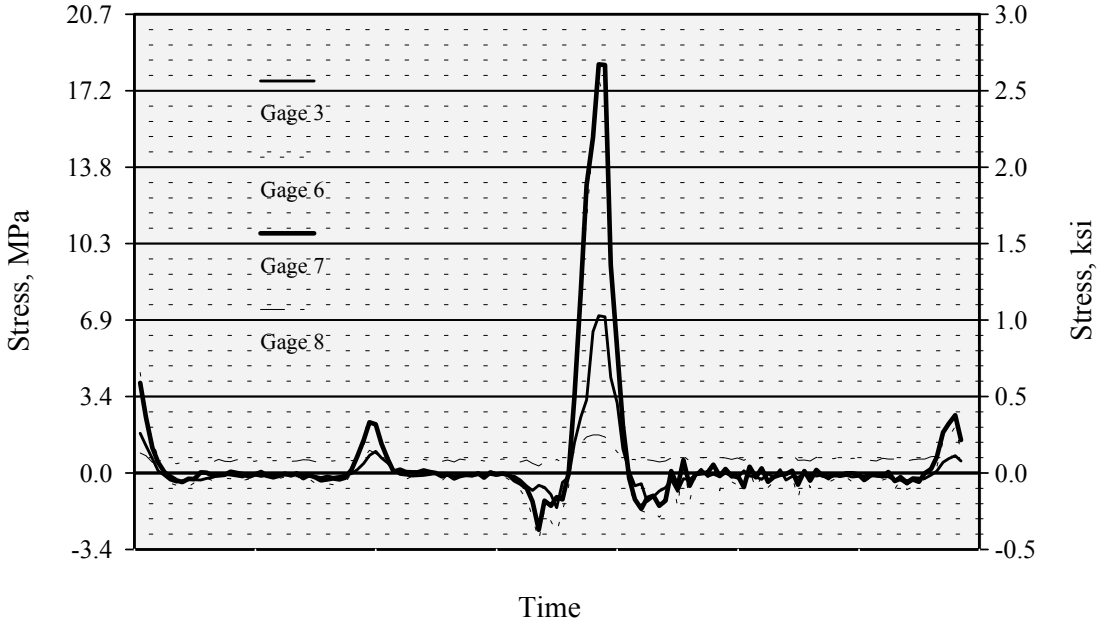

Figure 4-16: Stress histories for Gage Group 2B, Truck Pass 2 (test truck centered in center lane).

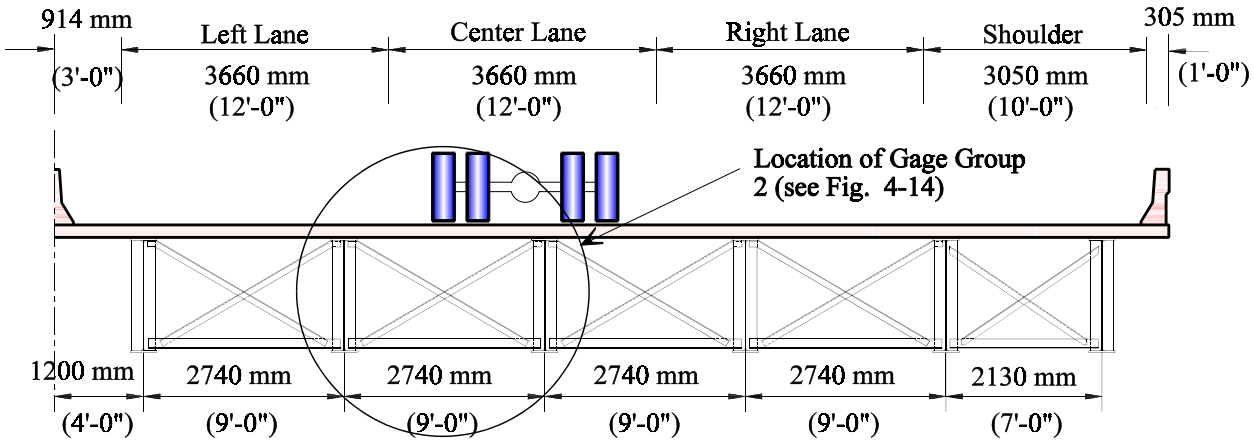

Figure 4-17: Test truck position for Gage Group 2, Truck Pass 2.

Table 4-2: Maximum measured stress ranges for Gage Group 2, Truck Pass 2 (test truck centered in driving lane).

Gage No.	Location	Max. Stress Range, MPa	Max. Stress Range, ksi
1	Bottom flange, Girder No. 2	5.5 (T)	0.80 (T)
2	Bottom flange, Girder No. 3	6.7 (T)	0.97 (T)
3	Lower strut, neutral axis	9.0 (T)	1.3 (T)
4	Diagonal, neutral axis	6.9 (T)	1.0 (T)
5	Diagonal, neutral axis	14.0 (C)	2.1 (C)
6	Lower strut, top	2.1 (T)	3.0 (T)
7	Lower strut, bottom	14.0 (C)	2.1 (T)
8	Upper strut, neutral axis	1.4 (T)	0.20 (T)

In addition to the cross frame diaphragm member, the bottom flanges of each girder in a cross section were strain gaged to study the load distribution characteristics of the structure. Figure 4-18 shows the gage locations for Gage Group 4, which is located along Diaphragm Line 21 (positive moment region of bending). Figures 4-19 and 4-20 provide the stress histories for Gage Group 4 with the test vehicle centered in the center lane as shown in Fig. 4-17. Table 4-3 provides the maximum recorded stress range for each of the eight gages in the group. Note that Gage No. 2 reads the highest maximum tensile stress level, 5.1 MPa (0.74 ksi), since the test vehicle is approximately centered above Girder No. 2, to which it was attached. Gage No. 1 has the highest recorded stress range due to slightly more vibrational stresses and reversal of moment.

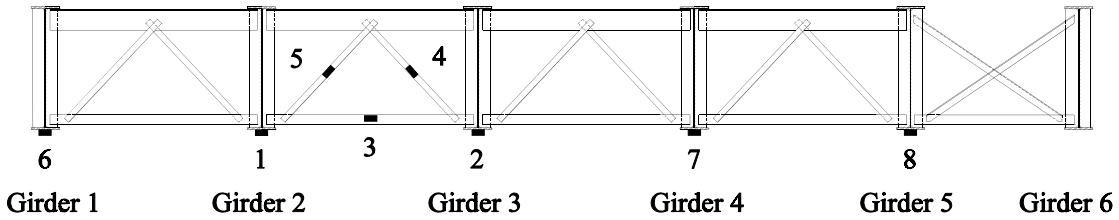

Figure 4-18: Strain gage locations for Gage Group 4, Town Lake Bridge.

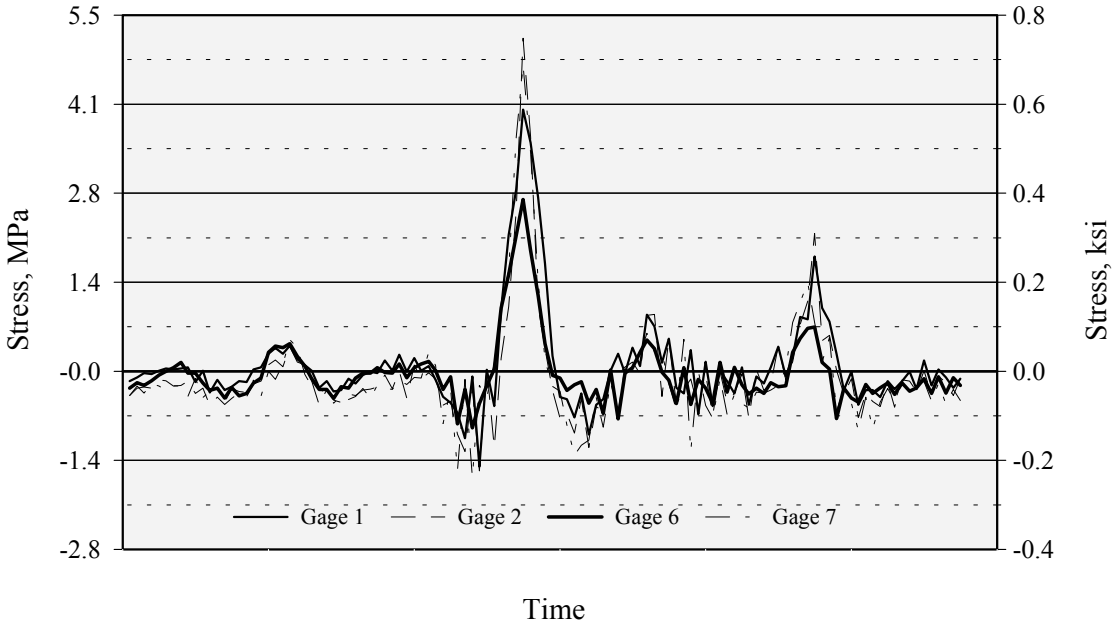

Figure 4-19: Stress histories for Gage Group 4A, Truck Pass 2 (test truck centered in center lane).

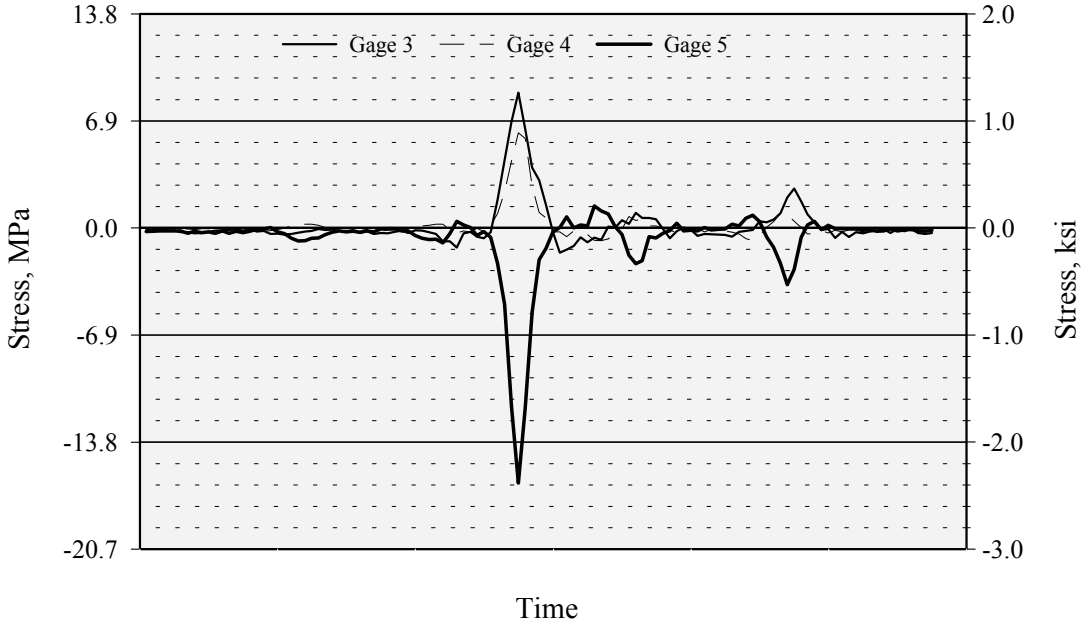

Figure 4-20: Stress histories for Gage Group 4B, Truck Pass 2 (test truck centered in center lane).

Table 4-3: Maximum measured stress ranges for Gage Group 4, Truck Pass 2 (test truck centered in center lane).

Gage Number	Location	Max. Stress Range, MPa	Max. Stress Range, ksi
1	Bottom flange, Girder No. 3	6.76 (T)	0.98 (T)
2	Bottom flange, Girder No. 2	6.55 (T)	0.95 (T)
3	Lower strut, Bay B	16.5 (C)	2.39 (T)
4	Diagonal, Bay B	11.4 (T)	1.66 (T)
5	Diagonal, Bay B	5.10 (T)	0.74 (T)
6	Bottom flange, Girder No. 1	6.07 (T)	0.88 (T)
7	Bottom flange, Girder No. 4	5.86 (T)	0.85 (T)
8	Bottom flange, Girder No. 5	3.96 (T)	0.57 (T)

4.4 Finite Element Modeling

Diaphragm removal was not an option at the Town Lake Bridge since the diaphragm fatigue cracking was not as severe as that experienced by the Midland County Bridge. Therefore, a finite element model of the bridge was developed in order to evaluate the influence of the diaphragms on the load distribution characteristics of the structure. Figure 4-21 shows a plot of half of the northbound 134 m (440 ft) unit, though the entire unit was modeled. The bridge was modeled to capture the global deformations under the action of vehicle live loading. A longitudinal mesh density was chosen to accommodate diaphragm lines, field splices, skewed supports, and transitions of the girder cross section. Non-composite action was assumed over the interior supports between field splices, but positive moment regions were modeled compositely. Many nodes were needed throughout the length of the bridge, especially near the interior supports, in order to correctly model the features listed above. Transverse mesh density was chosen to accommodate girder lines and lines of loading within each traffic lane. Solid elements were used for the deck, plane stress elements for the web, and space frame elements for the flanges and diaphragm members.

The finite element model was compared to the field test data to determine how accurately the behavior of the bridge was modeled. Fig. 4-22 shows a plot of a stress history from field tests compared to a stress history developed from finite element modeling for the bottom flange stresses in Girder No. 3 for Truck Pass 2. The finite element stress values were multiplied by the AASHTO impact fraction, 20 percent in this case, to better correspond with the field tests values. This was done because the field data was taken with the test truck traveling at 80.5 km/hr (50 mph) across the bridge. Comparison of the peak stress value shows that the model predicted value is 9 percent below that actually measured in the field. This is excellent agreement, since finite element solutions are inherently more stiff due to the limited number of degrees of freedom used in modeling the structure.

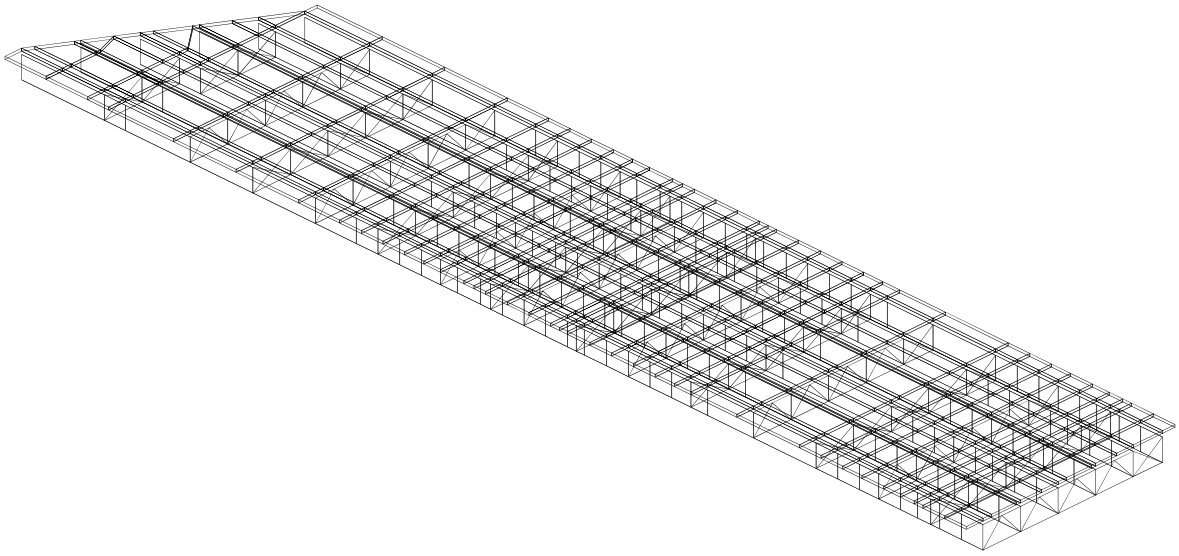

Figure 4-21: Finite element model of Town Lake Bridge.

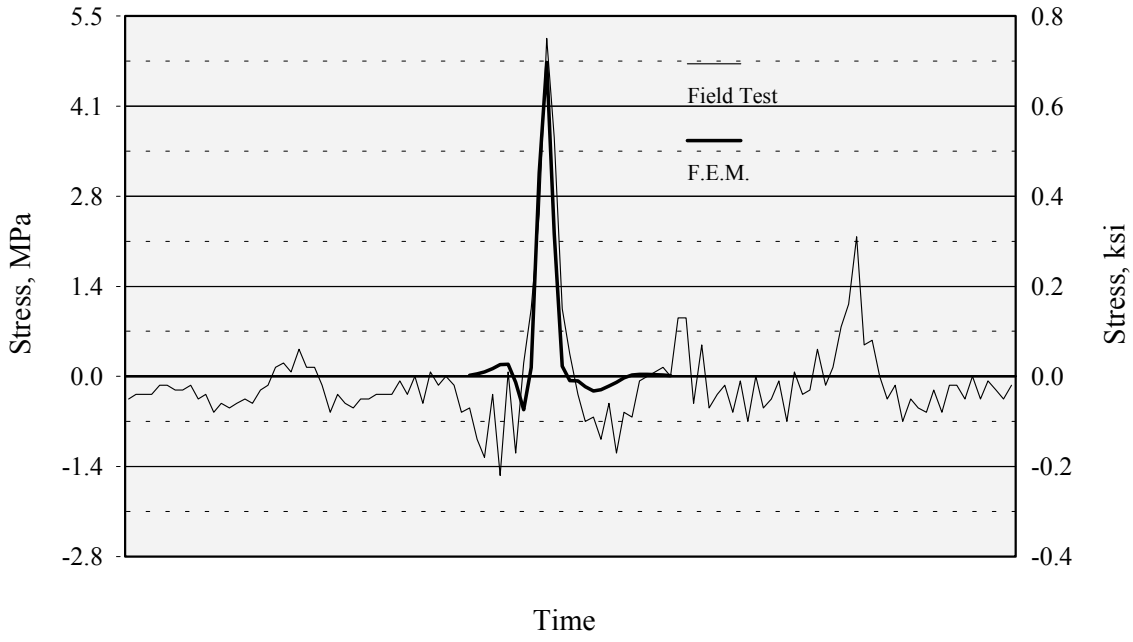

Figure 4-22: Comparison of measured and FEM stress histories.

Similar to the Midland County Bridge, an analysis was performed to study what effect diaphragm removal would have on the flange stress of the girders. Figure 4-23 shows the predicted stress histories from the finite element analysis for the bottom flange stresses in the positive moment region of bending. The as-built (diaphragms spaced at 4.6 m (15 ft)) condition results in a maximum stress of 3.8 MPa (0.55 ksi). Removal of all diaphragms from the structure increases the flange stress by 45 percent to 5.5 MPa (0.80 ksi). While this increase is not as large as the increase measured in the Midland County Bridge, it is still significant in terms of fatigue and strength considerations. When an AASHTO line girder analysis is used to predict the flange stresses, it overestimates the as-built condition by 320 percent. As was the case with the Midland County Bridge, the magnitude of the moment reversal was also reduced. Figure 4-24 shows a similar plot and behavior for the bottom flange stresses in the negative moment region of bending.

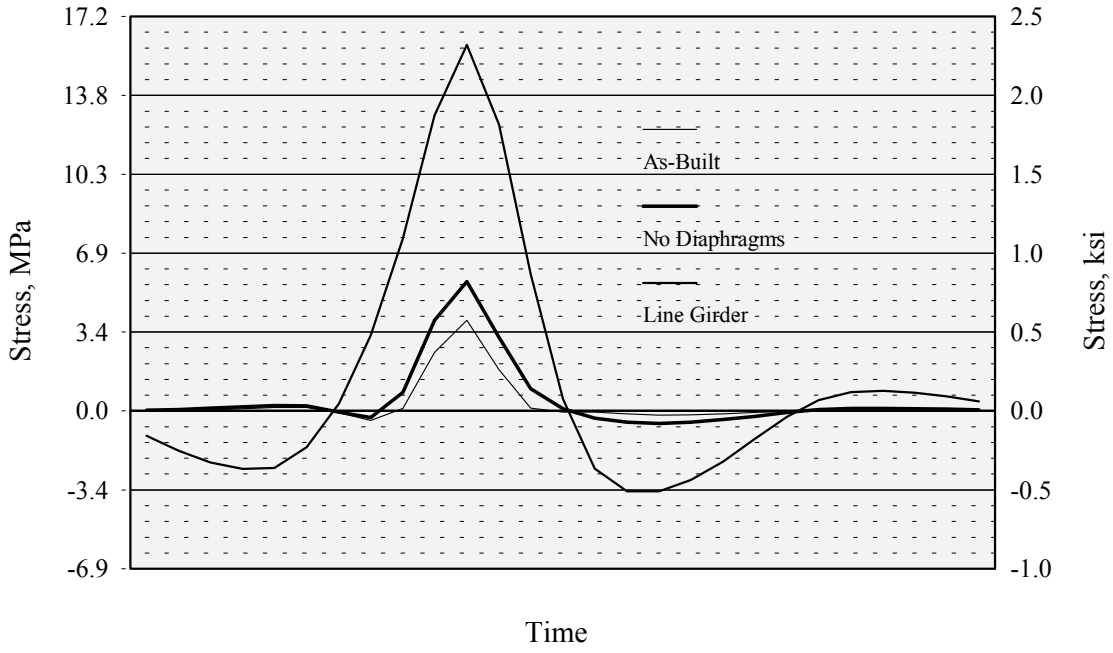

Figure 4-23: Comparison of stress histories for positive moment region of bending.

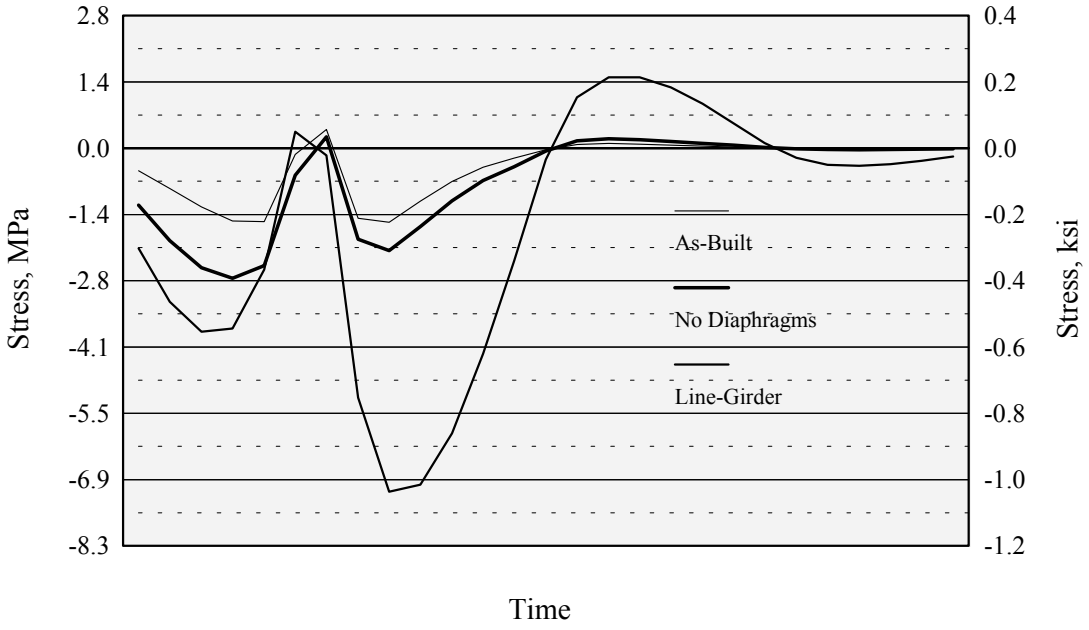

Figure 4-24: Comparison of stress histories for negative moment region of bending.

The finite element model of the Town Lake Bridge was also used to investigate the effect the bridge skew had on the load distribution characteristics of the structure. Figures 4-25 and 4-26 show comparison plots of stress histories considering the as-built case, no diaphragms, no bridge skew, and a skewed wheel load pattern. The skewed wheel load pattern was used to investigate whether its effect would negate the effect of the bridge skew. As indicated by the results in Fig. 4-25, the skew had little effect on the flange stresses in the positive moment region of bending. As expected, no diaphragms result in the highest stresses. As indicated by Fig. 4-26, the bridge skew has more of an effect in the negative moment region of bending. Here, the non-skew case results in the highest bending moment, whereas a bridge skew decreases the bending moment.

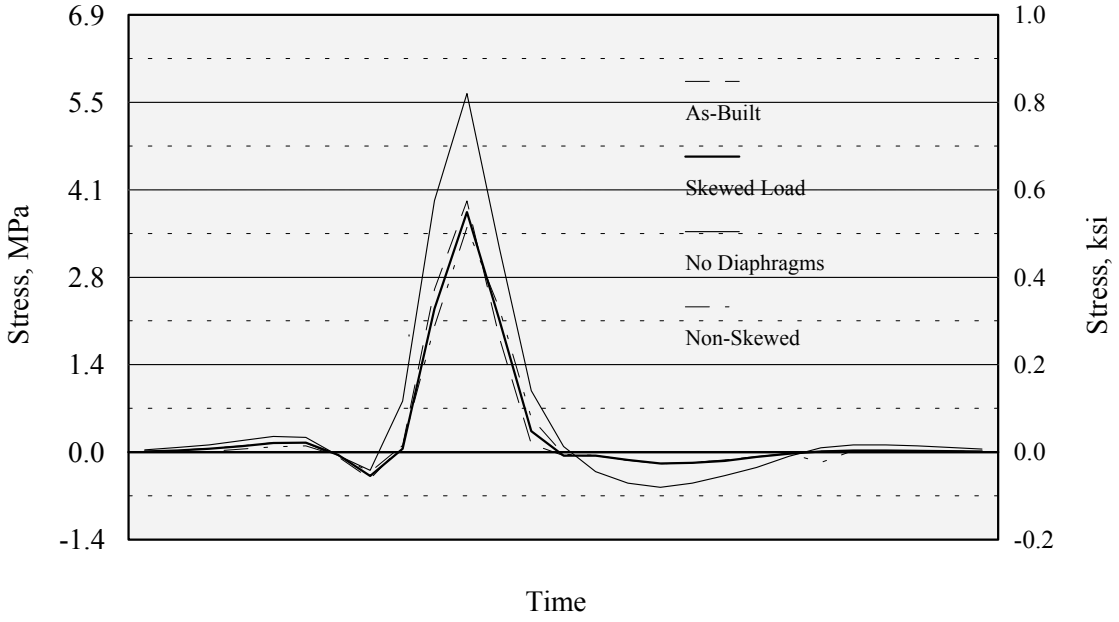

Figure 4-25: Comparison of stress histories for FEM diaphragm study, positive moment region of bending.

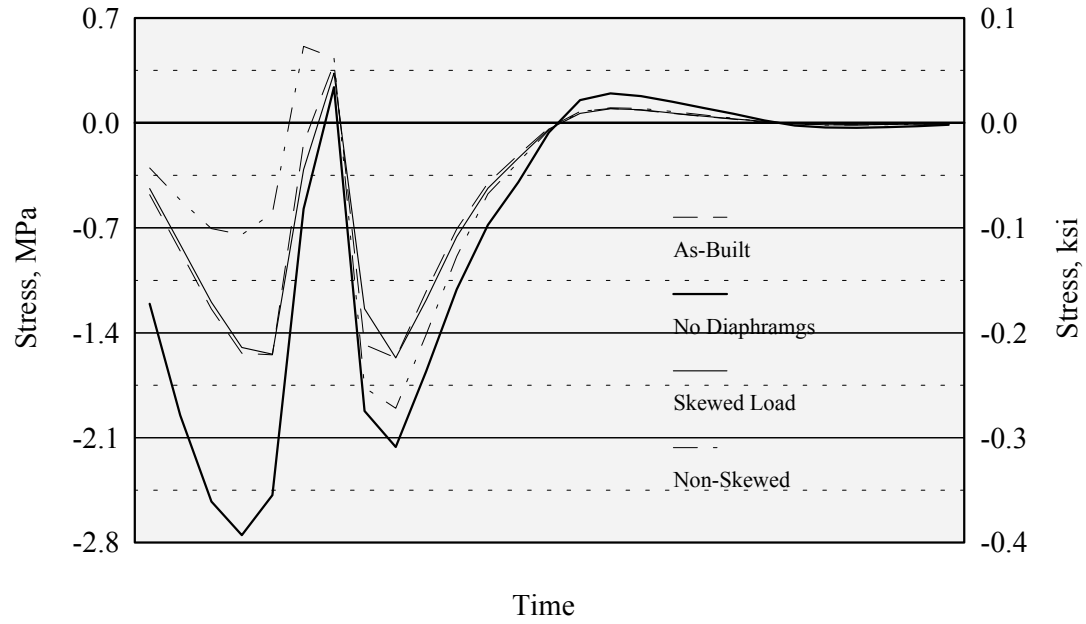

Figure 4-26: Comparison of stress histories for FEM diaphragm study, negative moment region of bending.

5. COLETO CREEK BRIDGE INVESTIGATION

5.1 Background

To provide calibration for the analytical portion of the current study, a non-skewed bridge was necessary for field testing. Through discussion with TxDOT personnel, the Coleto Creek Bridge was selected. This bridge carries U.S. Highway 59 southwest of Victoria, Texas, in Victoria County. Though this bridge had not experienced any detectable fatigue damage to date, its relatively low traffic volume made it ideal for static load testing where temporary bridge closure was necessary.

The structure is a two-lane, three-span continuous structure with an overall length of 83.8 m (275 ft). The structure has individual spans of 22.9 m (75 ft), 38.1 m (125 ft), and 22.0 m (75 ft). The cross section, shown in Fig. 5-1, is comprised of three welded plate girders with 1220 mm by 9.5 mm (48 in by 0.375 in) web plate. The flange size varied from 305 mm by 19 mm (12 in by 0.75 in) to 356 mm by 28.5 mm (14 in by 1.125 in) to meet the required moment capacity. Flange cover plates, 330 mm by 19 mm (13 in by 0.75 in) were used in the negative moment regions. A 165 mm (6.5 in) reinforced concrete slab has an overall width of 9.80 m (32.2 ft) with an 8.53 m (28 ft) roadway.

Two types of cross frame diaphragms were used. Type A, similar to that shown in Fig. 4-5 and Type B (Fig. 4-4). The diaphragm spacing is nominally 4.88 m (16 ft) but shortened to 3.35 m (11 ft) to make up differences in the individual span lengths. The diaphragm types alternated along the length of the structure with the heavier diaphragm, Type A, used at supports and expansion joints. A partial framing plan of the structure is shown in Fig. 5-2.

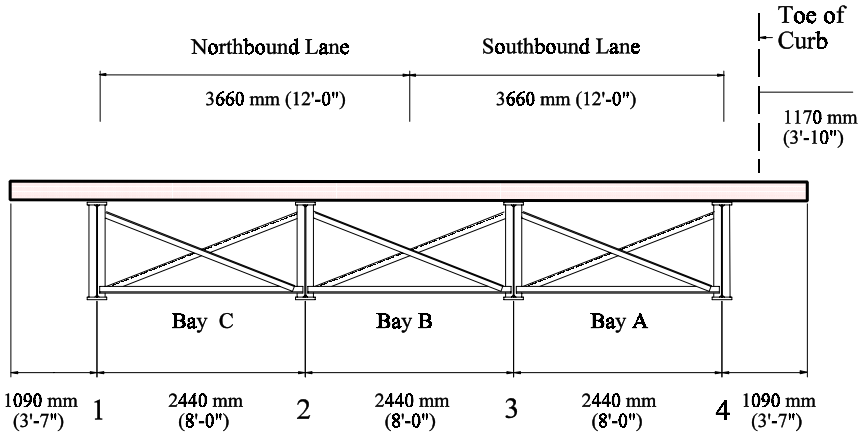

Figure 5-1: Coleto Creek Bridge cross section.

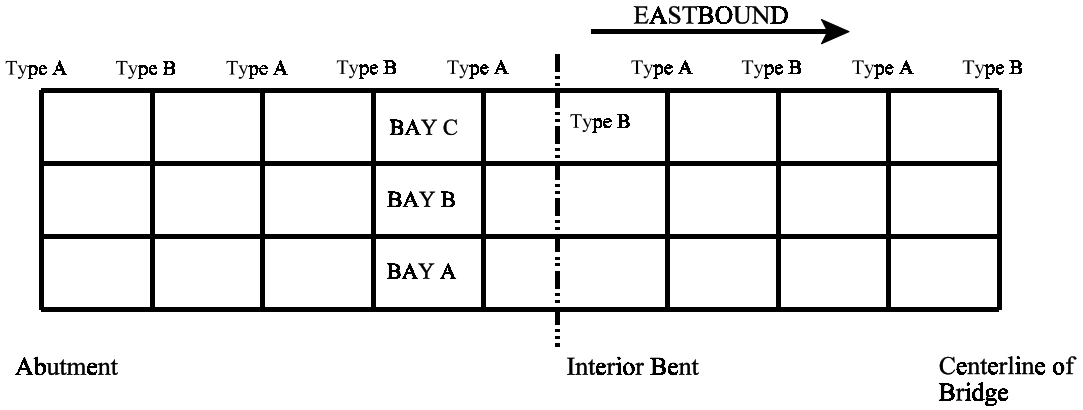

Figure 5-2: Partial framing plan for Coleto Creek Bridge.

5.2 Load Testing

Field tests were performed on the Coleto Creek Bridge to determine the load distribution between girders and to provide data for correlation with the analytical portion of the study. Both static and dynamic (test vehicle traveling at 80.5 km/hr (50 mph)) tests were conducted. The

tests were performed on December 15, 1993, in cooperation with the Texas Department of Transportation.

The data acquisition system used on the previous bridges was also used for the Coleto Creek Bridge study. Five gage groups of eight channels each were located as shown in Fig. 5-3. Table 5-1 summarizes each of the gage groups. Figure 5-4 shows the gage locations for Gage Group 1 and is representative of the other groups.

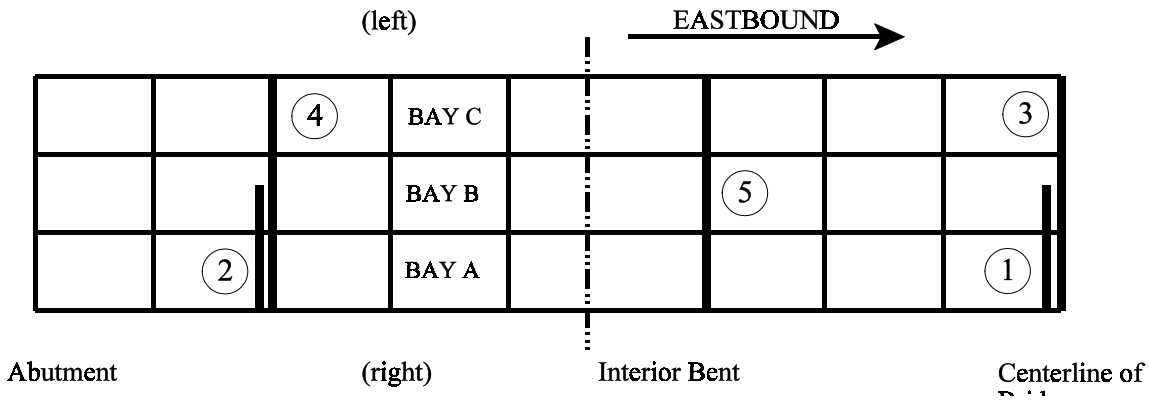

Figure 5-3: Gage group locations for Coleto Creek Bridge.

Table 5-1: Summary of gage group locations, Coleto Creek Bridge.

Gage Group Number	Description of Gage Group Locations
1	Type B diaphragm members at midspan of center span.
2	Type A diaphragm members, positive moment region of bending.
3	Bottom flanges at midspan of center span.
4	Bottom flanges, positive moment region of bending.
5	Bottom flanges, negative moment region of bending.

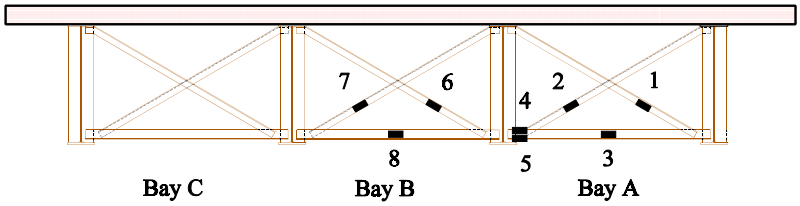

Figure 5-4: Gage Group 1, midspan diaphragm location (cross frame members)

The tests were conducted using a TxDOT vehicle with the weight and axle configuration shown in Fig. 5-5. The gross vehicle weight was measured at 197.0 kN (44.26 kips). The vehicle was positioned statically at various locations along the structure and laterally in the roadway width to obtain maximum stresses. Stress histories were also obtained for the test vehicle at various speeds. A complete description of the field testing, as well as all stress measurements for the Coleto Creek Bridge, can be found in Appendix D.

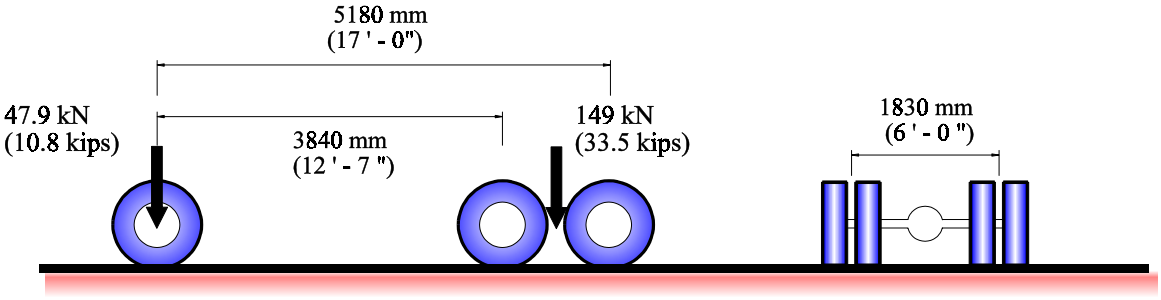

Figure 5-5: Test truck axial weight and configuration, Coleto Creek Bridge.

A typical set of stress measurements for the Coleto Creek Bridge is shown in Table 5-2. These data are for Gage Group 1 with the test vehicle stopped directly above the gage group location in four different lateral roadway positions. Figure 5-6 shows the test vehicle position for Truck Position 2 where the center of the right rear wheel group is 1.17 m (3.83 ft) from the curb toe. For Truck Position 1, this distance is 0.56 m (1.83 ft), 1.78 m (5.83 ft) for Truck Position 3, and 2.39 m (7.83 ft) for Truck Position 4.

Table 5-2: Static load stress values for Gage Group 2.

Truck Position	Gage Number and maximum measured static stress (MPa (ksi))							
	1	2	3	4	5	6	7	8
1	-1.32	-4.71	2.55	0.24	3.89	4.89	-2.59	-6.19
	-0.19	-0.68	0.37	0.03	0.56	0.71	-0.38	-0.90
2	-7.79	0.27	8.67	2.40	19.32	8.42	-8.02	2.67
	-1.13	-0.04	1.26	0.35	2.80	1.22	-1.16	0.39
3	-12.79	-4.30	12.29	3.44	30.65	8.36	-13.78	11.10
	-1.86	-0.62	1.78	0.50	4.45	1.21	-2.00	1.61
4	-12.13	12.72	10.97	2.72	33.39	3.86	-15.53	19.98
	-1.76	-1.85	-1.59	0.39	4.85	0.56	-2.25	2.90

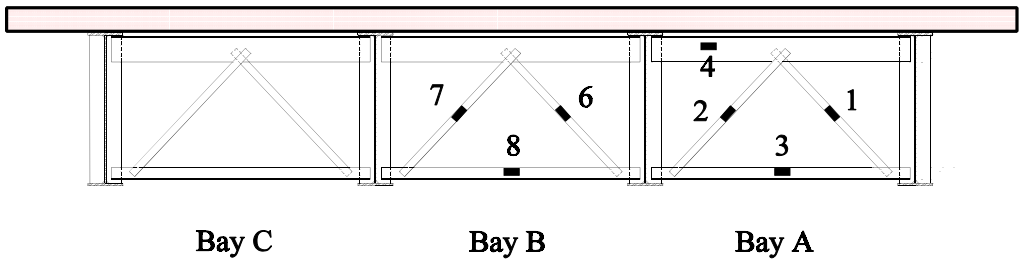

Figure 5-6: Gage Group No. 2, Type A diaphragm members (positive moment region).

The stress histories for Gage Group 2 with the test vehicle traversing the structure at 80 km/hr (50 mph) and centered in the passing lane is shown in Fig. 5-7. Table 5-3 provides the maximum recorded stress range for each of the eight gages in the group. Note that the maximum stress occurs in the bottom strut of the Bay A diaphragm.

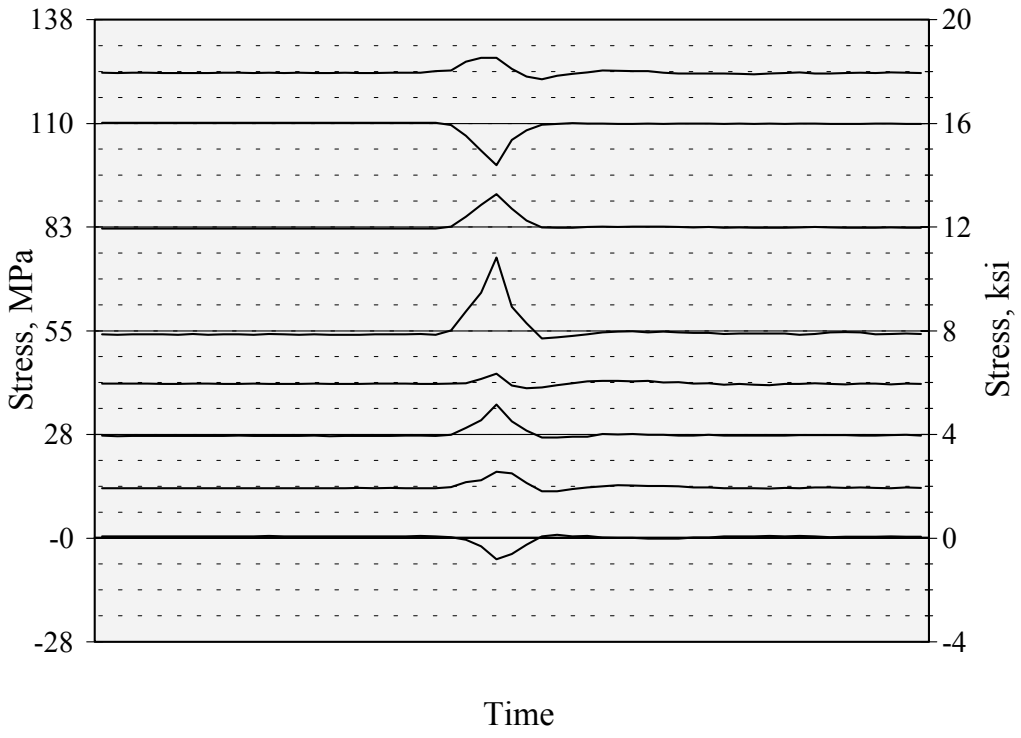

Figure 5-7: Stress histories for Gage Group 2, Truck Pass 2.

Table 5-3: Maximum measured stress ranges and direction for Gage Group 2, Truck Pass 2 (test truck centered in passing lane).

Number	Location	Max. Stress Range, MPa	Max. Stress Range, ksi
1	Bottom flange, Girder No. 1	7.9 (C)	1.0 (T)
2	Bottom flange, Girder No. 2	5.5 (T)	0.8 (C)
3	Bottom flange, Girder No. 3	9.0 (T)	1.3 (T)
4	Bottom flange, Girder No. 4	4.1 (T)	0.6 (T)
5	Bottom flange, Girder No. 5	21 (T)	3.1 (T)
6	Web, Girder No. 2	9.0 (C)	1.3 (T)
7	Web, Girder No. 3	11 (C)	1.6 (T)
8	Web, Girder No. 4	5.5 (T)	0.8 (C)

6. ANALYTICAL STUDY OF DIAPHRAGM BEHAVIOR

6.1 Objective and Scope

From previous research on various slab-girder bridges (Chapter Two), it can be seen that no conclusive results have been obtained for the use of diaphragms in concrete slab-on-steel girder bridges. Most studies which have considered diaphragms have done so in development of a load distribution factor formula based upon common parameters that describe the geometry of a highway bridge. These formulas have assumed diaphragms to be present in the bridge models used in their development, at the standard 7.62 m (25 ft) spacing required by the AASHTO specifications. However, no explicit parameter describing the diaphragms' effect on lateral load distribution has been included in formulas for load distribution factors, nor has any attempt been made to determine the forces transmitted by the diaphragms through their connections with the main longitudinal girders. This has been absent from the AASHTO design specifications, leaving designers to guess at what these forces may be. Additionally, there is no guarantee that previous studies have been comprehensive in covering all aspects of slab-girder bridges.

The objective of this portion of the study is twofold. First, to determine the contribution diaphragms can make to live load lateral distribution in concrete slab-on-steel girder highway bridges and ultimately to determine the need for diaphragms in this type of bridge. Second, to predict the forces diaphragm members transmit under vehicle live load by rational means so the diaphragms and connections can be properly designed.

The bridges used in this study conform to the following assumptions:

- Simple spans,
- Two design lanes,
- Non-horizontally curved,
- Composite construction,

- Full depth X-brace diaphragms, and
- The slab edges are free from crash barriers or other excess stiffness.

The case with two lanes loaded controls the design of two, three, and most four lane bridges, so the results are applicable to bridges with three and four lanes. This will keep the number of required load cases to a minimum. Orthotropic plate theory will be used to classify bridges in this study. The orthotropic plate theory will ensure that all practical two-lane bridge configurations will be studied by reducing the number of parameters required to describe a highway bridge. Any bridge configuration and cross section which can be realistically idealized as an orthotropic plate will be covered by this study.

Although only simple spans will be studied, it will be applicable to the positive moment regions of continuous span structures with variable stiffness girders, since these behave the same as simple spans with respect to load distribution. Separate results will be given for interior and exterior girders, as necessary.

Both the stiffness and spacing of diaphragms will be investigated separately, with different stiffnesses being investigated at only one spacing, and different spacings being investigated for only one stiffness of diaphragm. This is adequate since the effects of diaphragm stiffness and spacing are linear and can be added together using the principle of superposition if necessary.

The criterion for evaluation of diaphragm contribution will be the change in D values for interior and exterior girders. Finite element modeling will be used to evaluate the effects of including the diaphragms in the bridge models and will also be used for evaluating the live load effect in the line-girder idealization.

The assumptions listed above for diaphragm contribution to lateral distribution are also used for the method developed for diaphragm force prediction. Different load cases are used to evaluate the effect for strength design and fatigue design of the members. A method for

prediction of the forces in diaphragms for the strength and fatigue limit states is given. The same bridges used to determine the diaphragm contribution to live load lateral distribution are used for the diaphragm force prediction. The method developed is applicable to any bridge cross section which can be idealized as an orthotropic plate. However, the transverse moments of very wide bridges are larger than those in the two-lane bridges studied and extrapolation of the results to three and four lane bridges is not recommended. Finite element modeling will be used to predict the forces in the diaphragm members under the vehicle loading.

Since many bridges have skewed geometry, a correction factor to account for any possible increase in diaphragm forces due to skew is developed. Field measurements of forces in diaphragms of actual concrete slab-on-steel girder highway bridges will be used to verify the accuracy of the method developed for predicting the diaphragm member forces. These measurements are obtained from continuous span bridges with variable stiffness longitudinal girders. Although these parameters are not explicitly investigated, the method developed is applicable to bridges of this type, as the comparisons between field data and predicted data show.

6.2 Orthotropic Plate Theory for Highway Bridges

Highway bridges have often been idealized as orthotropic plates. Orthotropic plates are defined as having different material properties along two perpendicular axes. A concrete slab-on-steel girder bridge has a longitudinal stiffness based primarily on the stiffness of the longitudinal girders, and a transverse stiffness based primarily upon the concrete deck stiffness. For this reason, orthotropic plate theory reasonably approximates the behavior of concrete slab-on-steel girder highway bridges, provided that certain assumptions are met. The assumptions necessary for idealizing a highway bridge as an orthotropic plate are as follows:

- The width is constant.
- There is a uniform transverse distribution of longitudinal stiffness, satisfied by four or more longitudinal girders per cross section.
- The longitudinal stiffness has no transverse variation.

Bakht and Jaeger (1985) have characterized the behavior of orthotropic plates in terms of two parameters, α and θ. Orthotropic plates with identical α and θ values will have the same patterns of load distribution for similar load configuration. The parameter α can be thought of as a measure of the ratio of representative torsional rigidity to representative flexural rigidity. The parameter θ can be regarded as a measure of the ratio of deflection stiffness due to flexure in the longitudinal and transverse directions.

Bakht and Jaeger (1985) have shown that by classifying bridges idealized as orthotropic plates by their α values, bridges of similar construction fall within specific ranges. The effect of planform ratio of a bridge idealized as an orthotropic plate is reflected in the θ value of the plate. Figure 6 shows the α - θ space and how the α and θ values vary with the effects of bridge type and planform ratio.

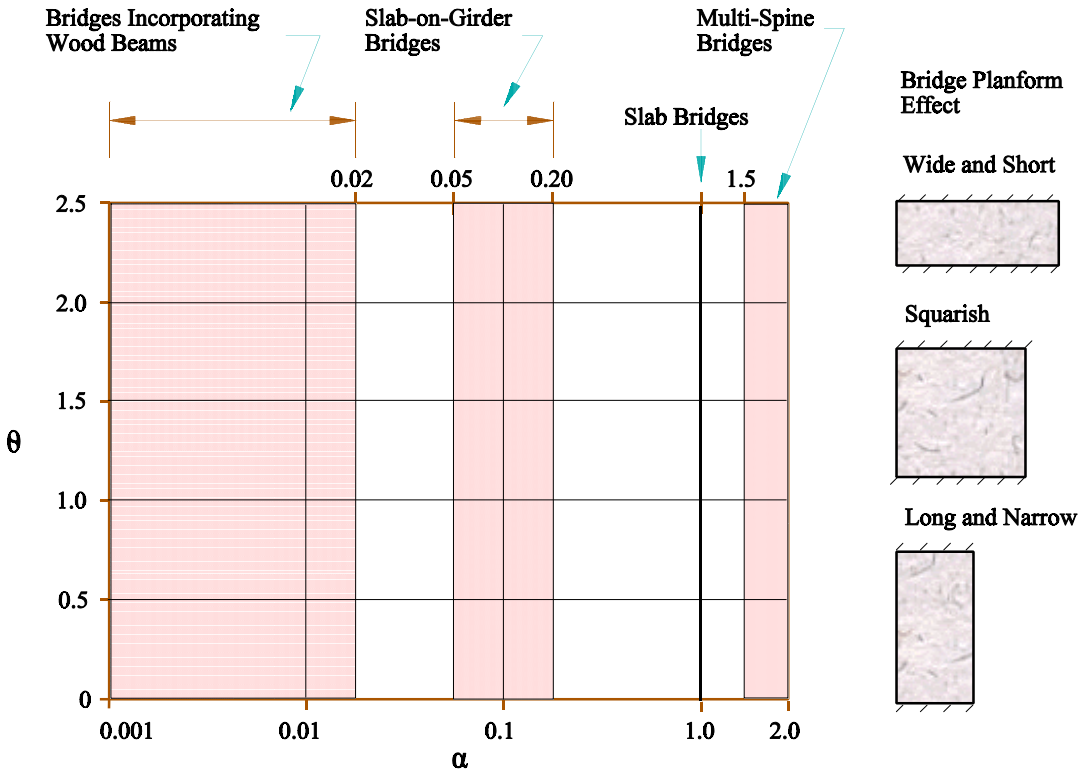

Figure 6-1: Space for α - θ (Bakht and Jaeger 1985).

6.3 Calculation of α and θ

The parameters α and θ are derived from orthotropic plate theory and are given in Eqs. (6-1) and (6-2). The subscripts x and y refer to the longitudinal and transverse directions, respectively.

$$\alpha = \frac{D_{xy} + D_{yx} + D_1 + D_2}{2(D_x D_y)^{0.5}} \tag{6-1}$$

$$\theta = \frac{b}{L}\left(\frac{D_x}{D_y}\right)^{0.25} \tag{6-2}$$

The variables in Eqs. (6-1) and (6-2) are defined as follows:

D_x	=	longitudinal flexural rigidity per unit width
D_y	=	transverse flexural rigidity per unit length
D_{xy}	=	longitudinal torsional rigidity per unit width
D_{yx}	=	transverse torsional rigidity per unit length
D_1	=	longitudinal coupling rigidity per unit width
D_2	=	transverse coupling rigidity per unit length
b	=	one half of the bridge width, mm (ft)
L	=	span length of bridge, mm (ft)

Bakht and Jaeger (1985) show that calculation of these plate rigidities is based upon properties of the bridge, as given by Eqs. (6-3) through (6-8).

$$D_x = \frac{E_s I_g}{S} \tag{6-3}$$

$$D_y = \frac{E_c t^3}{12} \tag{6-4}$$

$$D_{xy} = \frac{G_c t^3}{6} \tag{6-5}$$

$$D_{yx} = \frac{G_c t^3}{6} \tag{6-6}$$

$$D_1 = \nu_c D_y \tag{6-7}$$

$$D_2 = \nu_c D_y \tag{6-8}$$

In these equations, the subscript g refers to the girder and c refers to the concrete deck. The term I_g refers to the composite moment of inertia of the steel girder and its associated width of the deck slab, taken equal to the girder spacing. It has been shown in most practical cases that the reduction of the flexural rigidity of a T-beam due to shear lag effects is negligible so far as load distribution is concerned (Bakht and Jaeger 1982). It is, therefore, sufficiently accurate to ignore the shear lag and use the full slab width. The longitudinal torsional rigidity does not include a

term for the contribution of the steel girder to this rigidity, since the torsional inertia of a steel I-girder section is small. Additionally, these equations are for composite construction only.

Variable stiffness girders can be evaluated for α and θ by using an average stiffness value for the girder since only D_x is affected by the longitudinal variation of stiffness. Each span of continuous span bridges can be evaluated for α and θ by using the span length between the interior supports. Orthotropic plate theory does not include any contribution of the diaphragms to the stiffness of the structure, so they are not included in the calculation of α and θ. A separate parameter will be developed to account for diaphragms.

6.4 Application of Orthotropic Plate Theory

Bakht and Moses (1988) used the α - θ space to establish realistic limits of bridge geometry and planform ratio for slab-on-girder bridges. In their study they establish 0.05 to 0.20 as a realistic range for α, and 0.50 to 2.0 as a realistic range for θ in slab-on-girder highway bridges. These ranges are shown on the α - θ space in Fig. 6-2. Concrete slab-on-concrete girder bridges can have α values of up to 0.20 since the longitudinal torsional inertia of the girders is significant. However, for concrete slab-on-steel girder bridges, it is recommended that the limits for α in this study be narrowed to a maximum value of 0.17. Since the value of α for a concrete slab-on-steel girder bridge depends heavily on the slab thickness, it would be unrealistic to obtain values of up to 0.20. This would require bridges with slab thicknesses of 305 mm (12 in) or more, even with moderate girder spacings.

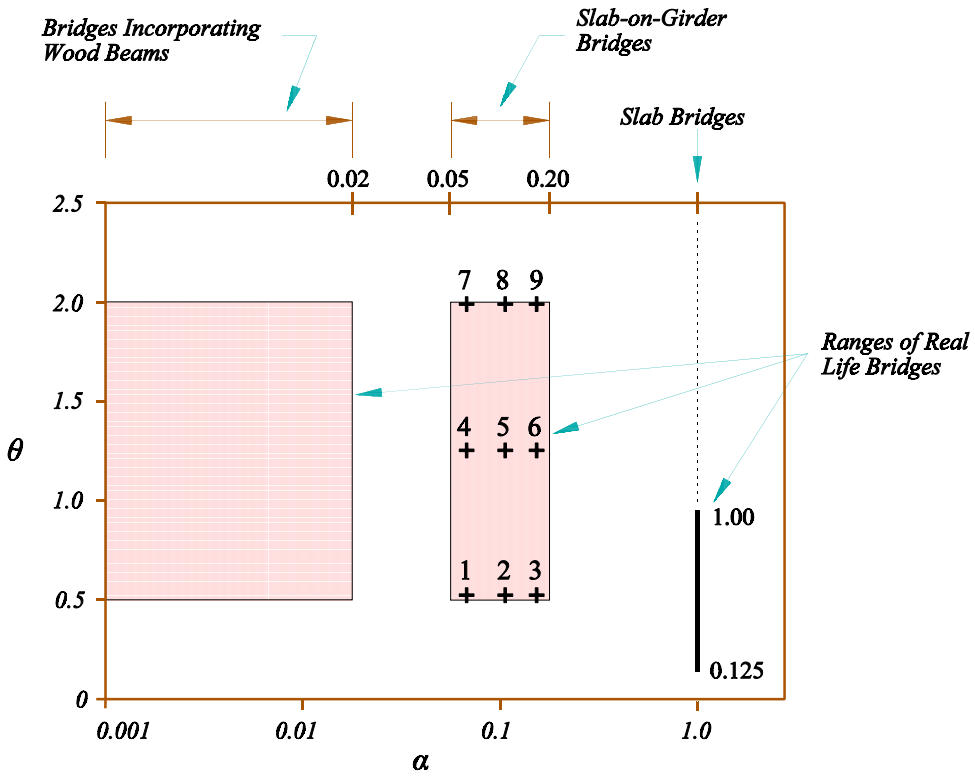

Figure 6-2: Realistic ranges for α - θ space (Bakht and Moses 1988).

The parameter α is essentially a summation of torsional rigidities and since the longitudinal girders of a concrete slab-on-steel girder bridge do not significantly contribute to the overall torsional rigidity, α becomes a function of slab thickness. Bridges with low α values have thin deck slabs and bridges with high α values have thick deck slabs. θ varies primarily with the planform of the bridge, but for two lane bridges, as used in this study, the variation in θ is due mostly to span length. High θ values accompany short span lengths and low θ values accompany long span lengths. Bridges with the combinations of low α/low θ values and high α/high θ values represent the extremes of practical bridge cross sections and occur less frequently than bridges with combinations of high α/low θ or low α/high θ.

Selection of bridges on which to base the current study was accomplished by using the realistic range of the α - θ space with the narrowed limits for α mentioned above. Nine pairs of α and θ values were chosen which covered the entire practical range of the α - θ space and are shown in Fig. 6-2 with a "+" mark in the α - θ space for slab-girder bridges. The number beside each "+" mark corresponds to the bridge number listed in the first column of Table 6-1. Three different cross sections of typical concrete slab-on-steel girder bridges with constant stiffness girders were chosen with α values of 0.06, 0.11, and 0.17, and their span lengths were adjusted to fit the required θ values of 0.53, 1.25, and 2.00. These cross sections are based loosely on standard designs for simple span bridges used by the Texas Department of Transportation. Use of the α - θ space guarantees that a limited number of cross sections adequately covers the range of varying bridge designs used in practice. Table 6-1 lists the girder size, girder spacing, slab thickness, span length, bridge width, and number of girders for each bridge corresponding to a pair of α and θ values. The number given in the first column of Table 6-1 corresponds to the numbers shown in the α - θ space of Fig. 6-2 and show where each bridge configuration plots in the practical ranges for α and θ. The "P.G." in the girder size column refers to a plate girder section consisting of a 10 mm x 1220 mm (3/8 in x 48 in) web with 25 mm x 305 mm (1 in x 12 in) wide flanges. Although only one plate girder section is used in the study, deeper sections with variable stiffness are still covered by the study as long as the bridge can be realistically idealized as an orthotropic plate whose α and θ values fall within the limits used in this study. The finite element method will be used to conduct the study on the nine bridges to determine the diaphragm contribution to lateral load distribution and to predict the diaphragm member forces. Use of the α - θ space will ensure that the realistic spectrum of concrete slab-on-steel girder highway bridges is studied.

Table 6-1: Bridge configurations used in study.

No.	α	θ	Girder Size	Girder Spacing mm (in)	Slab Thickness mm (in)	Span Length mm (ft)	Bridge Width mm (ft)	No. of Girders
1	0.06	0.53	W920x238 (W36x160)	1220 (48)	127 (5)	34 140 (112)	8530 (28)	7
2	0.11	0.53	P.G.	2430 (96)	203 (8)	29 260 (96)	9750 (32)	4
3	0.17	0.53	W920x238 (W36x160)	1830 (72)	254 (10)	21 940 (72)	9140 (30)	5
4	0.06	1.25	W920x238 (W36x160)	1220 (48)	127 (5)	14 330 (47)	8530 (28)	7
5	0.11	1.25	P.G.	2430 (96)	203 (8)	12 190 (40)	9750 (32)	4
6	0.17	1.25	W920x238 (W36x160)	1830 (72)	254 (10)	9140 (30)	9140 (30)	5
7	0.06	2.00	W920x238 (W36x160)	1220 (48)	127 (5)	8990 (29.5)	8530 (28)	7
8	0.11	2.00	P.G.	2430 (96)	203 (8)	7620 (25)	9750 (32)	4
9	0.17	2.00	W920x238 (W36x160)	1830 (72)	254 (10)	5715 (18.75)	9140 (30)	5

6.5 Determination of *D* Values

The *D* value provides a measure of the load distribution characteristics of a bridge. For a given girder spacing, the higher the *D* value the more evenly loads are distributed between adjacent girders. The *D* value can be determined by rearranging Eq. (6-1) as follows:

$$D = \frac{S}{D.F.} \tag{6-9}$$

It should be recalled that D has units of length.

In the design of a slab on steel girder highway bridge a single beam is analyzed using classical beam theory for the maximum response produced by a single line of wheels of the design vehicle. This is referred to as a line-girder analysis. Since the girders of highway bridges are always slender, meaning the span to girder depth ratio is greater than 10, longitudinal moment controls the design. The results from the line-girder analysis give the maximum moment in a girder due to the loading of a single line of wheels.

The distribution factor is a scalar multiplier which takes into account the increase or decrease in longitudinal moment that a single girder must carry. This local increase or decrease arises from the transverse positioning of multiple lines of wheels on a bridge under actual loading. The distribution factor will have a value less than one for small girder spacings. The results from the line girder analysis are multiplied by the distribution factor to account for the effects of lateral distribution of the live load. Since only linear structural analysis is used, the single line of wheel loads could also be multiplied by the distribution factor before the line girder analysis is done. This gives the same results.

In the current study, detailed finite element analysis will be used for determining the maximum response in the girders of the nine multi-girder bridges used for this study. However, since stresses are more easily calculated from the finite element output, bottom flange stresses will be used instead to determine the maximum response in the beams of a multi-beam bridge. It is analogous to using stresses since linear elastic solutions are assumed, but no processing of the stress distribution across a critical section is required (Bishara et al. 1993). The distribution factor is therefore defined as follows:

$$D.F. = \frac{\text{Max. bottom flange stress in a girder under all load conditions}}{\text{Max. bottom flange stress obtained from line girder analysis}} \quad (6\text{-}10)$$

The maximum bottom flange stress under all load conditions refers to the envelope stress value obtained from the various transverse positionings of the live load vehicles. Since only simple-span bridges are being used for this study, the critical section, or place where the maximum stresses occur, will always be at midspan. *D.F.*s, and consequently *D* values, will be calculated for each girder of each bridge at midspan only. As previously explained, the results obtained for the simple spans used in this study will be applicable to the positive moment regions of continuous span bridges.

6.6 Finite Element Method

Many different discretization schemes have been used to model highway bridges using the finite element method. For the current study, solid elements are used to model the concrete decks, shell elements are used to model the girder webs, space frame elements are used to model the girder flanges, and space truss elements are used for all diaphragm cross-bracing members. Figure 6-3 provides an exploded view of a small portion of a highway bridge modeled in this fashion. The elements are reduced in size to provide clarity and show the girder flanges modeled with space frame elements. Longitudinal bending of the girder flange members about their own neutral axes is not included. The material properties used in all finite element models are as follows: E_c = 21,500 MPa (3122 ksi), ν_c = 0.2, E_s = 200,000 MPa (29,000 ksi), ν_s = 0.3.

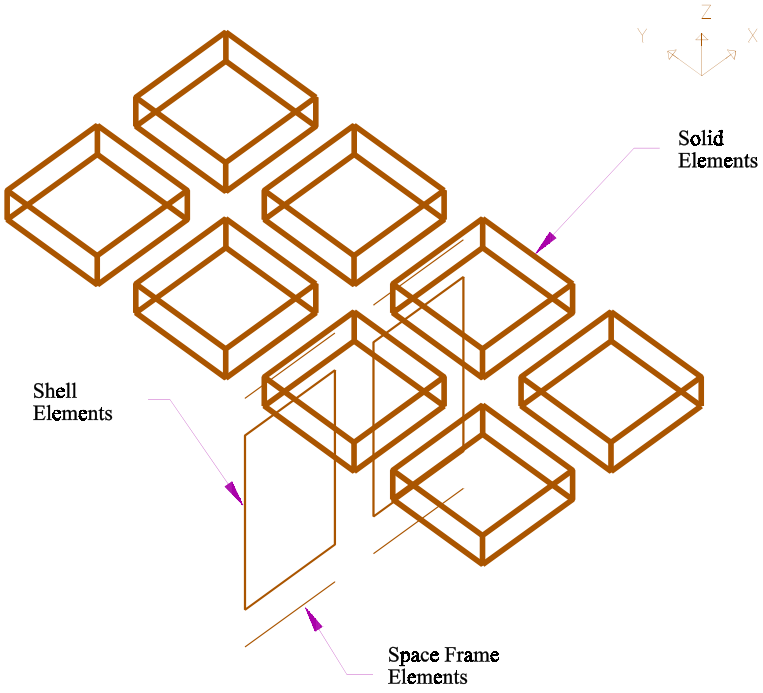

Figure 6-3: Finite element discretization scheme.

The finite element method is used to determine the maximum bottom flange stresses in all bridge superstructures studied and in their counterpart line girders. Since it is an approximate technique, some errors are inherent in the computation of the maximum bottom flange stresses. Finite discretization of a continuum and roundoff are two sources of error. Bathe (1982) contains a complete discussion of all possible errors in a finite element analysis. The line-girder analysis can be performed in closed form solution, but a correction for the distribution factors is necessary. Since the bottom flange stresses in the bridge superstructure would contain the errors described above and the line girder stresses would not. Tarhini and Frederick (1992) performed their analysis in this manner and used an 8 percent correction in determining their distribution

factors. However, since the line girder bottom flange stresses are evaluated with the finite element method, errors in the computation of the distribution factors cancel each other. Identical longitudinal mesh densities and discretization schemes are used for each bridge and associated line girder. The line girder contains additional boundary conditions for the free edges of its portion of the slab. The deck nodes at any cross section of a line girder are constrained to the same vertical deflection as the top of the flange, which prevents any transverse curvature of the slab. Using finite element solutions for both the bridge superstructures and line girders ensures that any errors inherent in the approximate solutions obtained from finite element analysis cancel in determining the distribution factors. Figure 6-4 shows the finite element mesh of a 12.2 m (40 ft) long, simply supported bridge. Figure 6-5 shows the finite element mesh for the line girder model of the same bridge.

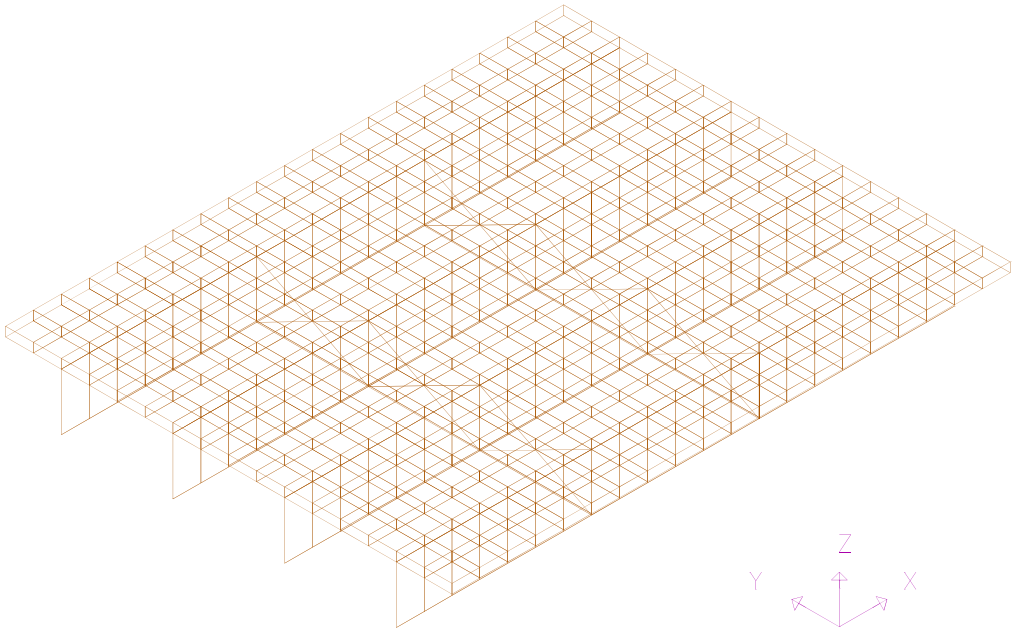

Figure 6-4: Typical finite element mesh for slab-on-girder highway bridge.

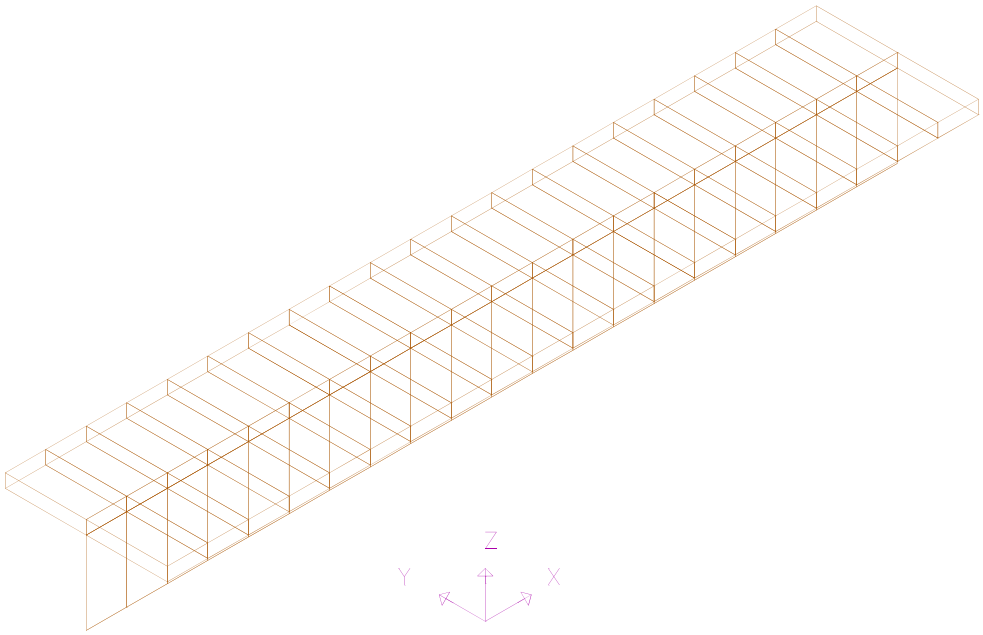

Figure 6-5: Typical finite element mesh for line girder analysis.

The finite element method is also used to determine the forces in the diaphragm cross-frame members under the vehicle loading. Since relatively dense meshes are used to model the bridges, reasonable approximations of these forces can be obtained.

6.6.1 Vehicle Live Loading

The design loading for all bridges will consist of either the AASHTO HS-20 truck or alternate military loading, depending upon which loading gives the maximum response for a particular bridge. Figure 6-6 shows the HS-20 truck load and Fig. 6-7 depicts the design tandem, sometimes referred to as the alternate military load. The design tandem will control for span lengths less than 17.1 m (56 ft), and the truck will control for span lengths between 17.1 m (56 ft) and 42.7 m (140 ft). The AASHTO lane loading, which consists of a longitudinally uniform

distributed load, will not be used in the study. This load controls the design for bridges with span lengths exceeding 42.7 m (140 ft).

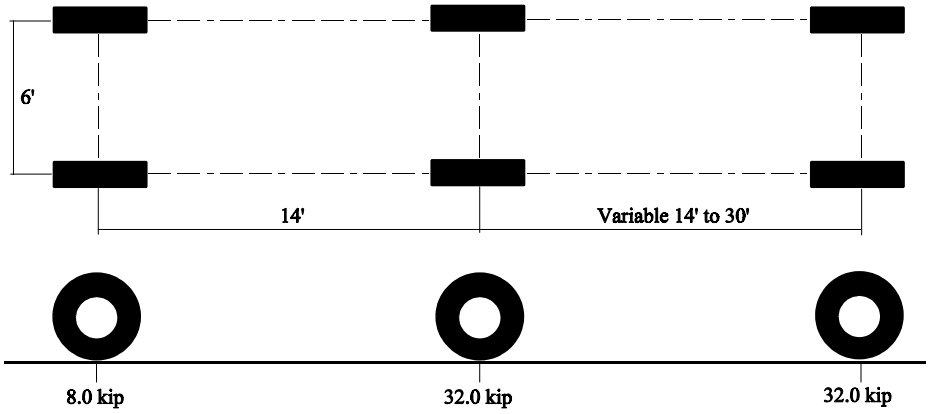

Figure 6-6: AASHTO HS-20 truck axle weights and configuration.

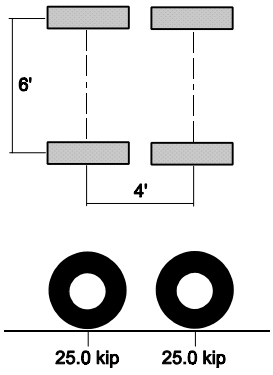

Figure 6-7: AASHTO design tandem axle weights and configuration.

The transverse positioning of the design loads in each lane is varied in order to determine the maximum effect in any single bridge girder. A distance of 1.22 m (4 ft) is used as the minimum distance between multiple vehicles positioned side by side on a bridge. Figure 6-8 shows one such transverse arrangement of the design loading with two vehicles on the bridge. These loads are applied to the finite element bridge models as concentrated nodal loads, located longitudinally so as to produce the maximum stresses in the bottom flanges of the bridge girders. The solid element deck of the finite element models will attenuate these concentrated loads, producing results which are realistic and which resemble the actual tire contact areas of real vehicles.

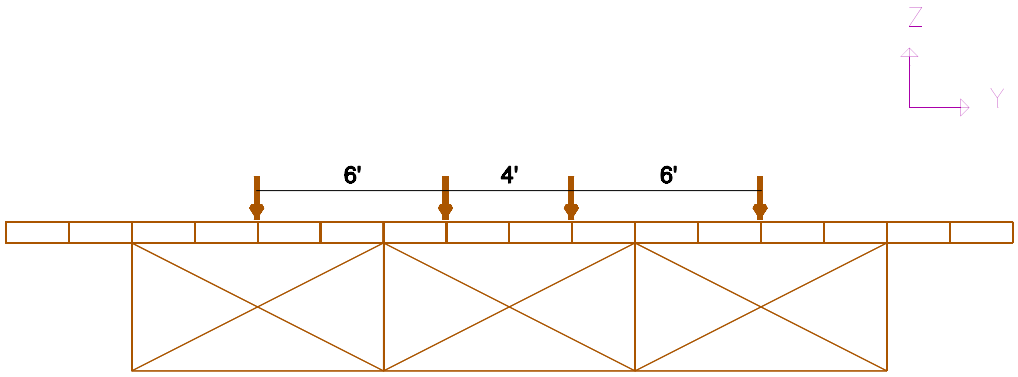

Figure 6-8: Transverse positioning of multiple vehicles.

The positioning of the vehicle wheels near the edge of a bridge can greatly affect the results obtained for an exterior girder. Figure 6-9 shows the relationship between the vehicle-edge distance and the vehicle-girder distance. Bakht and Jaeger (1985) have developed methods for correcting an increased vehicle-edge distance, which allows a reduction in the required strength of an exterior girder. However, the AASHTO specifications do not allow for any reduction in the required strength of an exterior girder. In this study the vehicle-girder distance is zero. For all bridges studied, the overhang is equal to one-half of the girder spacing, which varies from the vehicle-edge distance somewhat. However, since only three different girder spacings are being used in the current study, 1.22 m (4 ft), 1.83 m (6 ft), and 2.44 (8 ft), the

vehicle-edge distance only varies between 7 and 12.5 percent of the bridge width. This produces realistic results with respect to exterior girders.

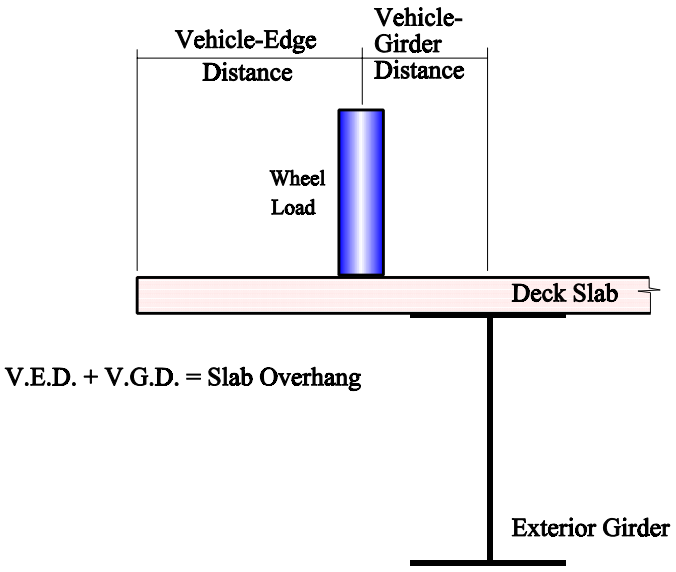

Figure 6-9: Vehicle-edge distance of live load.

The line girder analysis is performed in much the same way, with only one line of wheels or half-axle loads being applied directly above the longitudinal girder. The longitudinal position for each line of wheels is identical to the longitudinal position used for the corresponding bridge model, such that the maximum effect in the line-girder is attained.

6.6.2 Diaphragm Truss Model

The only type of diaphragm used in the finite element models is the full-depth X-brace with equal cross sectional areas for the diagonals and lower strut as shown in Fig. 6-10. This particular diaphragm design is typical of those used by the Texas Department of Transportation and other transportation authorities around the country when stay-in-place deck forms are used. In all finite element models it is assumed that the diaphragm members carry only axial loads. A cross frame diaphragm essentially behaves like a panel of a truss bridge. The lower strut is

similar to a chord member which, when coupled with the slab, forms a stiff member capable of carrying moment. The diagonals carry the shear force analogous to the web of an I-beam carrying shear.

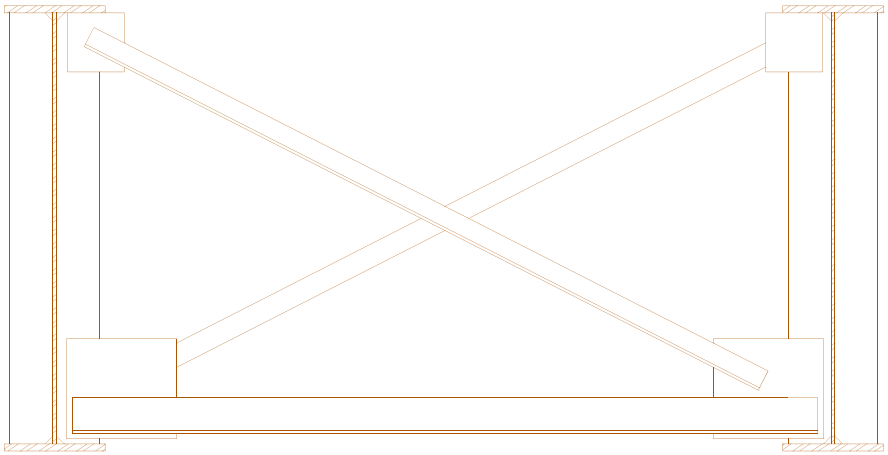

Figure 6-10: Typical full depth X-brace diaphragm.

Since the diaphragm is a deep member, its shear stiffness is of importance. A method for classifying this shear stiffness consisted of evaluating the vertical deflection of one side of the diaphragm relative to the other under a point load, as shown in Fig. 6-11. This was accomplished with the finite element method, using boundary conditions as shown in Fig. 6-11. All members were assumed to carry only axial loads. The shear stiffness of the diaphragm is defined, as in Eq. (6-11), as the load divided by this deflection.

$$Diaphragm\ \ Stiffness\ \ ' \ \frac{P}{\Delta} \tag{6-11}$$

Table 6-2 gives the cross sectional area of the diaphragm members used in each bridge model to obtain the stiffnesses, as defined above, of 43.8 kN/mm, 122 kN/mm, and 219 kN/mm (250 k/in, 700 k/in, and 1250 k/in).

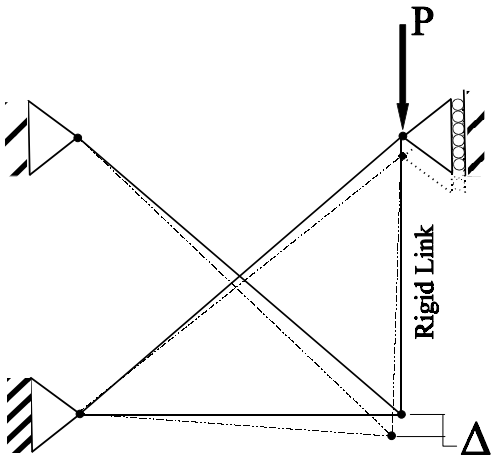

Figure 6-11: Characterization of diaphragm stiffness.

Table 6-2: Cross sectional areas of diaphragm members, mm^2 (in^2).

	Diaphragm Stiffness, kN/mm (k/in)		
α	43.8 kN/mm (250 k/in)	122 kN/mm (700 k/in)	219 kN/mm (1250 k/in)
0.06	465 (0.72)	1290 (2.00)	2323 (3.60)
0.11	1484 (2.30)	4194 (6.50)	7419 (11.50)
0.17	1110 (1.72)	3135 (4.86)	5613 (8.70)

In addition to the full depth X-brace, another common diaphragm cross-frame arrangement is the inverted K-brace as seen in Fig. 6-12. Although this type of diaphragm is not included in any of the finite element models of bridge superstructures, its stiffness is evaluated relative to that of the full depth X-brace using the same procedure explained above for the X-brace. Table 6-3 gives the relative stiffness of the K-brace to that of the X-brace for members with the same cross sectional areas. It can be seen that the X-brace is approximately twice as

stiff as the K-brace. Its load distribution behavior will be the same as an X-brace with the same shear stiffness.

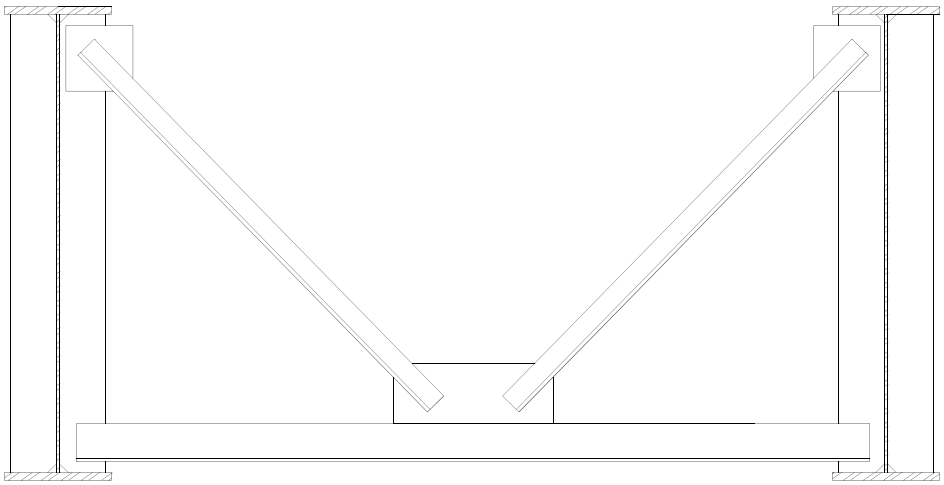

Figure 6-12: Typical K-brace cross frame

Table 6-3: Relative stiffness of K-brace to X-brace.

α	Cross-Section Area, mm^2 (in^2)	Relative Stiffness
0.06	465 (0.72)	0.50
	1290 (2.00)	0.50
	2323 (3.60)	0.50
0.11	1484 (2.30)	0.58
	4194 (6.50)	0.58
	7419 (11.50)	0.58
0.17	1110 (1.72)	0.58
	3135 (4.86)	0.58
	5613 (8.70)	0.58

It is also common for the X-brace and K-brace to have a top strut which serves as a gusset plate for attachment of the diagonals and also, in the days before stay-in-place forms, as a

support for the formwork for the concrete deck. It has been shown through field testing that the top strut carries no load and serves no purpose so far as the stiffness of the diaphragm is concerned once the slab has been cast (Keating and Crozier 1992).

6.6.3 Diaphragm-deck Stiffness Ratio

A second method for classifying diaphragm behavior recognizes that the diaphragms and slab form an indeterminant system which transversely distributes the vehicle live load. If diaphragms are not present in the bridge, the slab distributes the load in transverse flexure. When diaphragms are present, a truss system is formed with the slab acting as one chord and the diaphragm lower strut acting as the other chord. The mechanism of transverse distribution changes when the diaphragms are present, with transverse shear being the predominant mode of load transfer from one girder to the next. However, the distribution of axial forces through the diaphragm cross-frame members is similar to that obtained for a truss where the top and bottom chords carry large axial forces at the locations of maximum deflection and the diagonals carry large axial forces where the relative deflection of the girders is small. For two trucks positioned near the center of the bridge, the exterior girders deflect the least and the girder(s) near the centerline deflect(s) the most. In this case, the diagonals attached to the exterior girders will carry large axial forces and diagonals near the centerline will carry small forces. Conversely, the lower strut members will have large axial forces occurring under the point of maximum deflection, which for the loading case described is at the centerline of the bridge. This distribution of forces is analogous to the forces in a beam loaded symmetrically near its centerline. The largest moment occurs at midspan of the beam, with large shears generated at the supports.

It is assumed that the transverse moments are carried by the slab and diaphragm in the proportion of each component's stiffness to the sum of the two stiffnesses, as defined in Eq. (6-12). Figure 6-13 shows the terms used in defining the stiffness ratio. Equations (6-12) and (6-13) are used to calculate the stiffnesses of the deck slab and deck slab in combination with diaphragm cross-frames, respectively.

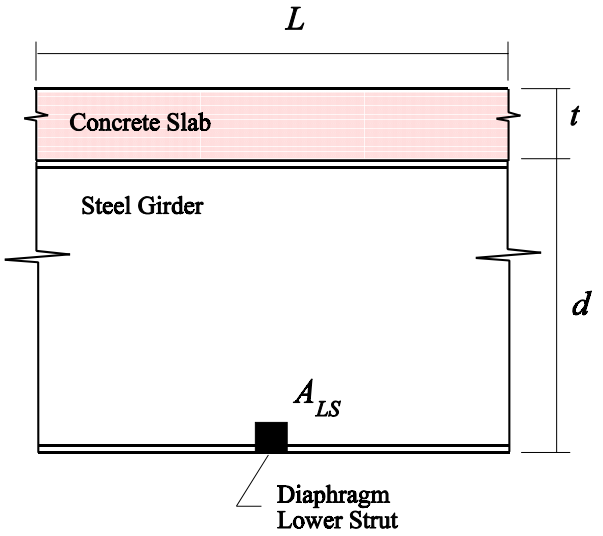

Figure 6-13: Diaphragm-deck stiffness ratio.

$$Stiffness\,Ratio = \frac{K_D}{K_D + K_S} \tag{6-12}$$

$$K_s = Lt^3 E_c \tag{6-13}$$

$$K_D = E_c\left(Lt^3 + A_{LS}\left(\frac{E_s}{E_c}\right)\left(d - \frac{t}{2}\right)^2\right) \tag{6-14}$$

The term K_s is the stiffness of the deck in the transverse direction. The term K_D is the stiffness of the diaphragm, considering the contribution of the diaphragm lower strut and deck, to form a stiff member with high moment of inertia. The calculation of the stiffness ratio is based upon classical structural analysis of indeterminant systems, whereby the load follows the stiffness. The diaphragm-deck stiffness ratio recognizes that using a lower strut with large cross sectional areas will attract more of the load and distribute it transversely.

6.6.4 Skewness

Since many highway bridges are built with skewed geometry, meaning the supports for the girders are not perpendicular to the roadway centerline, it is necessary to classify the skewness of a bridge for later use in predicting the diaphragm forces in such bridges. Figure 6-14 shows a plan view of a skewed bridge, where φ is the skew angle, S is the girder spacing,

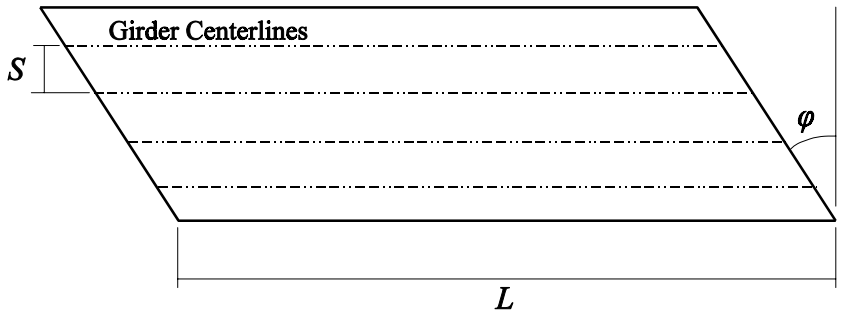

Figure 6-14: Plan view of skewed bridge.

and L is the span length. Jaeger and Bakht (1982) define the skewness as a dimensionless ratio equal to the offset of the critical section between adjacent girders compared to the span length, as defined in Eq. (6-15).

$$Skewness = \frac{S\tan\varphi}{L} \tag{6-15}$$

Keating and Crozier (1992) have shown that the behavior of highly skewed bridges is significantly different from that of non-skewed bridges, particularly the forces in the diaphragms. Since many highway bridges are built with skewed geometry, the method for predicting diaphragm member forces requires a correction for skewness.

The correction factor is developed by determining the forces in one bridge with varying skew angles. The bridge chosen has α and θ values of 0.11 and 0.53, respectively, and the same properties as the non-skewed bridge of the same α and θ used in this study. Skew angles of 30,

45, and 60 degrees are used, giving skewness values of 0.05, 0.08, and 0.14. Only midspan diaphragms, passing through the geometric center of the skewed bridge, are included in the analysis. The loading consists of one design truck with its transverse position fixed over the centerline of the bridge. Predicting these forces with only midspan diaphragms provides an upper-bound value for the diaphragm forces, since additional lines of diaphragms reduce the forces in the diaphragms at midspan.

6.7 Diaphragm Stiffness Effect on Lateral Distribution

Finite element models of the nine bridges chosen to cover the practical range of the α - θ space are evaluated under highway loadings to determine what effect diaphragms have on the D values, and therefore what potential economies might arise from including the diaphragm effects in the design of a concrete slab-on-steel girder bridge. D values are calculated for each girder of each bridge for the diaphragm stiffnesses of 43.8 kN/mm, 122 kN/mm, and 219 kN/mm (250 k/in, 700 k/in, and 1250 k/in). Results are also given for the condition where no diaphragms are included in the structural models of the bridges. Since only simple span bridges are considered, the critical section in analysis and design occurs at midspan, so D values are only calculated at midspan. The D values are shown in Figs. 6-20 through 6-28 in graphical form. Only one half of the results for each bridge are shown, since the bridge is symmetrical about a longitudinal centerline, and results for the other half mirror the results shown. The bridges are referred to by their α and θ values.

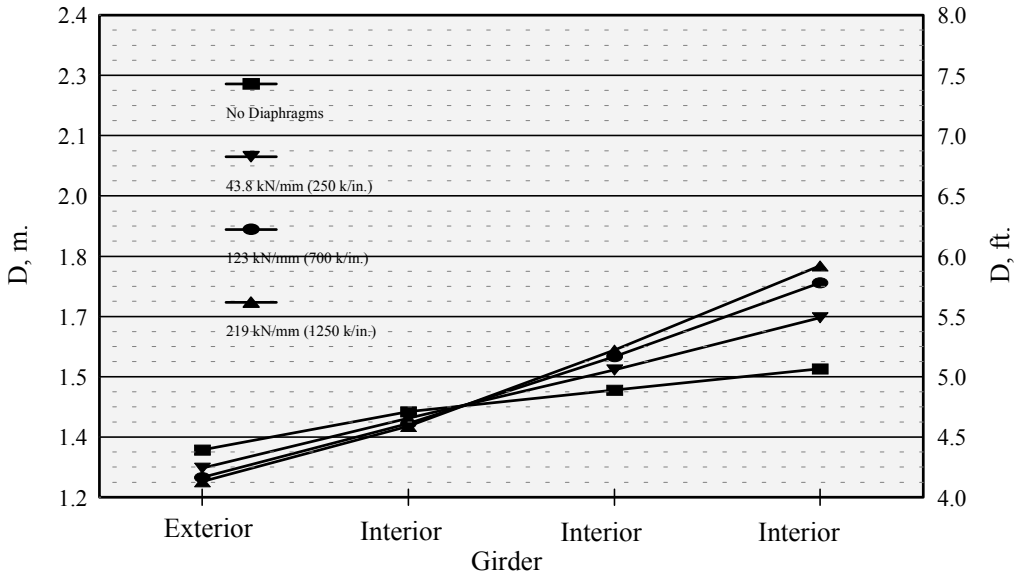

Figure 6-15: Diaphragm stiffness effect for Bridge No. 1 (α =0.06, θ = 0.53).

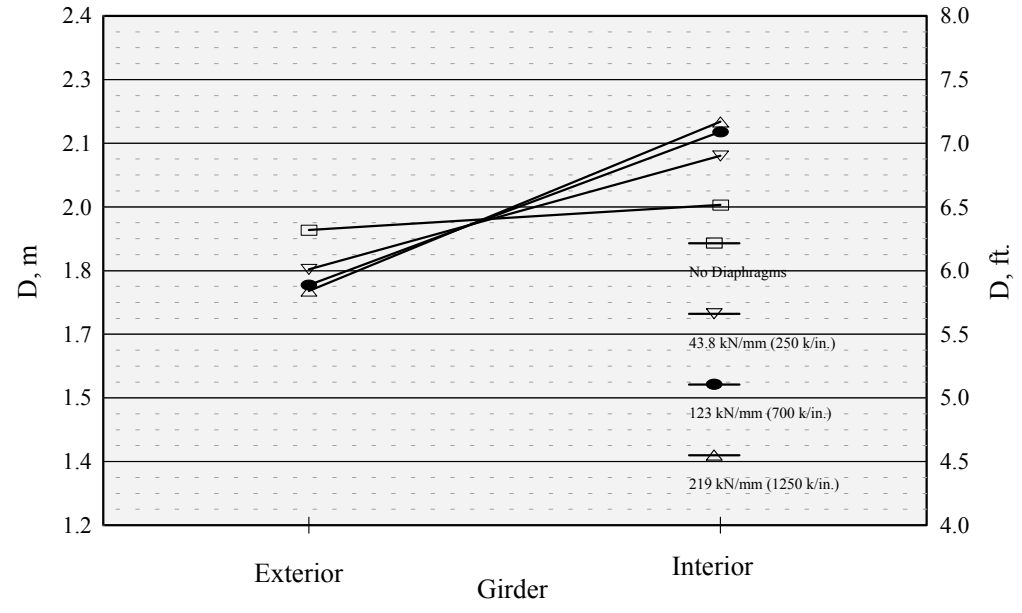

Figure 6-16: Diaphragm stiffness effect for Bridge No. 2 (α =0.11, θ = 0.53).

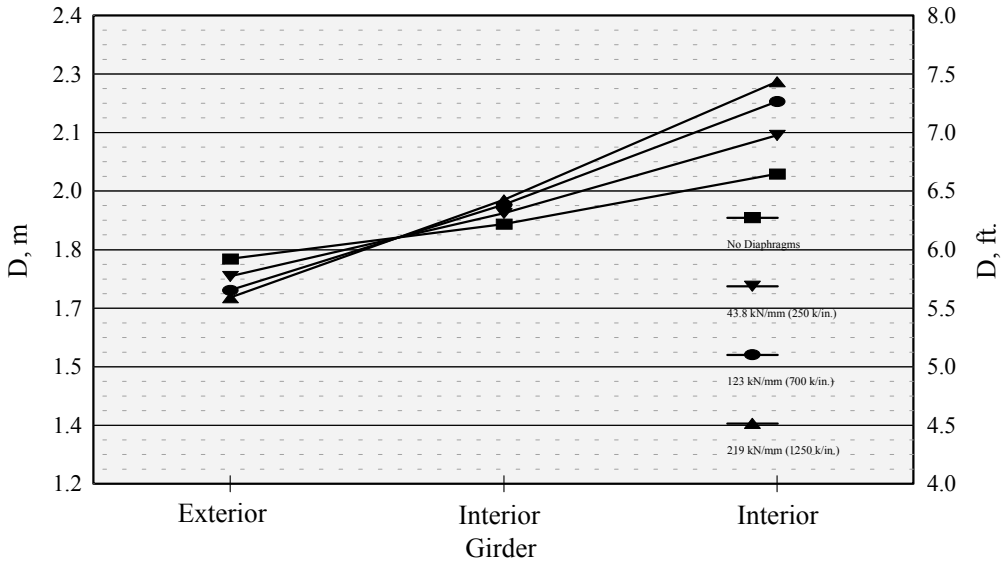

Figure 6-17: Diaphragm stiffness effect for Bridge No. 3 ($\alpha = 0.17$, $\theta = 0.53$).

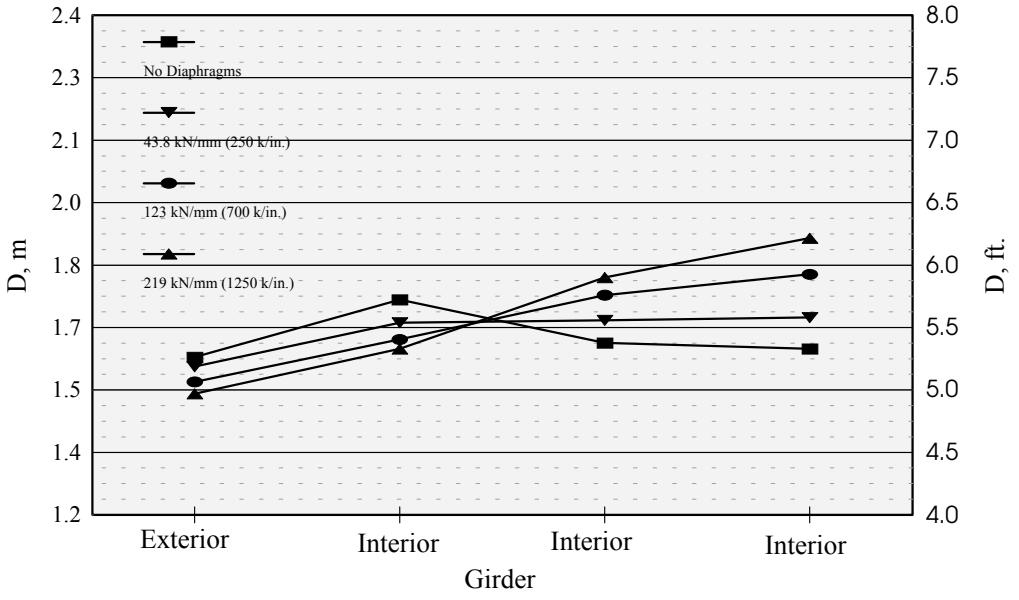

Figure 6-18: Diaphragm stiffness effect for Bridge No. 4 ($\alpha = 0.17$, $\theta = 0.53$).

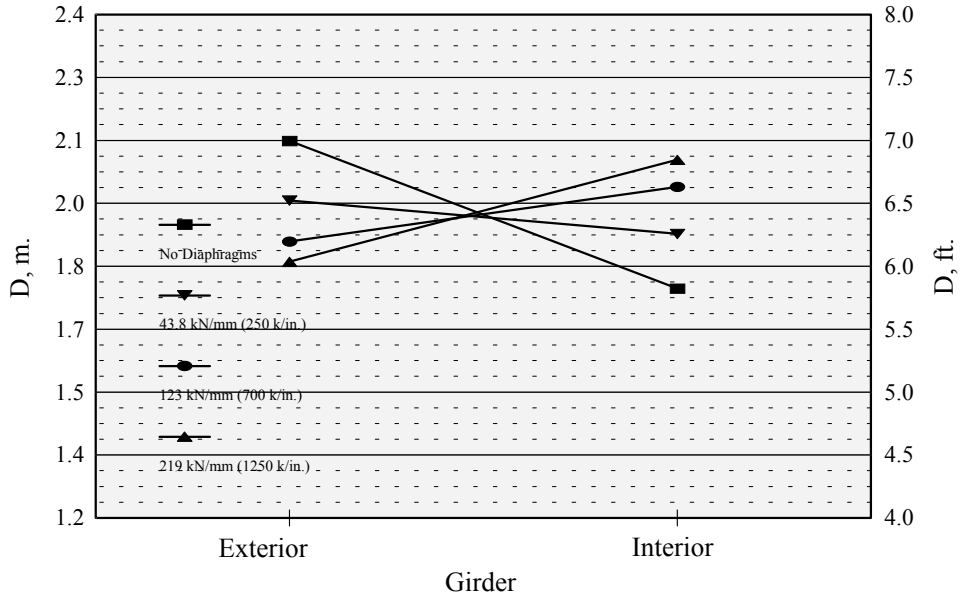

Figure 6-19: Diaphragm stiffness effect for Bridge No. 5 ($\alpha = 0.11$, $\theta = 1.25$).

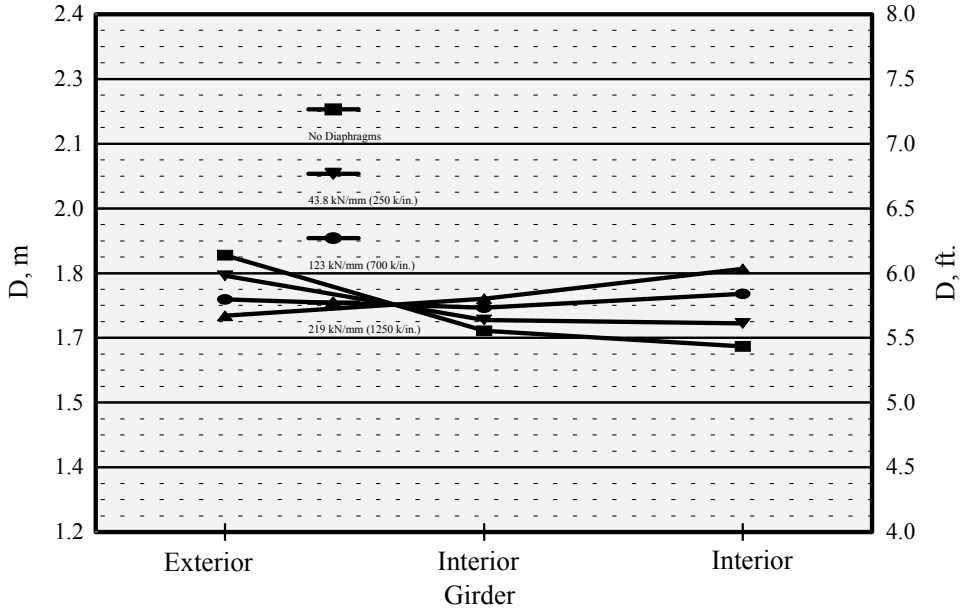

Figure 6-20: Diaphragm stiffness effect for Bridge No. 6 ($\alpha = 0.17$, $\theta = 1.25$).

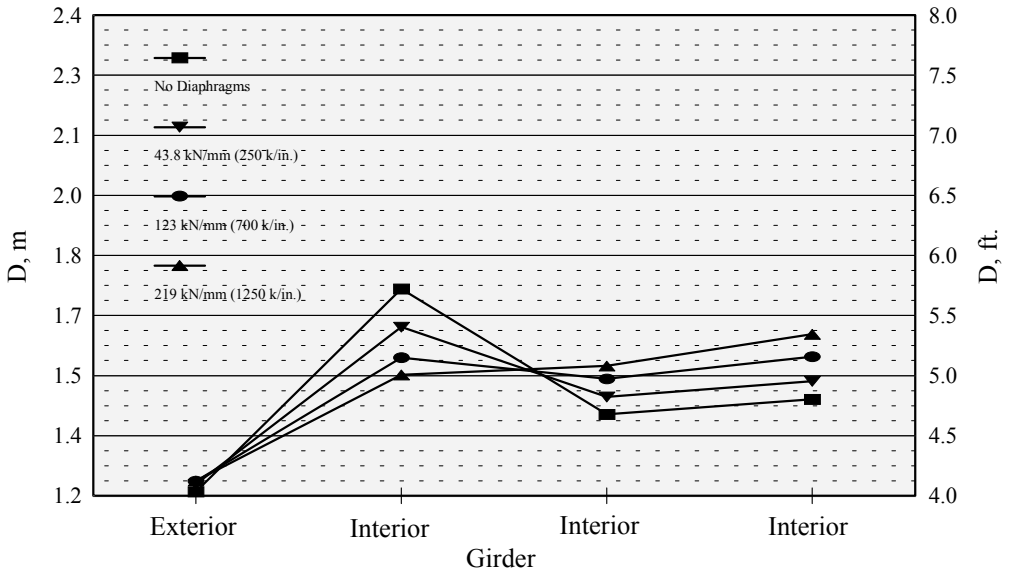

Figure 6-21: Diaphragm stiffness effect for Bridge No. 7 ($\alpha = 0.06$, $\theta = 2.00$).

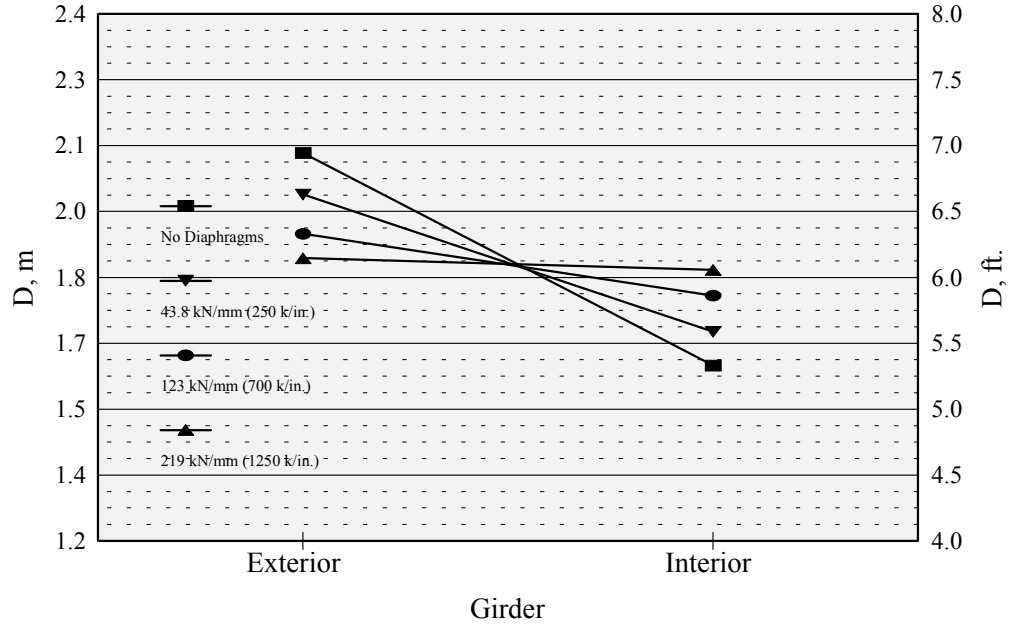

Figure 6-22: Diaphragm stiffness effect for Bridge No. 8 ($\alpha = 0.11$, $\theta = 2.00$).

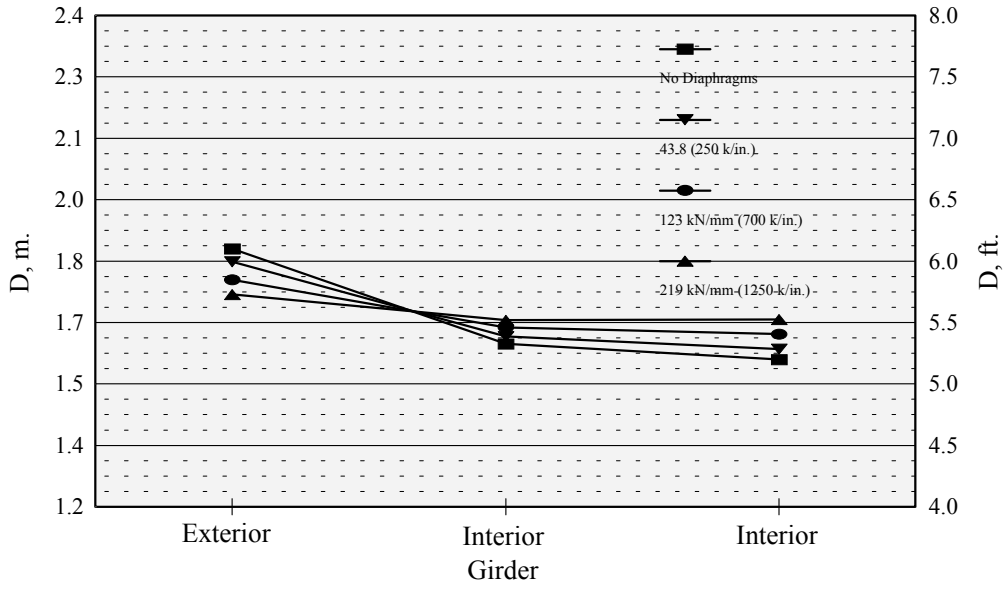

Figure 6-23: Diaphragm stiffness effect for Bridge No. 9 ($\alpha = 0.17$, $\theta = 2.00$).

It can be seen in the figures that a definite trend occurs for interior girders where midspan diaphragms of various stiffnesses have been included. For girders nearest to the longitudinal centerline, *D* increases as the diaphragm stiffness increases. For all other interior girders there is some variation in *D*. This variation seems to correspond with the distance from the girder centerline to the bridge centerline. The nearer the girder is to the bridge centerline, the greater is the increase in the *D* value. An increased *D* value corresponds to an decrease in the design longitudinal moment capacity of the girder. It can be seen that the load distribution in a highway bridge is not a constant, but varies across the width of the bridge. The pattern of this variation appears parabolic, with the interior girders having the greatest *D* values.

The three bridges with θ values of 0.53 exhibited a more uniform transverse distribution of load when no diaphragms were included in the finite element models. When diaphragms are

present, the interior girders have increased D values but the exterior girders have decreased D values. This effect is exaggerated by an increased stiffness of the diaphragm.

For exterior girders, D tends to decrease as the diaphragm stiffness increases, but there are some exceptions. The factor which contributes to this behavior is the vehicle-edge distance, which greatly affects the load distribution pattern for exterior girders. Bakht and Jaeger (1985) developed a correction factor to account for the vehicle-edge distance when determining D values for highway bridges idealized as orthotropic plates. It is reasonable that if an orthotropic plate is affected by the vehicle-edge distance, then the girders of a concrete slab-on-steel girder highway bridge would also be affected by the vehicle-edge distance.

6.8 Diaphragm Spacing Effect on Lateral Distribution

Finite element models of the nine bridges chosen to cover the practical α - θ space are evaluated under highway loadings to determine what effect diaphragms at $L/2$, $L/3$, $L/4$, and $L/8$ spacings, where L is the span length, have upon the D values. The list of span lengths for each bridge can be found in Table 6-1. For all of these runs, a constant diaphragm stiffness of 43.8 kN/mm (250 k/in) is used for each bridge. D values are calculated for each girder of each bridge and results are also given for the condition where no diaphragms are included in the structural models of the bridges. Since only simple span bridges are considered, the critical section in analysis and design occurs at midspan, so D values are only calculated at midspan. The D values for the various bridges are given in Figs. 6-24 through 6-33. Again, it should be noted that the bridges are referred to by their α and θ values.

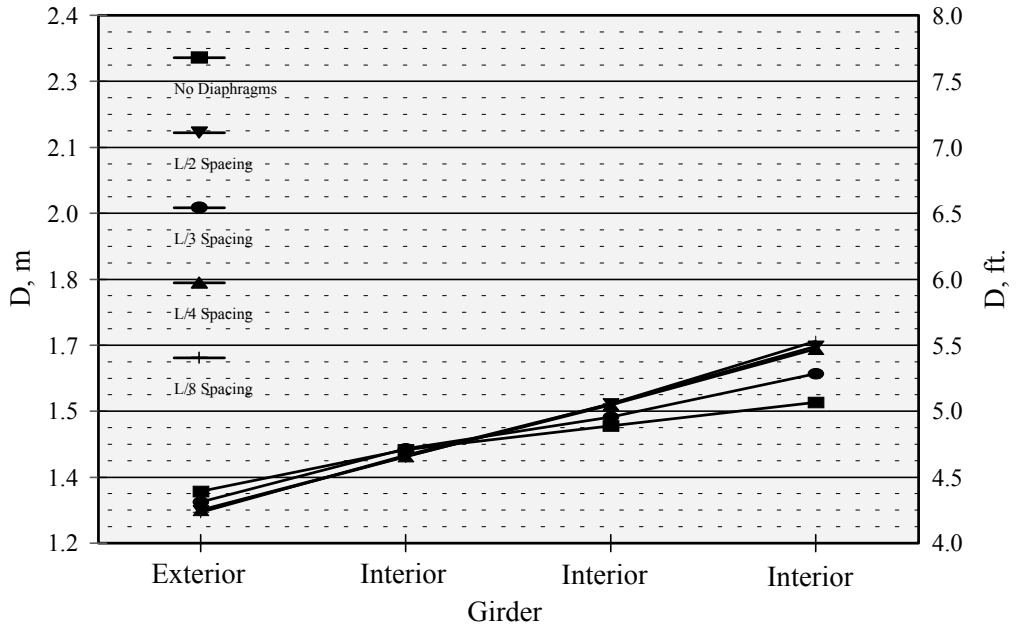

Figure 6-24: Diaphragm spacing effect for Bridge No. 1 ($\alpha = 0.06$, $\theta = 0.53$).

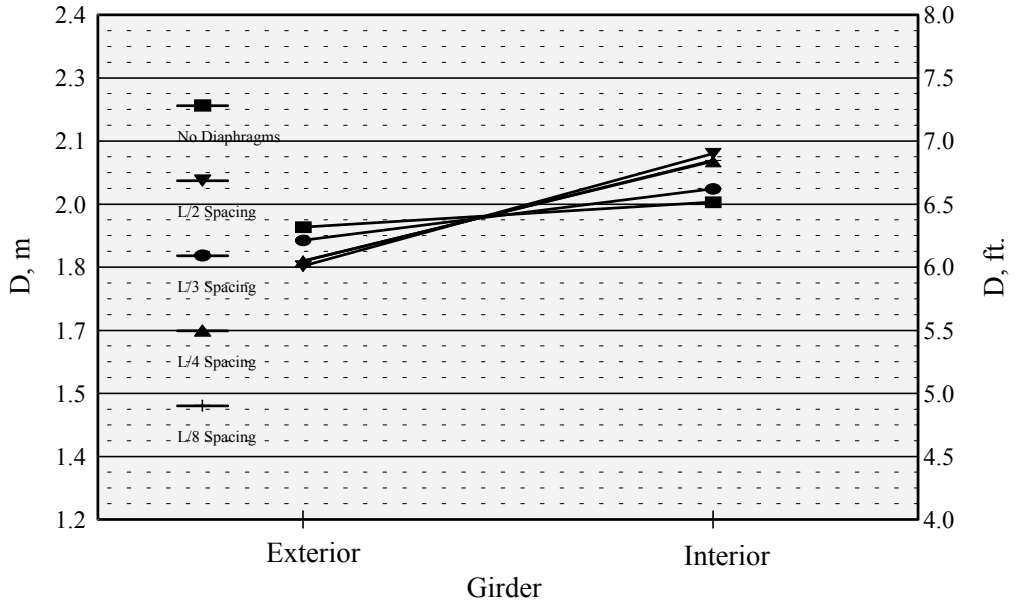

Figure 6-25: Diaphragm spacing effect for Bridge No. 2 ($\alpha = 0.11$, $\theta = 0.53$).

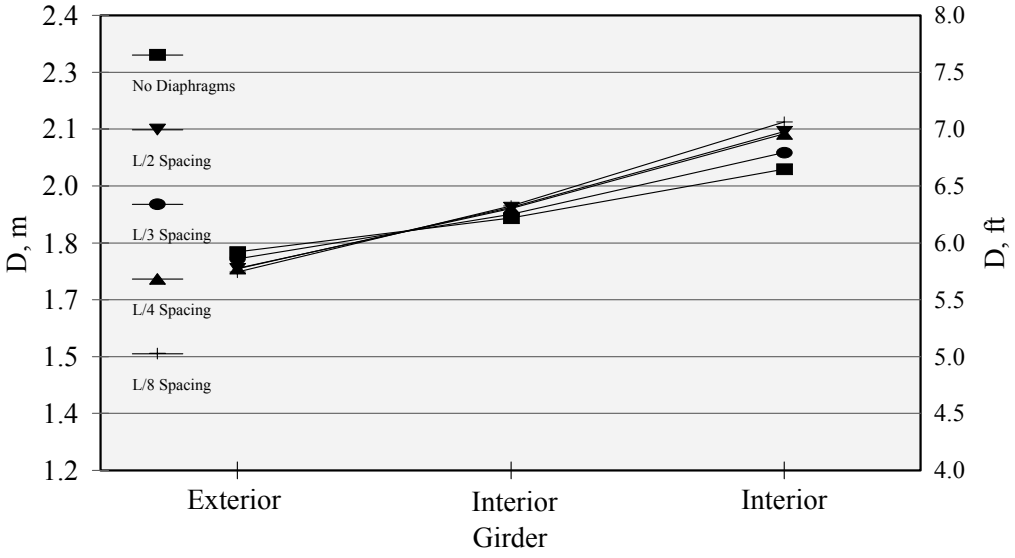

Figure 6-26: Diaphragm spacing effect for Bridge No. 3 ($\alpha = 0.17$, $\theta = 0.53$).

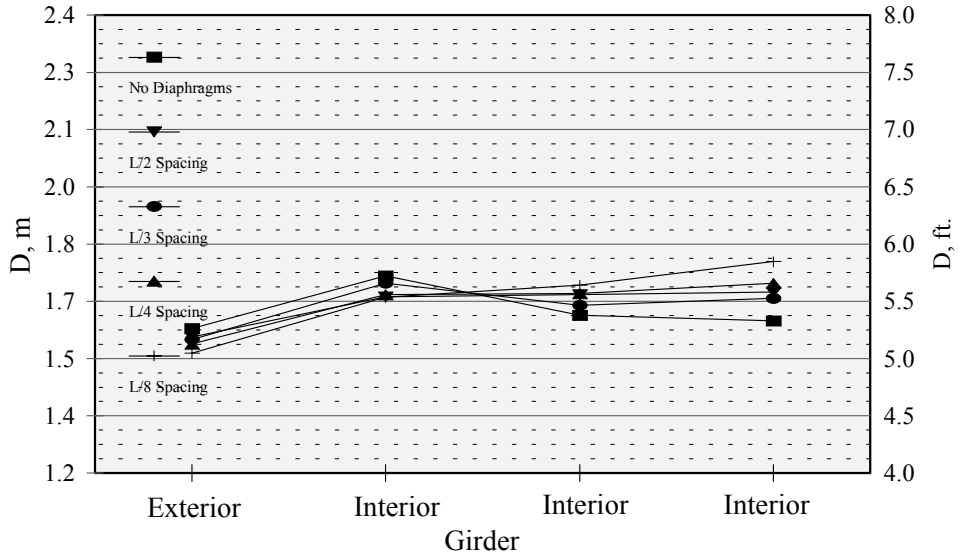

Figure 6-27: Diaphragm spacing effect for Bridge No. 4 ($\alpha = 0.06$, $\theta = 1.25$).

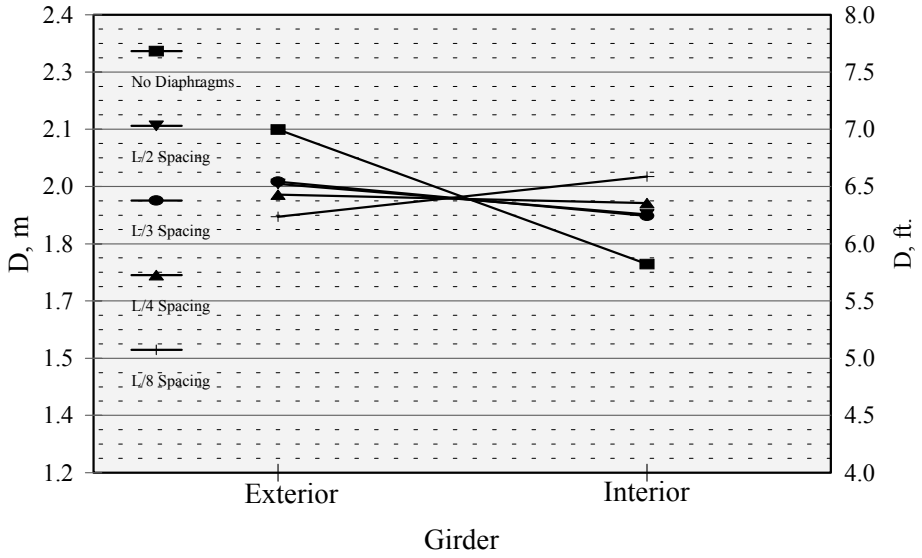

Figure 6-28: Diaphragm spacing effect for Bridge No. 5 ($\alpha = 0.11$, $\theta = 1.25$).

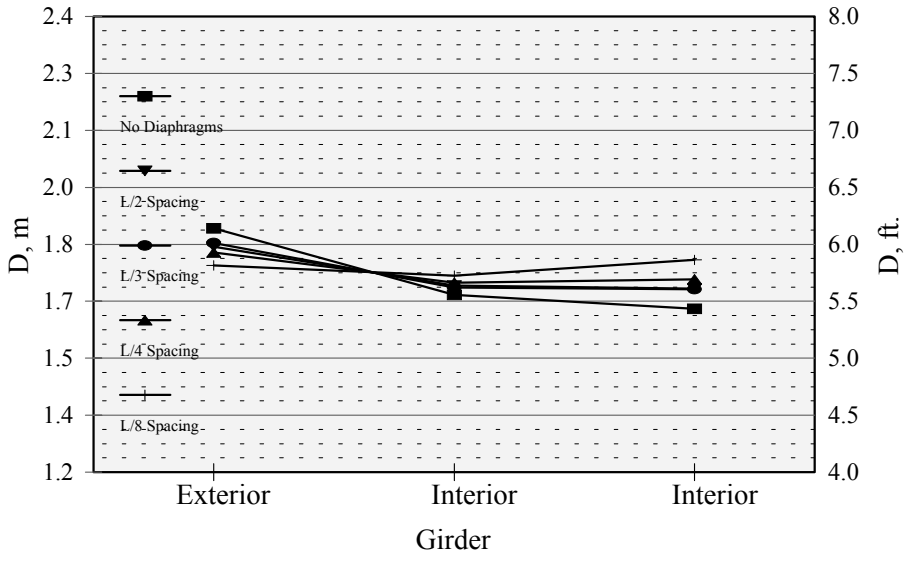

Figure 6-29: Diaphragm spacing effect for Bridge No. 6 ($\alpha = 0.17$, $\theta = 1.25$).

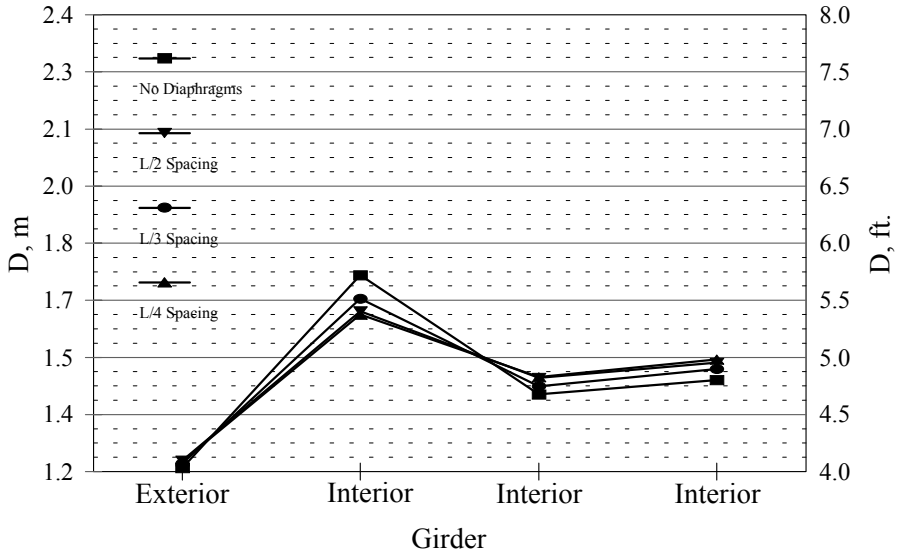

Figure 6-30: Diaphragm spacing effect for Bridge No. 7 ($\alpha = 0.06$, $\theta = 2.00$).

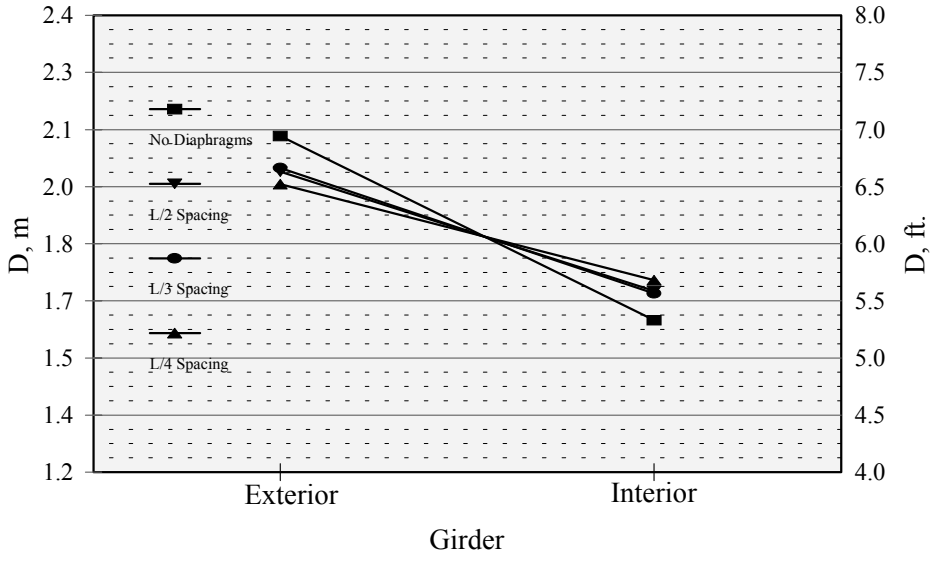

Figure 6-31: Diaphragm spacing effect for Bridge No. 8 ($\alpha = 0.11$, $\theta = 2.00$).

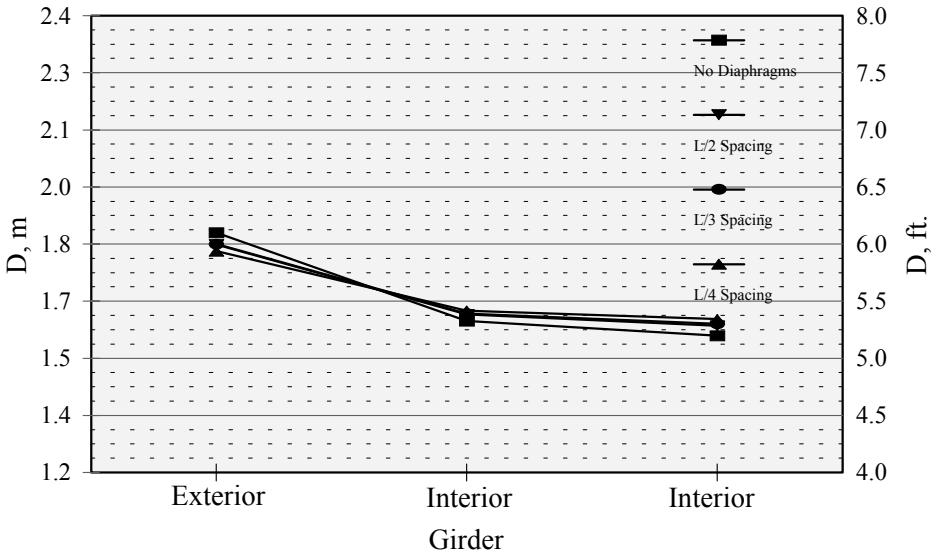

Figure 6-32: Diaphragm spacing effect for Bridge No. 9 ($\alpha = 0.11$, $\theta = 2.00$).

In comparing the results for the diaphragm spacing effect, several observations can be drawn. Excluding the *L*/3 spacing, as the spacing is decreased the interior girder *D* values increase. The *L*/3 spacing has a much less marked effect on interior girder *D* values because the diaphragm lines do not correspond with the midspan of the bridge where the differential deflections of the girders are greatest. As for the other spacings, the *L*/2 spacing produces almost as much increase in the *D* value as the *L*/4 or *L*/8 spacing. Again, because the differential deflections of the girders are greatest at midspan, the increase in *D* values can be attributed almost entirely to the midspan diaphragms, with additional lines of diaphragms contributing little to additional increases in the *D* value.

Exterior girders experience decreased *D* values as the spacing of the diaphragms is decreased. The vehicle-edge distance, as explained in the preceding section, is responsible for this decrease in *D* values for exterior girders.

6.9 Diaphragm Force Prediction

Although the contribution of diaphragms to live load lateral distribution is negligible, diaphragms will likely be used in concrete slab-on-steel girder highway bridges for construction purposes and wind bracing. For this reason, a method is required that can predict the forces the diaphragm members must transmit under vehicle live loading. The current study indicates that the diaphragm-deck stiffness ratio is appropriate in describing the forces in the diaphragms under vehicle live load. The same finite element models of highway bridges used in the diaphragm contribution section are used for this portion of the study. The analysis includes two additional bridge structures with θ values of 1.00 in order to eliminate a large gap in predicting the diaphragm member forces between θ values of 0.53 and 1.25. The cross sections for these two bridges are the same as those used for the bridges with α values of 0.11 and 0.17. The same diaphragm stiffnesses are used for these two bridges as well.

Values of the diaphragm lower strut forces are recorded for each of the stiffnesses of diaphragms used for each bridge. Only the midspan diaphragms are included in the models because this corresponds to the maximum location of differential deflection for the girders of the bridge, thereby producing the highest forces in the diaphragm members. Separate load cases are used to predict the maximum diaphragm lower strut forces, corresponding to the strength limit state and the fatigue limit state. The strength limit state uses two HS-20 trucks positioned in adjacent lanes to predict the maximum forces occurring in the diaphragm members. The fatigue limit state uses only one HS-20 truck with a fixed spacing of 9.1 m (30 ft) between the 142 kN (32 kip) axles. The transverse positioning of the vehicle live load is varied.

6.9.1 Strength

A graph of the diaphragm lower strut forces vs. the diaphragm-deck stiffness ratio is shown in Figure 6-33. It can be seen that the data plots non-linearly for each value of θ. The parameter θ describes the ratio of longitudinal and transverse deflection stiffness and also the planform of the bridge. The maximum forces in the diaphragms occur when the vehicle live load

is placed symmetrically on the bridge, nearest to the longitudinal centerline. This is confirmed by using several transverse positionings of the vehicle live load in the finite element analyses. Bakht and Jaeger (1985) also state that the maximum transverse moments in a bridge occur at the center of the bridge cross section. Keating and Crozier (1992) have also shown through field measurements that the maximum diaphragm forces occur for a load centrally placed on a bridge. Curve fitting techniques are used to fit a piecewise, upper-bound curve for each value of θ, as shown in Figure 6-34.

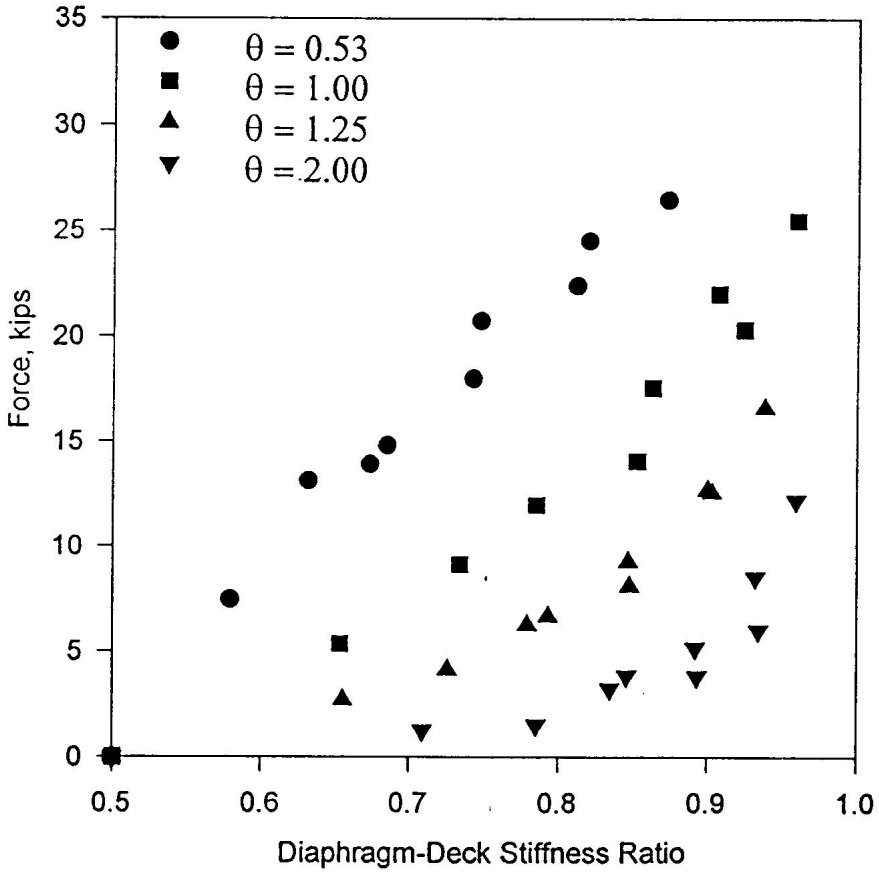

Figure 6-33: Diaphragm forces under strength loading.

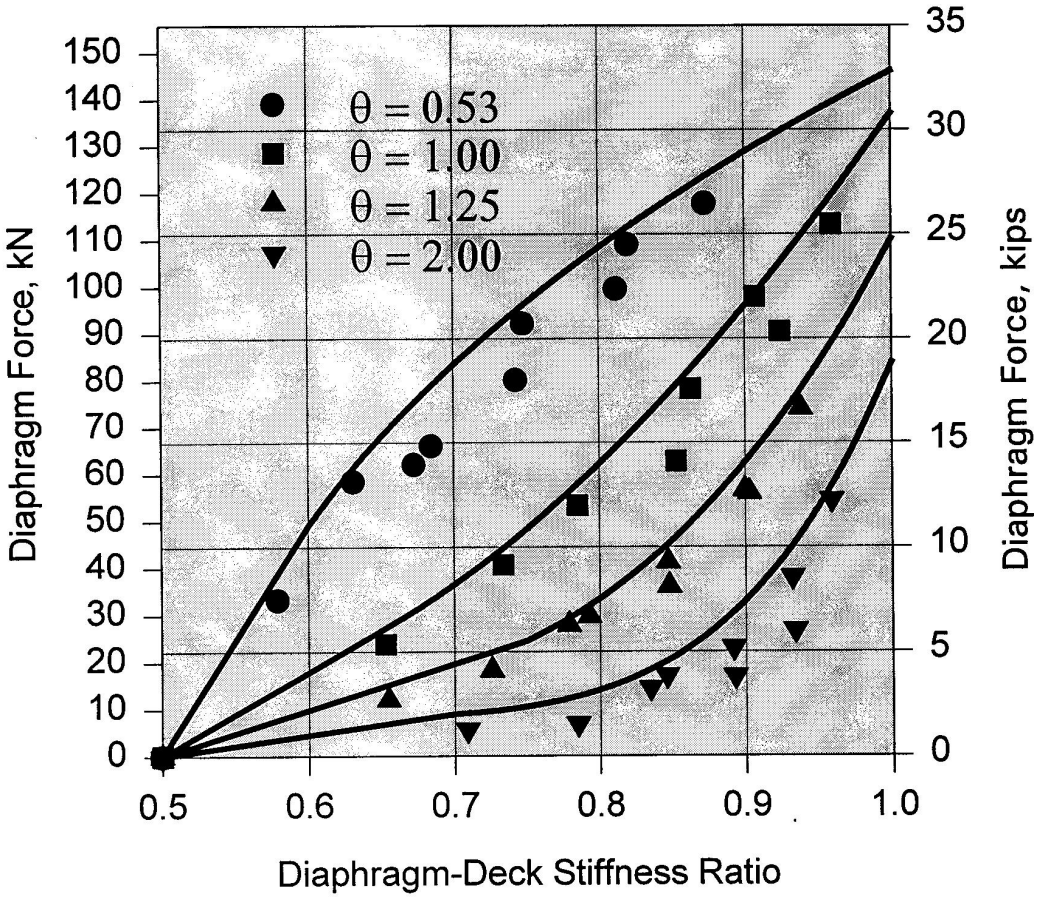

Figure 6-34: Upper-bound fit of diaphragm force prediction for strength.

As stated above, separate runs were made to predict the forces occurring in the diaphragms under fatigue loading. The AASHTO LRFD specifications specify using this fatigue load so that the forces predicted are not overly conservative. A graph of lower strut forces vs. diaphragm-deck stiffness ratios is shown in Figure 6-36. It can again be seen that the parameter θ efficiently groups the data. A large shift occurs for $\theta = 0.53$. This is due to the fact that low θ values correspond to longer spans, thus allowing all axles of the HS-20 truck to be placed on the bridge models. A curve fitting program was used to establish the best fit curve for each value of θ, and these curves are shown in Figure 6-35 along with the data.

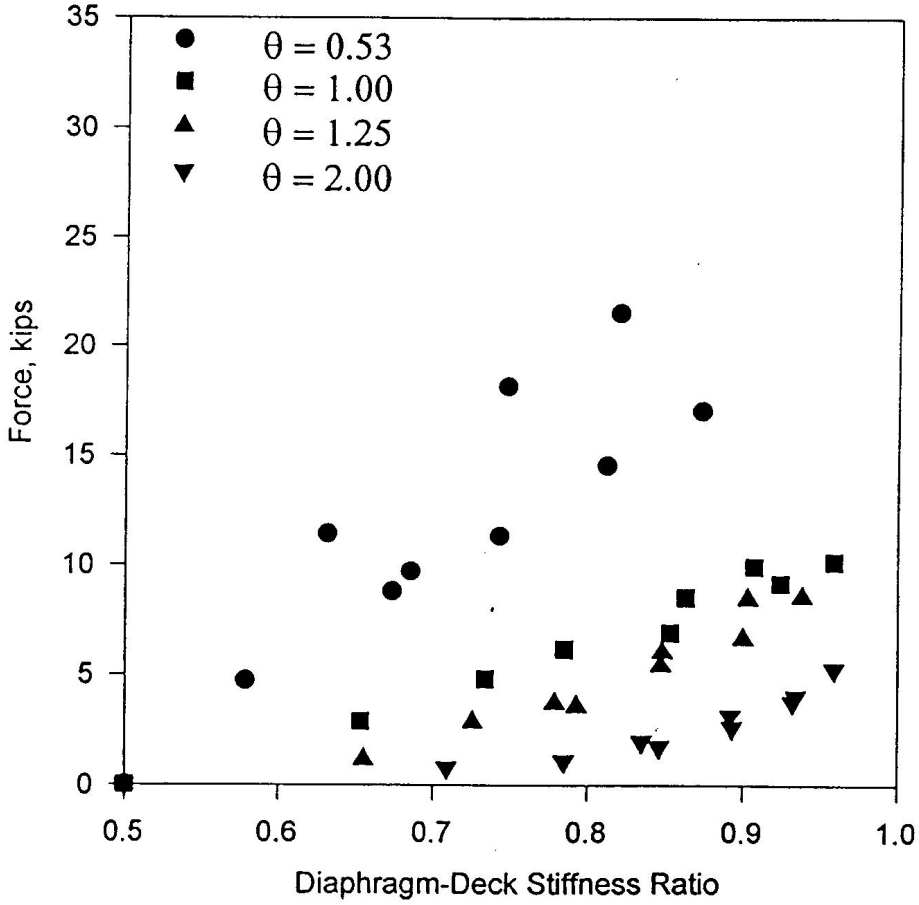

Figure 6-35: Diaphragm forces under fatigue loading.

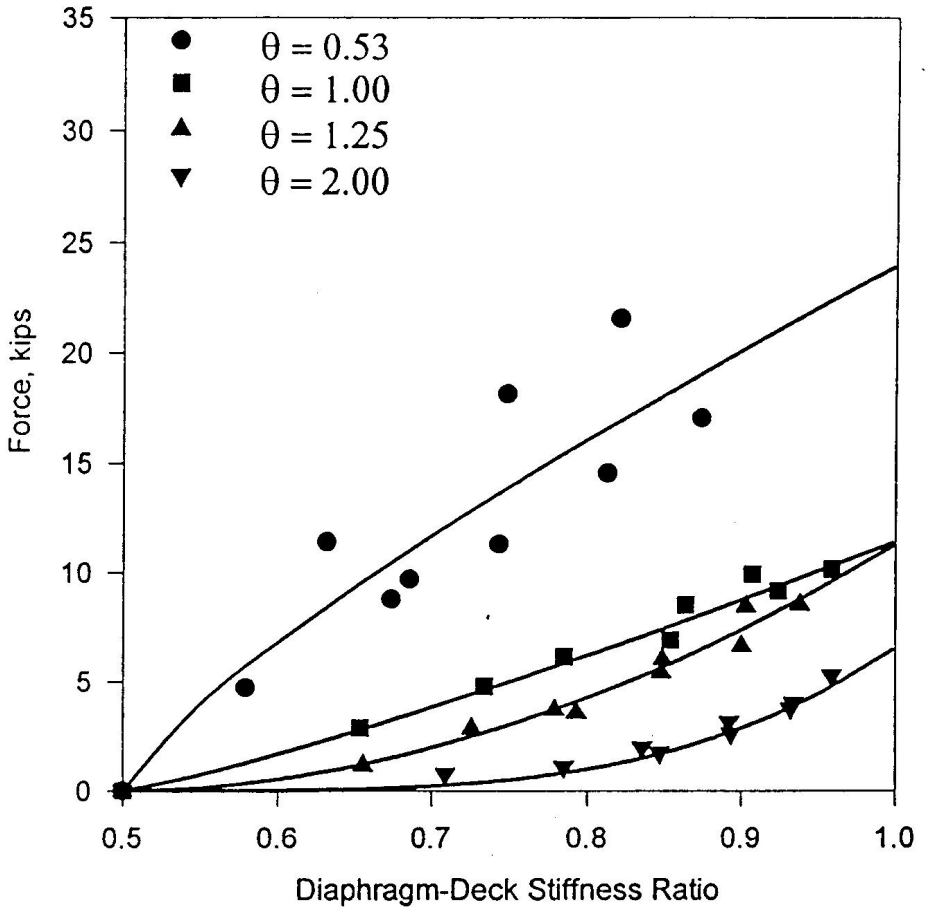

Figure 6-36: Curve fit for diaphragm forces under fatigue loading.

6.9.2 Skew Correction Factor

Since a majority of highway bridges are skewed, it is desired to determine what effect the skewed construction would have on diaphragm member forces. A single bridge with midspan diaphragms is analyzed for this, and the skew angle is varied. The bridge chosen is the same as the bridge used in the original study on diaphragm contribution to lateral load distribution, with α and θ values equal to 0.11 and 0.53, respectively. The skewness is used as the measure of skew in the bridge geometry, with values of 0.05, 0.08, and 0.14 used in the study. Figure 6-37 shows

the percent change in the diaphragm forces for these values of skewness compared to the diaphragm forces in the straight bridge. It can be seen that for values of skewness below 0.050 there is almost no change in the diaphragm forces. However, the difference in the diaphragm forces deviates rapidly as the skewness exceeds the 0.050 value, with a 22.1 percent difference in the forces for the 0.14 value of skewness.

6.9.3 Comparison with Field Data

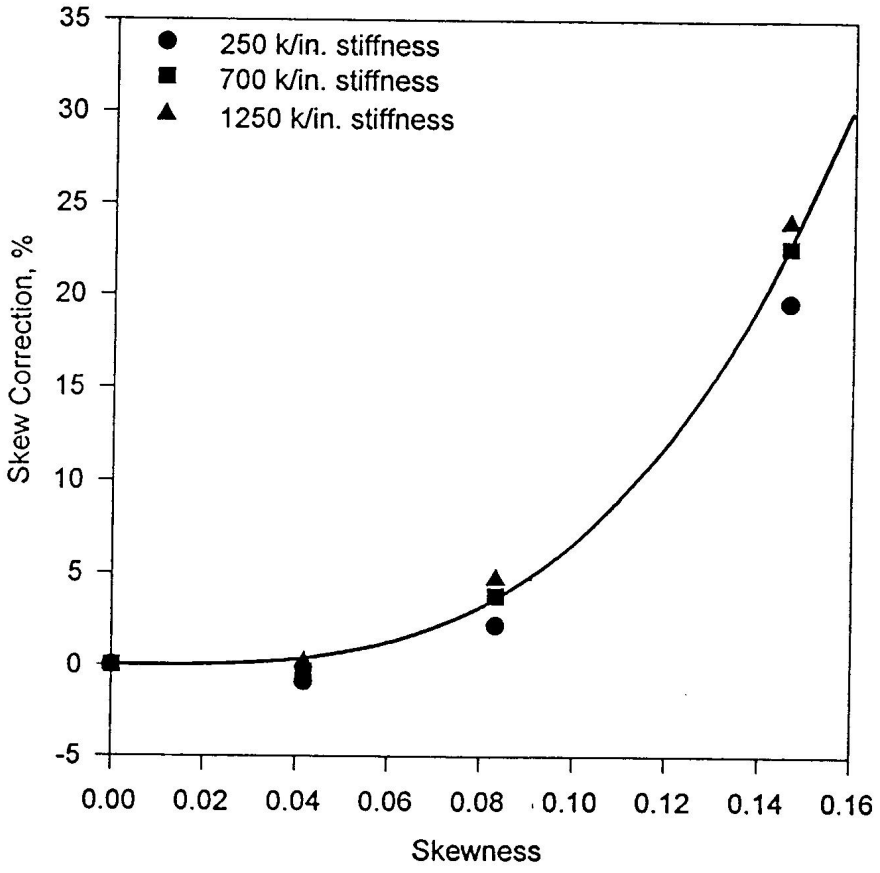

Figure 6-37: Deviation of diaphragm forces with bridge skewness.

Measured diaphragm forces from three Texas bridges were available to compare with the forces predicted by the developed method. The first bridge, located in Victoria, Texas, is a three span continuous plate girder bridge. This bridge is non-skewed, with a 2.44 m (8 ft) girder spacing, 165 mm (6.5 in.) thick concrete deck, and spans of 22.9-38.1-22.9 m (75-125-75 ft). The θ value of the bridge is 0.48. The stiffness ratio is calculated in Eqs. (6-16) through (6-19).

$$K_s = 38{,}100\,\text{mm}(165\,\text{mm})^3 21{,}500\,\text{MPa} = 3.68\times10^{12}\ \text{kN-mm}^2$$
$$\left(K_s = 125\,\text{ft}(6.5\,\text{in.})^3(3122\,\text{ksi}) = 107.2\times10^{6}\ \text{k-in.}^2\right) \tag{6-16}$$

$$K_D = 21{,}500\,\text{MPa}\left(38{,}000)(165)^3\%(1968)^2\left(\frac{200{,}000\,\text{MPa}}{21{,}500\,\text{MPa}}\right)\right(1$$
$$\left(K_D = 3122\,\text{ksi}\left(125\text{ft}(6.5\,\text{in.})^3\%3.05\,\text{in.}^2\left(\frac{29{,}000\,\text{ksi}}{3122\,\text{ksi}}\right)\right(49\,\text{in} \tag{6-17}$$

$$\left(K_D = 1.00\times10^{12}\ \text{kN-mm}^2\right)$$
$$\left(K_D = 348.6\times10^{6}\ \text{k-in.}^2\right) \tag{6-18}$$

$$\textit{Stiffness Ratio} = \frac{1.00\times10^{12}}{(1.00\%3.38)\times10^{12}} = 0.76$$
$$\textit{Stiffness Ratio} = \frac{348.6\times10^{6}}{(348.6\%107.2)\times10^{6}} = 0.76 \tag{6-19}$$

Using Fig. 6-36 with 0.76 stiffness ratio and θ of 0.48, the predicted diaphragm lower strut force is 71 kN (16 kips). Equation (6-20) shows the lower strut force corrected for the ratio of the gross vehicle weight of the test truck to the HS-20 truck and a correction for the transverse moment assuming a linear distribution with maximum value at the center of the bridge cross section.

$$Predicted\ Force = 71\ \text{kN}(0.61)_{GVW}(0.71)_{M_T} = 31\ \text{kN}$$
$$\left(Predicted\ Force = 16\ \text{kips}(0.61)_{GVW}(0.71)_{M_T} = 6.93\ \text{kips}\right) \quad (6\text{-}20)$$

The force measured in the field is 32 kN (7.2 kips). Static measurements were taken, so no correction for impact forces is necessary. Comparing this value to the predicted value of 31 kN (6.93 kips) gives a -4 percent error, which is excellent agreement. A possible reason for the measured value exceeding the predicted value is a reduced modulus of elasticity for the concrete deck due to creep effects. The bridge has been in service for approximately 35 years.

Two additional bridges were field tested to determine diaphragm forces. One is located in Midland, Texas, and the other in Austin, Texas. Comparisons of predicted diaphragm forces to actual diaphragm forces, similar to those shown above, were made in an identical manner for these two bridges. Table 6-4 shows the relevant values used in these comparisons and the percent errors obtained. The term φ represents the correction factor, obtained from Fig. 6-36, for the skewed bridge geometry.

Table 6-4: Comparison of measured and predicted diaphragm forces.

Bridge	Stiff. Ratio	θ	Correction Factors				Predicted Force kN (kips)	Actual Force kN (kips)	% Error
			GW	M_T	φ	IM			
Victoria	0.76	0.48	0.61	0.71	-	-	31 (6.9)	32 (7.2)	-4
Midland	0.72	0.53	0.61	0.85	1.12	0.75	32 (7.3)	30 (6.8)	+7
Austin	0.81	0.86	0.37	0.84	1.01	0.75	12 (2.8)	20 (4.4)	-36

The large error between predicted and measured forces associated with the Austin bridge can be attributed to several factors. First, during the testing it was difficult to isolate the test truck from other traffic on the bridge since it is located just south of downtown Austin on a busy

section of Interstate 35. Additional vehicles may have contributed to the forces being higher than predicted. Second, the bridge is extremely wide, containing three 3.7 m (12 ft) traffic lanes, a 1.2 m (4 ft) inside shoulder and a 3.0 m (10 ft) outside shoulder. Additionally, the northbound and southbound structures were constructed 2.4 m (8 ft) from each other and later made continuous by bridging this gap with a slab and diaphragms, effectively doubling the bridge width.

7. RECOMMENDATIONS AND CONCLUSIONS

Cross frame diaphragms have been used extensively in steel girder highway bridges. The AASHTO bridge specifications have mandated their use at a maximum 7.62 m (25 ft) spacing when the bridge span length exceeds 38.1 m (125 ft). However, their contribution to the overall load carrying capacity of the bridge has never been codified. Explicit design for diaphragm member forces has not existed in the bridge design process, with the except of horizontally curved structures.

Cross frame diaphragms are, however, subject to live load forces and stresses that may lend to fatigue cracking development. The cracking can be in the diaphragm members or, more commonly, in the connection of the diaphragm to the longitudinal girder. Common practice dictated that no welded attachment be used between the end of a diaphragm connection plate and the tension flange of the girder. This unstiffened web gap is then susceptible to out-of-plane distortion resulting from the diaphragm member forces occurring as a result of the three-dimensional behavior of the structure.

The results of this study have shown that a reduction in longitudinal girder moments, achieved by the presence of diaphragm cross-frames in the bridge, may produce a lighter, cheaper structure. However, no decrease in moment can be assumed from the results presented in this study. Inclusion of diaphragms results in a decrease in girder moments for girders near the centerline of the bridge, but only because these girders are controlled by the vehicle live loading being positioned symmetrically near the centerline of the bridge.

Walker (1987) described the effect of having an eccentric load vs. a non-eccentric load on a highway bridge. He states that the reduction in longitudinal girder bending moment only occurs for interior girders under a non-eccentric loading pattern. There is no practical way to translate this reduction in girder moments into design of a lighter girder section unless it can be

guaranteed that the loading on the bridge will always be non-eccentric. This cannot be guaranteed under normal highway truck loading.

Inclusion of diaphragms in a bridge may actually increase the exterior girder moments slightly. The diaphragm stiffness and spacing, vehicle-edge distance, and presence of concrete crash barriers along the sides of a bridge are factors which must be taken into account to determine if the exterior girder moments will increase by including diaphragms.

Though no reduction in longitudinal girder moments can be assumed by including diaphragms in a bridge, complete removal of diaphragms must take into account other beneficial effects of diaphragms. Diaphragms do distribute load transversely and in so doing reduce the slab bending stresses. They also distribute wind loading and other horizontal forces and provide stability of the longitudinal girder compression flanges. Deck replacement schemes may require diaphragm bracing.

7.1 Recommendations

It is recommended that permanent cross frame diaphragm removal be considered as an option in the repair of fatigue damage at unstiffened web gaps. While cross frame diaphragms do contribute to the load-carrying distribution of the structure, their partial removal results in insignificant increases in girder flange stresses.

For the prediction of diaphragm forces, the plots of data and curve fits show that the data is tightly grouped, especially for the θ values of 1.25 and 2.00. From finite element modeling, it can be seen that the diaphragm-deck stiffness ratio and θ value provide an accurate means of assessing the forces in the diaphragms of concrete slab-on-steel girder bridges. This is further validated by the close comparisons of the predicted diaphragm forces with the field test data. It is therefore recommended that the method developed for the prediction of diaphragm forces be used for the analysis and design of diaphragms in concrete slab-on-steel girder highway bridges. Figures 7-1, 7-2, and 7-3 may be used to predict the diaphragm forces for the strength and

fatigue limit states, respectively, in concrete slab-on-steel girder highway bridges of straight or skewed geometry.

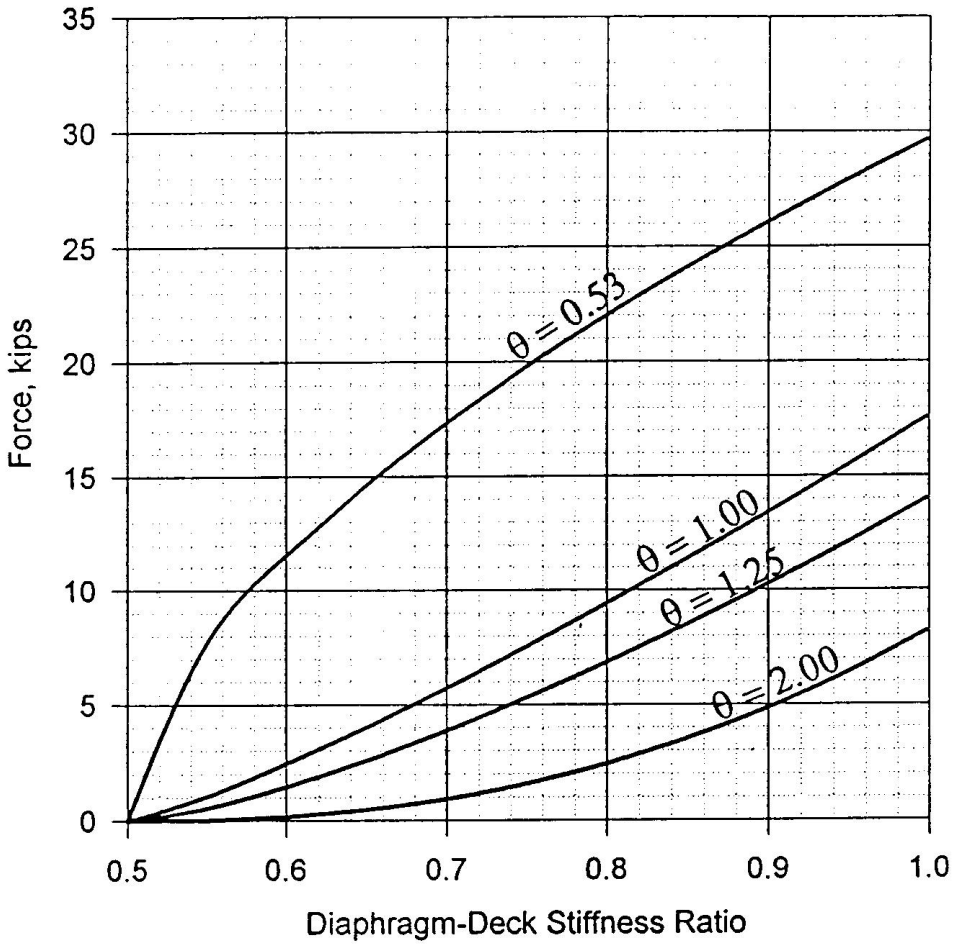

Figure 7-1: Diaphragm force prediction for strength.

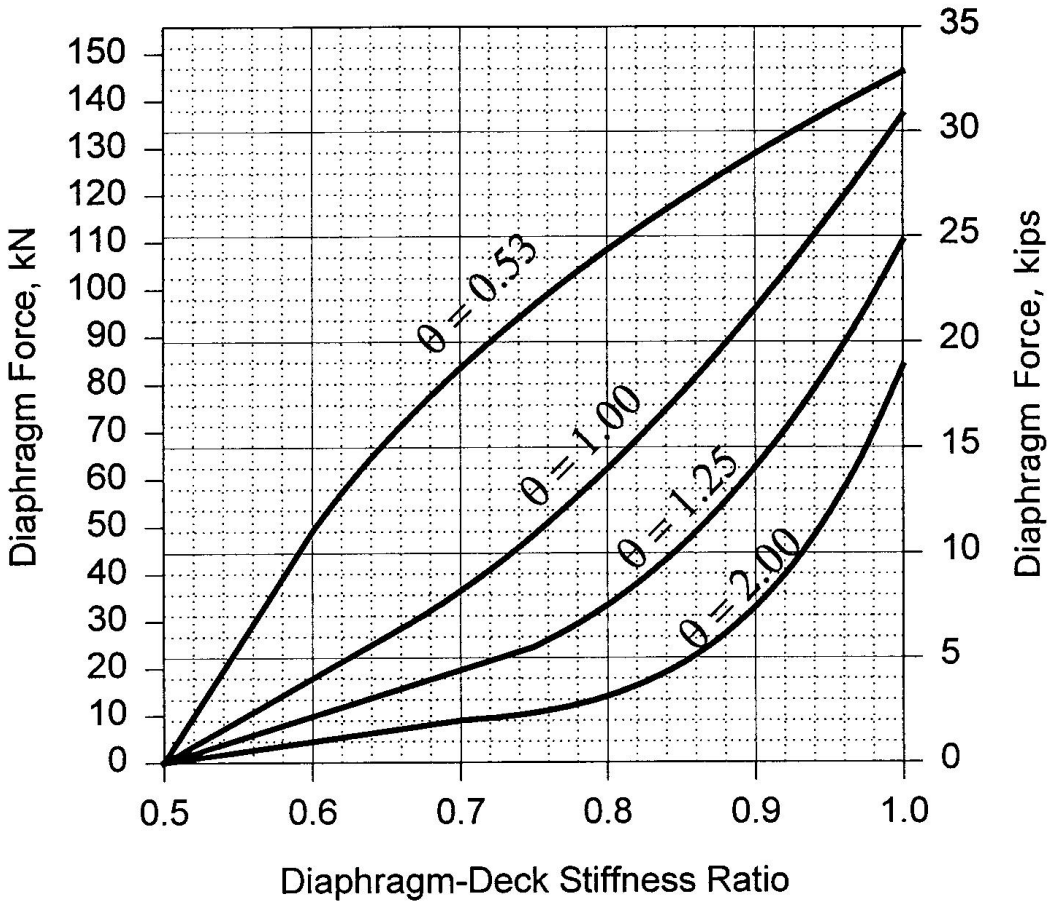

Figure 7-2: Diaphragm force prediction for fatigue.

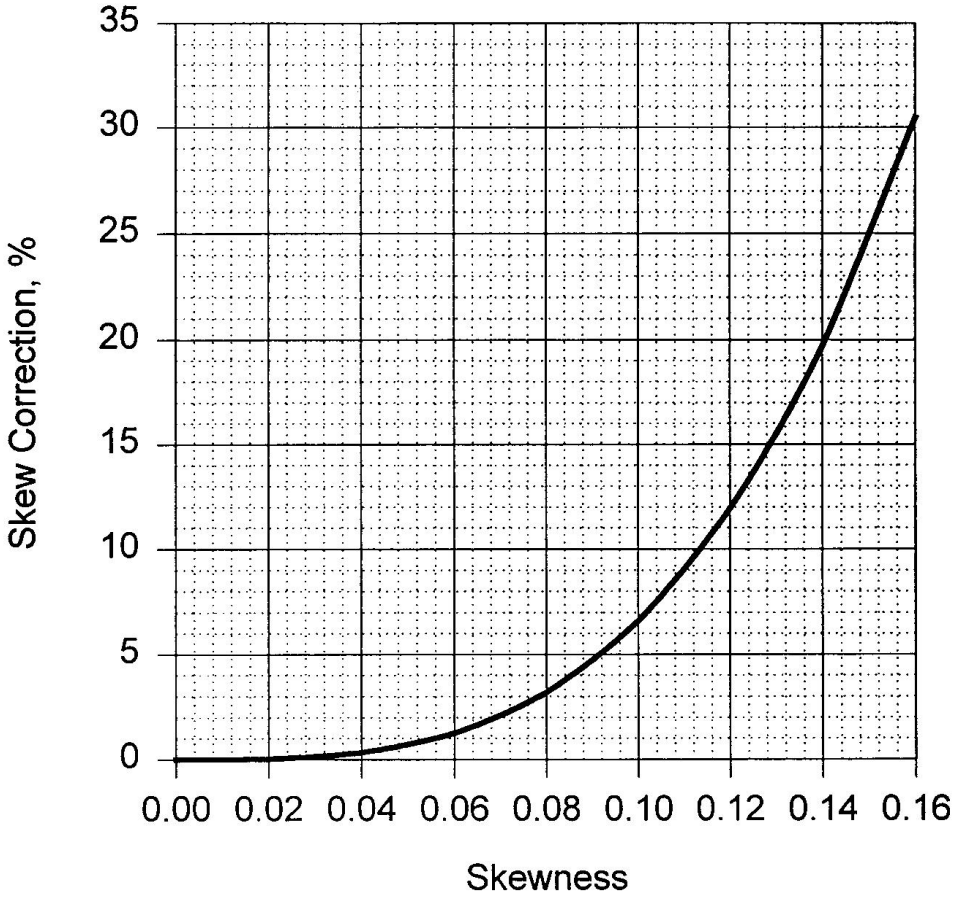

Figure 7-3: Skew correction factor for force prediction.

The results reported herein should not be used to provide a procedure for the design of cross frame diaphragm members. Experience has shown that explicitly sizing individual members for maximum design load conditions results in increase member sizes. This increases the overall stiffness of the diaphragms, increasing their load carrying contribution to the structure, resulting in even larger member sizes. Minimum diaphragm member sizes, only that

necessary to provide girder stability, should be used.

Fatigue cracking that has occurred at diaphragm connection plates should be repaired using the methods outlined in TxDOT Research Report 1360-1. Three procedures for the removal or arresting of the fatigue cracking are provided. To prevent the reinitiation of fatigue damage, the driving force behind the cracking must also be removed, either by providing a rigid attachment between the diaphragm connection plate or the permanent removal of the diaphragms. Other types of fatigue damage, though not as common as that found at unstiffened web gaps, can be repaired using the procedures outlined in Appendix E.

Diaphragms should not be used as a means of increasing the redundancy of the structure and providing alternate load paths in the event of the fracture of a longitudinal girder. Load paths through cross frame diaphragms require increased diaphragm member sizes, leading to increased out-of-plane distortion. Many fractures in girders can be attributed fatigue initiation at diaphragm locations.

7.2 Conclusions

The primary focus of this research study has been to determine what contribution diaphragms in concrete slab-on-steel girder bridges have on lateral distribution of live load and to predict the forces in the diaphragms under vehicle live load. Orthotropic plate theory has been used to idealize concrete slab-on-steel girder highway bridges and also to classify the stiffness properties of a highway bridge, allowing a small number of bridges to represent the entire practical range of concrete slab-on-steel girder bridges.

Finite element modeling techniques have been used to evaluate the vehicle live load effects of nine bridges chosen to represent the spectrum of practical concrete slab-on-steel girder highway bridges. The finite element results were used to calculate distribution factors. From these it was determined that diaphragms of a given stiffness and spacing could not reduce the required design longitudinal moment capacity in all girders of a bridge, but only those near the

bridge centerline. Inclusion of diaphragms does not necessarily give a more even distribution of the longitudinal girder moments. However, the diaphragms do distribute vehicle live loads laterally, loads which must be carried by the deck slab in their absence.

The finite element method was also used to predict the forces in the members of a diaphragm cross-frame. The diaphragm lower strut forces were shown to vary significantly with the stiffness of the diaphragm and the configuration of the bridge. The diaphragm-deck stiffness ratio and the orthotropic plate parameter θ can accurately describe this variation, as evidenced by the close comparison of the predicted forces and actual forces measured on three real bridges. Use of the diaphragm-deck stiffness ratio and θ will allow for a close approximation of the actual forces in a diaphragm, thereby allowing proper design and detailing of the diaphragms and their connections to the longitudinal girders.

A review of steel bridge inspection records indicated that distortion-induced fatigue cracking at diaphragm connections has been the most prevalent form of fatigue damage in the state of Texas. While other types of fatigue damage have occurred, this damage has not been as widespread.

7.3 Recommendations for Additional Research

This research study report provided a thorough investigation into the fatigue and load distribution behavior of cross frame diaphragms in simple span structures. Additional finite element analysis is warranted to determine cross frame behavior in continuous mulitspan bridges. Additionally, a more detailed analysis should be performed to determine the influence the concrete slab has on load distribution and how the slab can be designed to reduce or eliminate the need for cross frame diaphragms.

References

American Association of State Highway and Transporation Officials, *Standard Specifications for Highway Bridges*, 15th ed., 1992.

American Association of State Highway and Transporation Officials, *Highway Bridge Specifications - Load and Resistance Factor Design*, 1994.

Azizinamini, A., Kathol, S., and Beacham, M.W., "Influence of Cross Frames on Load Resisting Capacity of Steel Girder Bridges," *Engineering Journal*, American Institute of Steel Construction, Volume 32, No. 3, 1995.

Bakht, B. and Jaeger, L.G., Bridge Analysis Simplified, McGraw-Hill, 1985.

Bakht, B. and Moses, F., "Lateral Distribution Factors for Highway Bridges," *Journal of Structural Engineering*, ASCE, Vol. 114, No. 8, 1988, 1785-1803.

Bathe, K., Finite Element Procedures in Engineering Analysis, Prentice-Hall, 1982.

Bishara, A.G., Liu, M.C., and El-Ali, N.D., "Wheel Load Distribution on Simply Supported Skew I-Beam Composite Bridges," *Journal of Structural Engineering, ASCE*, Vol. 119, No. 2, 1993, 399-419.

Diaz, M. and Andrews, "Detailed Structural Condition Report for Bridge 06-165-0005-15-201 (IH 20 WestBound) and 06-165-0005-15202 (HI 20 WestBound)," ARE, Inc., Engineering Consultants, July 9-17, 1990.

Jaeger, L.G. and Bakht, B., "The Grillage Analogy in Bridge Analysis," *Canadian Journal of Civil Engineering*, Vol. 9, No. 2, 1982, 224-235.

Keating, P.B. and Crozier, A.R., *Evaluation and Repair of Fatigue Damage to Midland County Bridges*, Texas Transportation Institute, Report 1313-1F, 1992.

Keating, P.B., Wilson, S.D., and Kohutek, T.L., *Evaluation of Repair Procedures for Web Gap Fatigue Damage*, Texas Transportation Institute, Report 1360-1, 1996.

Kostem, C.N. and deCastro, E.S., "Effects of Diaphragms on Lateral Load Distribution in Beam-Slab Bridges," *Transportation Research Record, Bridge Tests*, No. 645, 1977, 6-9.

Newmark, N.M., "Design of I-Beam Bridges," *Journal of the Structural Division*, ASCE, Vol. 74, No. 1, 1948, 305-330.

Saindon, K.C. *Live Load Effects in Diaphragms of Concrete Slab-on-Steel Girder Highway Bridges*, Thesis, submitted to the Civil Engineering Department in partial fulfillment of the M.S. Degree, Texas A&M University, College Station, Texas, 1994.

Tarhini, K.M. and Frederick, G.R., "Wheel Load Distribution in I-Girder Highway Bridges," *Journal of Structural Engineering*, ASCE, Vol. 118, No. 5, 1992, 1285-1294.

Walker, W.H., "Lateral Load Distribution in Multi-Girder Bridges," *Engineering Journal*, AISC, Vol. 24, No. 1, 1987, 21-28.

Zwerneman, F.J., Poynter, P.G., Rauf, A, and Yang, J., *Fatigue Assessment of Bridge Members Based on In-Service Stresses*, School of Civil and Environmental Engineering, Oklahoma State University, Interim Report No. 1, 1995.

APPENDIX - A

STRESS HISTORIES

for

MIDLAND COUNTY BRIDGE
(IH-20 Eastbound)
FIELD TEST 2
(No Diaphragms)

Test Date
October 6, 1992

Table A-1: Summary of recorded test truck passages, Field Test No. 2.

Filename	Gage Group	Truck Pass	Truck Position	Number of Scans
MID5P1	5	1	Truck centered in passing lane	93
MID5P2	5	2	Truck centered in driving lane	86
MID5P3	5	3	Truck centered in right shoulder	87
Scan Rate changed from 0.10 sec. to 0.0125 sec.				
MID5P4	5	4	Truck centered in passing lane	47
MID5P5	5	5	Truck centered in right lane	81
MID8P1	6	1	Truck centered in driving lane	60
MID8P2	6	2	Truck centered in right shoulder	74
MID8P3	6	3	Truck centered right shoulder	80
MID9P1	9	1	Truck centered in passing lane	76
MID9P2	9	2	Truck centered in driving lane	65
MID9P3	9	3	Truck centered in right shoulder	76
MID10P1	10	1	Truck centered in passing lane	76
MID10P2	10	2	Truck centered in driving lane	71
MID10P3	10	3	Truck centered in right shoulder	89

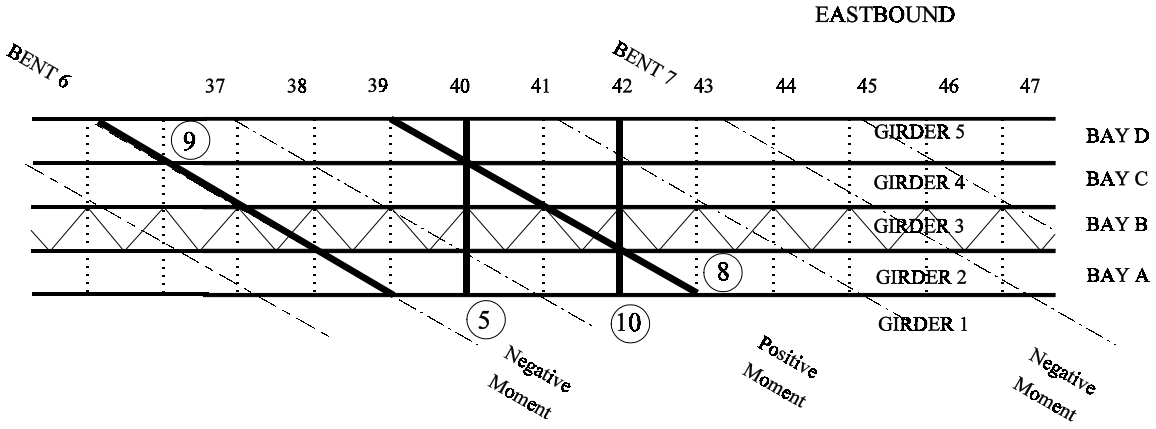

Figure A-1: Gage group locations on Eastbound structure, Field Test No. 2.

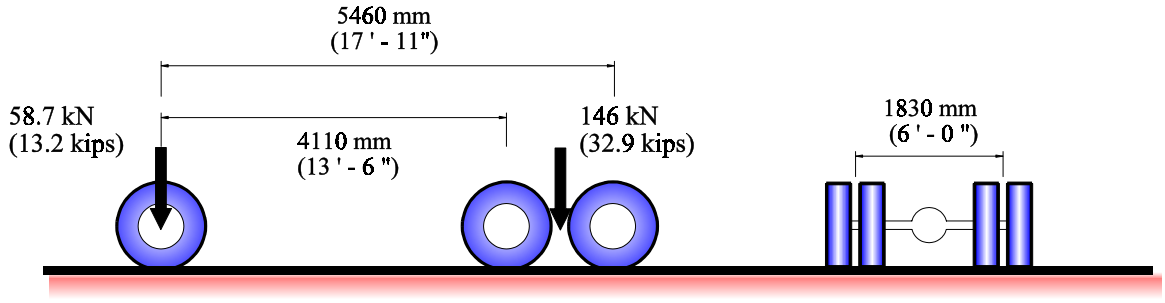

Figure A-2: Test truck axial weight and configuration, Field Test No. 2.

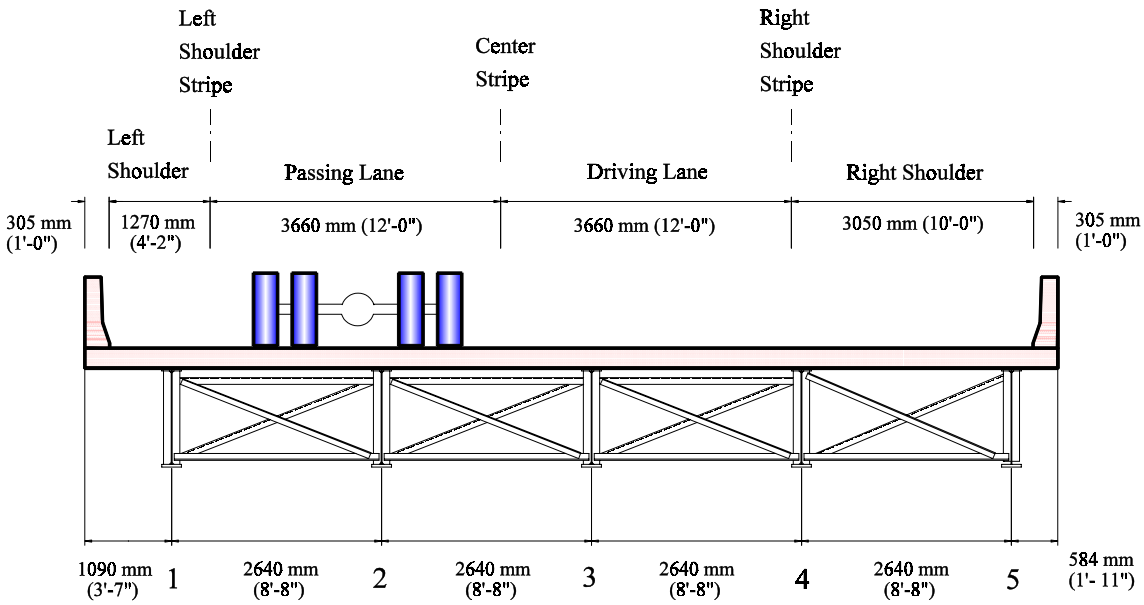

Figure A-3: Location for test truck positioned in center of passing lane (Pass No. 1).

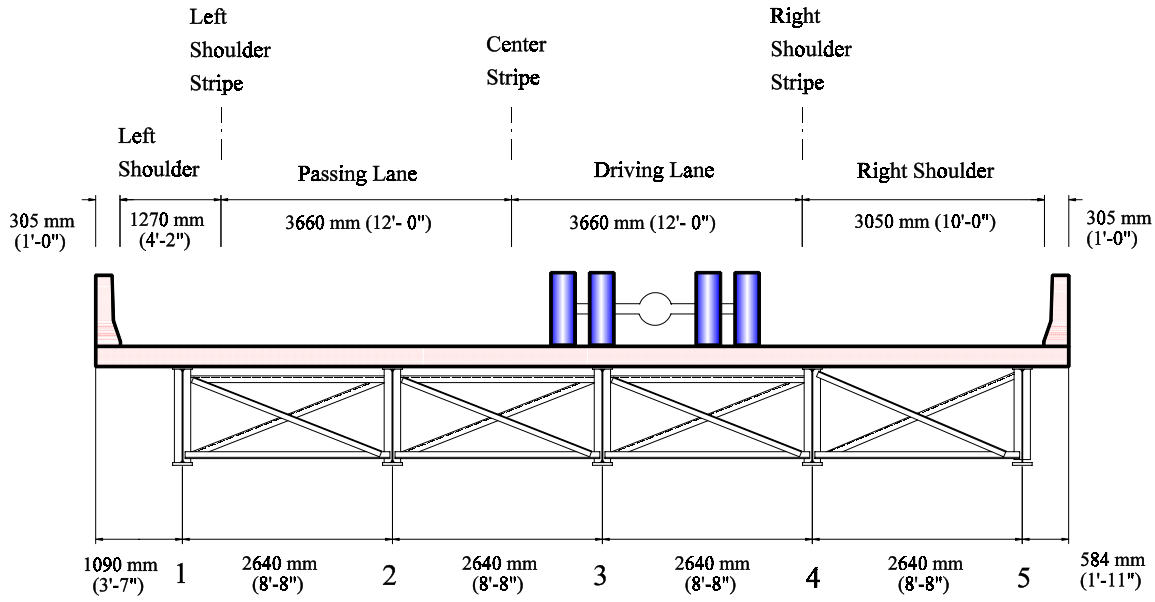

Figure A-4: Location for test truck positioned in center of driving lane (Pass No. 2).

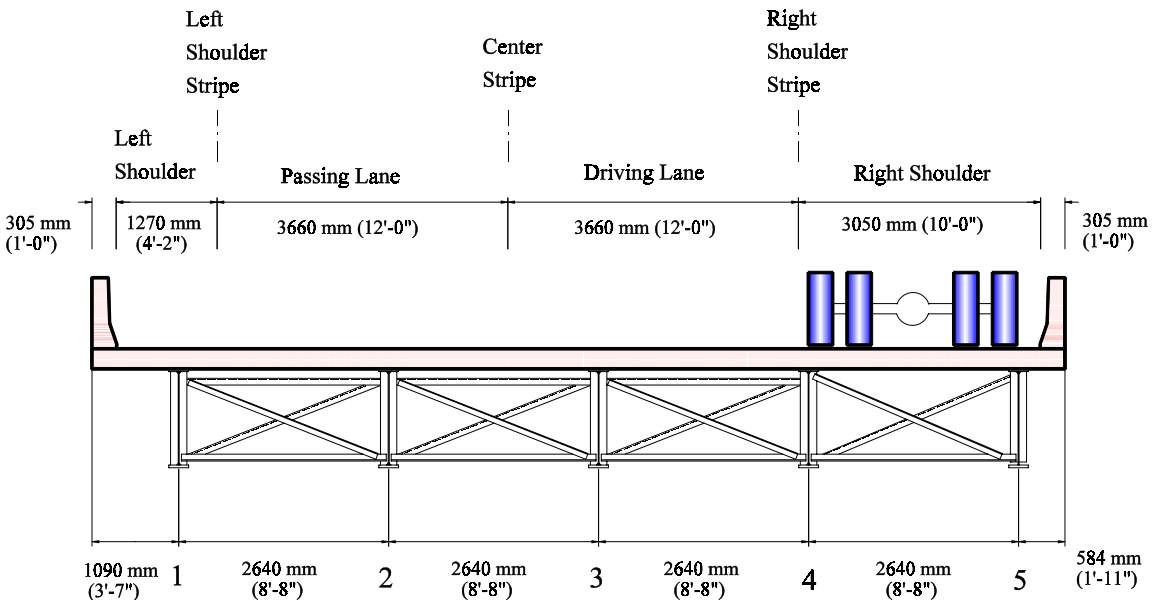

Figure A-5: Location for test truck positioned in center of right shoulder lane (Pass No. 3).

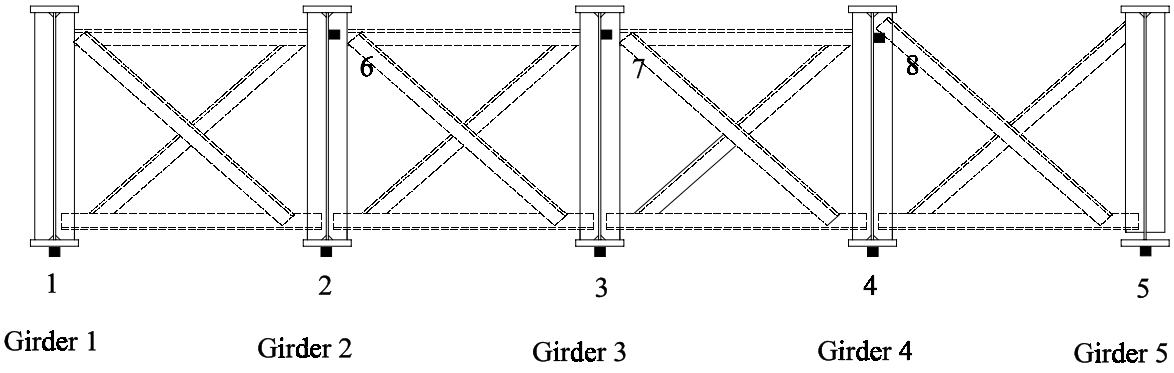

Figure A-6: Gage Group No. 5-2 location, Diaphragm Line 40 (positive bending moment region).

Table A-2: Gage locations of Group No. 5-2.

Gage Number	Position
1	bottom flange, Girder No. 1
2	bottom flange, Girder No. 2
3	bottom flange, Girder No. 3
4	bottom flange, Girder No. 4
5	bottom flange, Girder No. 5
6	web plate, Girder No. 2, long. direction (191 mm (7.5 in) below flange)
7	web plate, Girder No. 3, long. direction (191 mm (7.5 in) below flange)
8	web plate, Girder No. 3, long. direction (191 mm (7.5 in) below flange)

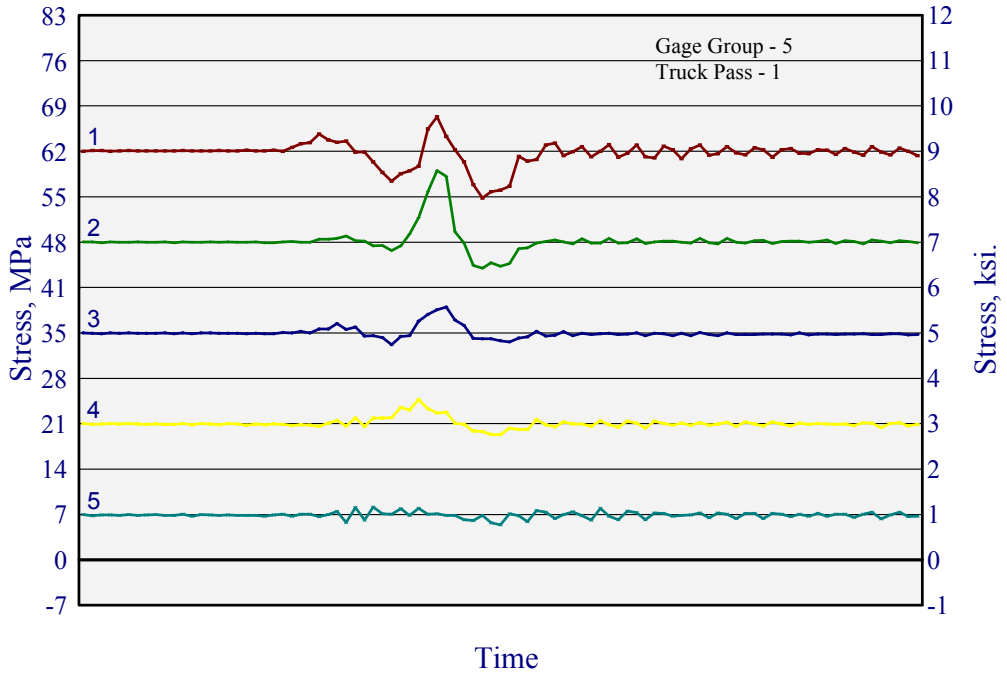

Figure A-7: Bottom flange stress histories for Gage Group 5, Truck Pass 1 (test truck centered in passing plane).

Table A-3: Maximum measured stress ranges and direction for Gage Group 5, Truck Pass 1 (test truck centered in passing lane).

Number	Location	Max. Stress Range, MPa	Max. Stress Range, ksi
1	Bottom flange, Girder No. 1	12 (C)	1.8 (C)
2	Bottom flange, Girder No. 2	15 (T)	2.2 (T)
3	Bottom flange, Girder No. 3	5.5 (T)	0.8 (T)
4	Bottom flange, Girder No. 4	5.5 (T)	0.8 (T)
5	Bottom flange, Girder No. 5	2.8 (T)	0.4 (T)
6	Web, Girder No. 2	2.8 (C)	0.4 (C)
7	Web, Girder No. 3	4.8 (C)	0.7 (C)
8	Web, Girder No. 4	1.4 (T)	0.2 (T)

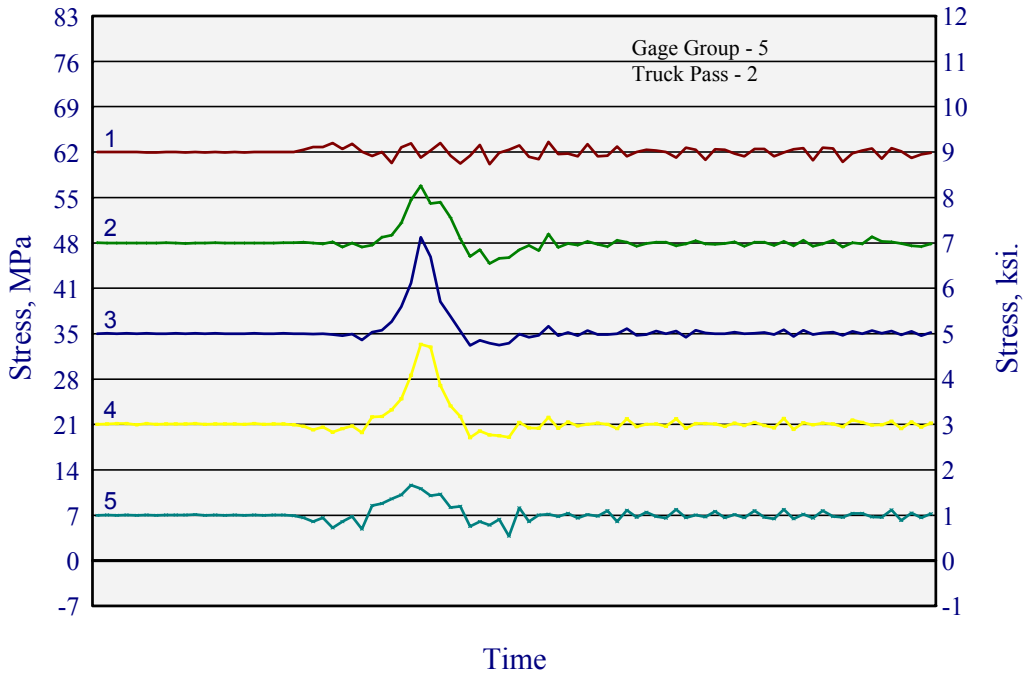

Figure A-8: Bottom flange stress histories for Gage Group 5, Truck Pass 2 (test truck centered in driving lane).

Table A-4: Maximum measured stress ranges and direction for Gage Group 5, Truck Pass 2 (test truck centered in driving lane).

Gage Number	Location	Max. Stress Range, MPa	Max. Stress Range, ksi
1	Bottom flange, Girder No. 1	3.5 (C)	0.5 (C)
2	Bottom flange, Girder No. 2	12 (T)	1.7 (T)
3	Bottom flange, Girder No. 3	17 (T)	2.4 (T)
4	Bottom flange, Girder No. 4	14 (T)	2.1 (T)
5	Bottom flange, Girder No. 5	7.6 (T)	1.1 (T)
6	Web, Girder No. 2	0.7 (T)	0.1 (T)
7	Web, Girder No. 3	2.1 (T)	0.3 (T)
8	Web, Girder No. 4	0.7 (C)	0.1 (C)

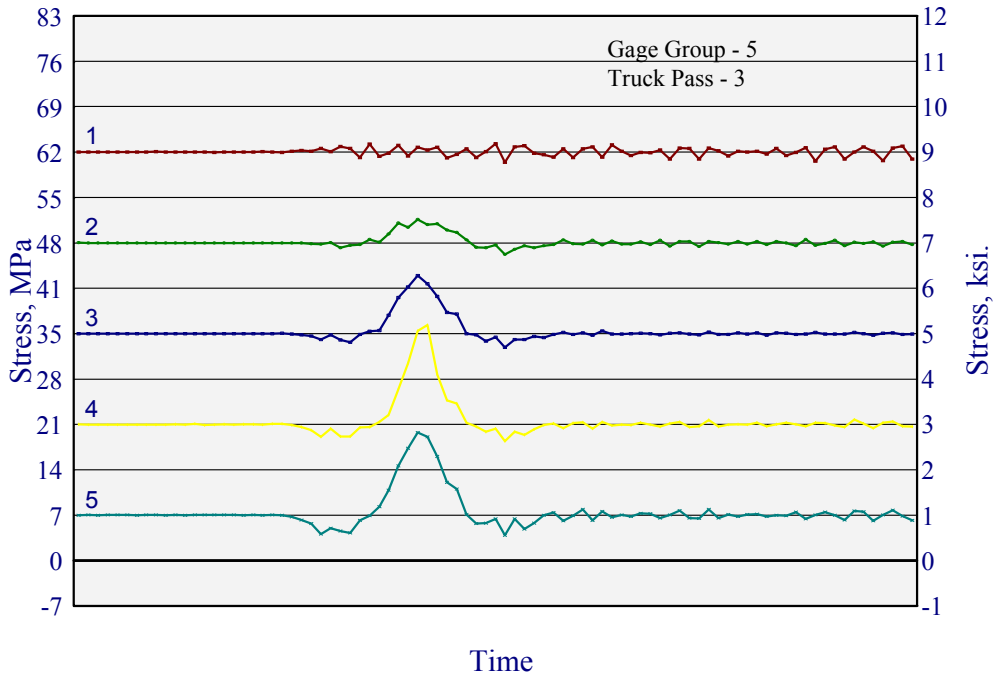

Figure A-9: Bottom flange stress histories for Gage Group 5 Truck Pass 3 (test truck centered in right shoulder).

Table A-5: Maximum measured stress ranges and direction for Gage Group 5, Truck Pass 3 (test truck centered in right shoulder).

Gage Number	Location	Max. Stress Range, MPa	Max. Stress Range, ksi
1	Bottom flange, Girder No. 1	2.8 (C)	0.4 (C)
2	Bottom flange, Girder No. 2	5.5 (T)	0.8 (T)
3	Bottom flange, Girder No. 3	11 (T)	1.6 (T)
4	Bottom flange, Girder No. 4	18 (T)	2.6 (T)
5	Bottom flange, Girder No. 5	16 (T)	2.3 (T)
6	Web, Girder No. 2	0.7 (C)	0.1 (C)
7	Web, Girder No. 3	0.3 (T)	0.05 (T)
8	Web, Girder No. 4	0.7 (T)	0.1 (T)

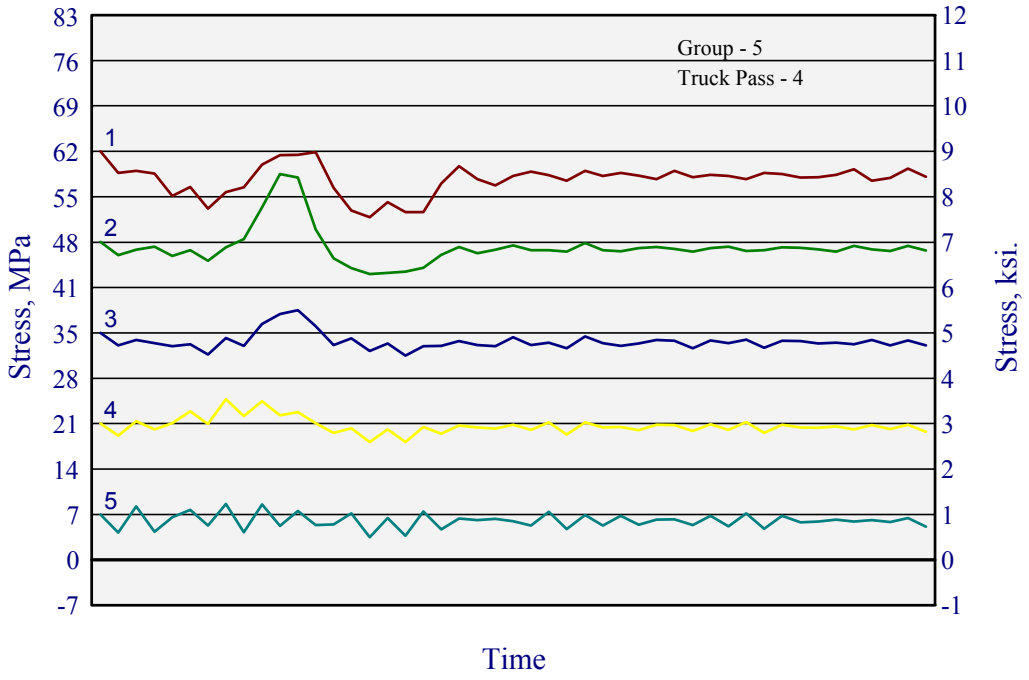

Figure A-10: Bottom flange stress histories for Gage Group 5, Truck Pass 4 (test truck centered in passing lane).

Table A-6: Maximum measured stress ranges and direction for Gage Group 5, Truck Pass 4 (test truck centered in passing lane).

Gage Number	Location	Max. Stress Range, MPa	Max. Stress Range, ksi
1	Bottom flange, Girder No. 1	10 (C)	1.5 (C)
2	Bottom flange, Girder No. 2	15 (T)	2.2 (T)
3	Bottom flange, Girder No. 3	6.9 (C)	1.0 (C)
4	Bottom flange, Girder No. 4	6.2 (T)	0.9 (T)
5	Bottom flange, Girder No. 5	4.8 (C)	0.7 (C)
6	Web, Girder No. 2	3.5 (C)	0.5 (C)
7	Web, Girder No. 3	1.4 (T)	0.2 (T)
8	Web, Girder No. 4	0.7 (T&C)	0.1 (T&C)

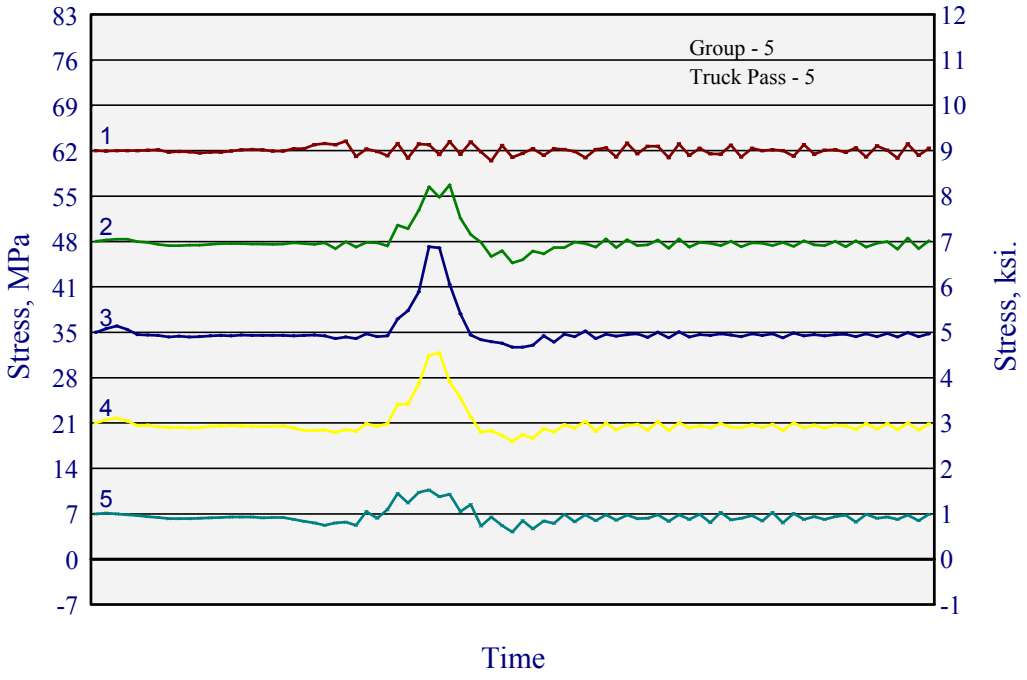

Figure A-11: Bottom flange stress histories for Gage Group 5, Truck Pass 5 (test truck centered in driving lane).

Table A-7: Maximum measured stress ranges and direction for Gage Group 5, Truck Pass 5 (test truck centered in driving lane).

Gage Number	Location	Max. Stress Range, MPa	Max. Stress Range, ksi
1	Bottom flange, Girder No. 1	2.8 (C)	0.4 (C)
2	Bottom flange, Girder No. 2	12 (T)	1.7 (T)
3	Bottom flange, Girder No. 3	15 (T)	2.2 (T)
4	Bottom flange, Girder No. 4	13 (T)	1.9 (T)
5	Bottom flange, Girder No. 5	6.2 (T)	0.9 (T)
6	Web, Girder No. 2	0.7 (C)	0.1 (C)
7	Web, Girder No. 3	1.4 (T)	0.2 (T)
8	Web, Girder No. 4	0.7 (C)	0.1 (C)

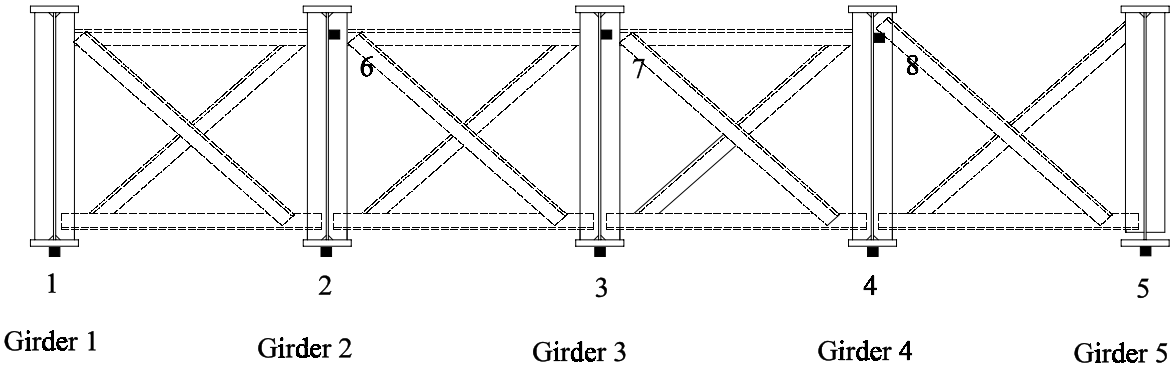

Figure A-12: Gage Group No. 8-2 location, in-line on the skew (positive moment region).

Table A-8: Gage locations for Group No. 8-2.

Gage Number	Position
1	bottom flange, Girder No. 1
2	bottom flange, Girder No. 2
3	bottom flange, Girder No. 3
4	bottom flange, Girder No. 4
5	bottom flange, Girder No. 5
6	web plate, Girder No. 2, long. direction (191 mm (7.5 in below flange)
7	web plate, Girder No. 3, long. direction (191 mm (7.5 in) below flange)
8	web plate, Girder No. 3, long. direction (191 mm (7.5 in) below flange)

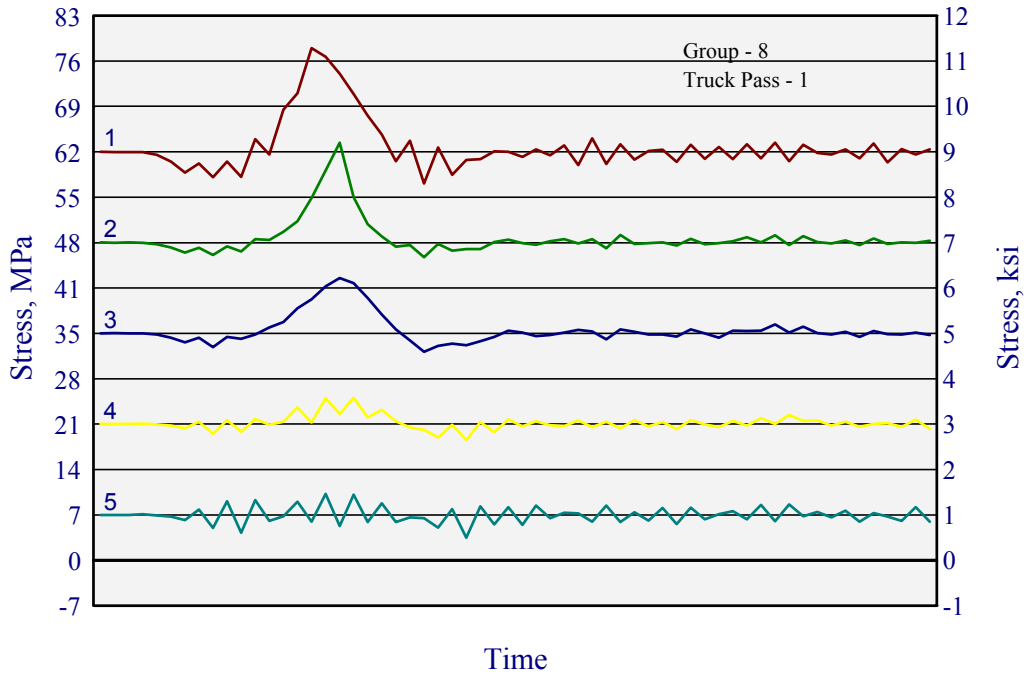

Figure A-13: Bottom flange stress histories for Gage Group 8, Truck Pass 1 (test truck centered in passing lane).

Table A-9: Maximum measured stress ranges and direction for Gage Group 8, Truck Pass 1 (test truck centered in passing lane).

Gage Number	Location	Max. Stress Range, MPa	Max. Stress Range, ksi
1	Bottom flange, Girder No. 1	21 (T)	3.0 (T)
2	Bottom flange, Girder No. 2	17 (T)	2.5 (T)
3	Bottom flange, Girder No. 3	11 (T)	1.6 (T)
4	Bottom flange, Girder No. 4	6.2 (T)	0.9 (T)
5	Bottom flange, Girder No. 5	7.0 (C)	1.0 (C)
6	Web, Girder No. 2	1.4 (T)	0.2 (T)
7	Web, Girder No. 3	0.7 (T)	0.1 (T)
8	Web, Girder No. 4	0.7 (C)	0.1 (C)

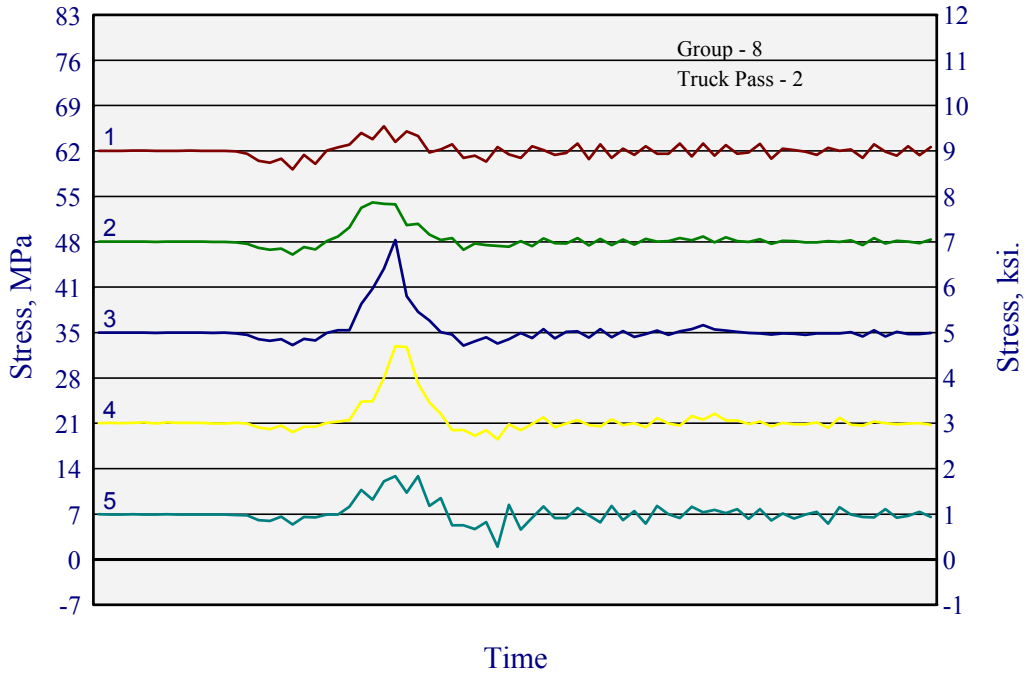

Figure A-14: Bottom flange stress histories for Gage Group 8, Truck Pass 2 (test truck centered in driving lane).

Table A-10: Maximum measured stress ranges and direction for Gage Group 8, Truck Pass 2 (test truck centered in driving lane).

Gage Number	Location	Max. Stress Range, MPa	Max. Stress Range, ksi
1	Bottom flange, Girder No. 1	7.0 (T)	1.0 (T)
2	Bottom flange, Girder No. 2	8.3 (T)	1.2 (T)
3	Bottom flange, Girder No. 3	16 (T)	2.3 (T)
4	Bottom flange, Girder No. 4	14 (T)	2.0 (T)
5	Bottom flange, Girder No. 5	11 (T)	1.6 (T)
6	Web, Girder No. 2	0.7 (T)	0.1 (T)
7	Web, Girder No. 3	2.1 (C)	0.3 (C)
8	Web, Girder No. 4	0.7 (C)	0.1 (C)

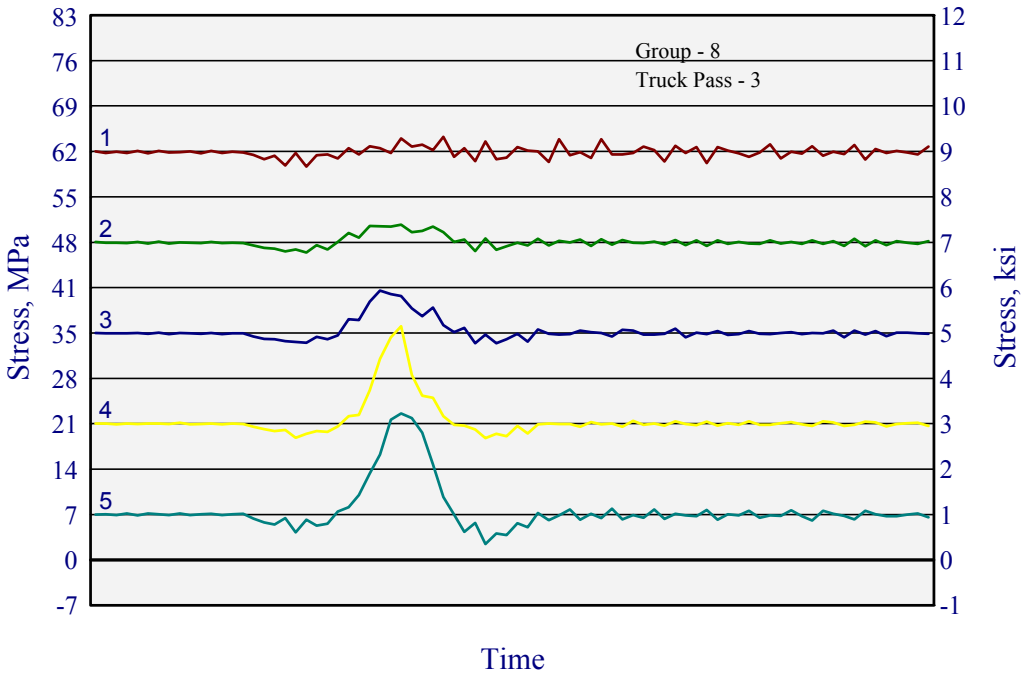

Figure A-15: Flange stress histories for Gage Group 8 Truck Pass 3 (test truck centered in right shoulder).

Table A-11: Maximum measured stress ranges and direction for Gage Group 8, Truck Pass 3 (test truck centered in right shoulder).

Gage Number	Location	Max. Stress Range, MPa	Max. Stress Range, ksi
1	Bottom flange, Girder No. 1	4.8 (C)	0.7 (C)
2	Bottom flange, Girder No. 2	4.1 (T)	0.6 (T)
3	Bottom flange, Girder No. 3	8.3 (T)	1.2 (T)
4	Bottom flange, Girder No. 4	17 (T)	2.5 (T)
5	Bottom flange, Girder No. 5	20 (T)	2.9 (T)
6	Web, Girder No. 2	0.7 (T)	0.1 (T)
7	Web, Girder No. 3	0.7 (C)	0.1 (C)
8	Web, Girder No. 4	0.7 (C)	0.1 (C)

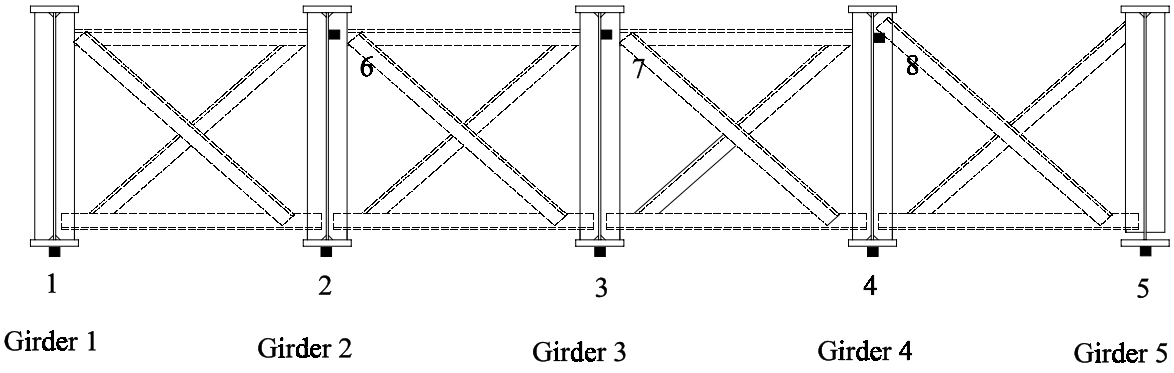

Figure A-16: Gage Group No. 9-2 location, in-line on the skew (negative moment region).

Table A-12: Gage locations for Group No. 9-2.

Gage Number	Position
1	bottom flange, Girder No. 1
2	bottom flange, Girder No. 2
3	bottom flange, Girder No. 3
4	bottom flange, Girder No. 4
5	bottom flange, Girder No. 5
6	web plate, Girder No. 2, long. direction (191 mm (7.5 in) below flange)
7	web plate, Girder No. 3, long. direction (191 mm (7.5 in) below flange)
8	web plate, Girder No. 3, long. direction (191 mm (7.5 in) below flange)

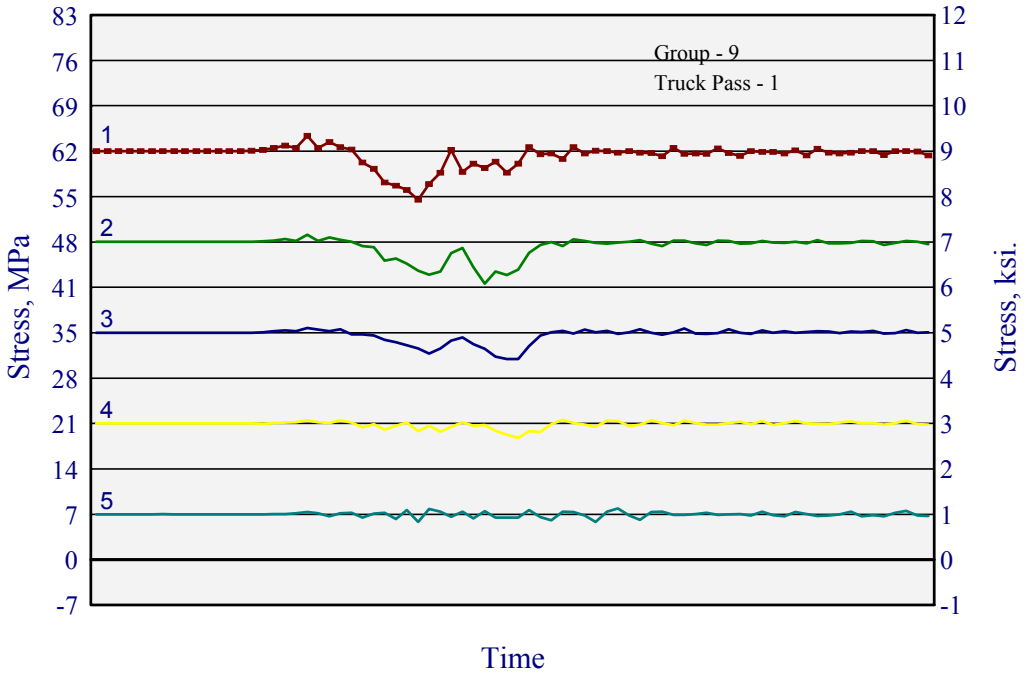

Figure A-17: Bottom flange stress histories for Gage Group 9, Truck Pass 1 (test truck centered in passing lane).

Table A-13: Maximum measured stress ranges and direction for Gage Group 9, Truck Pass 1 (test truck centered in passing lane).

Gage Number	Location	Max. Stress Range, MPa	Max. Stress Range, ksi
1	Bottom flange, Girder No. 1	10 (C)	1.4 (C)
2	Bottom flange, Girder No. 2	7.6 (C)	1.1 (C)
3	Bottom flange, Girder No. 3	4.8 (C)	0.7 (C)
4	Bottom flange, Girder No. 4	2.8 (C)	0.4 (C)
5	Bottom flange, Girder No. 5	2.1 (C)	0.3 (C)
6	Web, Girder No. 2	3.5 (T)	0.5 (T)
7	Web, Girder No. 3	1.4 (T)	0.2 (T)
8	Web, Girder No. 4	0.7 (C)	0.1 (C)

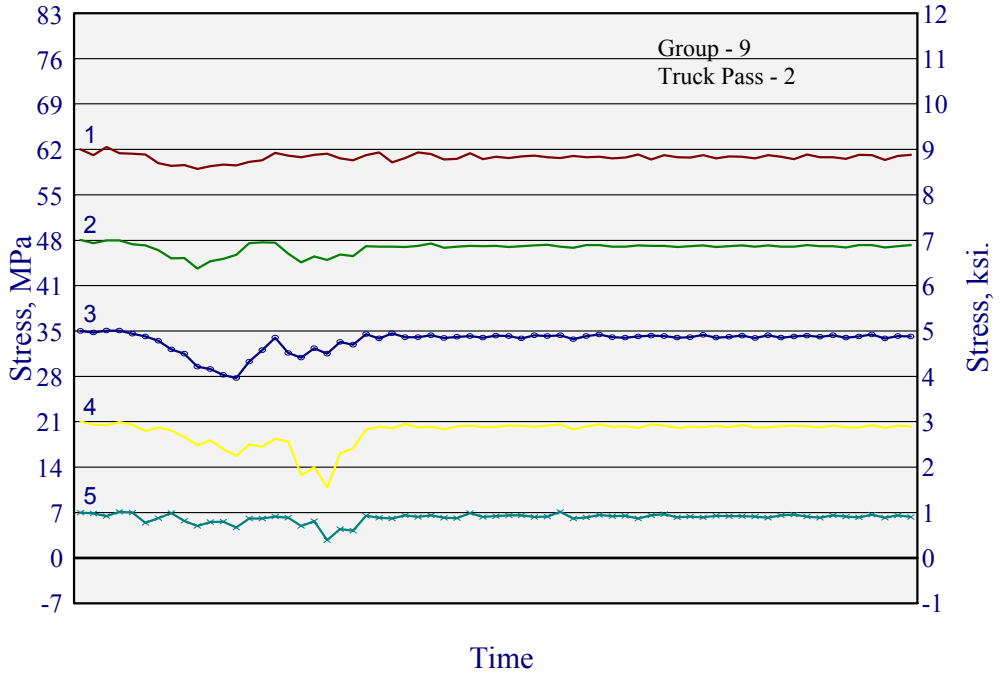

Figure A-18: Bottom flange stress histories for Gage Group 9, Truck Pass 2 (test truck centered in driving lane).

Table A-14: Maximum measured stress ranges and direction for Gage Group 9, Truck Pass 2 (test truck centered in driving lane).

Gage Number	Location	Max. Stress Range, MPa	Max. Stress Range, ksi
1	Bottom flange, Girder No. 1	3.5 (C)	0.5 (C)
2	Bottom flange, Girder No. 2	4.1 (C)	0.6 (C)
3	Bottom flange, Girder No. 3	7.6 (C)	1.1 (C)
4	Bottom flange, Girder No. 4	10 (C)	1.4 (C)
5	Bottom flange, Girder No. 5	4.1 (C)	0.6 (C)
6	Web, Girder No. 2	1.4 (T)	0.2 (T)
7	Web, Girder No. 3	4.8 (T)	0.7 (T)
8	Web, Girder No. 4	2.1 (T)	0.3 (T)

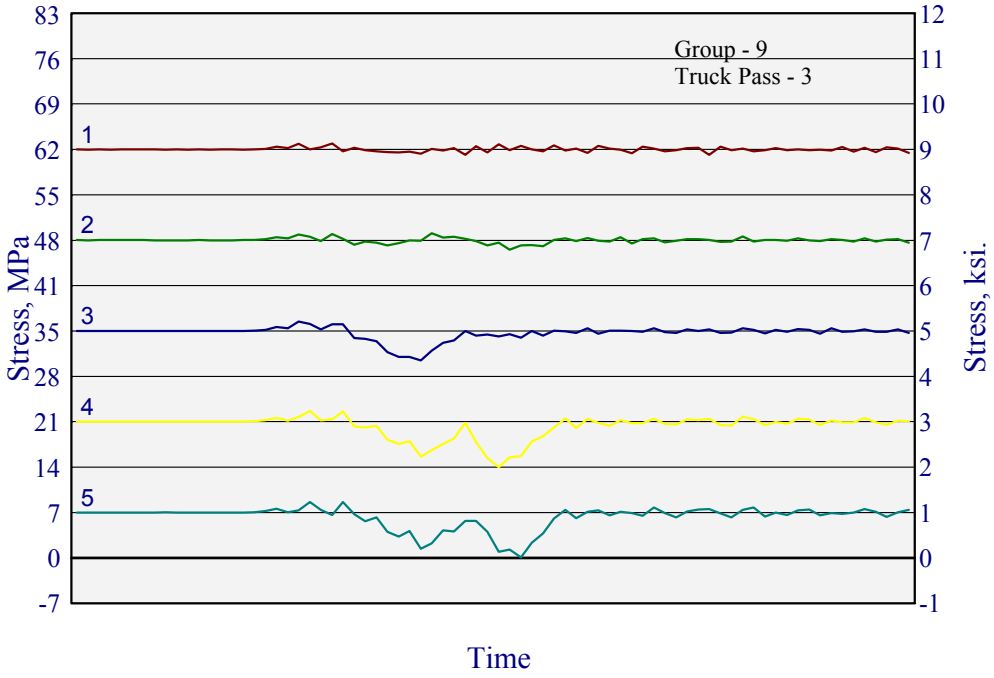

Figure A-19: Bottom flange stress histories for Gage Group 9, Truck Pass 3 (test truck centered in right shoulder).

Table A-15: Maximum measured stress ranges and direction for Gage Group 9, Truck Pass 3 (test truck centered in right shoulder).

Gage Number	Location	Max. Stress Range, MPa	Max. Stress Range, ksi
1	Bottom flange, Girder No. 1	1.4 (T)	0.2 (T)
2	Bottom flange, Girder No. 2	2.8 (C)	0.4 (C)
3	Bottom flange, Girder No. 3	6.2 (C)	0.9 (C)
4	Bottom flange, Girder No. 4	8.3 (C)	1.2 (C)
5	Bottom flange, Girder No. 5	8.3 (C)	1.2 (C)
6	Web, Girder No. 2	0.7 (T)	0.1 (T)
7	Web, Girder No. 3	1.4 (T)	0.2 (T)
8	Web, Girder No. 4	2.1 (T)	0.3 (T)

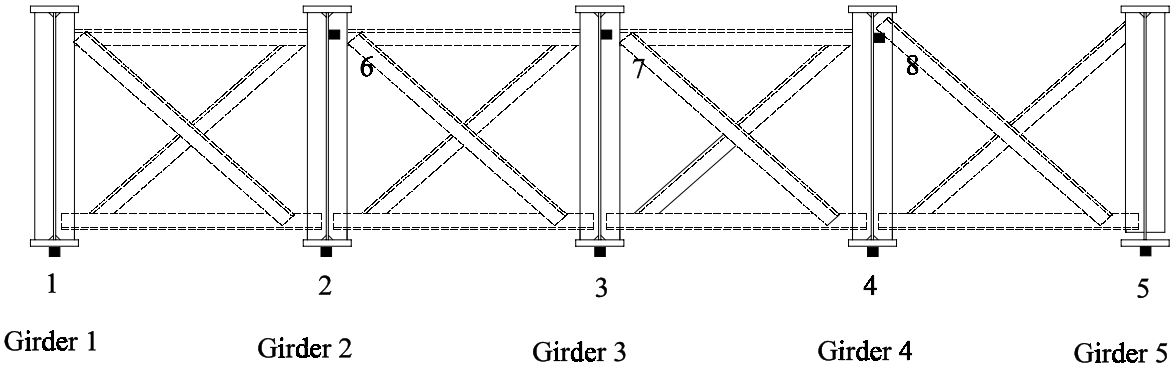

Figure A-20: Gage Group No. 10-2 location, Diaphragm Line 42 (positive bending moment region).

Table A-16: Gage locations for Group No. 10-2.

Gage Number	Position
1	bottom flange, Girder No. 1
2	bottom flange, Girder No. 2
3	bottom flange, Girder No. 3
4	bottom flange, Girder No. 4
5	bottom flange, Girder No. 5
6	web plate, Girder No. 2, long. direction (191 mm (7.5 in) below flange)
7	web plate, Girder No. 3, long. direction (191 mm (7.5 in) below flange)
8	web plate, Girder No. 3, long. direction (191 mm (7.5 in) below flange)

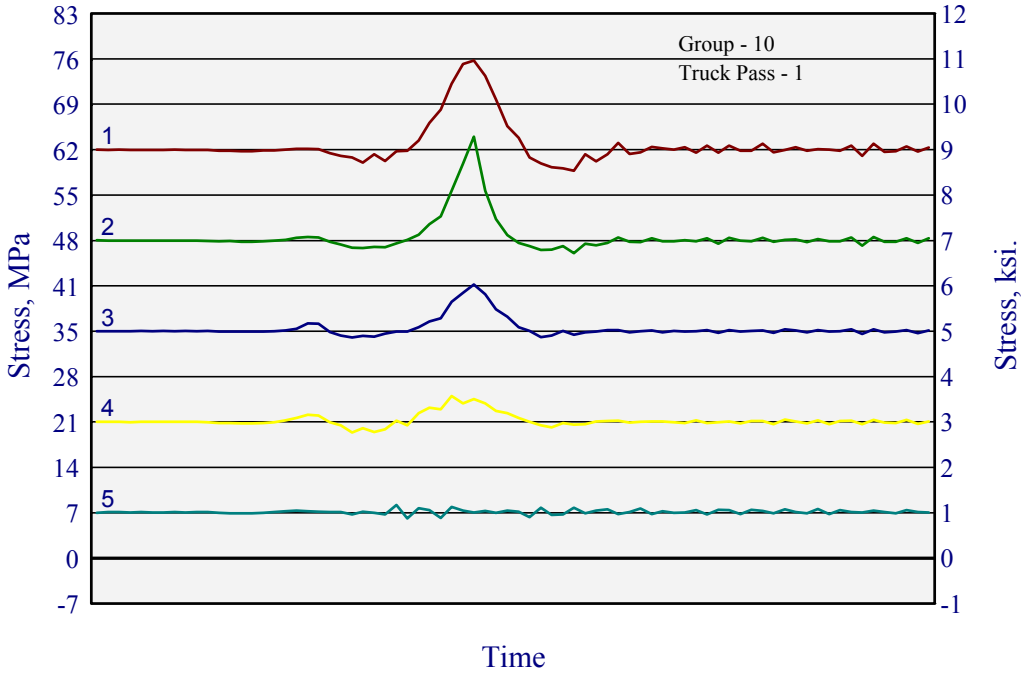

Figure A-21: Bottom flange stress histories for Gage Group 10, Truck Pass 1 (test truck centered in passing lane).

Table A-17: Maximum measured stress ranges and direction for Gage Group 10, Truck Pass 1 (test truck centered in passing lane).

Gage Number	Location	Max. Stress Range, MPa	Max. Stress Range, ksi
1	Bottom flange, Girder No. 1	17 (T)	2.4 (T)
2	Bottom flange, Girder No. 2	18 (T)	2.6 (T)
3	Bottom flange, Girder No. 3	8.3 (T)	1.2 (T)
4	Bottom flange, Girder No. 4	5.5 (T)	0.8 (T)
5	Bottom flange, Girder No. 5	2.1 (T)	0.3 (T)
6	Web, Girder No. 2	1.4 (T)	0.2 (T)
7	Web, Girder No. 3	0.7 (C)	0.1 (C)
8	Web, Girder No. 4	0.7 (C)	0.1 (C)

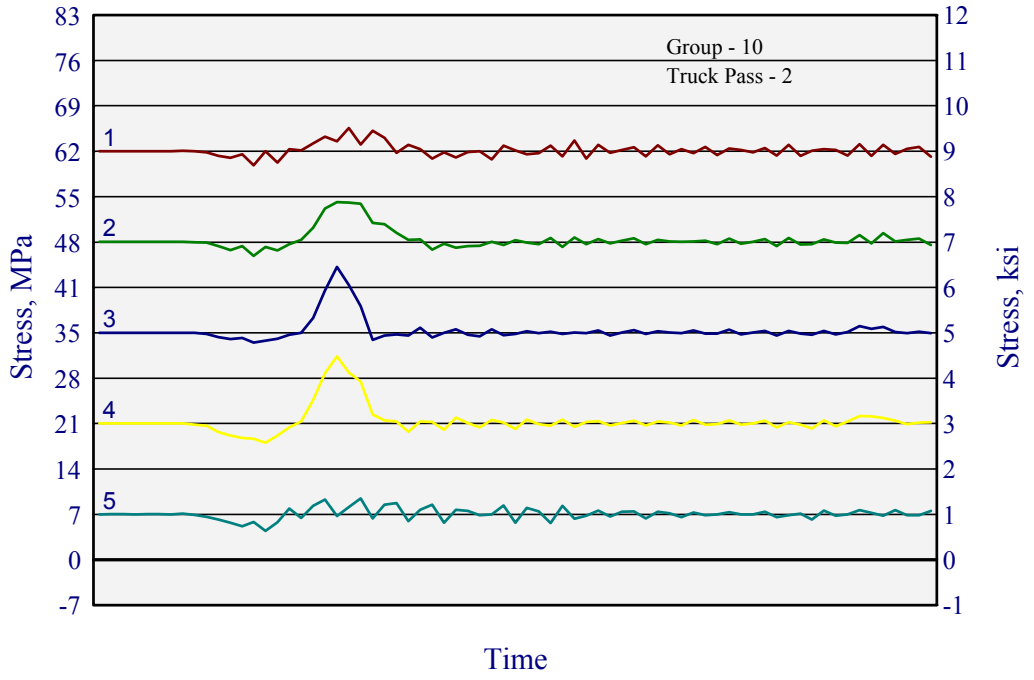

Figure A-22: Bottom flange stress histories for Gage Group 10, Truck Pass 2 (test truck centered in driving lane).

Table A-18: Maximum measured stress ranges and direction for Gage Group 10, Truck Pass 2 (test truck centered in driving lane).

Gage Number	Location	Max. Stress Range, MPa	Max. Stress Range, ksi
1	Bottom flange, Girder No. 1	5.5 (T)	0.8 (T)
2	Bottom flange, Girder No. 2	8.3 (T)	1.2 (T)
3	Bottom flange, Girder No. 3	12 (T)	1.7 (T)
4	Bottom flange, Girder No. 4	13 (T)	1.9 (T)
5	Bottom flange, Girder No. 5	4.8 (C)	0.7 (C)
6	Web, Girder No. 2	0.7 (T)	0.1 (T)
7	Web, Girder No. 3	0.7 (C)	0.1 (C)
8	Web, Girder No. 4	1.4 (T)	0.2 (T)

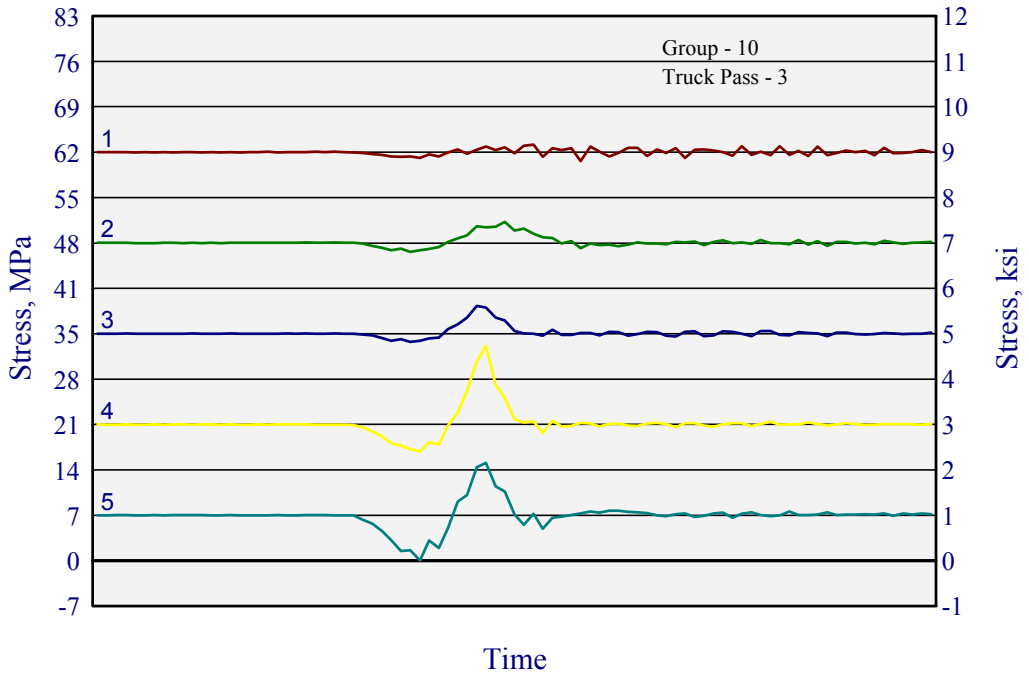

Figure A-23: Bottom flange stress histories for Gage Group 10, Truck Pass 3 (test truck centered in right shoulder).

Table A-19: Maximum measured stress ranges and direction for Gage Group 10, Truck Pass 3 (test truck centered in right shoulder).

Gage Number	Location	Max. Stress Range, MPa	Max. Stress Range, ksi
1	Bottom flange, Girder No. 1	2.8 (C)	0.4 (C)
2	Bottom flange, Girder No. 2	4.8 (T)	0.7 (T)
3	Bottom flange, Girder No. 3	5.5 (T)	0.8 (T)
4	Bottom flange, Girder No. 4	16 (T)	2.3 (T)
5	Bottom flange, Girder No. 5	15 (T)	2.2 (T)
6	Web, Girder No. 2	0.7 (T)	0.1 (T)
7	Web, Girder No. 3	0.7 (T)	0.1 (T)
8	Web, Girder No. 4	1.4 (T)	0.2 (T)

APPENDIX - B

STRESS HISTORIES

for

MIDLAND COUNTY BRIDGE
(IH-20 Eastbound)
FIELD TEST 3
(New Diaphragms)

Test Date
November 11-12, 1992

Table B-1: Summary of recorded test truck passages, Field Test No. 3.

Filename	Gage Group	Truck Pass	Truck Position	Number of Scans
M5PS1	5	1	Truck centered in passing lane	96
M5PS2	5	2	Truck centered in driving lane	80
M5PS3	5	3	Truck centered in right shoulder	81
M8PS1	8	1	Truck centered in driving lane	121
M8PS2	8	2	Truck centered in right shoulder	106
M8PS3	8	3	Truck centered right shoulder	96
M9PS1	9	1	Truck centered in passing lane	110
M9PS2	9	2	Truck centered in driving lane	100
M9PS3	9	3	Truck centered in right shoulder	88
M10PS1	10	1	Truck centered in passing lane	83
M10PS2	10	2	Truck centered in driving lane	72
M10PS3	10	3	Truck centered in right shoulder	78
M11PS1	11	1	Truck centered in passing lane	85
M11PS2	11	2	Truck centered in driving lane	69
M11PS3	11	3	Truck centered in right shoulder	84
M12PS1	12	1	Truck centered in passing lane	103
M12PS2	12	2	Truck centered in driving lane	83
M12PS3	12	3	Truck centered in right shoulder	87
M13PS1	13	1	Truck centered in passing lane	86
M13PS2	13	2	Truck centered in driving lane	98
M13PS3	13	3	Truck centered in right shoulder	86
M14PS1	14	1	Truck centered in passing lane	110
M14PS2	14	2	Truck centered in driving lane	67
M14PS3	14	3	Truck centered in right shoulder	70

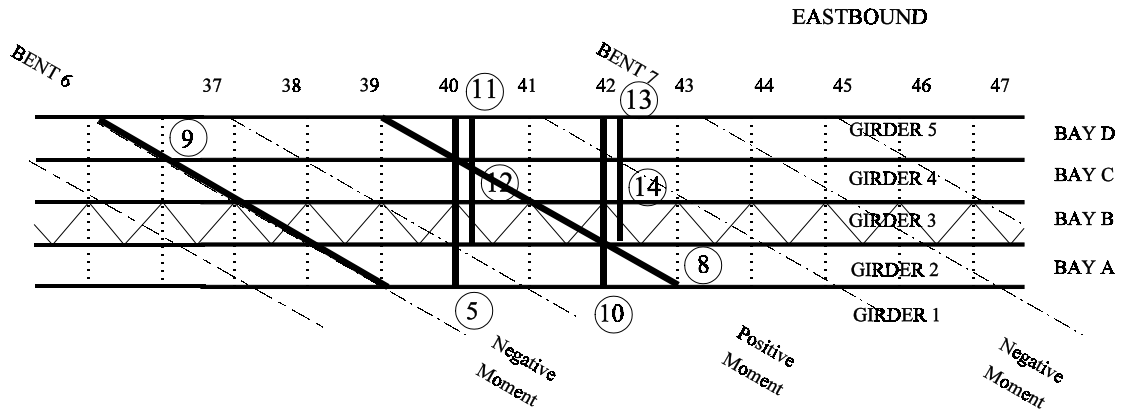

Figure B-1: Gage group locations on Eastbound structure, Field Test No. 3.

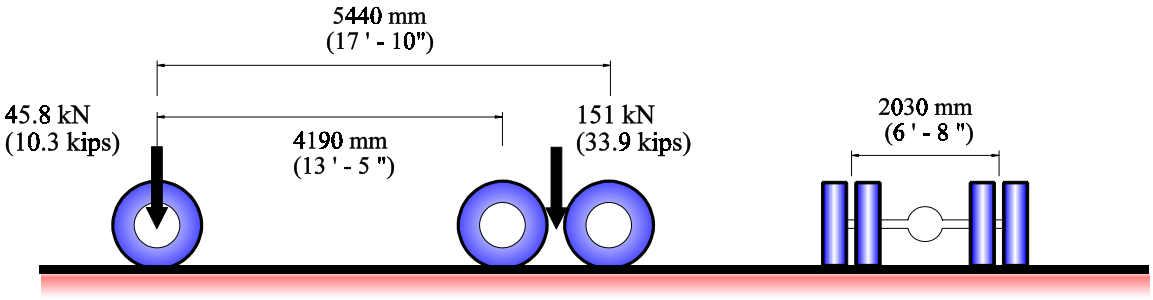

Figure B-2: Test truck axial weight and configuration, Field Test No. 3.

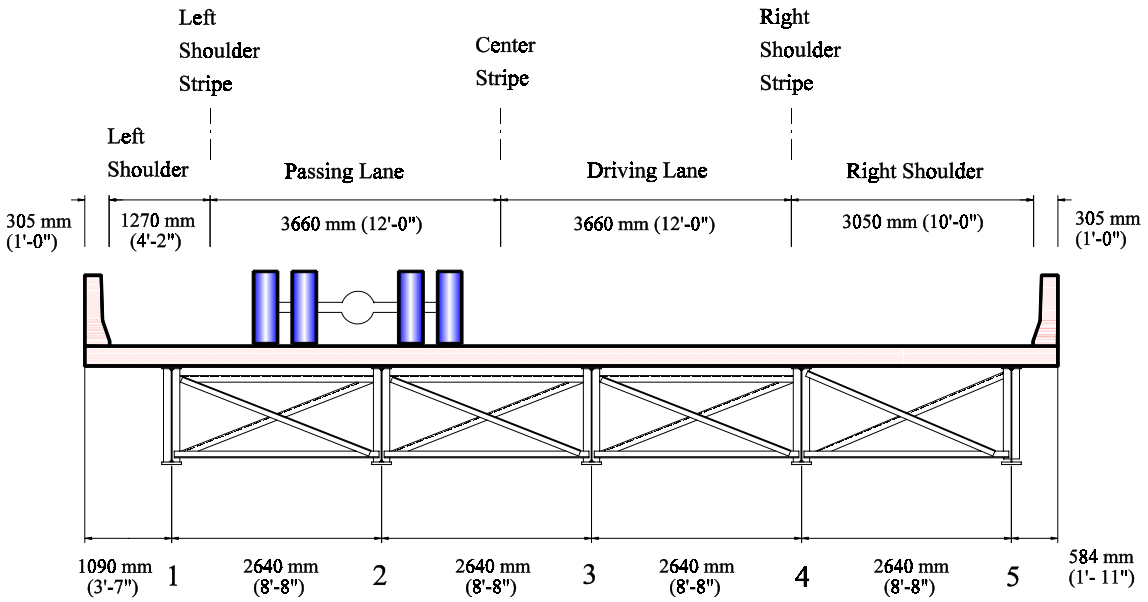

Figure B-3: Location for test truck positioned in center of passing lane (Pass No. 1).

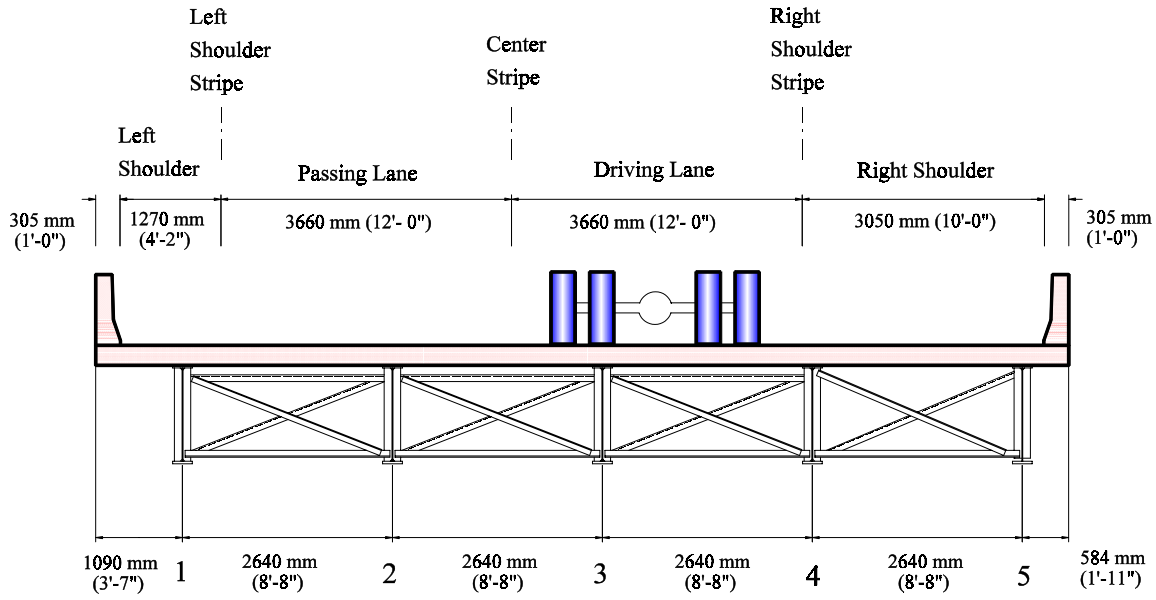

Figure B-4: Location for test truck positioned in center of driving lane (Pass No. 2).

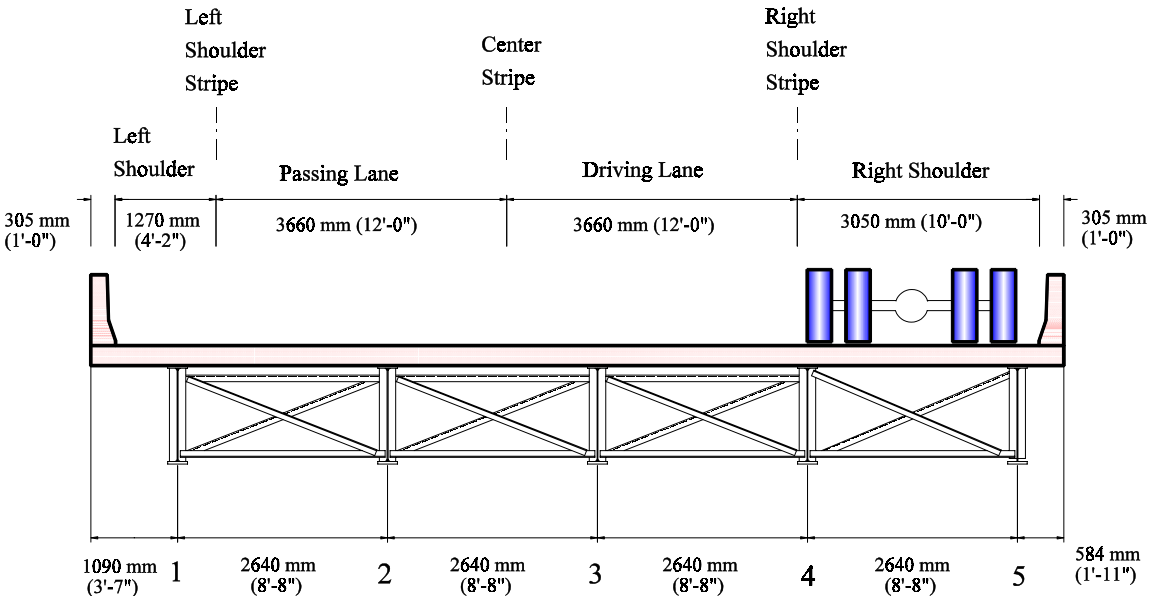

Figure B-5: Location for test truck positioned in center of right shoulder lane (Pass No. 3).

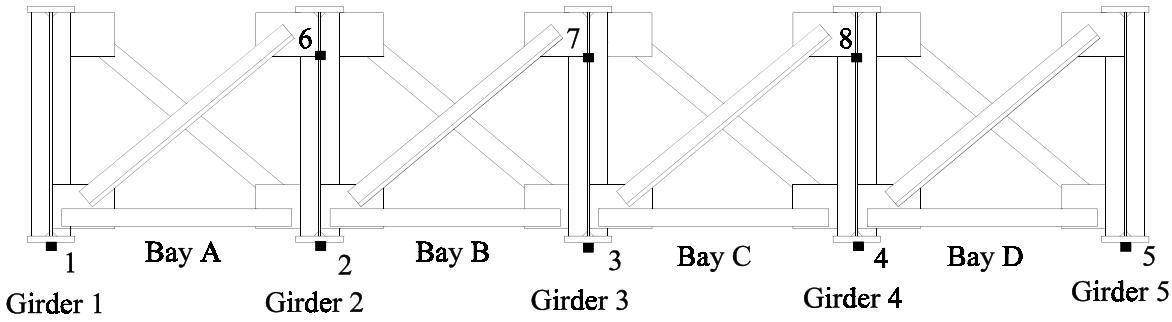

Figure B-6: Gage Group No. 5-3, Diaphragm Line 40 (positive bending moment region).

Table B-2: Gage locations for Group No. 5-3.

Gage Number	Position
1	bottom flange, Girder No. 1
2	bottom flange, Girder No. 2
3	bottom flange, Girder No. 3
4	bottom flange, Girder No. 4
5	bottom flange, Girder No. 5
6	web plate, Girder No. 2, long. direction (191 mm (7.5 in) below flange)
7	web plate, Girder No. 3, long. direction (191 mm (7.5 in) below flange)
8	web plate, Girder No. 4, long. direction (191 mm (7.5 in) below flange)

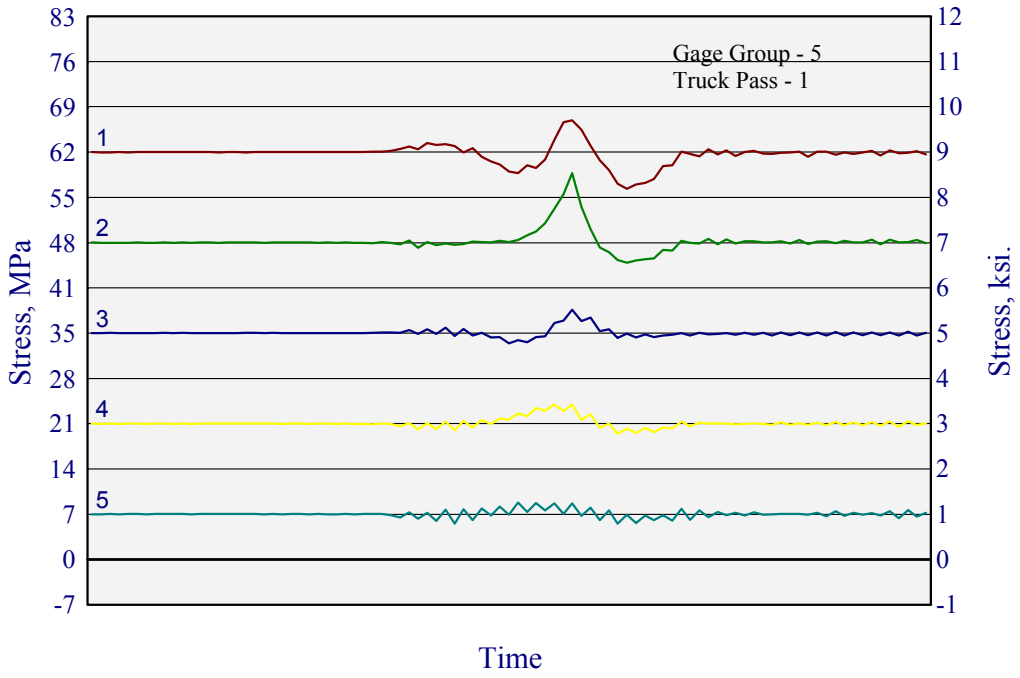

Figure B-7: Bottom flange stress histories for Gage Group 5, Truck Pass 1 (test truck centered in passing lane).

Table B-3: Maximum measured stress ranges and direction for Gage Group 5, Truck Pass 1 (test truck centered in passing lane).

Gage Number	Location	Max. Stress Range, MPa	Max. Stress Range, ksi
1	Bottom flange, Girder No. 1	10 (C)	1.5 (C)
2	Bottom flange, Girder No. 2	13 (T)	1.9 (T)
3	Bottom flange, Girder No. 3	4.8 (T)	0.7 (T)
4	Bottom flange, Girder No. 4	4.1 (T)	0.6 (T)
5	Bottom flange, Girder No. 5	3.4 (T)	0.5 (T)
6	Web, Girder No. 2	3.4 (C)	0.5 (C)
7	Web, Girder No. 3	0.7 (T)	0.1 (T)
8	Web, Girder No. 4	0.7 (T)	0.1 (T)

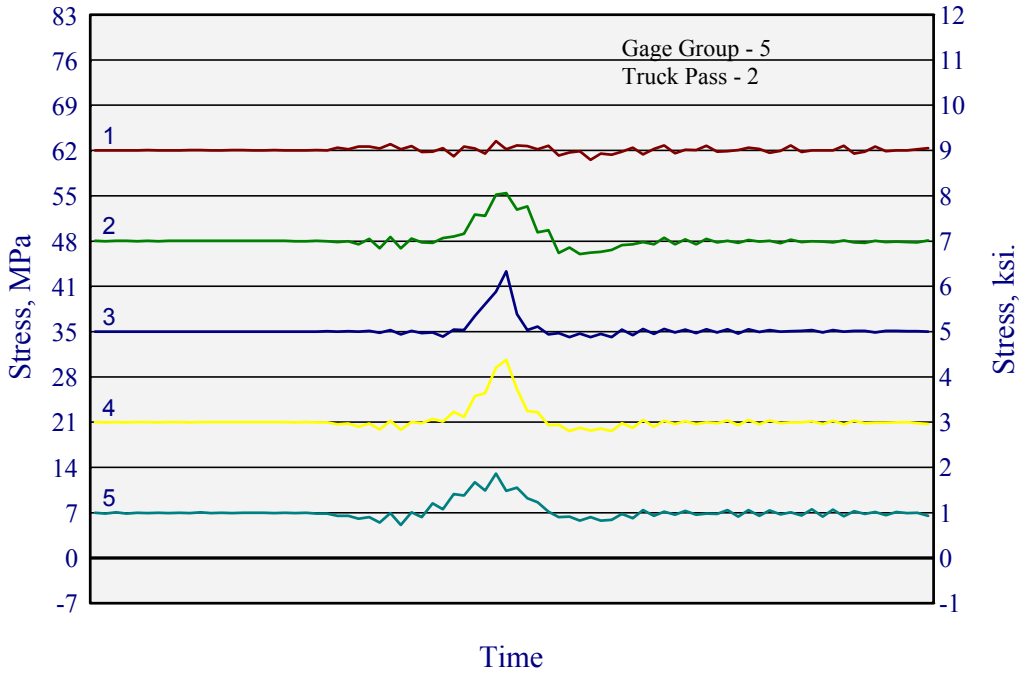

Figure B-8: Bottom flange stress histories for Gage Group 5, Truck Pass 2 (test truck centered in driving lane).

Table B-4: Maximum measured stress ranges and direction for Gage Group 5, Truck Pass 2 (test truck centered in driving lane).

Gage Number	Location	Max. Stress Range, MPa	Max. Stress Range, ksi
1	Bottom flange, Girder No. 1	2.8 (C)	0.4 (C)
2	Bottom flange, Girder No. 2	9.0 (T)	1.3 (T)
3	Bottom flange, Girder No. 3	9.6 (T)	1.4 (T)
4	Bottom flange, Girder No. 4	11 (T)	1.6 (T)
5	Bottom flange, Girder No. 5	7.6 (T)	1.1 (T)
6	Web, Girder No. 2	0.7 (T)	0.1 (T)
7	Web, Girder No. 3	2.8 (T)	0.4 (T)
8	Web, Girder No. 4	0.7 (T)	0.1 (T)

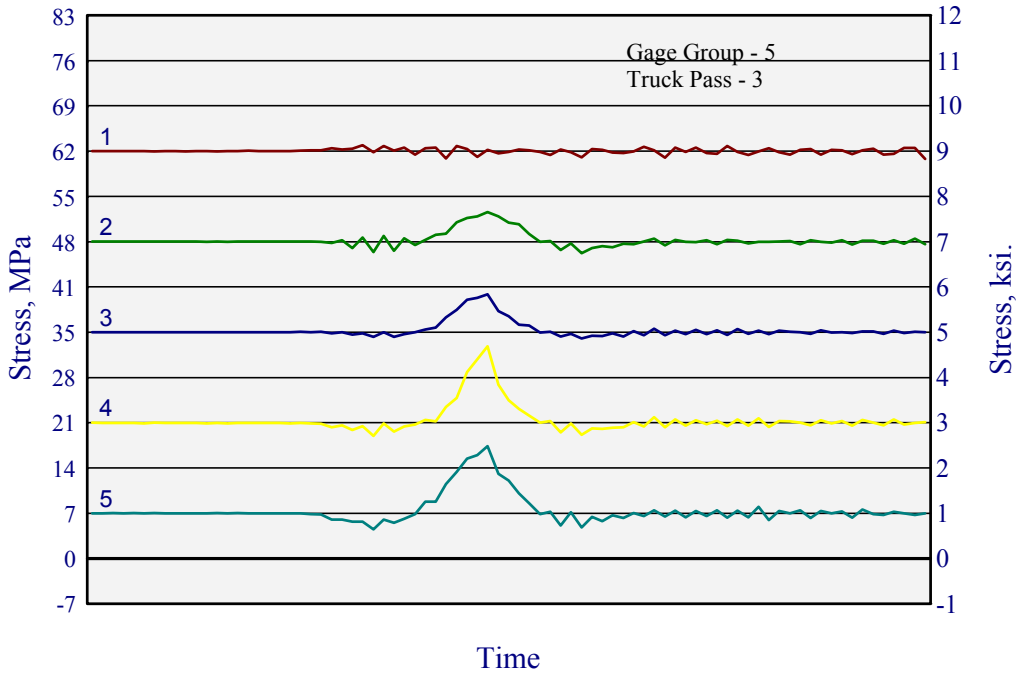

Figure B-9: Bottom flange stress histories for Gage Group 5 Truck Pass 3 (test truck centered in right shoulder).

Table B-5: Maximum measured stress ranges and direction for Gage Group 5, Truck Pass 3 (test truck centered in right shoulder).

Gage Number	Location	Max. Stress Range, ksi	Max. Stress Range, ksi
1	Bottom flange, Girder No. 1	2.1 (C)	0.3 (C)
2	Bottom flange, Girder No. 2	6.2 (T)	0.9 (T)
3	Bottom flange, Girder No. 3	6.9 (T)	1.0 (T)
4	Bottom flange, Girder No. 4	13 (T)	1.9 (T)
5	Bottom flange, Girder No. 5	12 (T)	1.8 (T)
6	Web, Girder No. 2	0.7 (C)	0.1 (C)
7	Web, Girder No. 3	0.7 (T)	0.1 (T)
8	Web, Girder No. 4	0.7 (T)	0.1 (T)

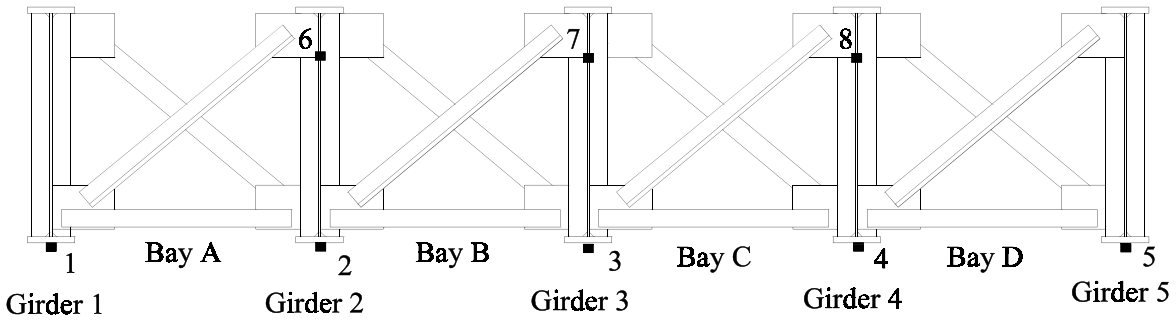

Figure B-10: Gage Group No. 8-3, In-line on the skew (positive bending moment region).

Table B-6: Gage locations for Group No. 8-3.

Gage Number	Position
1	bottom flange, Girder No. 1
2	bottom flange, Girder No. 2
3	bottom flange, Girder No. 3
4	bottom flange, Girder No. 4
5	bottom flange, Girder No. 5
6	web plate, Girder No. 2, long. direction (191 mm (7.5 in) below flange)
7	web plate, Girder No. 3, long. direction (191 mm (7.5 in) below flange)
8	web plate, Girder No. 4, long. direction (191 mm (7.5 in) below flange)

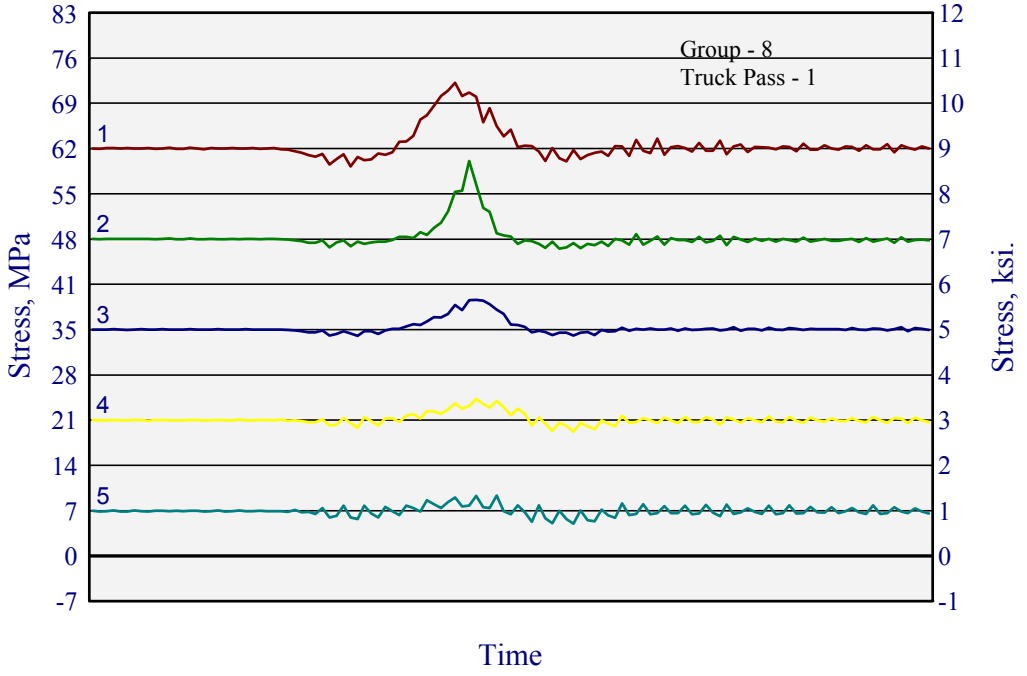

Figure B-11: Bottom flange stress histories for Gage Group 8, Truck Pass 1 (test truck centered in passing lane).

Table B-7: Maximum measured stress ranges and direction for Gage Group 8, Truck Pass 1 (test truck centered in passing lane).

Gage Number	Location	Max. Stress Range, MPa	Max. Stress Range, ksi
1	Bottom flange, Girder No. 1	12 (T)	1.8 (T)
2	Bottom flange, Girder No. 2	13 (T)	1.9 (T)
3	Bottom flange, Girder No. 3	5.5 (T)	0.8 (T)
4	Bottom flange, Girder No. 4	4.9 (T)	0.7 (T)
5	Bottom flange, Girder No. 5	4.1 (T)	0.6 (T)
6	Web, Girder No. 2	---	---
7	Web, Girder No. 3	---	---
8	Web, Girder No. 4	---	---

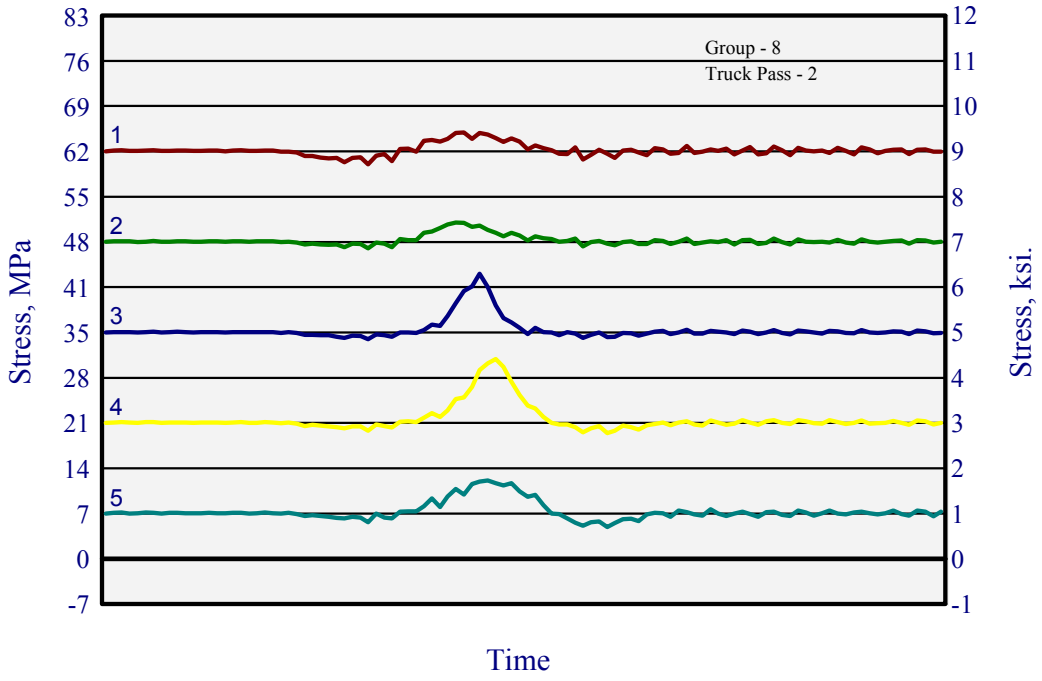

Figure B-12: Bottom flange stress histories for Gage Group 8, Truck Pass 2 (test truck centered in driving lane).

Table B-8: Maximum measured stress ranges and direction for Gage Group 8, Truck Pass 2 (test truck centered in driving lane).

Gage Number	Location	Max. Stress Range, ksi	Max. Stress Range, ksi
1	Bottom flange, Girder No. 1	4.8 (T)	0.7 (T)
2	Bottom flange, Girder No. 2	4.2 (T)	0.6 (T)
3	Bottom flange, Girder No. 3	10 (T)	1.4 (T)
4	Bottom flange, Girder No. 4	11 (T)	1.6 (T)
5	Bottom flange, Girder No. 5	7.0 (T)	1.0 (T)
6	Web, Girder No. 2	---	---
7	Web, Girder No. 3	---	---
8	Web, Girder No. 4	---	---

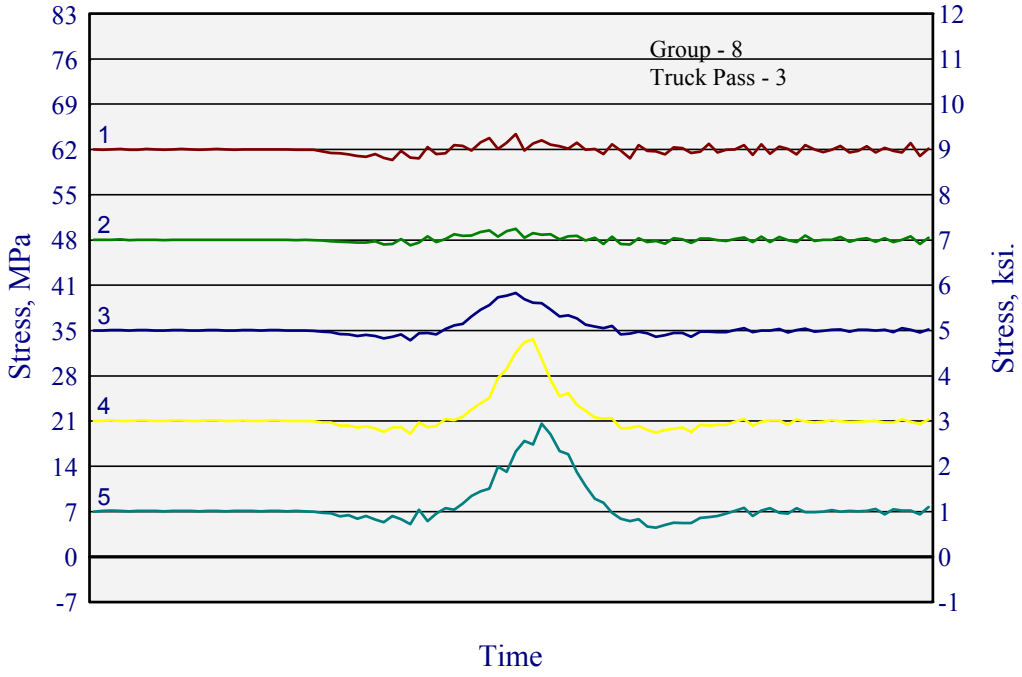

Figure B-13: Bottom flange stress histories for Gage Group 8, Truck Pass 3 (test truck centered in right shoulder).

Table B-9: Maximum measured stress ranges and direction for Gage Group 8, Truck Pass 3 (test truck centered in right shoulder).

Gage Number	Location	Max. Stress Range, ksi	Max. Stress Range, ksi
1	Bottom flange, Girder No. 1	4.1 (T)	0.6 (T)
2	Bottom flange, Girder No. 2	2.8 (T)	0.4 (T)
3	Bottom flange, Girder No. 3	0.7 (T)	1.0 (T)
4	Bottom flange, Girder No. 4	13.8 (T)	2.0 (T)
5	Bottom flange, Girder No. 5	15.8 (T)	2.3 (T)
6	Web, Girder No. 2	---	---
7	Web, Girder No. 3	---	---
8	Web, Girder No. 4	---	---

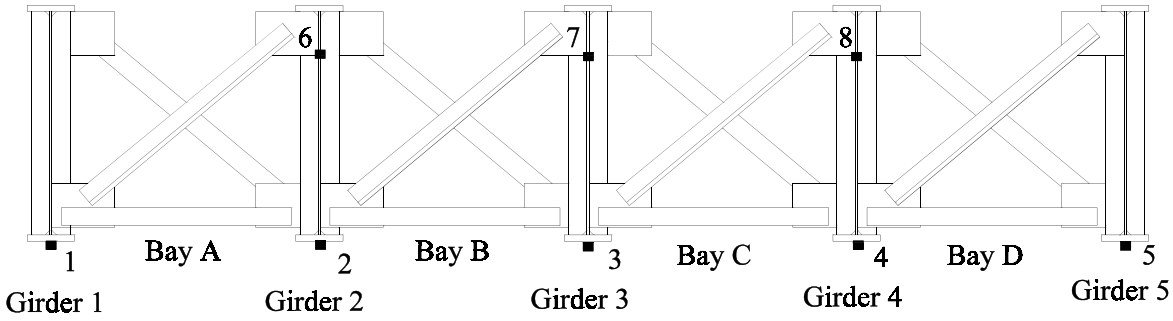

Figure B-14: Gage Group No. 9-3, In-line on the skew, (negative bending moment region).

Table B-10: Gage locations for Group No. 9-3.

Gage Number	Position
1	bottom flange, Girder No. 1
2	bottom flange, Girder No. 1
3	bottom flange, Girder No. 3
4	bottom flange, Girder No. 4
5	bottom flange, Girder No. 5
6	web plate, Girder No. 2, long. direction (191 mm (7.5 in) below flange)
7	web plate, Girder No. 3, long. direction (191 mm (7.5 in) below flange)
8	web plate, Girder No. 4, long. direction (191 mm (7.5 in) below flange)

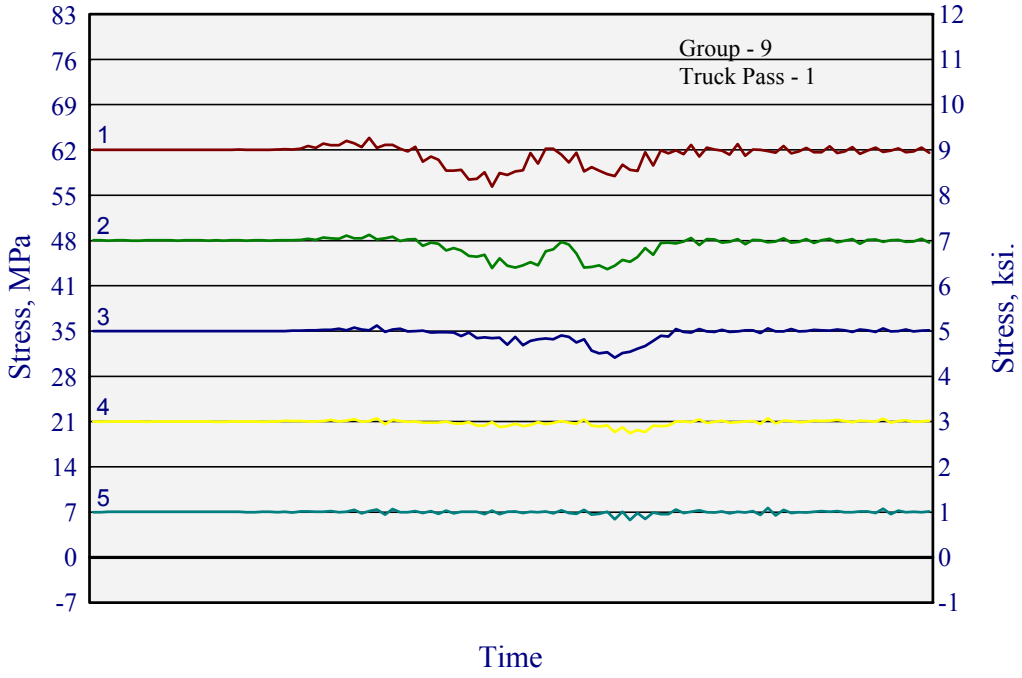

Figure B-15: Bottom flange stress histories for Gage Group 9, Truck Pass 1 (test truck centered in passing lane).

Table B-11: Maximum measured stress ranges and direction for Gage Group 9, Truck Pass 1 (test truck centered in passing lane).

Gage Number	Location	Max. Stress Range, MPa	Max. Stress Range, ksi
1	Bottom flange, Girder No. 1	7.6 (C)	1.1 (C)
2	Bottom flange, Girder No. 2	4.8 (C)	0.7 (C)
3	Bottom flange, Girder No. 3	4.8 (C)	0.7 (C)
4	Bottom flange, Girder No. 4	2.1 (C)	0.3 (C)
5	Bottom flange, Girder No. 5	2.1 (C)	0.3 (C)
6	Web, Girder No. 2	---	---
7	Web, Girder No. 3	---	---
8	Web, Girder No. 4	---	---

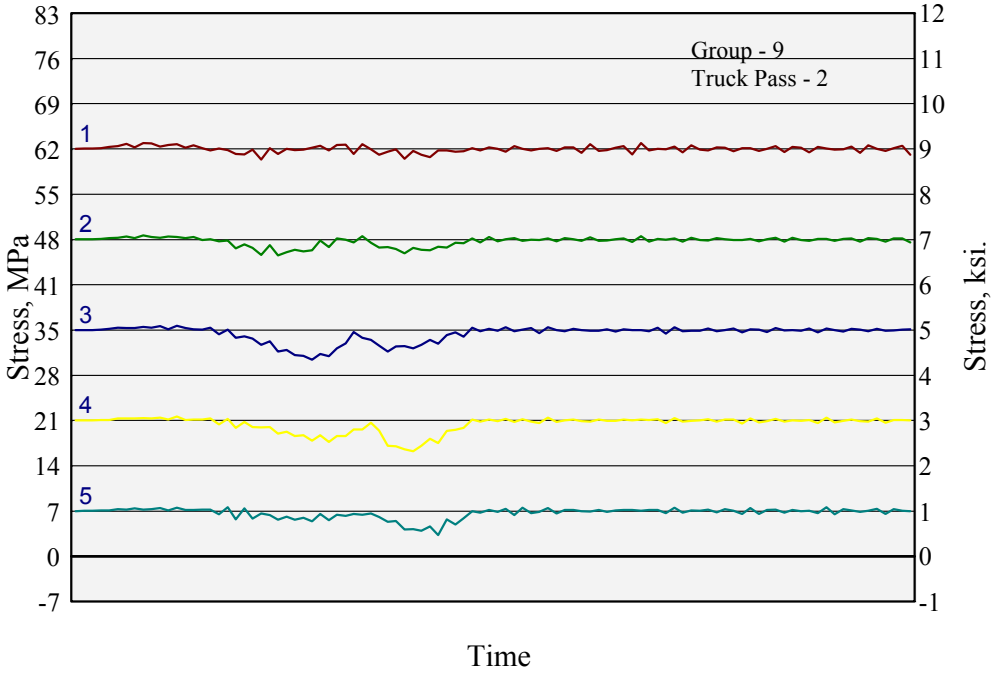

Figure B-16: Bottom flange stress histories for Gage Group 9, Truck Pass 2 (test truck centered in driving lane).

Table B-12: Maximum measured stress ranges and direction for Gage Group 9, Truck Pass 2 (test truck centered in driving lane).

Gage Number	Location	Max. Stress Range, MPa	Max. Stress Range, ksi
1	Bottom flange, Girder No. 1	2.1 (C)	0.3 (C)
2	Bottom flange, Girder No. 2	2.8 (C)	0.4 (C)
3	Bottom flange, Girder No. 3	4.8 (C)	0.7 (C)
4	Bottom flange, Girder No. 4	5.5 (C)	0.8 (C)
5	Bottom flange, Girder No. 5	4.1 (C)	0.6 (C)
6	Web, Girder No. 2	---	---
7	Web, Girder No. 3	---	---
8	Web, Girder No. 4	---	---

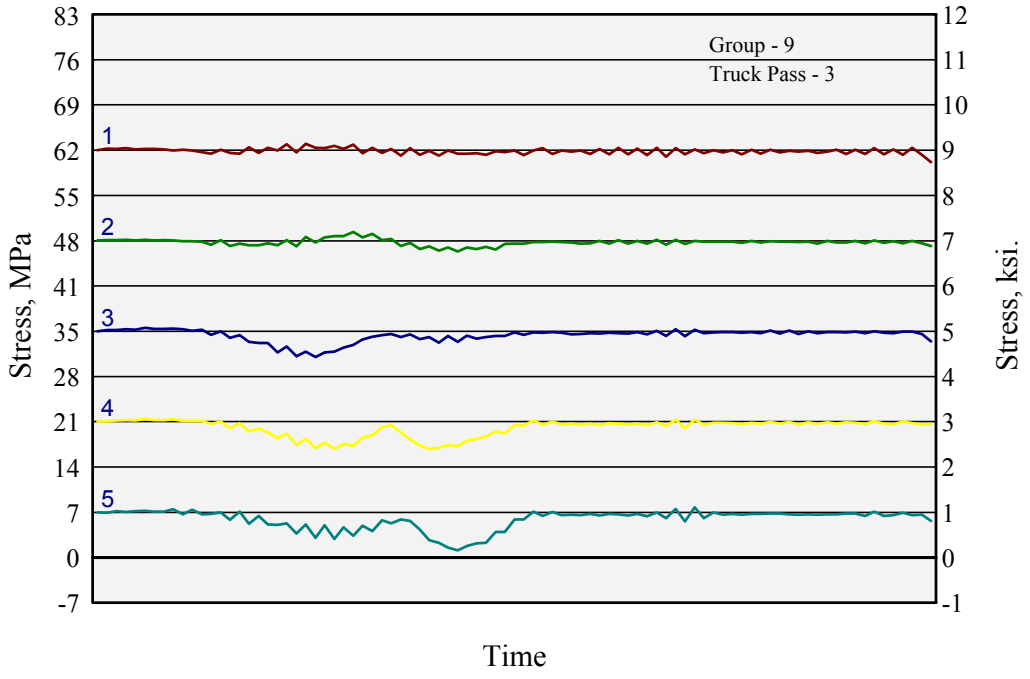

Figure B-17: Bottom flange stress histories for Gage Group 9 Truck Pass 3 (test truck centered in right shoulder).

Table B-13: Maximum measured stress ranges and direction for Gage Group 9, Truck Pass 3 (test truck centered in right shoulder).

Gage Number	Location	Max. Stress Range, MPa	Max. Stress Range, ksi
1	Bottom flange, Girder No. 1	2.8 (C)	0.4 (C)
2	Bottom flange, Girder No. 2	2.8 (C)	0.4 (C)
3	Bottom flange, Girder No. 3	4.1 (C)	0.6 (C)
4	Bottom flange, Girder No. 4	4.8 (C)	0.7 (C)
5	Bottom flange, Girder No. 5	6.2 (C)	0.9 (C)
6	Web, Girder No. 2	---	---
7	Web, Girder No. 3	---	---
8	Web, Girder No. 4	---	---

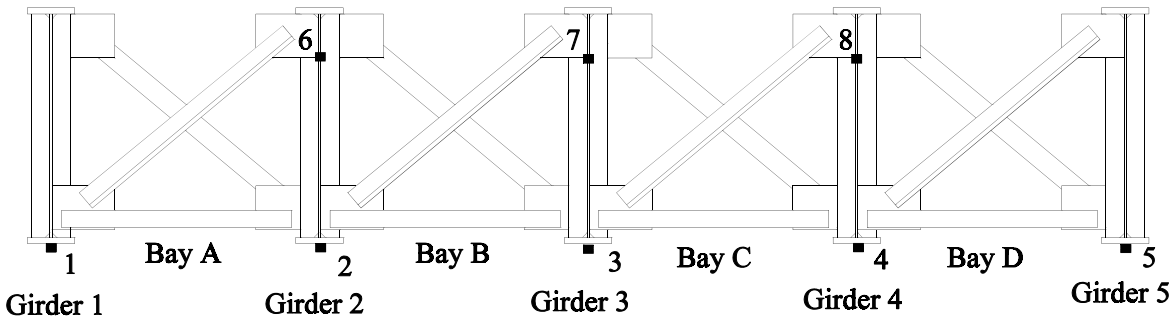

Figure B-18: Gage Group No. 10-3, Diaphragm Line 42 (positive bending moment region).

Table B-14: Gage locations for Group No. 10-3.

Gage Number	Position
1	bottom flange, Girder No. 1
2	bottom flange, Girder No. 2
3	bottom flange, Girder No. 3
4	bottom flange, Girder No. 4
5	bottom flange, Girder No. 5
6	web plate, Girder No. 2, long. direction (191 mm (7.5 in) below flange)
7	web plate, Girder No. 3, long. direction (191 mm (7.5 in) below flange)
8	web plate, Girder No. 4, long. direction (191 mm (7.5 in) below flange)

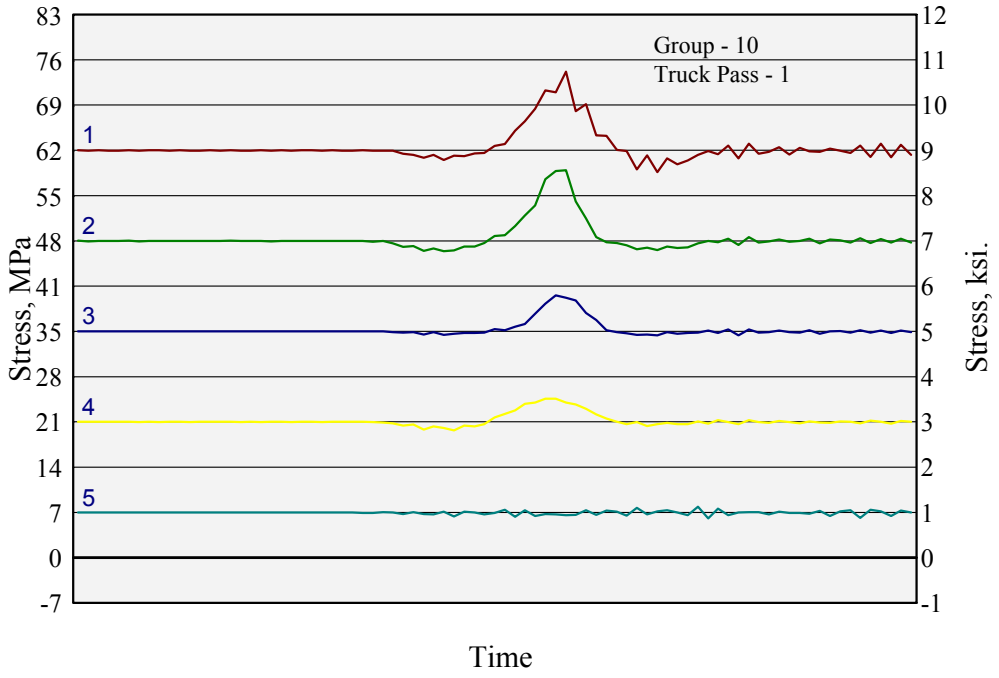

Figure B-19: Bottom flange stress histories for Gage Group 10, Truck Pass 1 (test truck centered in passing lane).

Table B-15: Maximum measured stress ranges and direction for Gage Group 10, Truck Pass 1 (test truck centered in passing lane).

Gage Number	Location	Max. Stress Range, MPa	Max. Stress Range, ksi
1	Bottom flange, Girder No. 1	15 (T)	2.2 (T)
2	Bottom flange, Girder No. 2	12 (T)	1.8 (T)
3	Bottom flange, Girder No. 3	6.2 (T)	0.9 (T)
4	Bottom flange, Girder No. 4	4.8 (T)	0.7 (T)
5	Bottom flange, Girder No. 5	2.1 (C)	0.3 (C)
6	Web, Girder No. 2	2.1 (C)	0.3 (C)
7	Web, Girder No. 3	0.7 (C)	0.1 (C)
8	Web, Girder No. 4	0.7 (C)	0.1 (C)

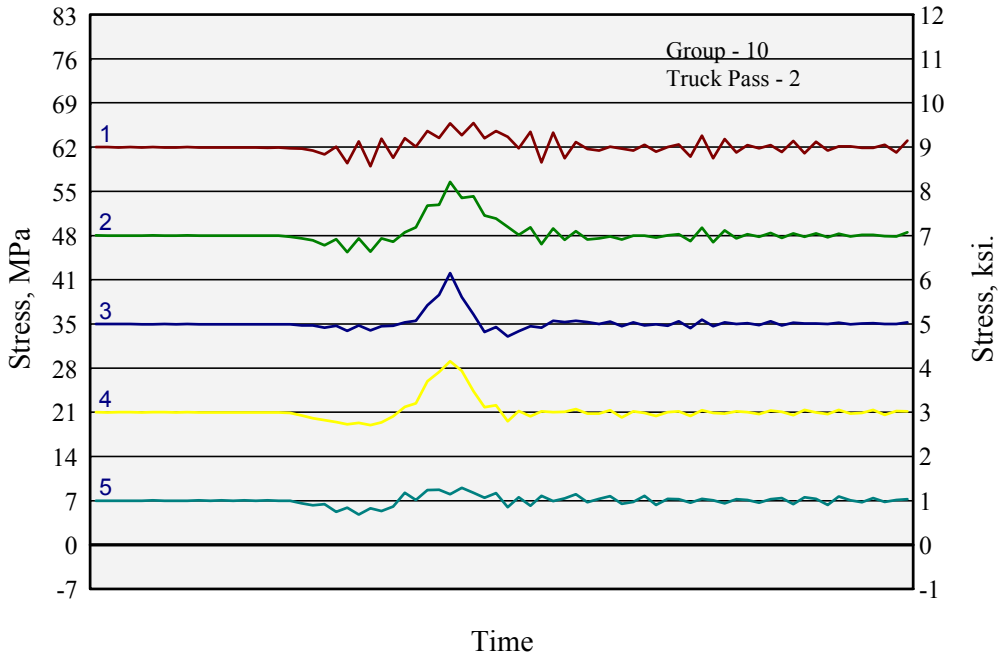

Figure B-20: Bottom flange stress histories for Gage Group 10, Truck Pass 2 (test truck in right lane).

Table B-16: Maximum measured stress ranges and direction for Gage Group 10, Truck Pass 2 (test truck centered in driving lane).

Gage Number	Location	Max. Stress Range, ksi	Max. Stress Range, ksi
1	Bottom flange, Girder No. 1	6.9 (T)	1.0 (T)
2	Bottom flange, Girder No. 2	11 (T)	1.6 (T)
3	Bottom flange, Girder No. 3	9.4 (T)	1.4 (T)
4	Bottom flange, Girder No. 4	9.6 (T)	1.4 (T)
5	Bottom flange, Girder No. 5	4.1 (C)	0.6 (C)
6	Web, Girder No. 2	0.7 (T)	0.1 (T)
7	Web, Girder No. 3	0.7 (T)	0.1 (T)
8	Web, Girder No. 4	1.4 (T)	0.2 (T)

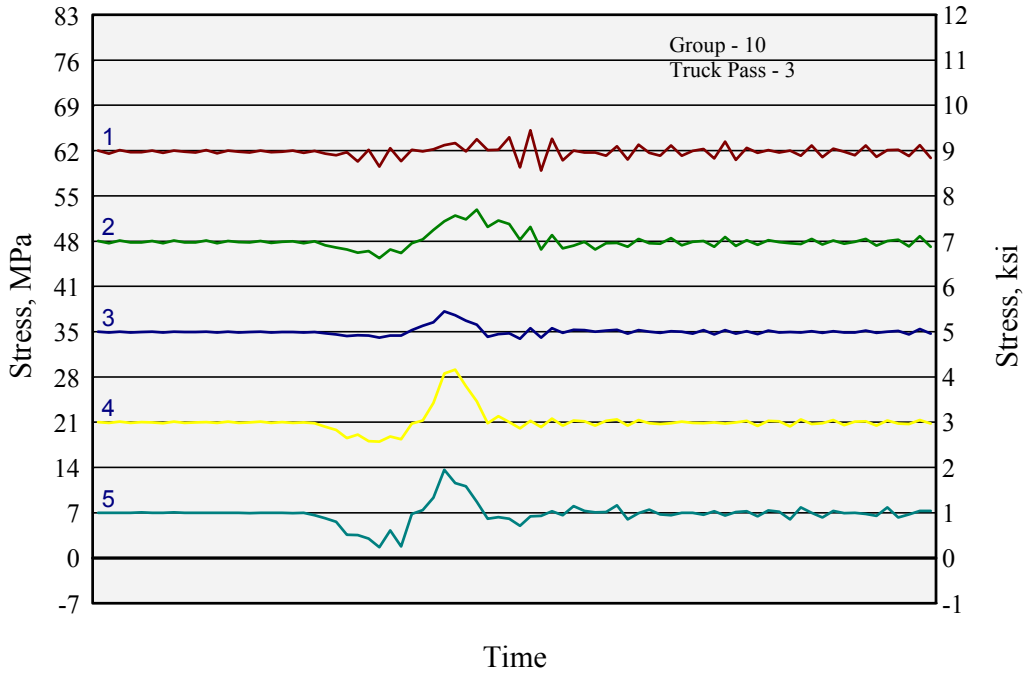

Figure B-21: Maximum flange stress histories for Gage Group 10, Truck Pass 3 (test truck centered in right shoulder).

Table B-17: Maximum measured stress ranges and direction for Gage Group 10, Truck Pass 3 (test truck centered in right shoulder).

Gage Number	Location	Max. Stress Range, ksi	Max. Stress Range, ksi
1	Bottom flange, Girder No. 1	6.2 (T)	0.9 (T)
2	Bottom flange, Girder No. 2	6.9 (T)	1.0 (T)
3	Bottom flange, Girder No. 3	4.1 (T)	0.6 (T)
4	Bottom flange, Girder No. 4	11 (T)	1.6 (T)
5	Bottom flange, Girder No. 5	12 (T)	1.7 (T)
6	Web, Girder No. 2	0.7 (T)	0.1 (T)
7	Web, Girder No. 3	0.7 (T)	0.1 (T)
8	Web, Girder No. 4	1.4 (T)	0.2 (T)

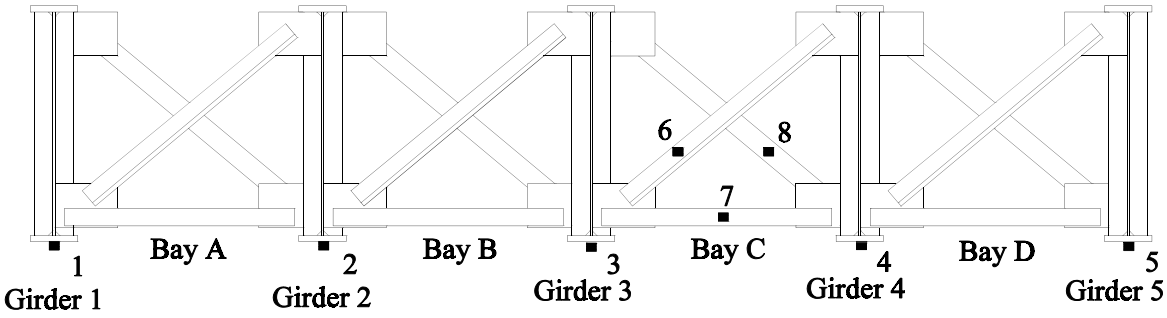

Figure B-22: Gage Group No. 11-3 between Diaphragm Lines 40 and 41.

Table B-18: Gage locations for Group No. 11-3.

Gage Number	Position
1	Bottom flange, Girder No. 1
2	Bottom flange, Girder No. 2
3	Bottom flange, Girder No. 3
4	Bottom flange, Girder No. 4
5	Bottom flange, Girder No. 5
6	Diaphragm cross frame, Bay C
7	Lower strut, Bay C
8	Diaphragm cross frame, Bay C

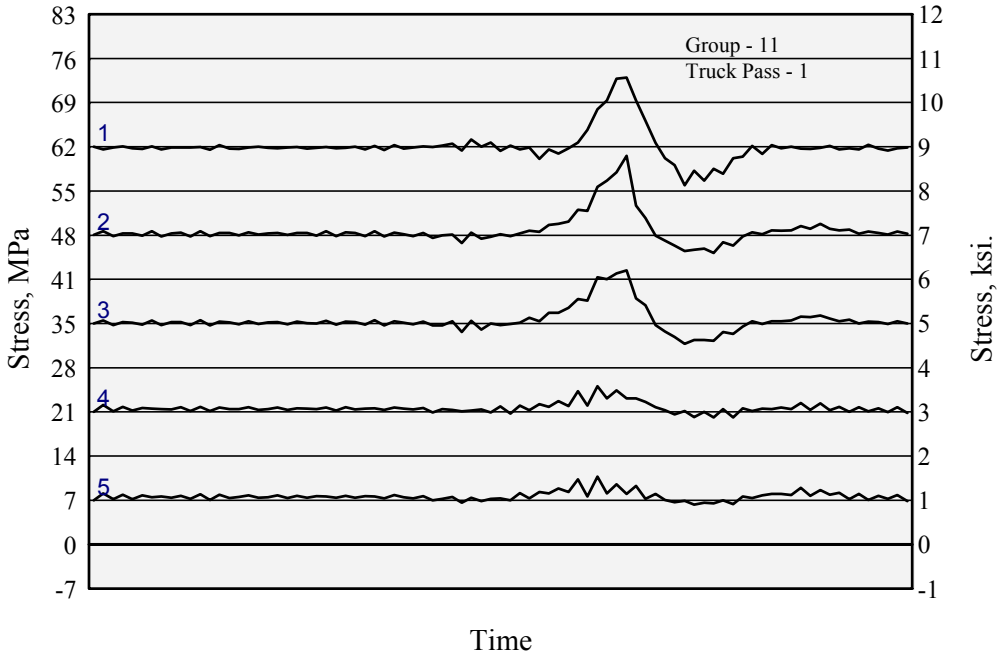

Figure B-23: Bottom flange stress histories for Gage Group 11, Truck Pass 1 (test truck centered in passing lane).

Table B-19: Maximum measured stress ranges and direction for Gage Group11, Truck Pass 1 (test truck centered in passing lane).

Gage Number	Location	Max. Stress Range, MPa	Max. Stress Range, ksi
1	Bottom flange, Girder No. 1	17 (T)	2.4 (T)
2	Bottom flange, Girder No. 2	15 (T)	2.2 (T)
3	Bottom flange, Girder No. 3	11 (T)	1.6 (T)
4	Bottom flange, Girder No. 4	4.8 (T)	0.7 (T)
5	Bottom flange, Girder No. 5	4.1 (T)	0.6 (T)
6	Diaphragm cross frame, Bay C	22 (T)	3.2 (T)
7	Lower strut, Bay C	13 (T)	1.9 (T)
8	Diaphragm cross frame, Bay C	7.6 (C)	1.1 (C)

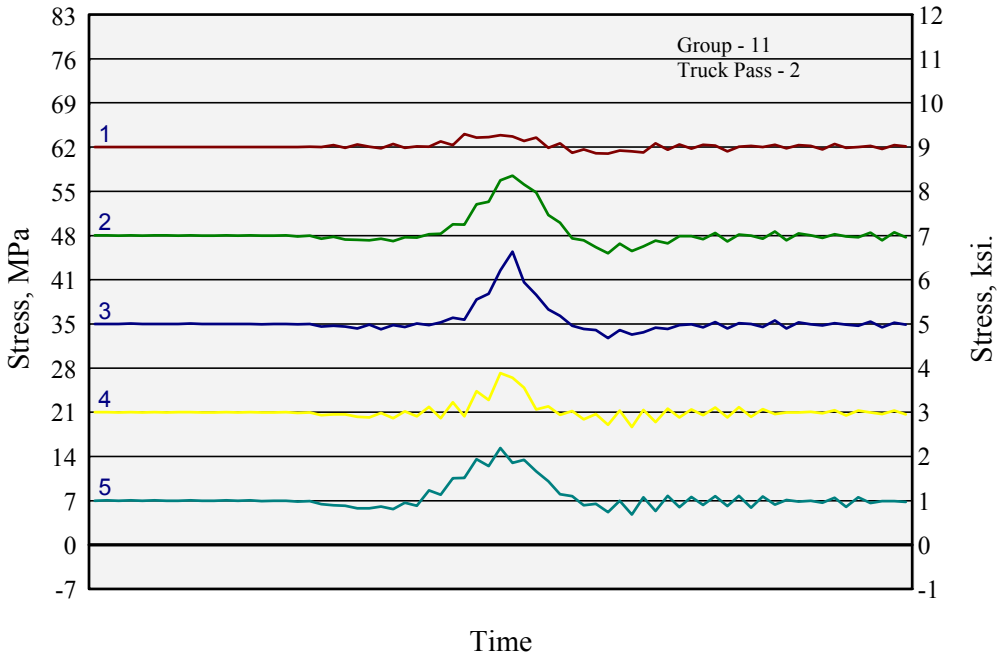

Figure B-24: Bottom flange stress histories for Gage Group 11, Truck Pass 2 (test truck centered in driving lane).

Table B-20: Maximum measured stress ranges and direction for Gage Group 11, Truck Pass 2 (test truck centered in driving lane).

Gage Number	Location	Max. Stress Range, MPa	Max. Stress Range, ksi
1	Bottom flange, Girder No. 1	2.8 (T)	0.4 (T)
2	Bottom flange, Girder No. 2	12 (T)	1.7 (T)
3	Bottom flange, Girder No. 3	13 (T)	1.9 (T)
4	Bottom flange, Girder No. 4	8.2 (T)	1.2 (T)
5	Bottom flange, Girder No. 5	10 (T)	1.5 (T)
6	Diaphragm cross frame, Bay C	28 (T)	4.0 (T)
7	Lower strut, Bay C	25 (T)	3.6 (T)
8	Diaphragm cross frame, Bay C	7.6 (T)	1.1 (T)

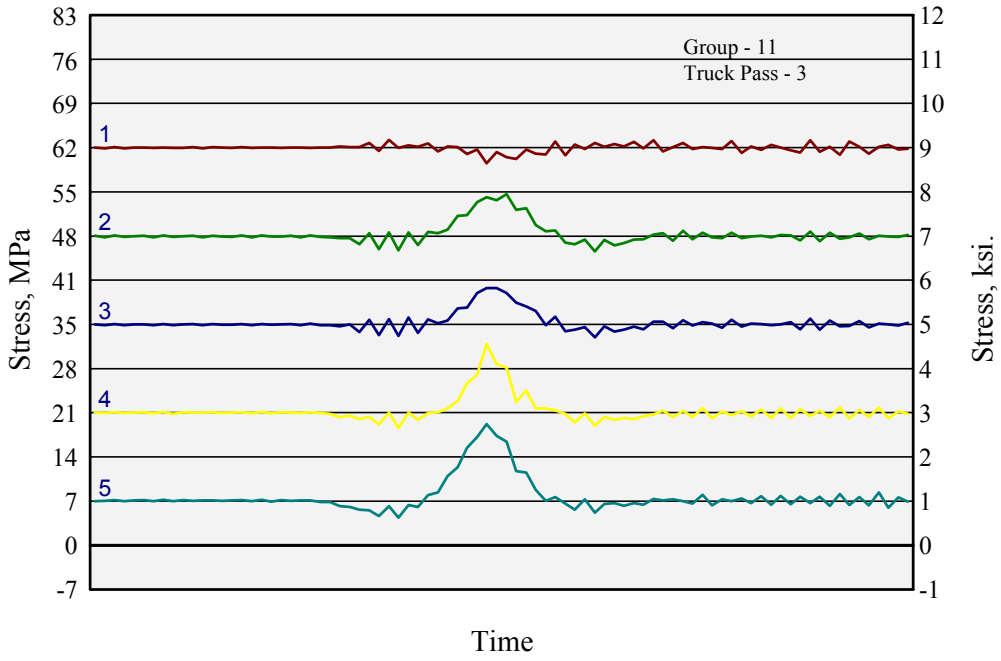

Figure B-25: Bottom flange stress histories for Gage Group 11, Truck Pass 3 (test truck centered in right shoulder).

Table B-21: Maximum measured stress ranges and direction for Gage Group 11, Truck Pass 3 (test truck centered in right shoulder).

Gage Number	Location	Max. Stress Range, MPa	Max. Stress Range, ksi
1	Bottom flange, Girder No. 1	3.4 (C)	0.5 (C)
2	Bottom flange, Girder No. 2	9.0 (T)	1.3 (T)
3	Bottom flange, Girder No. 3	7.6 (T)	1.1 (T)
4	Bottom flange, Girder No. 4	13 (T)	1.9 (T)
5	Bottom flange, Girder No. 5	14 (T)	2.1 (T)
6	Diaphragm cross frame, Bay C	11 (C)	1.6 (C)
7	Lower strut, Bay C	11 (T)	1.6 (T)
8	Diaphragm cross frame, Bay C	1.8 (T)	2.6 (T)

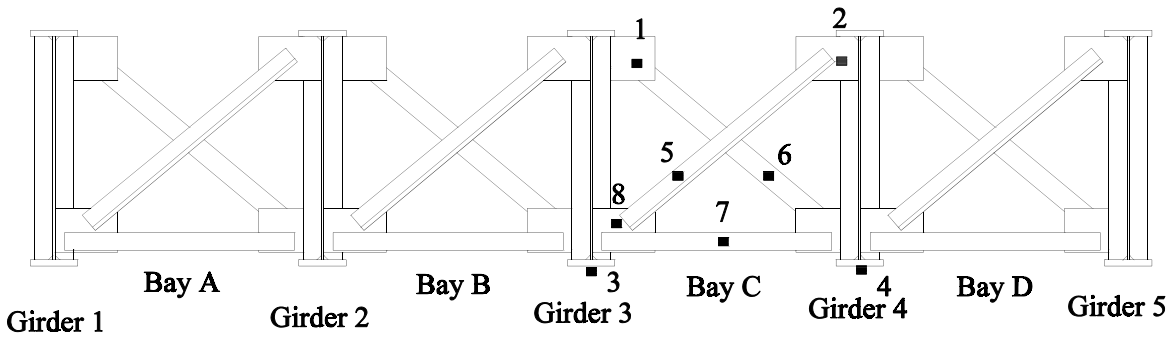

Figure B-26: Gage Group No. 12-3, between Diaphragm Lines 40 and 41 (bottom flanges, cross frame members, and gusset plates).

Table B-22: Gage locations for Group No. 12-3.

Gage Number	Position
1	Upper gusset plate, Girder No. 3
2	Upper gusset plate, Girder No. 4
3	Bottom flange, Girder No. 3
4	Bottom flange, Girder No. 4
5	Diaphragm cross frame, Bay C
6	Diaphragm cross frame, Bay C
7	Lower strut, Bay C
8	Lower gusset plate, Girder No. 3

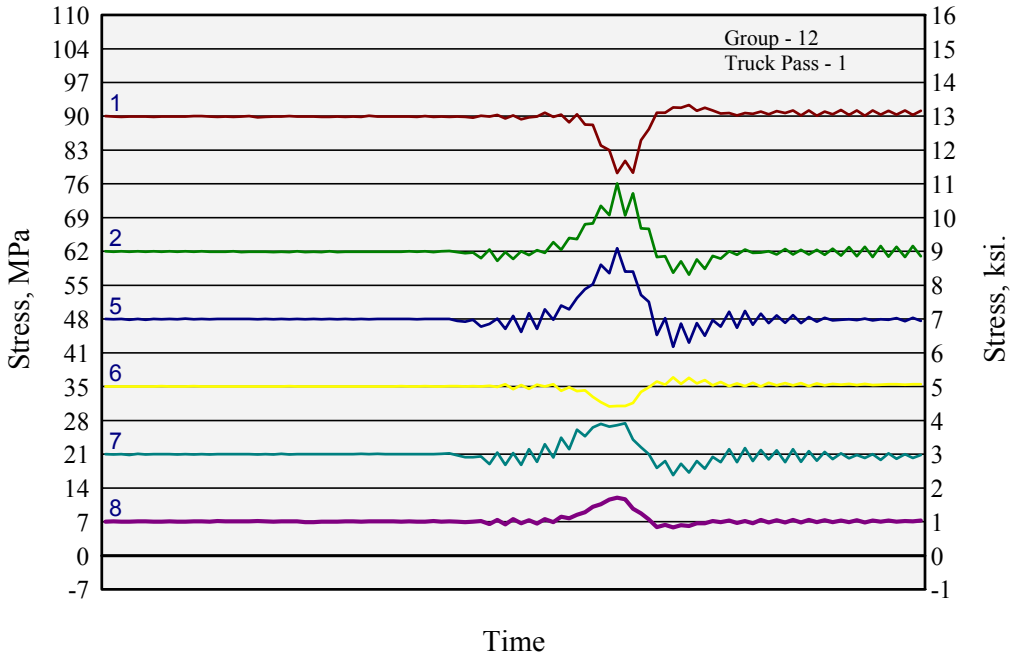

Figure B-27: Bottom flange stress histories for Gage Group 12, Truck Pass 1 (test truck centered in passing lane).

Table B-23: Maximum measured stress ranges and direction for Gage Group 12, Truck Pass 1 (test truck centered in passing lane).

Gage Number	Location	Max. Stress Range, MPa	Max. Stress Range, ksi
1	Upper gusset plate, Girder No. 3	14 (C)	2.0 (C)
2	Upper gusset plate, Girder No. 4	19 (T)	2.7 (T)
3	Bottom flange, Girder No. 3	11 (T)	1.6 (T)
4	Bottom flange, Girder No. 4	6.2 (T)	0.9 (T)
5	Diaphragm cross frame, Bay C	20 (T)	2.9 (T)
6	Diaphragm cross frame, Bay C	5.5 (C)	0.8 (C)
7	Lower strut, Bay C	10 (T)	1.5 (T)
8	Lower gusset plate, Girder No. 3	6.2 (T)	0.9 (T)

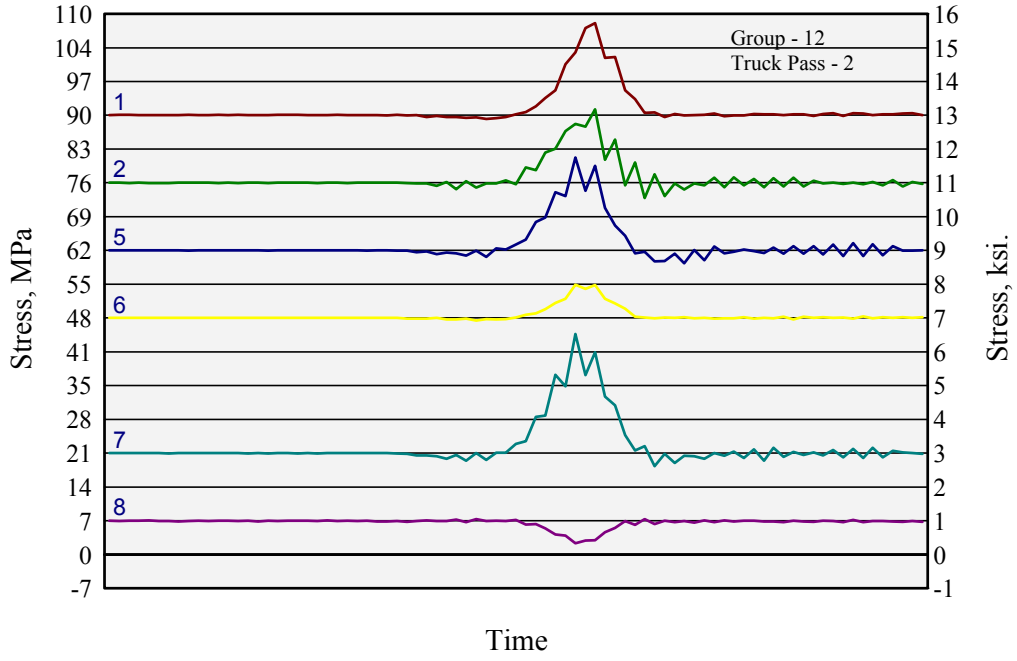

Figure B-28: Bottom flange stress histories for Gage Group 12, Truck Pass 2 (test truck centered in driving lane).

Table B-24: Maximum measured stress ranges and direction for Gage Group 12, Truck Pass 2 (test truck centered in driving lane).

Gage Number	Location	Max. Stress Range, MPa	Max. Stress Range, ksi
1	Upper gusset plate, Girder No. 3	19 (T)	2.8 (T)
2	Upper gusset plate, Girder No. 4	18 (T)	2.6 (T)
3	Bottom flange, Girder No. 3	11 (T)	1.6 (T)
4	Bottom flange, Girder No. 4	13 (T)	1.9 (T)
5	Diaphragm cross frame, Bay C	21 (T)	3.1 (T)
6	Diaphragm cross frame, Bay C	6.9 (T)	1.0 (T)
7	Lower strut, Bay C	26 (T)	3.8 (T)
8	Lower gusset plate, Girder No. 3	4.8 (C)	0.7 (C)

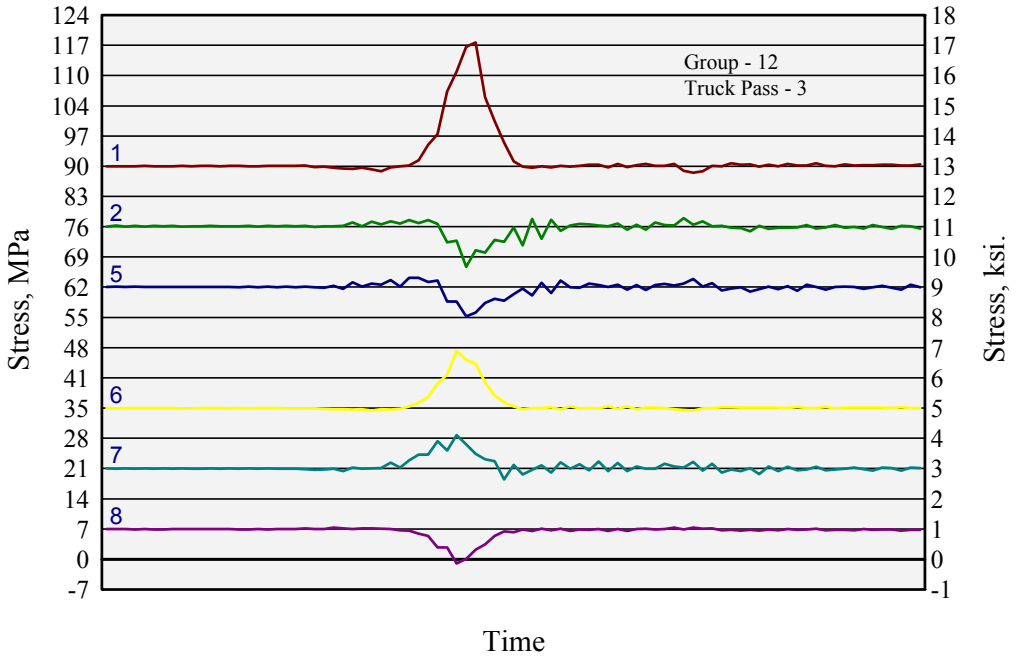

Figure B-29: Bottom flange stress histories for Gage Group 12, Truck Pass 3 (test truck centered in right shoulder).

Table B-25: Maximum measured stress ranges and direction for Gage Group 12, Truck Pass 3 (test truck centered in right shoulder).

Gage Number	Location	Max. Stress Range, MPa	Max. Stress Range, ksi
1	Upper gusset plate, Girder No. 3	29 (T)	4.2 (T)
2	Upper gusset plate, Girder No. 4	11 (C)	1.6 (C)
3	Bottom flange, Girder No. 3	7.6 (T)	1.1 (T)
4	Bottom flange, Girder No. 4	14 (T)	2.0 (T)
5	Diaphragm cross frame, Bay C	9.0 (C)	1.3 (C)
6	Diaphragm cross frame, Bay C	14 (T)	2.0 (T)
7	Lower strut, Bay C	9.4 (T)	1.4 (T)
8	Lower gusset plate, Girder No. 3	8.2 (C)	1.2 (C)

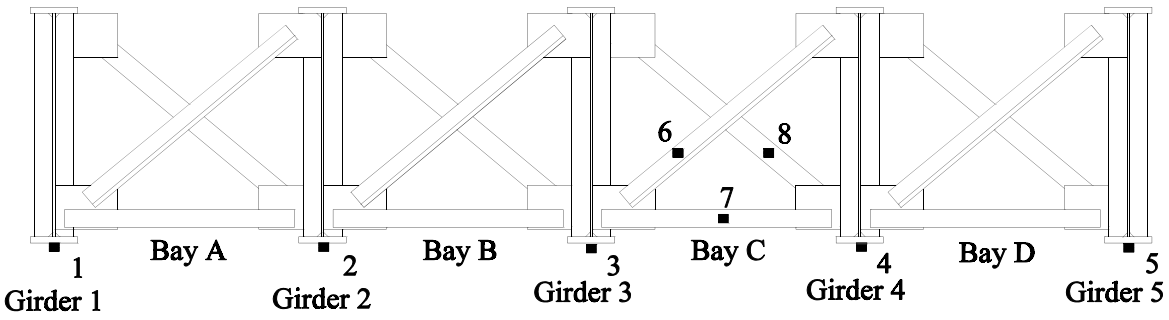

Figure B-30: Gage Group 13-3, between Diaphragm Lines 40 and 41 (bottom flanges and lower struts of cross frames).

Table B-26: Gage locations for Group No. 13-3.

Gage Number	Position
1	Bottom flange, Girder No. 1
2	Bottom flange, Girder No. 2
3	Bottom flange, Girder No. 3
4	Bottom flange, Girder No. 4
5	Bottom flange, Girder No. 5
6	Diaphragm cross frame, Bay C
7	Lower strut, Bay C
8	Diaphragm cross frame, Bay C

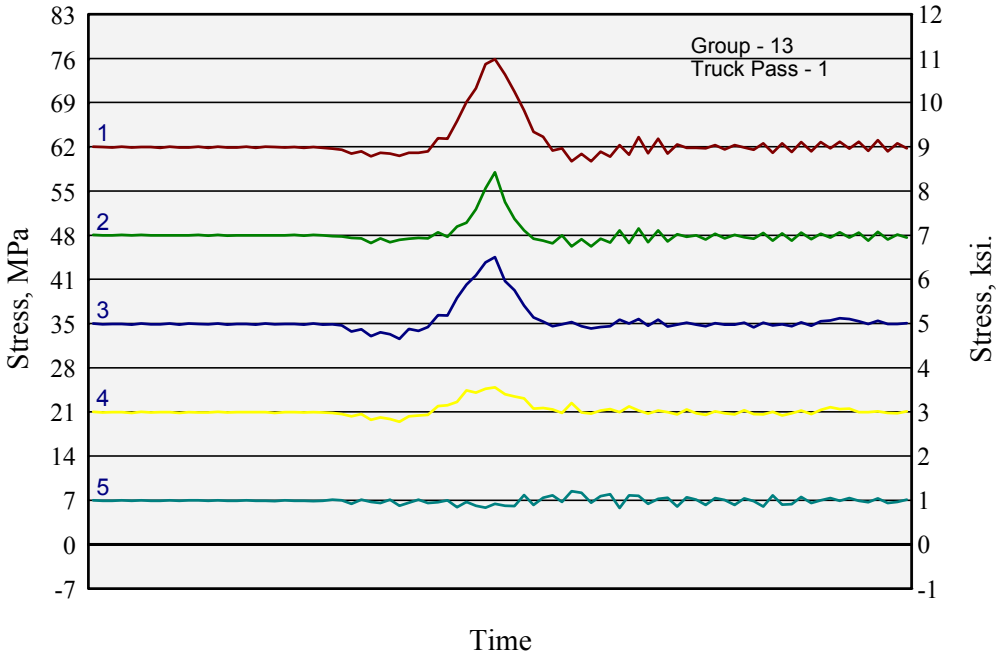

Figure B-31: Bottom flange stress histories for Gage Group 13, Truck Pass 1 (test truck centered in passing lane).

Table B-27: Maximum measured stress ranges and direction for Gage Group 13, Truck Pass 1 (test truck centered in passing lane).

Gage Number	Location	Max. Stress Range, MPa	Max. Stress Range, ksi
1	Bottom flange, Girder No. 1	16 (T)	2.3 (T)
2	Bottom flange, Girder No. 2	11 (T)	1.6 (T)
3	Bottom flange, Girder No. 3	12 (T)	1.8 (T)
4	Bottom flange, Girder No. 4	5.5 (T)	0.8 (T)
5	Bottom flange, Girder No. 5	2.8 (T)	0.4 (T)
6	Diaphragm cross frame, Bay C	13 (T)	1.9 (T)
7	Lower strut, Bay C	6.9 (T)	1.0 (T)
8	Diaphragm cross frame, Bay C	11 (C)	1.6 (C)

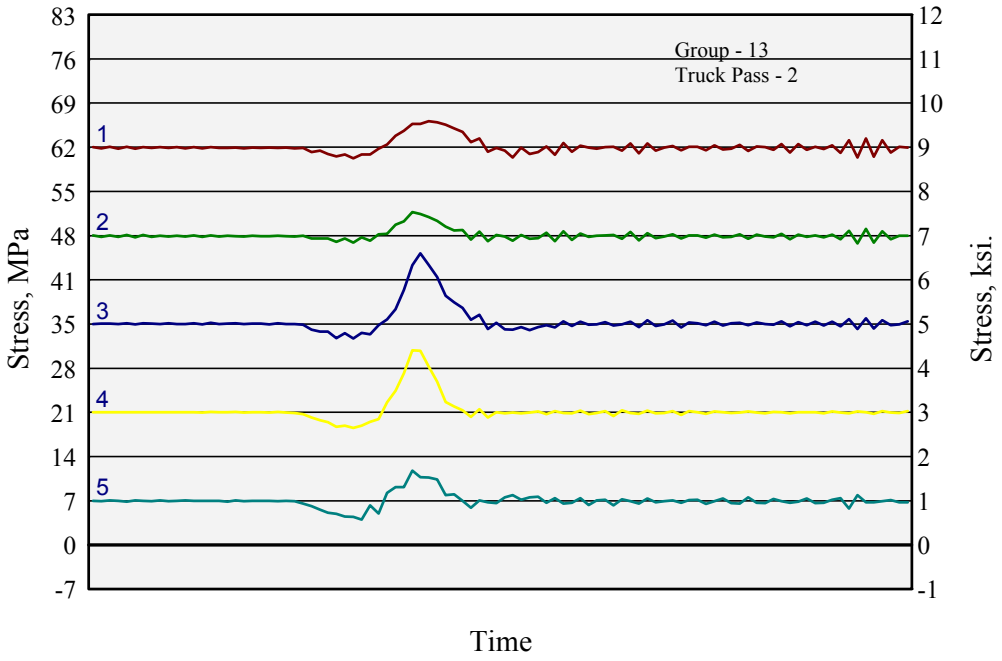

Figure B-32: Bottom flange stress histories for Gage Group 13, Truck Pass 2 (test truck centered in driving lane).

Table B- 28: Maximum measured stress ranges and direction for Gage Group 13, Truck Pass 2 (test truck centered in driving lane).

Gage Number	Location	Max. Stress Range, MPa	Max. Stress Range, ksi
1	Bottom flange, Girder No. 1	5.5 (T)	0.8 (T)
2	Bottom flange, Girder No. 2	4.8 (T)	0.7 (T)
3	Bottom flange, Girder No. 3	13 (T)	1.9 (T)
4	Bottom flange, Girder No. 4	12 (T)	1.7 (T)
5	Bottom flange, Girder No. 5	7.6 (T)	1.1 (T)
6	Diaphragm cross frame, Bay C	31 (T)	4.5 (T)
7	Lower strut, Bay C	28 (T)	4.0 (T)
8	Diaphragm cross frame, Bay C	7.6 (T)	1.1 (T)

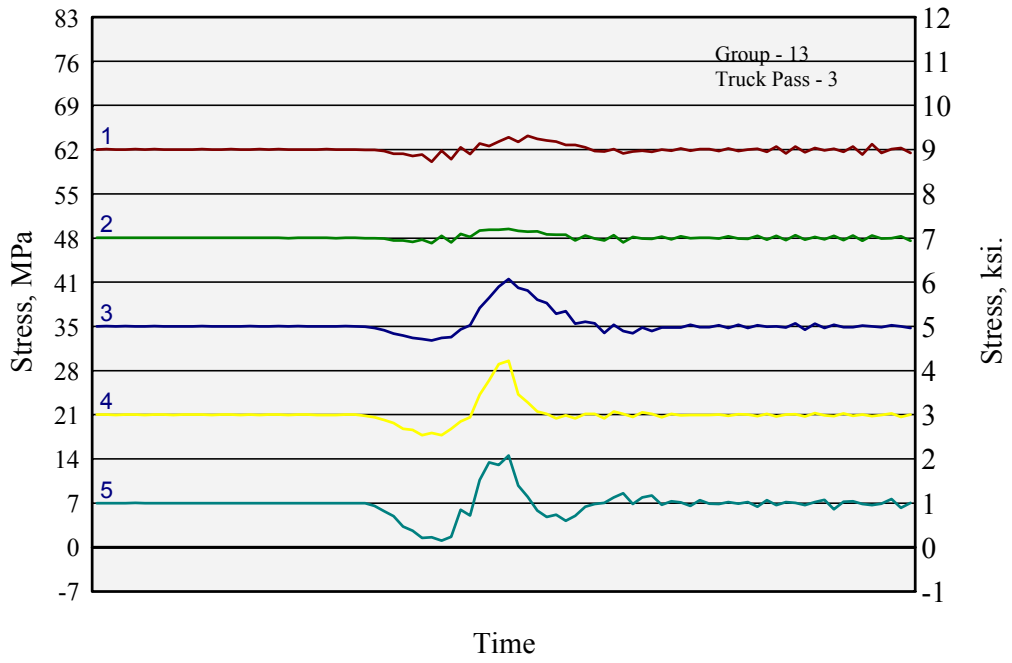

Figure B-33: Bottom flange stress histories for Gage Group 13, Truck Pass 3 (test truck centered in right shoulder).

Table B-29: Maximum measured stress ranges and direction for Gage Group 13, Truck Pass 3 (test truck centered in right shoulder).

Gage Number	Location	Max. Stress Range, MPa	Max. Stress Range, ksi
1	Bottom flange, Girder No. 1	4.1(T)	0.6 (T)
2	Bottom flange, Girder No. 2	2.1 (T)	0.3 (T)
3	Bottom flange, Girder No. 3	9.4 (T)	1.4 (T)
4	Bottom flange, Girder No. 4	12 (T)	1.7 (T)
5	Bottom flange, Girder No. 5	13 (T)	1.9 (T)
6	Diaphragm cross frame, Bay C	10 (T)	1.5 (T)
7	Lower strut, Bay C	20 (T)	2.9 (T)
8	Diaphragm cross frame, Bay C	19 (T)	2.7 (T)

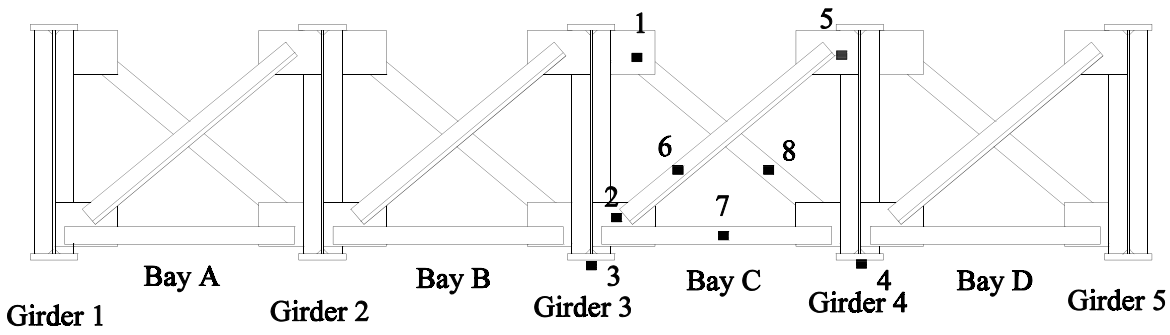

Figure B-34: Gage Group No. 14-3, between Diaphragm Lines 40 and 41 (bottom flanges, cross frame members, and gusset plates).

Table B-30: Gage locations for Group No. 14-3.

Gage Number	Position
1	Upper gusset plate, Girder No. 3
2	Upper gusset plate, Girder No. 3
3	Bottom flange, Girder No. 3
4	Bottom flange, Girder No. 4
5	Lower gusset plate, Girder No. 4
6	Diaphragm cross frame, Bay C
7	Lower strut, Bay C
8	Diaphragm cross frame, Bay C

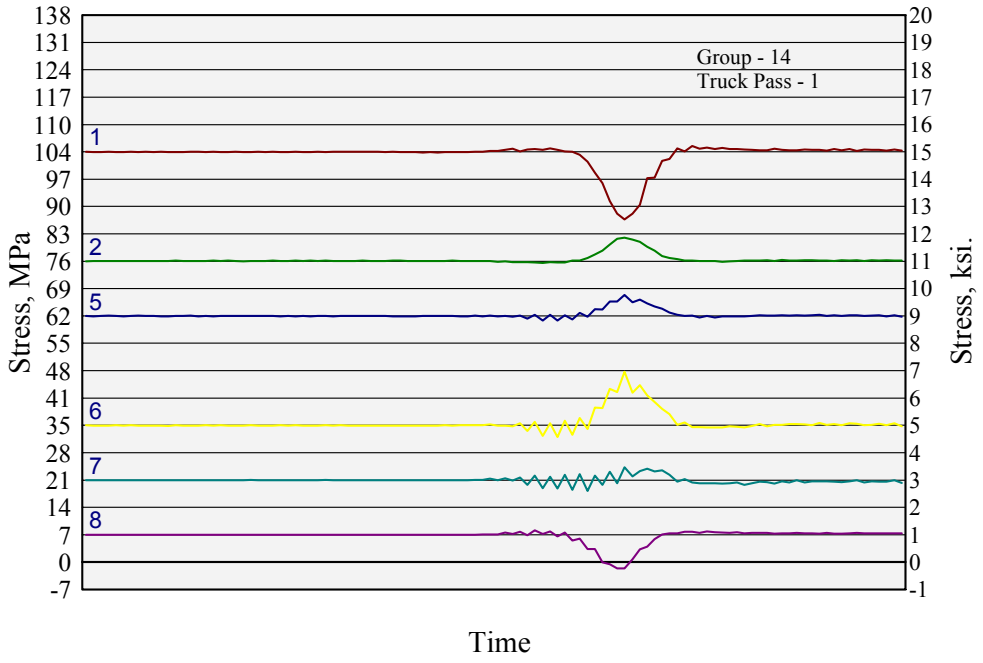

Figure B-35: Bottom flange stress histories for Gage Group 14, Truck Pass 1 (test truck centered in passing lane).

Table B-31: Maximum measured stress ranges and direction for Gage Group 14, Truck Pass 1 (test truck centered in passing lane).

Gage Number	Location	Max. Stress Range, ksi	Max. Stress Range, ksi
1	Upper gusset plate, Girder No. 3	18 (C)	2.6 (C)
2	Lower gusset plate, Girder No. 3	6.2 (T)	0.9 (T)
3	Bottom flange, Girder No. 3	12 (T)	1.7 (T)
4	Bottom flange, Girder No. 4	5.5 (T)	0.8 (T)
5	Upper gusset plate, Girder No. 4	6.2 (T)	0.9 (T)
6	Diaphragm cross frame, Bay C	16 (C)	2.3 (C)
7	Lower strut, Bay C	6.2 (C)	0.9 (C)
8	Diaphragm cross frame, Bay C	9.4 (T)	1.4 (T)

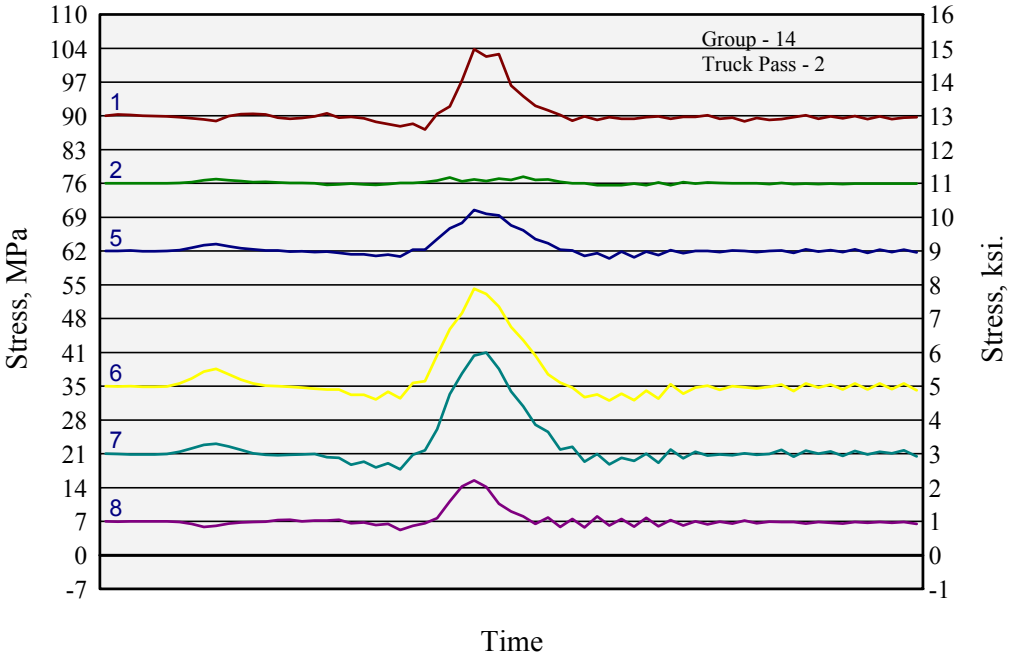

Figure B-36: Bottom flange stress histories for Gage Group 14, Truck Pass 2 (test truck centered in driving lane).

Table B-32: Maximum measured stress ranges and direction for Gage Group 14, Truck Pass 2 (test truck centered in driving lane).

Gage Number	Location	Max. Stress Range, MPa	Max. Stress Range, ksi
1	Upper gusset plate, Girder No. 3	16 (C)	2.3 (C)
2	Lower gusset plate, Girder No. 3	1.4 (T)	0.2 (T)
3	Bottom flange, Girder No. 3	140 (T)	2.0 (T)
4	Bottom flange, Girder No. 4	14 (T)	2.1 (T)
5	Upper gusset plate, Girder No. 4	9.4 (T)	1.4 (T)
6	Diaphragm cross frame, Bay C	23 (T)	3.3 (T)
7	Lower strut, Bay C	23 (T)	3.4 (T)
8	Diaphragm cross frame, Bay C	10 (C)	1.5 (C)

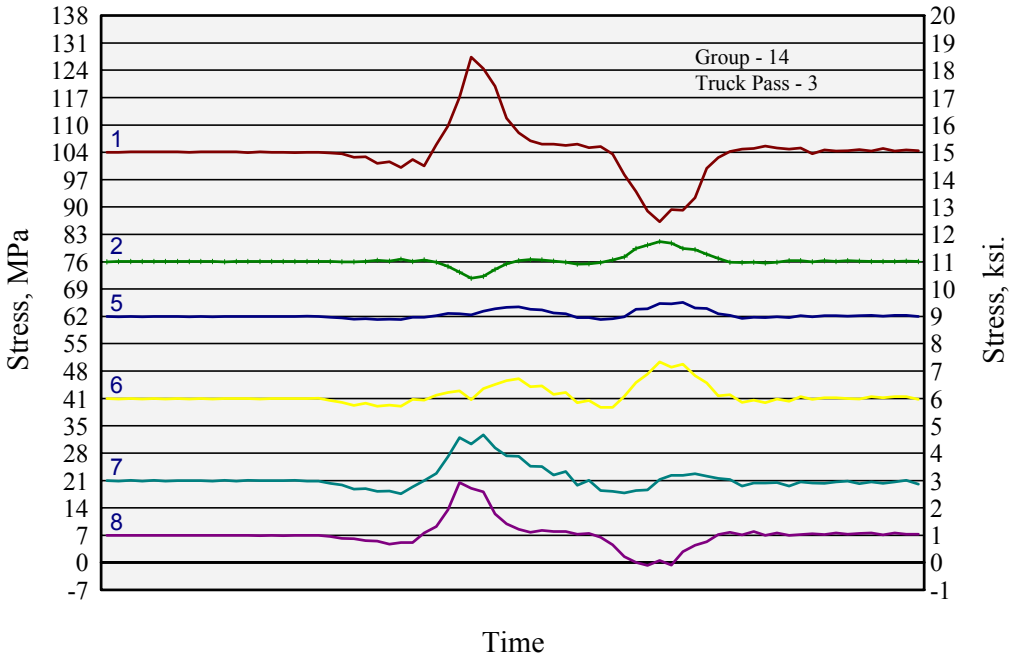

Figure B-37: Bottom flange stress histories for Gage Group 14, Truck Pass 3 (test truck centered in right shoulder).

Table B-33: Maximum measured stress ranges and direction for Gage Group 14, Truck Pass 3 (test truck centered in right shoulder).

Gage Number	Location	Max. Stress Range, MPa	Max. Stress Range, ksi
1	Upper gusset plate, Girder No. 3	41 (T)	5.9 (T)
2	Lower gusset plate, Girder No. 3	9.0 (T)	1.3 (T)
3	Bottom flange, Girder No. 3	12 (T)	1.8 (T)
4	Bottom flange, Girder No. 4	12 (T)	1.7 (T)
5	Upper gusset plate, Girder No. 4	4.1 (T)	0.6 (T)
6	Diaphragm cross frame, Bay C	11 (T)	1.6 (T)
7	Lower strut, Bay C	14 (T)	2.1 (T)
8	Diaphragm cross frame, Bay C	21 (T)	3.0 (T)

APPENDIX - C

STRESS HISTORIES

for

TOWN LAKE BRIDGE
(IH-35 Southbound)

Test Date
July 29, 1993

Table C-1: Summary of recorded test truck passages, Town Lake Bridge

Filename	Gage Group	Truck Pass	Truck Position	Number of Scans
TWN1PS1	1	1	Truck centered in left lane	133
TWN1PS2	1	2	Truck centered in center lane	123
TWN1PS3	1	3	Truck centered in right lane	148
TWN1TRK1	1	---	Truck centered in passing lane	137
TWN1TRK2	1	---	Truck centered in right lane	126
TWN2PS1	2	1	Truck centered in left lane	102
TWN2PS2	2	2	Truck centered in center lane	137
TWN2PS3	2	3	Truck centered right line w/ 18-wheeler in left lane	125
TWN2PS4	2	4	Truck centered in right lane	101
TWN3PS1	3	1	Truck centered in left lane	144
TWN3PS2	3	2	Truck centered in center lane	130
TWN3PS3	3	3	Truck centered in right lane	130
TWN4PS1	4	1	Truck centered in left lane	116
TWN4PS2	4	2	Truck centered in center lane	115
TWN4PS3	4	3	Truck centered in right lane	116
TWN4PS4	4	4	Group of approximately 20 passenger cars	144
TWN5PS1	5	1	Truck centered in left lane	117
TWN5PS2	5	2	Truck centered in center lane	114
TWN5PS3	5	3	Truck centered in right lane	117

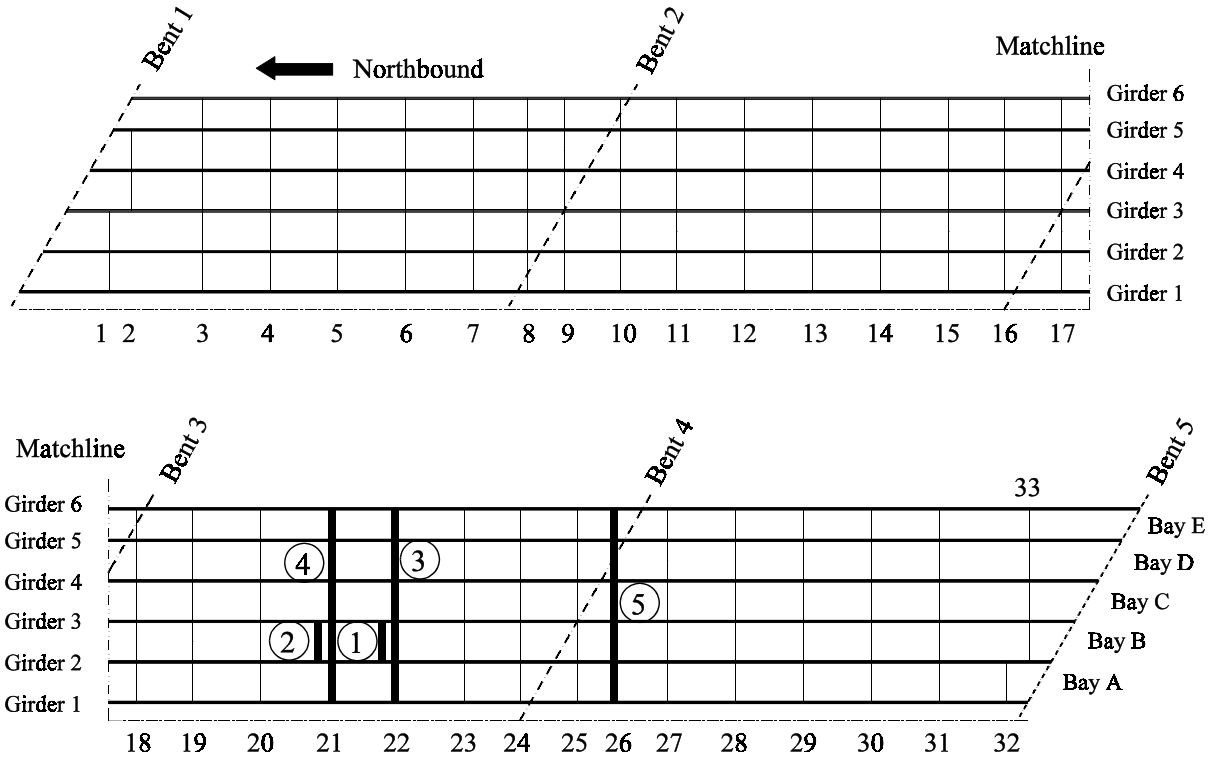

Figure C-1: Framing plan of 134.2 m (440 ft) unit.

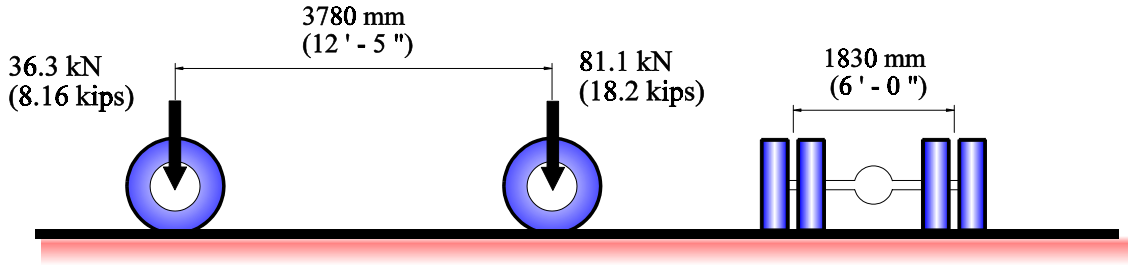

Figure C-2: Test truck axial weight and configuration, Field Test No. 2.

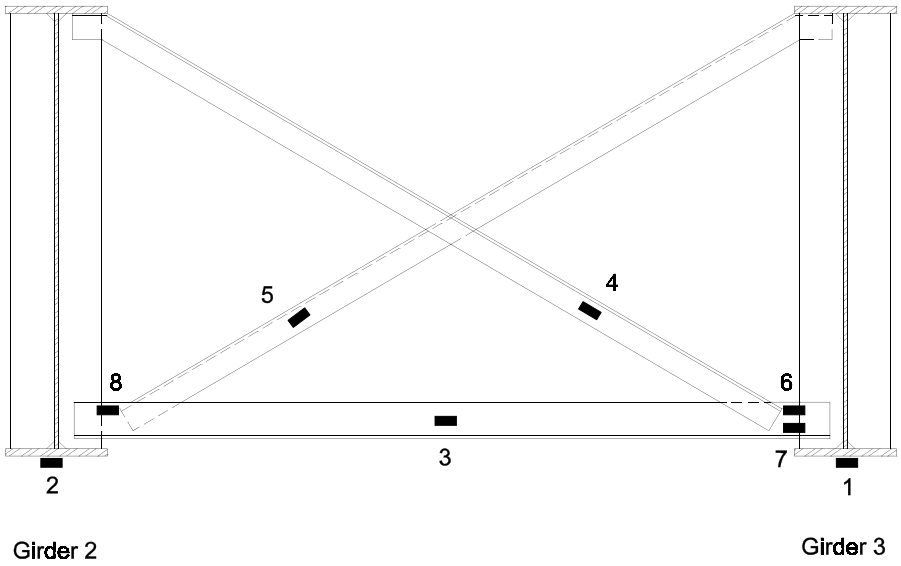

Figure C-3: Gage Group No. 1 location, Diaphragm B-22, Type D2 (positive bending moment region).

Table C-2: Gage locations of Gage Group No. 1.

Gage Number	Position
1	bottom flange, centerline of Girder No. 3
2	bottom flange, centerline of Girder No. 2
3	lower strut, neutral axis
4	diagonal, neutral axis
5	diagonal, neutral axis
6	lower strut, top
7	lower strut, bottom
8	lower strut, top

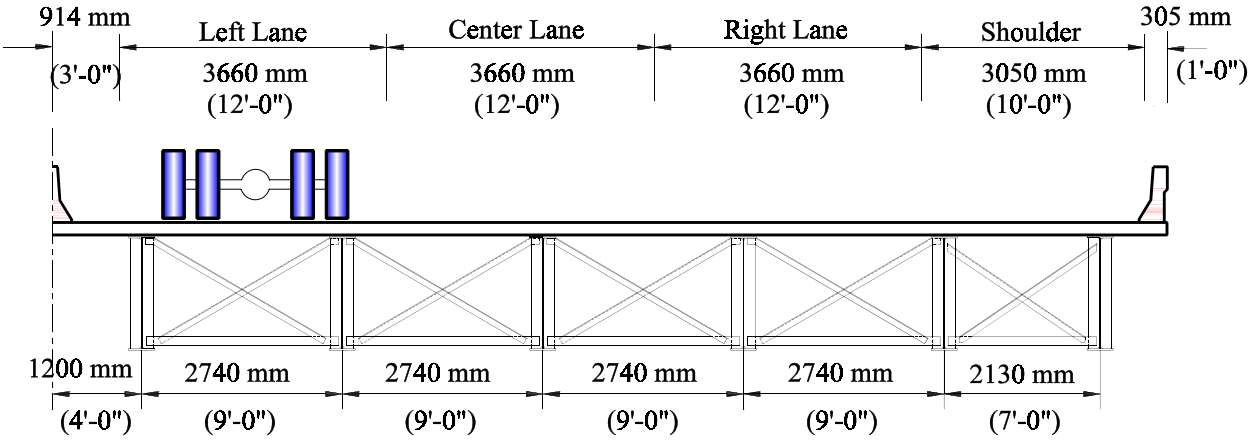

Figure C-4: Test truck position for Gage Group 1, Truck Pass 1 (test truck centered in left lane).

Table C-3: Maximum measured stress histories for Gage Group 1, Truck Pass 1 (test truck centered in left lane).

Gage Number	Location	Max. Stress Range, MPa	Max. Stress Range, ksi
1	Bottom flange, Girder No. 3	10 (T)	1.5 (T)
2	Bottom flange, Girder No. 2	8.4 (T)	1.2 (T)
3	Lower strut, neutral axis	17 (T)	2.4 (T)
4	Diagonal, neutral axis	14 (T)	2.0 (T)
5	Diagonal, neutral axis	13 (T)	1.9 (T)
6	Lower strut, top	72 (T)	10 (T)
7	Lower strut, bottom	35 (T)	5.1 (T)
8	Lower strut, top	35 (T)	5.1 (T)

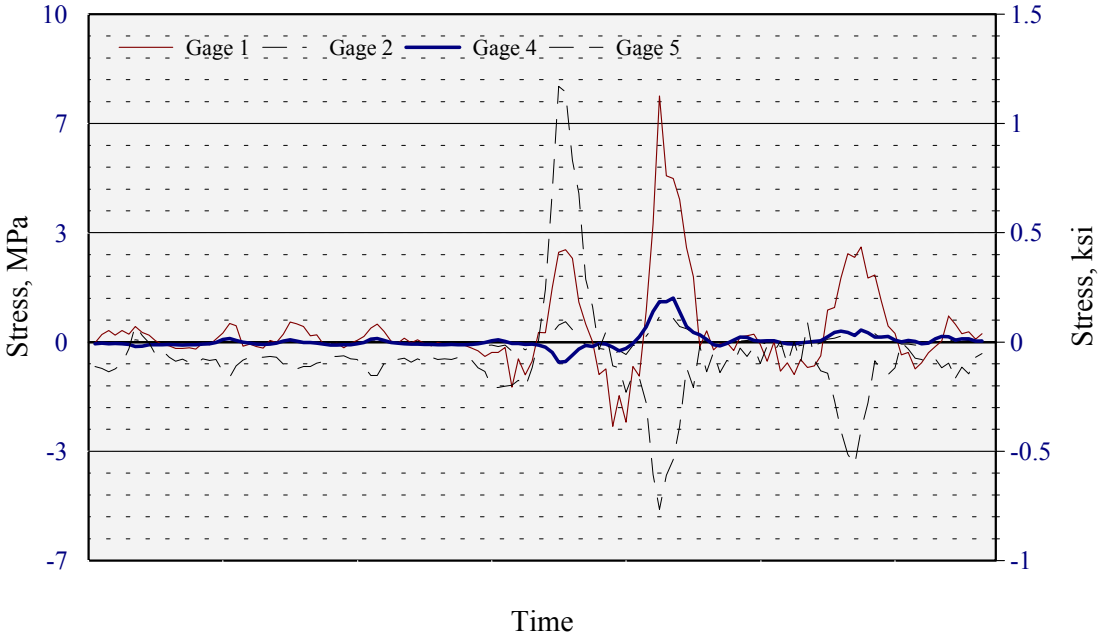

Figure C-5: Stress histories for Gage Group 1A, Truck Pass 1 (test truck centered in left lane).

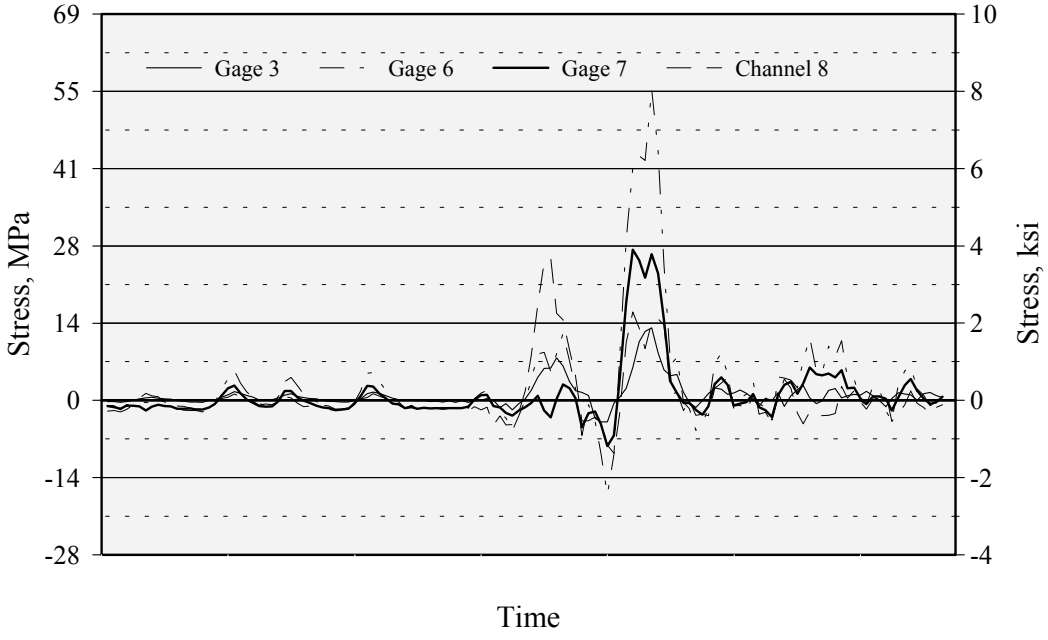

Figure C-6: Stress histories for Gage Group 1B, Truck Pass 1 (test truck centered in left lane).

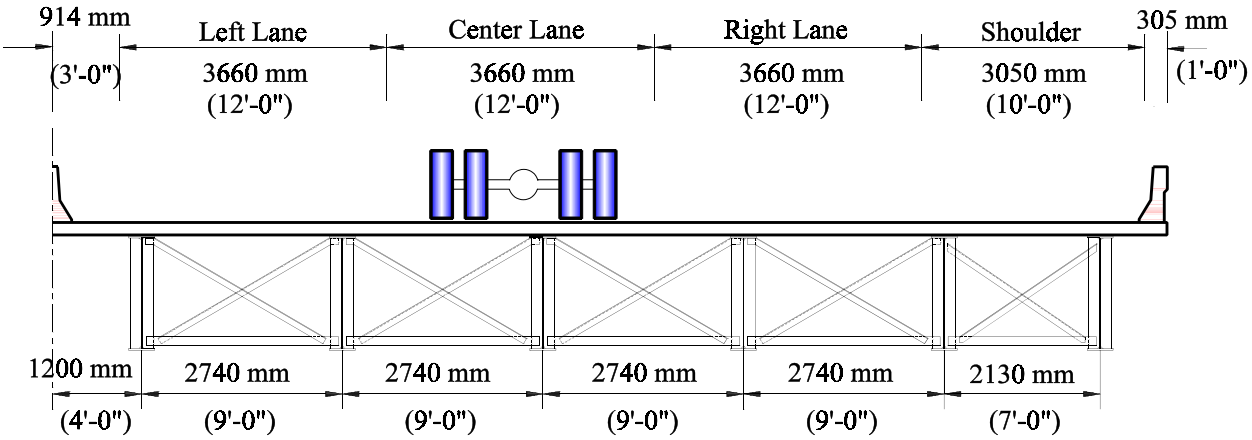

Figure C-7: Test truck position for Gage Group 1, Truck Pass 2 (test truck centered in center lane).

Table C-4: Maximum measured stress histories for Gage Group 1, Truck Pass 2 (test truck centered in center lane).

Gage Number	Location	Max. Stress Range, MPa	Max. Stress Range, ksi
1	Bottom flange, Girder No. 3	5.7 (T)	0.8 (T)
2	Bottom flange, Girder No. 2	5.0 (T)	0.7 (T)
3	Lower strut, neutral axis	13 (T)	1.9 (T)
4	Diagonal, neutral axis	9.5 (T)	1.4 (T)
5	Diagonal, neutral axis	4.3 (C)	0.6 (C)
6	Lower strut, top	57 (T)	8.2 (T)
7	Lower strut, bottom	29 (T)	4.1 (T)
8	Lower strut, top	23 (T)	3.3 (T)

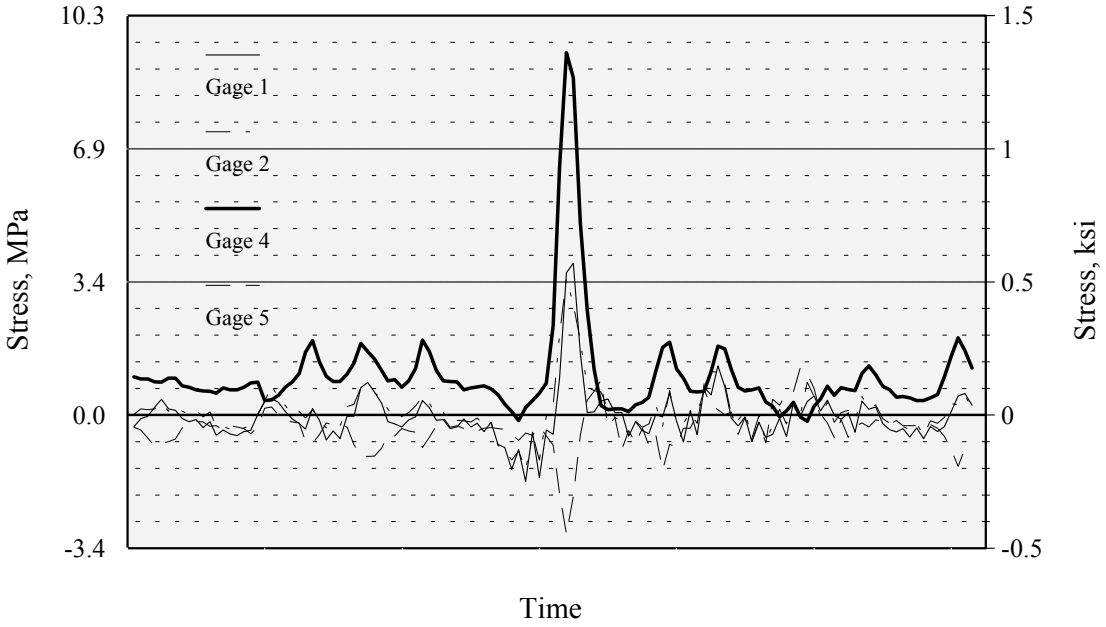

Figure C-8: Stress histories for Gage Group 1A, Truck Pass 2 (test truck centered in center lane).

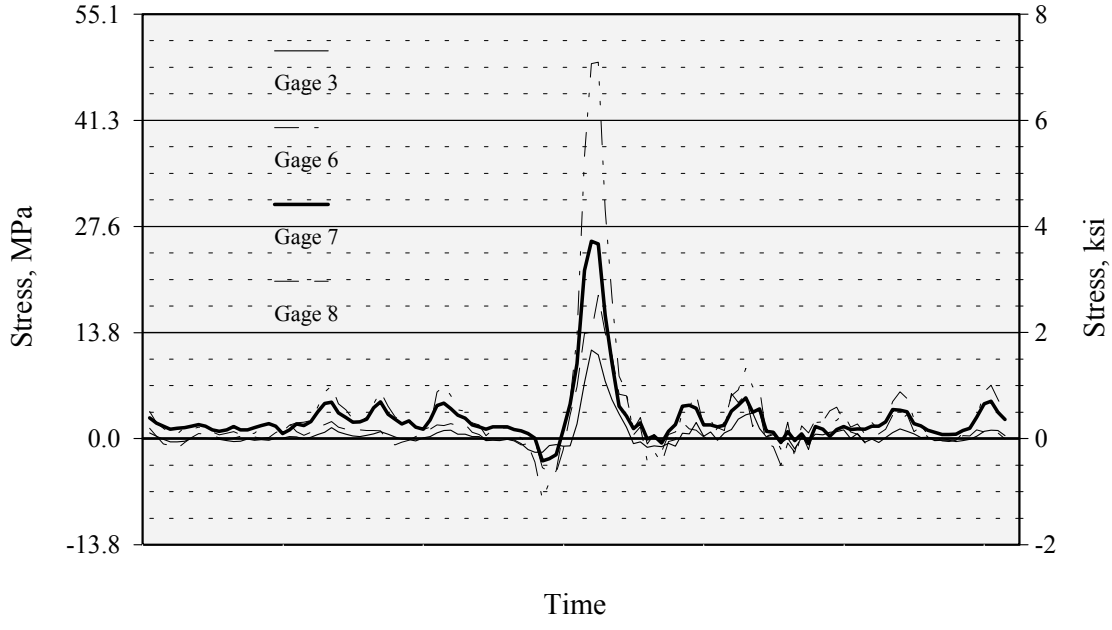

Figure C-9: Stress histories for Gage Group 1B, Truck Pass 2 (test truck centered in center lane).

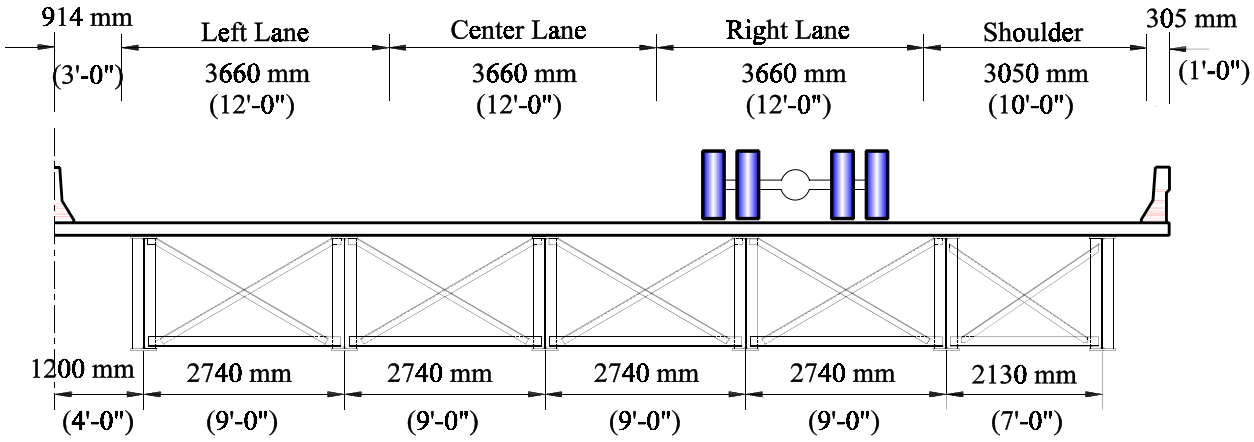

Figure C-10: Test truck position for Gage Group 1, Truck Pass 3 (test truck centered in right lane).

Table C-5: Maximum measured stress ranges for Gage Group 1, Truck Pass 3 (test truck centered in right lane).

Gage Number	Location	Max. Stress Range, MPa	Max. Stress Range, ksi
1	Bottom flange, Girder No. 3	5.1 (C)	0.7 (C)
2	Bottom flange, Girder No. 2	3.4 (T)	0.5 (T)
3	Lower strut, neutral axis	4.8 (C)	0.7 (C)
4	Diagonal, neutral axis	3.2 (T)	0.5 (T)
5	Diagonal, neutral axis	4.6 (T)	0.7 (T)
6	Lower strut, top	15 (T)	2.2 (T)
7	Lower strut, bottom	8.8 (T)	1.3 (T)
8	Lower strut, top	16 (T)	2.4 (T)

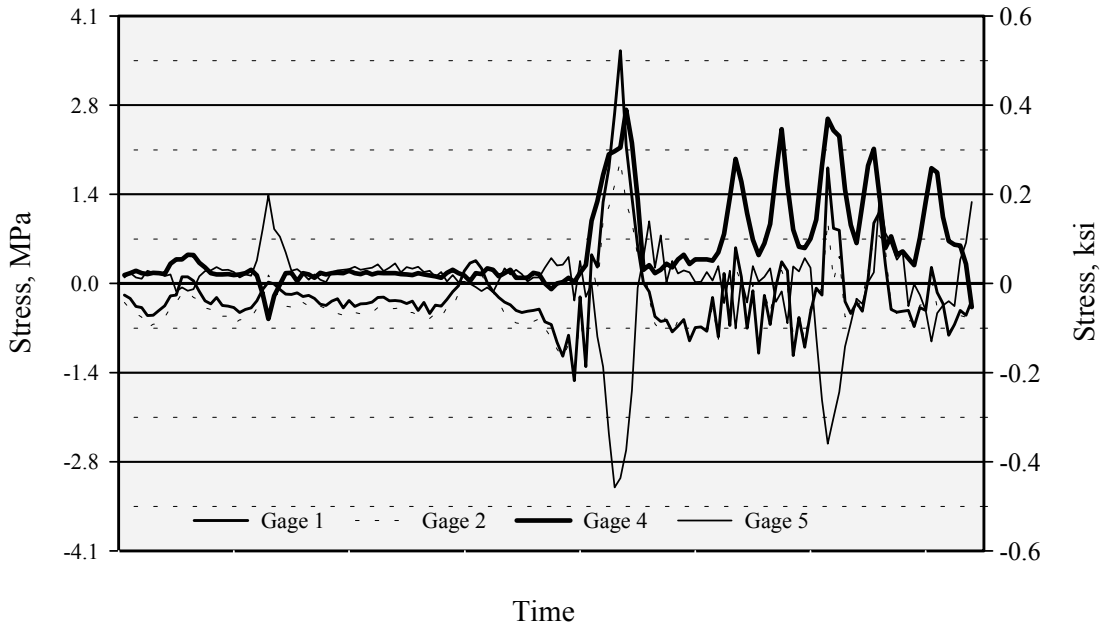

Figure C-11: Stress histories for Gage Group 1A, Truck Pass 3 (test truck centered in right lane).

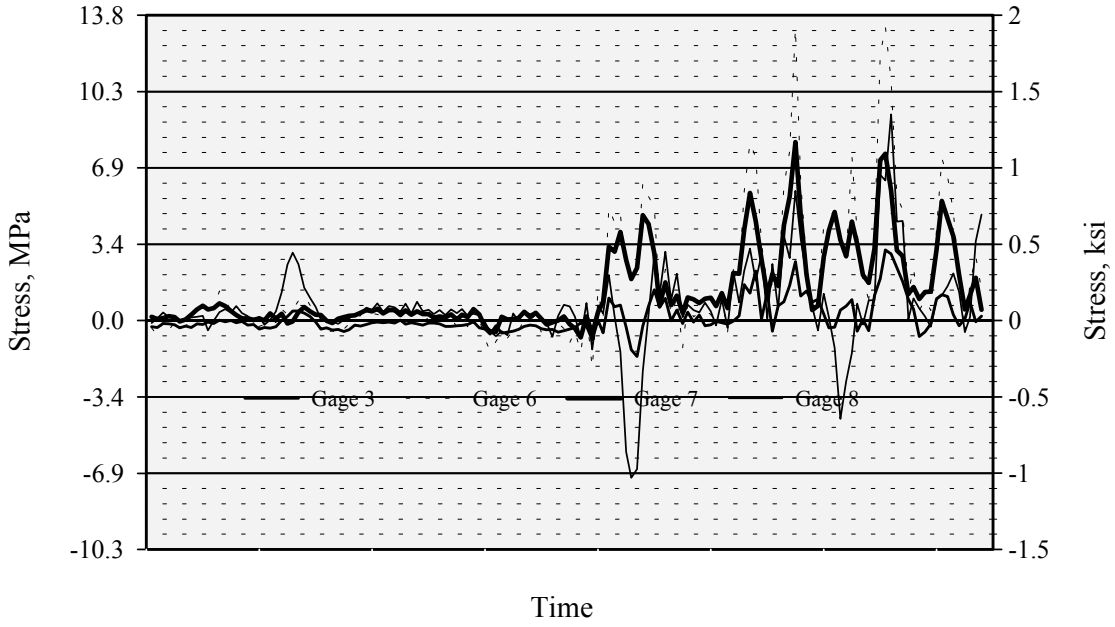

Figure C-12: Stress histories for Gage Group 1B, Truck Pass 3 (test truck centered in right lane).

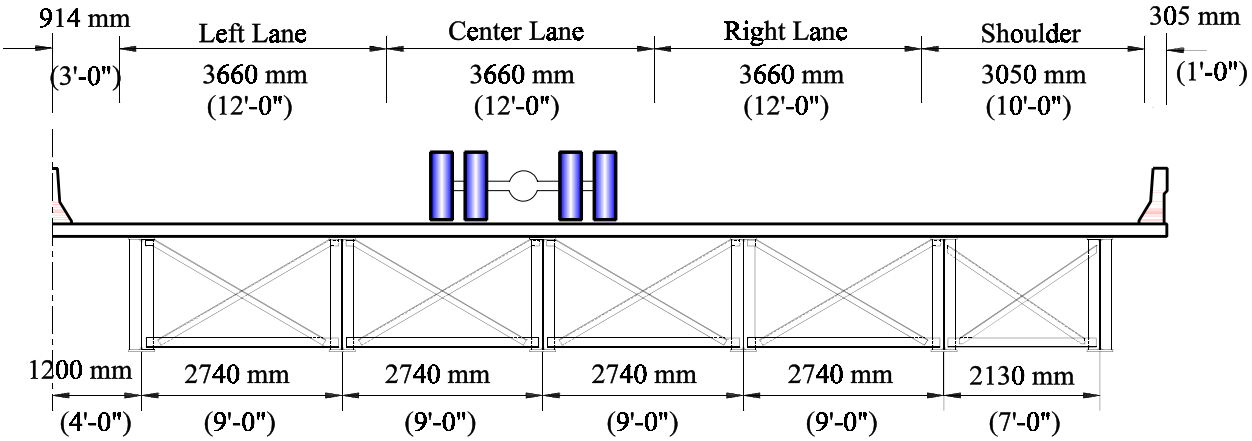

Figure C-13: Truck position for Gage Group 1, Truck Pass 4 (18-wheeler in center lane).

Table C-6: Maximum measured stress ranges for Gage Group 1, Truck Pass 4 (18-wheeler in center lane).

Gage Number	Location	Max. Stress Range, MPa	Max. Stress Range, ksi
1	Bottom flange, Girder No. 3	5.5 (C)	0.8 (C)
2	Bottom flange, Girder No. 2	4.6 (T)	0.7 (T)
3	Lower strut, neutral axis	13 (T)	2.0 (T)
4	Diagonal, neutral axis	7.3 (T)	1.1 (T)
5	Diagonal, neutral axis	3.6 (T)	0.5 (T)
6	Lower strut, top	51 (T)	7.4 (T)
7	Lower strut, bottom	27 (T)	3.9 (T)
8	Lower strut, top	22 (T)	3.2 (T)

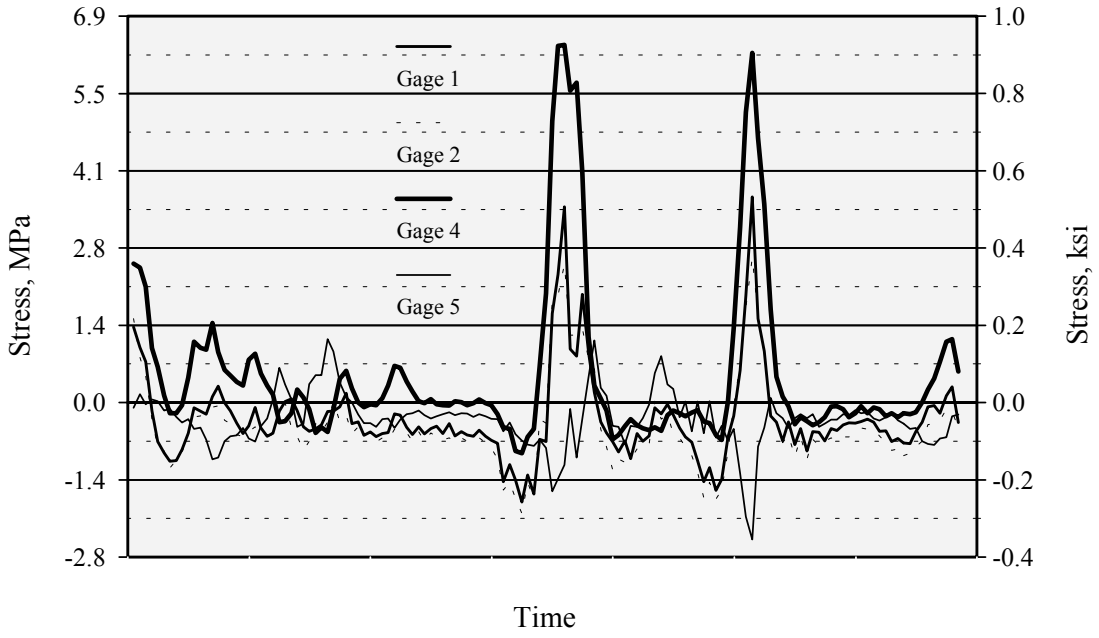

Figure C-14: Stress histories for Gage Group 1A, Truck Pass 4 (18-wheeler in center lane).

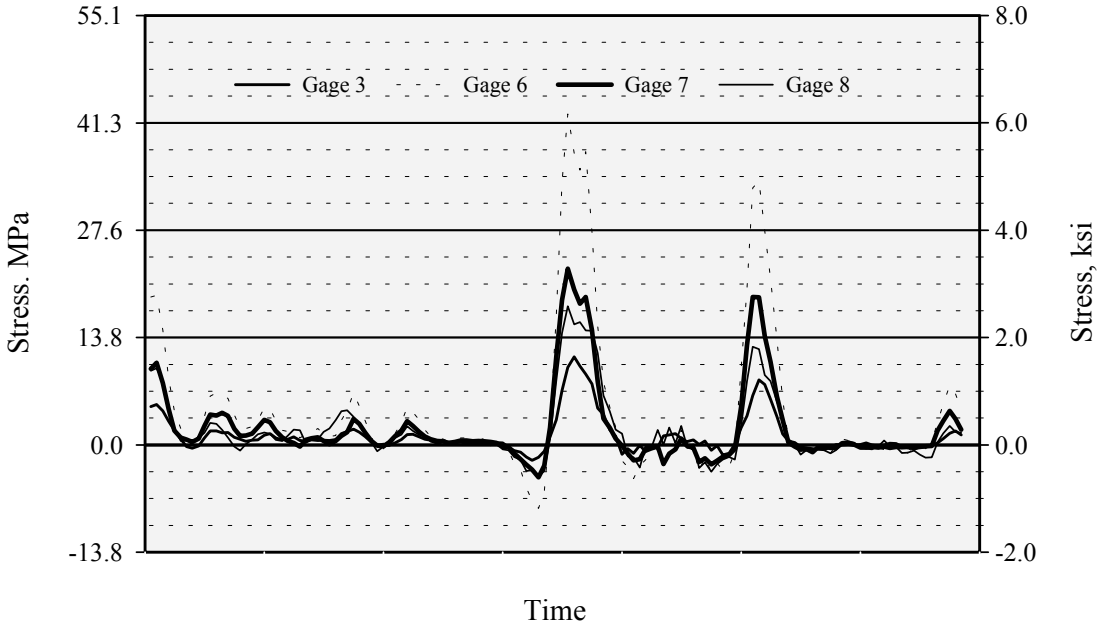

Figure C-15: Stress histories for Gage Group 1B, Truck Pass 4 (18-wheeler in center lane).

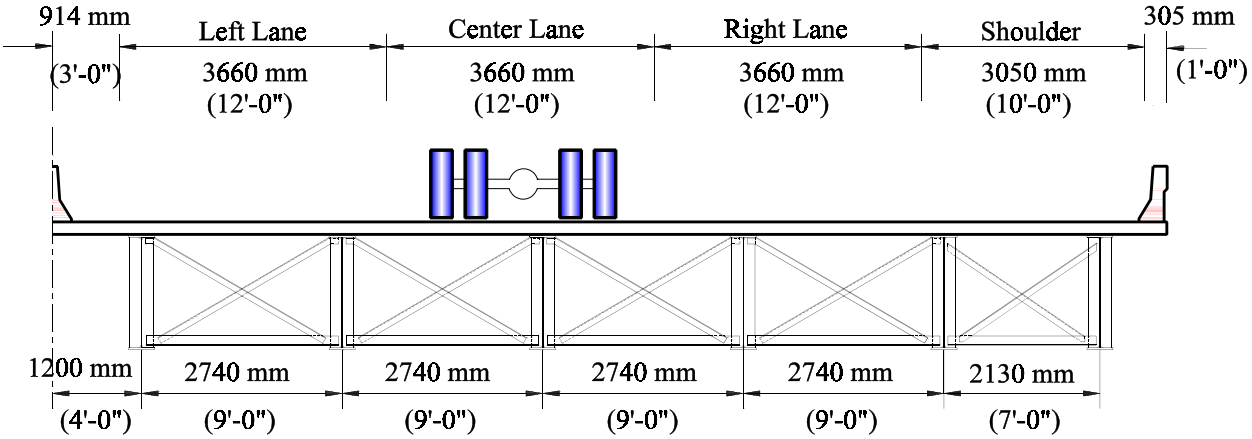

Figure C-16: Truck position for Gage Group 1, Truck Pass 5 (18-wheeler in center lane).

Table C-7: Maximum measured stress ranges for Gage Group 1, Truck Pass 5 (18-wheeler in center lane).

Gage Number	Location	Max. Stress Range, MPa	Max. Stress Range, ksi
1	Bottom flange, Girder No. 3	6.1 (T)	0.9 (T)
2	Bottom flange, Girder No. 2	5.7 (T)	0.8 (T)
3	Lower strut, neutral axis	16 (T)	2.3 (T)
4	Diagonal, neutral axis	11 (T)	1.6 (T)
5	Diagonal, neutral axis	9.0 (T)	1.3 (T)
6	Lower strut, top	61 (T)	8.8 (T)
7	Lower strut, bottom	29 (T)	4.3 (T)
8	Lower strut, top	28 (T)	4.1 (T)

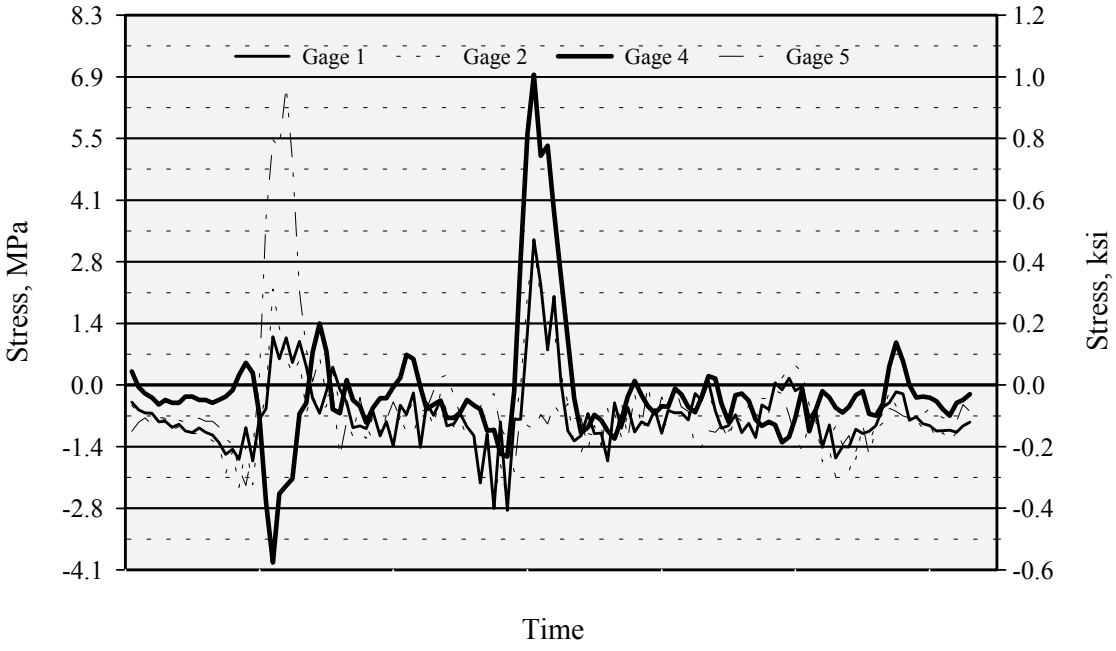

Figure C-17: Stress histories for Gage Group 1A, Truck Pass 5 (18-wheeler in center lane).

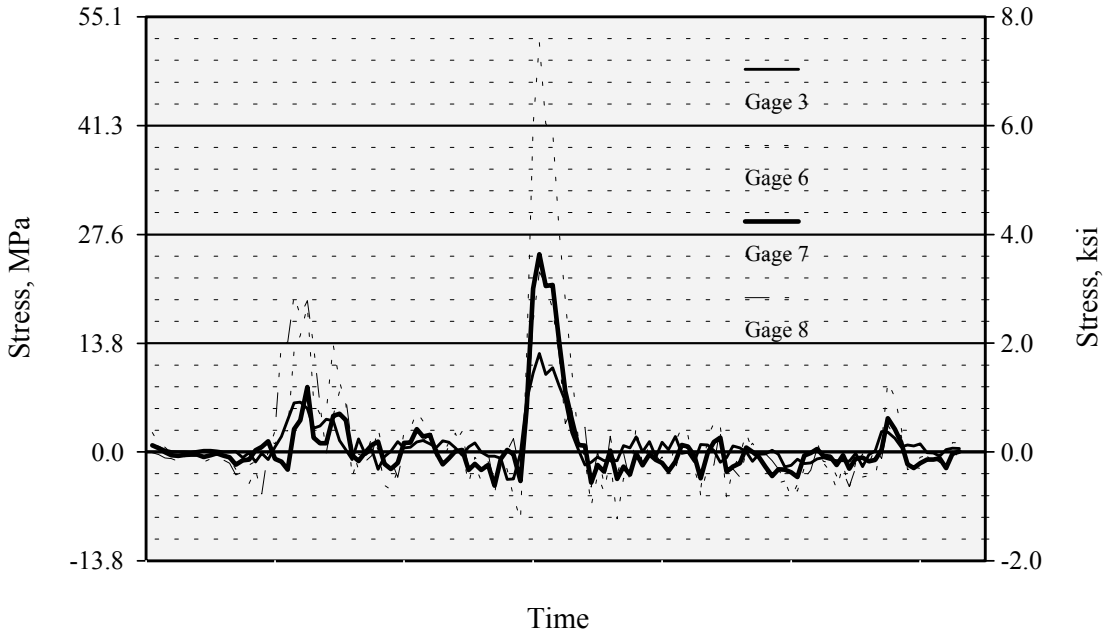

Figure C-18: Stress histories for Gage Group 1B, Truck Pass 5 (18-wheeler in center lane).

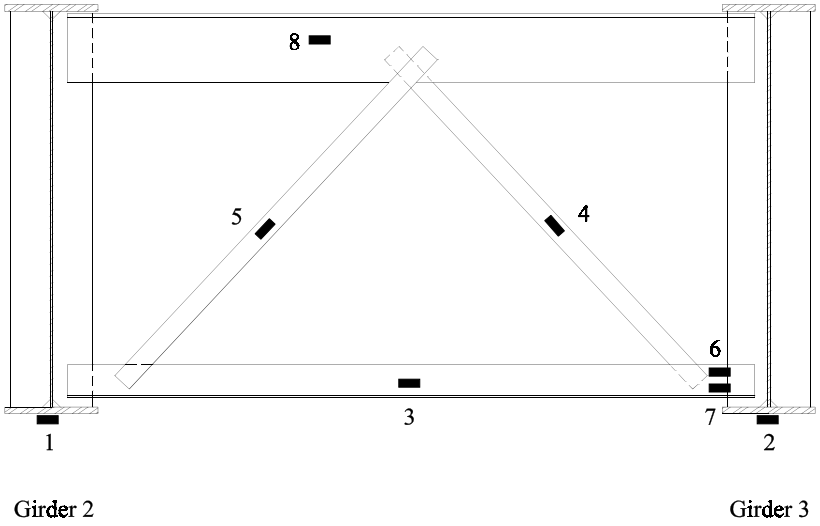

Figure C-19: Gage Group No. 2 location, Diaphragm B-21, Type D3 (positive bending moment region).

Table C-8: Gage locations for Group No. 2.

Gage Number	Position
1	Bottom flange, Girder No. 2, centerline of girder
2	Bottom flange, Girder No. 3, centerline of girder
3	Lower strut, neutral axis
4	Diagonal, neutral axis
5	Diagonal, neutral axis
6	Lower strut, top
7	Lower strut, bottom
8	Upper strut, neutral axis

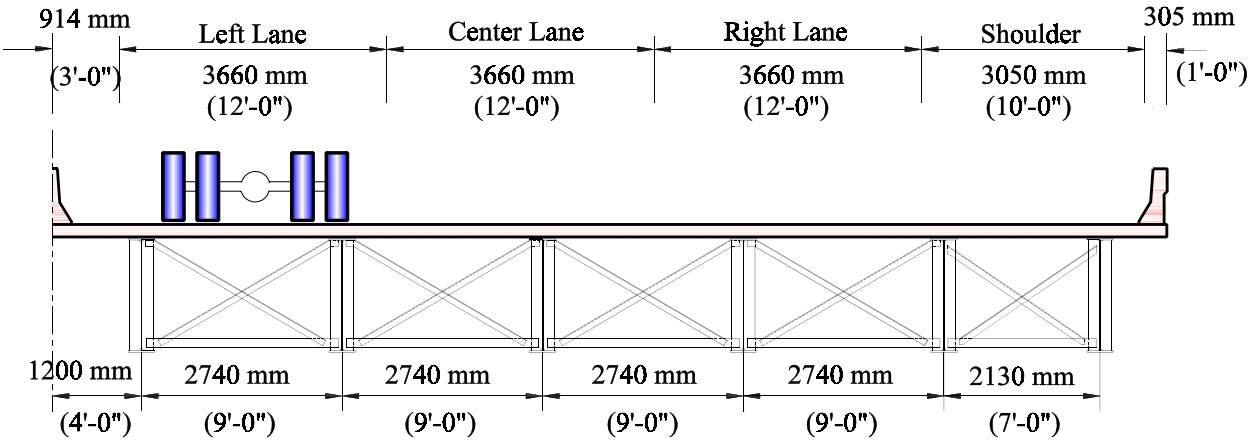

Figure C-20: Test truck position for Gage Group 2, Truck Pass 1 (test truck centered in left lane).

Table C-9: Maximum measured stress ranges for Gage Group 2, Truck Pass 1 (test truck centered in left lane).

Gage Number	Location	Max. Stress Range, MPa	Max. Stress Range, ksi
1	Bottom flange, Girder No. 2	4.8 (T)	0.69 (T)
2	Bottom flange, Girder No. 3	4.8 (T)	0.69 (T)
3	Lower strut, neutral axis	6.1 (T)	0.88 (T)
4	Diagonal, neutral axis	7.1 (C)	1.0 (C)
5	Diagonal, neutral axis	13 (C)	1.9 (C)
6	Lower strut, top	15 (R)	2.1 (R)
7	Lower strut, bottom	8.3 (R)	1.2 (R)
8	Upper strut, neutral axis	1.9 (T)	0.28 (T)

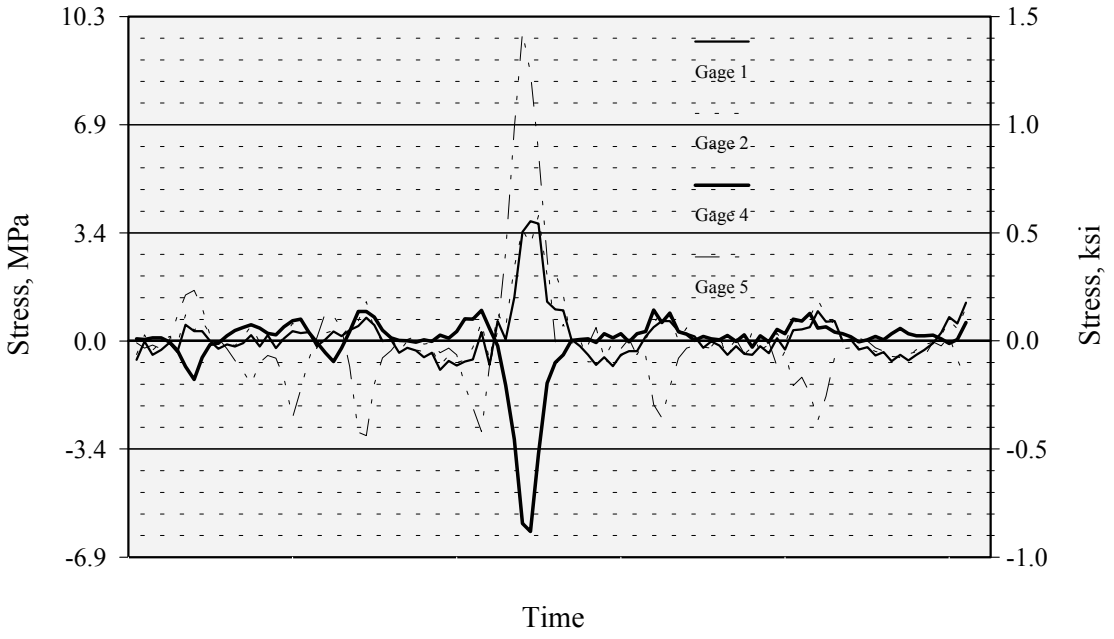

Figure C-21: Stress histories for Gage Group 2A, Truck Pass 1 (test truck centered in left lane).

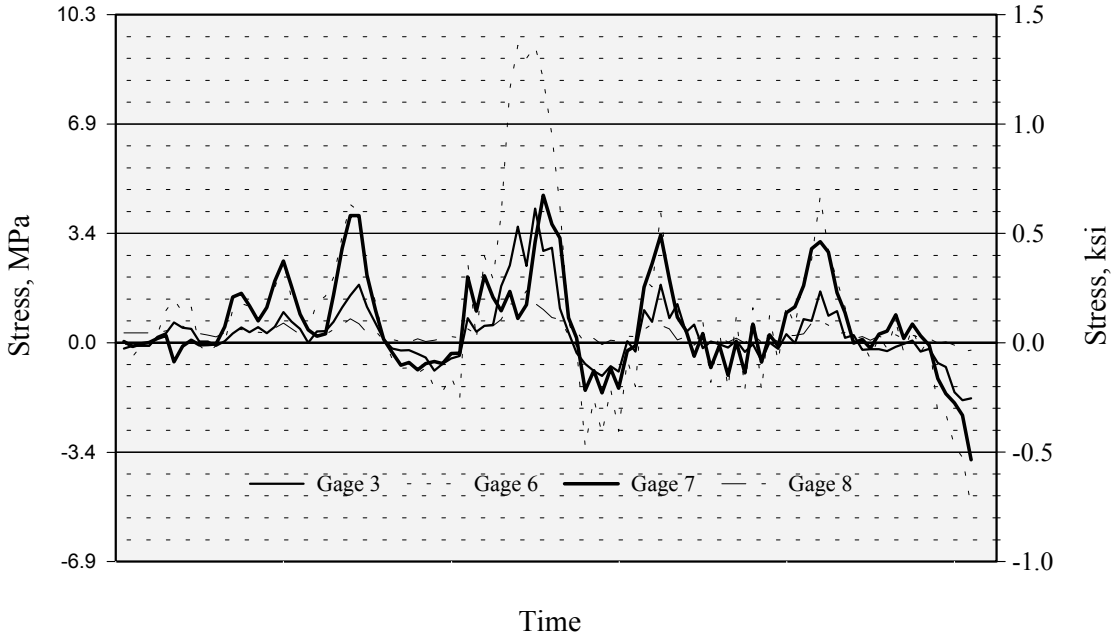

Figure C-22: Stress histories for Gage Group 2B, Truck Pass 1 (test truck centered in left lane).

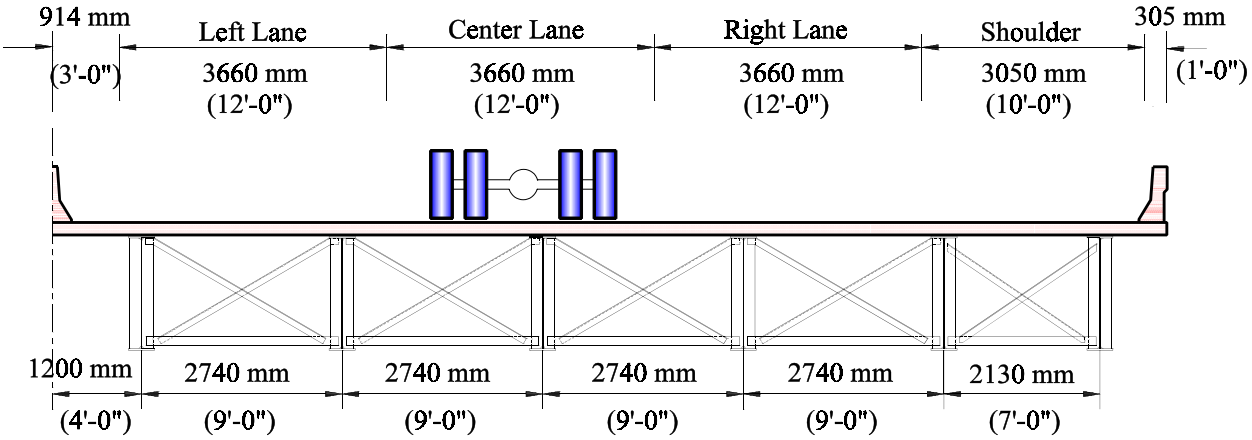

Figure C-23: Test truck position for Gage Group 2, Truck Pass 2 (test truck centered in center lane).

Table C-10: Maximum measured stress ranges for Gage Group 2, Truck Pass 2 (test truck centered in center lane).

Gage Number	Location	Max. Stress Range, MPa	Max. Stress Range, ksi
1	Bottom flange, Girder No. 2	5.5 (T)	0.8 (T)
2	Bottom flange, Girder No. 3	6.7 (T)	1.0 (T)
3	Lower strut, neutral axis	9.0 (T)	1.3 (T)
4	Diagonal, neutral axis	6.0 (T)	1.0 (T)
5	Diagonal, neutral axis	14 (C)	2.1 (C)
6	Lower strut, top	2.1 (T)	0.3 (T)
7	Lower strut, bottom	21 (T)	3.0 (T)
8	Upper strut, neutral axis	1.4 (T)	0.2 (T)

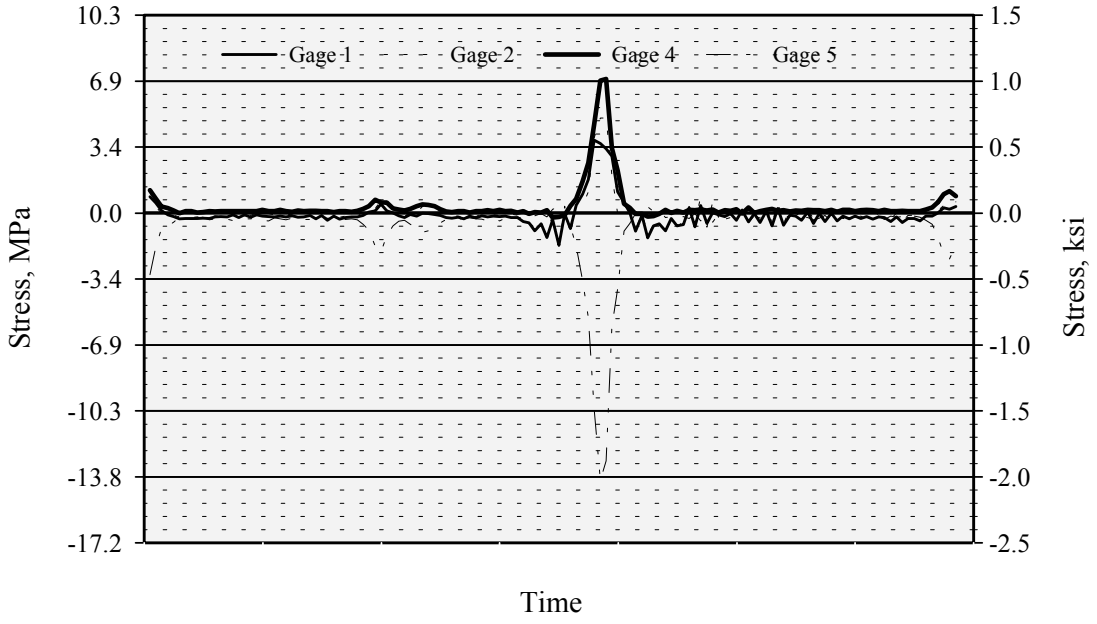

Figure C-24: Stress histories for Gage Group 2A, Truck Pass 2 (test truck centered in center lane).

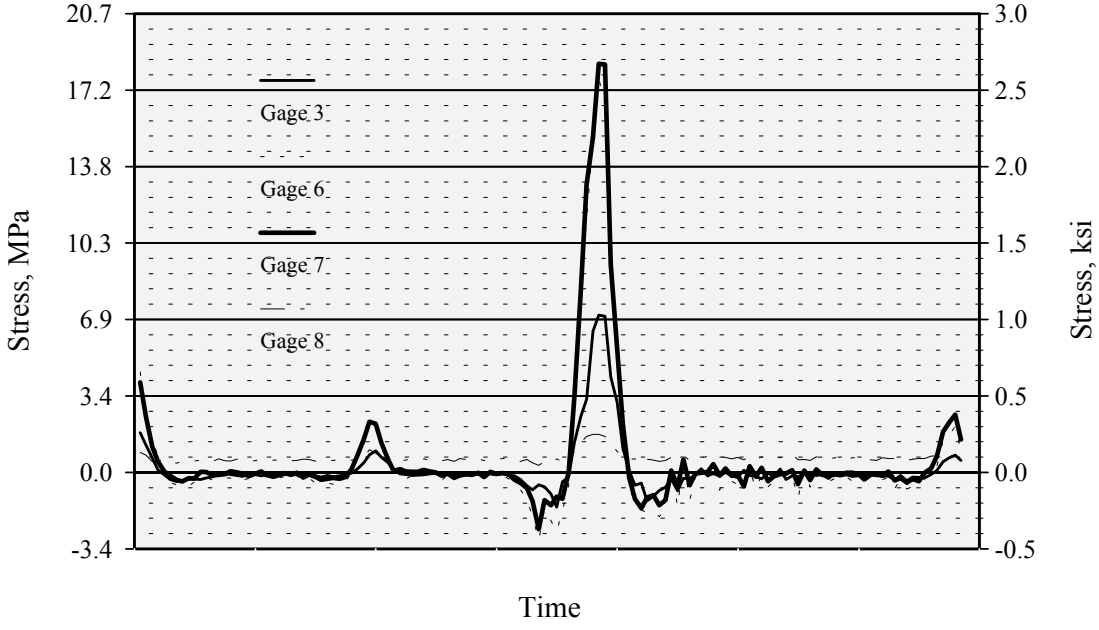

Figure C-25: Stress histories for Gage Group 2B, Truck Pass 2 (test truck centered in center lane).

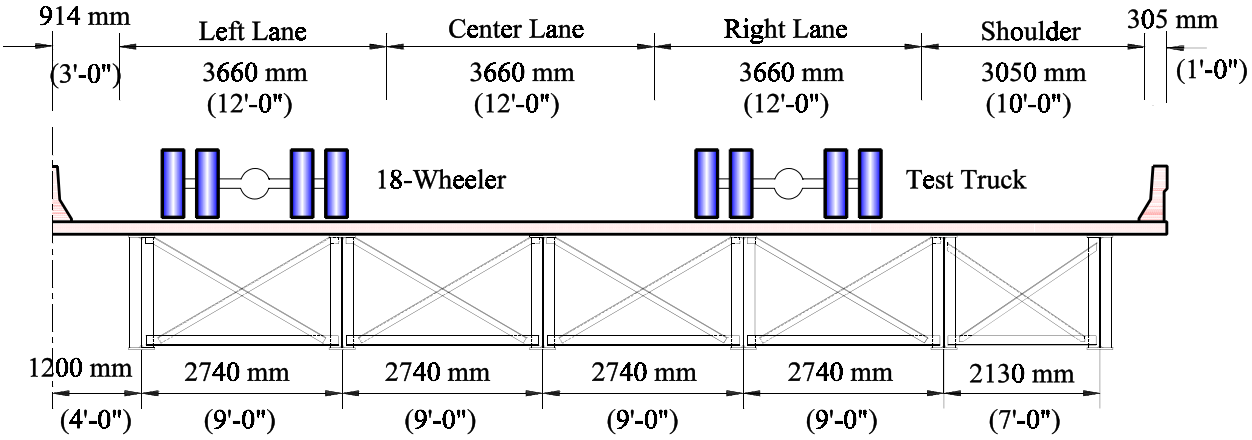

Figure C-26: Truck positions for Gage Group 2, Truck Pass 3 (test truck centered in right lane with 18-wheeler in left lane).

Table C-11: Maximum measured stress ranges for Gage Group 2, Truck Pass 2 (test truck centered in center lane).

Gage Number	Location	Max. Stress Range, MPa	Max. Stress Range, ksi
1	Bottom flange, Girder No. 2	1.4 (T)	0.2 (T)
2	Bottom flange, Girder No. 3	1.6 (T)	0.2 (T)
3	Lower strut, neutral axis	1.8 (T)	0.3 (T)
4	Diagonal, neutral axis	14 (C)	2.1 (C)
5	Diagonal, neutral axis	3.3 (T)	0.5 (T)
6	Lower strut, top	4.2 (T)	0.6 (T)
7	Lower strut, bottom	1.6 (T)	0.2 (T)
8	Upper strut, neutral axis	0.5 (T)	0.1 (T)

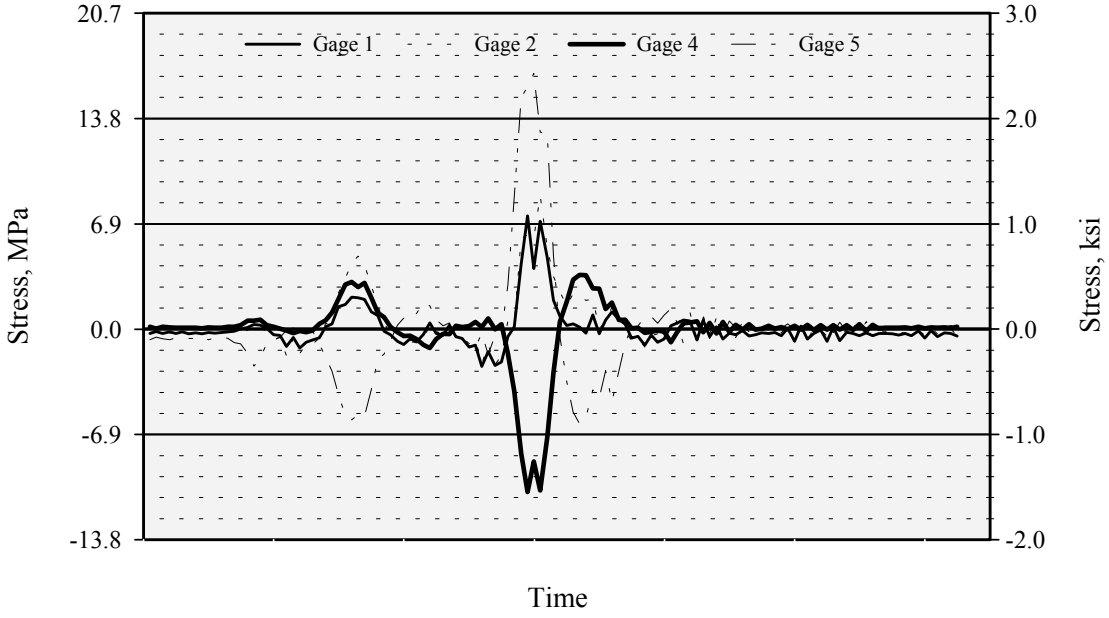

Figure C-27: Stress histories for Gage Group 2A, Truck Pass 3 (test truck in right lane with 18-wheeler in left lane).

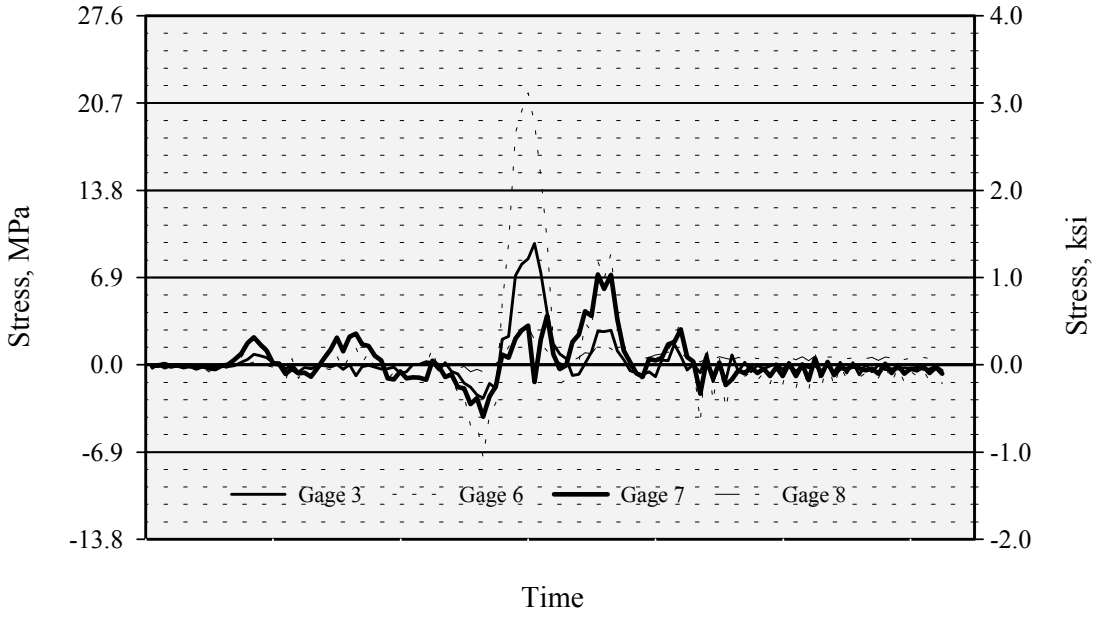

Figure C-28: Stress histories for Gage Group 2B, Truck Pass 3 (test truck in right lane with 18-wheeler in left lane).

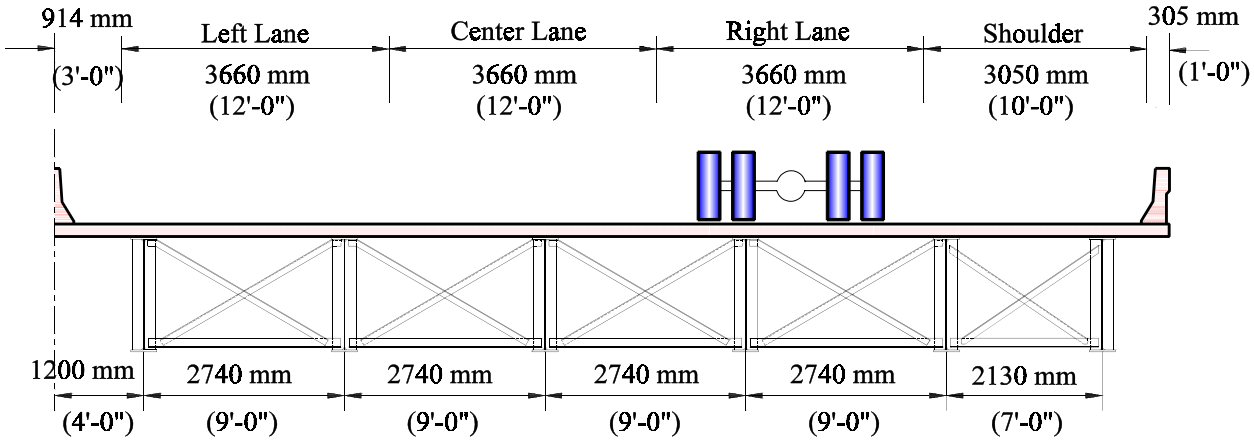

Figure C-29: Truck positions for Gage Group 2, Truck Pass 4 (test truck centered in right lane).

Table C-12: Maximum measured stress ranges for Gage Group 2, Truck Pass 4 (test truck centered in right lane).

Gage Number	Location	Max. Stress Range, MPa	Max. Stress Range, ksi
1	Bottom flange, Girder No. 2	5.5 (T)	0.8 (T)
2	Bottom flange, Girder No. 3	6.7 (T)	1.0 (T)
3	Lower strut, neutral axis	8.7 (T)	1.1 (T)
4	Diagonal, neutral axis	7.2 (T)	1.1 (T)
5	Diagonal, neutral axis	14 (C)	2.1 (C)
6	Lower strut, top	21 (R)	3.0 (R)
7	Lower strut, bottom	21 (T)	3.0 (T)
8	Upper strut, neutral axis	1.4 (T)	0.2 (T)

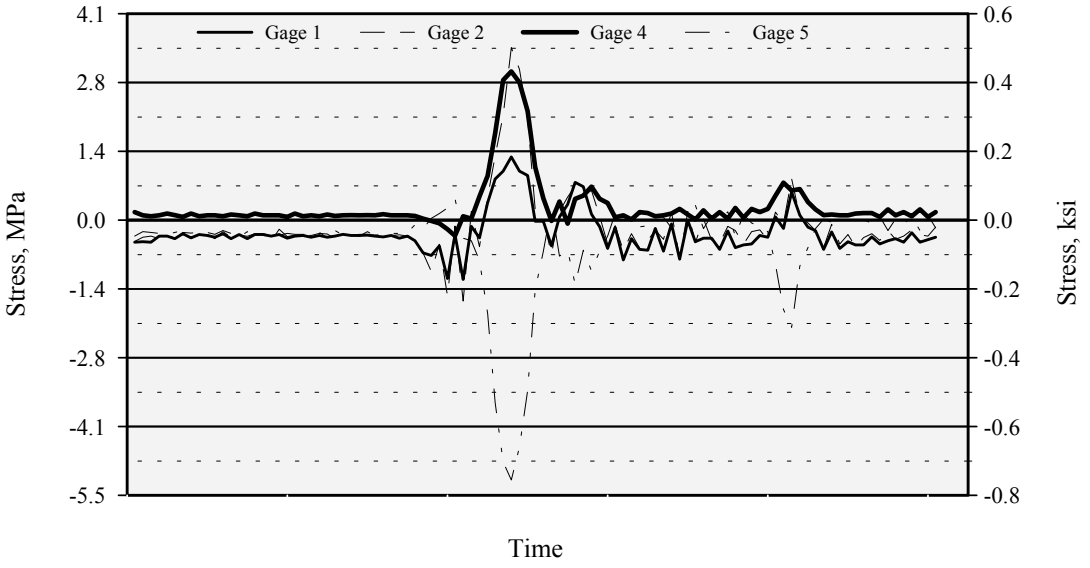

Figure C-31: Stress histories for Gage Group 2A, Truck Pass 4, (test truck centered in right lane).

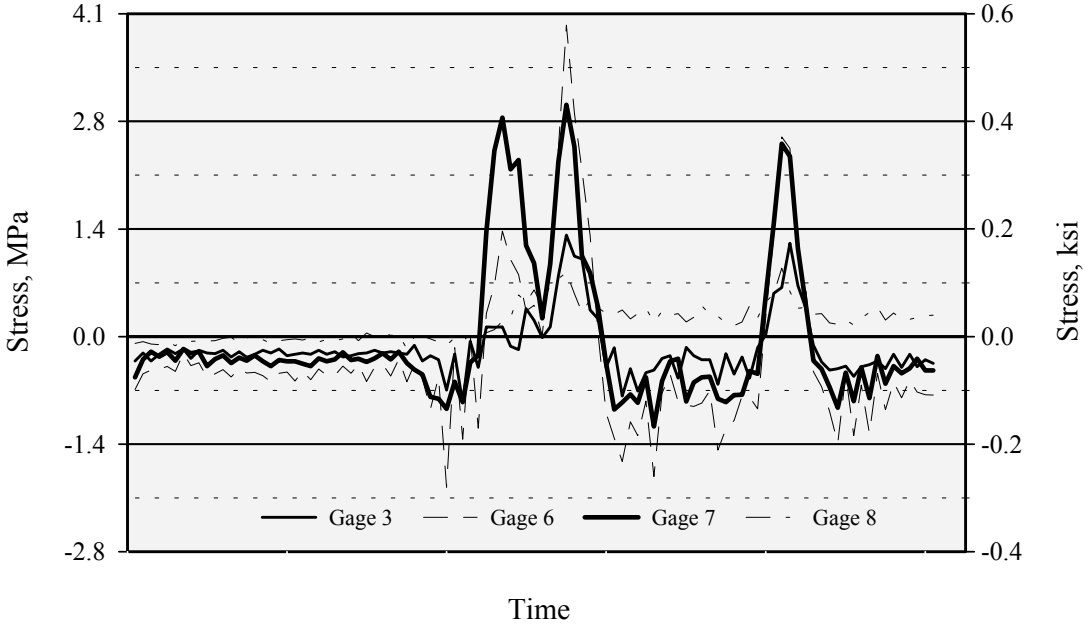

Figure C-30: Stress histories for Gage Group 2B, Truck Pass 4 (test truck centered in right lane).

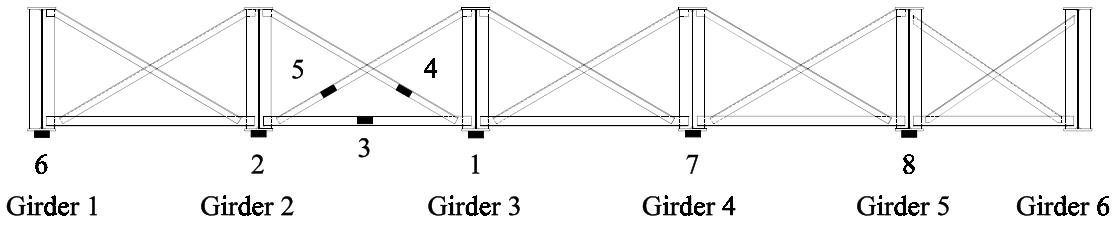

Figure C-32: Gage Group No. 3, Diaphragm Line 22
(positive bending moment region).

Table C-13: Gage locations for Gage Group 3.

Gage Number	Position
1	Bottom flange, centerline of girder
2	Bottom flange, centerline of girder
3	Lower strut, Neutral axis
4	Diagonal, Neutral axis
5	Diagonal, Neutral axis
6	Bottom flange, centerline of girder
7	Bottom flange, centerline of girder
8	Bottom flange, centerline of girder

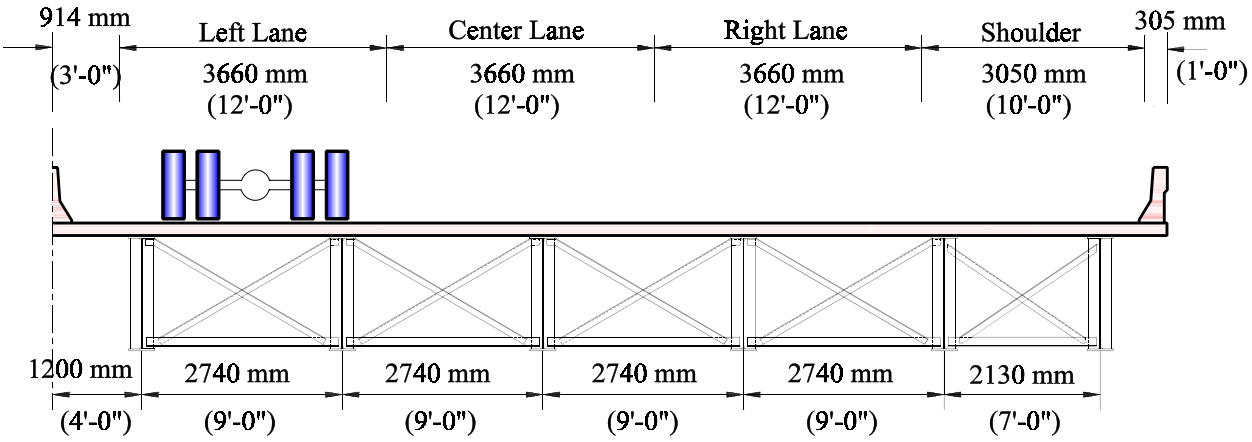

Figure C-33: Truck position for Gage Group 3, Truck Pass 1 (test truck centered in left lane).

Table C-14: Maximum measured stress ranges for Gage Group 3, Truck Pass 1, (test truck in left lane).

Gage Number	Location	Max. Stress Range, MPa	Max. Stress Range, ksi
1	Bottom flange, Girder No. 2	9.9 (T)	1.4 (T)
2	Bottom flange, Girder No. 3	11 (T)	1.6 (T)
3	Lower strut, neutral axis	12 (T)	1.8 (T)
4	Diagonal, neutral axis	14 (C)	2.1 (C)
5	Diagonal, neutral axis	23 (T)	3.3 (T)
6	Lower strut, top	29 (T)	4.2 (T)
7	Lower strut, bottom	11 (C)	1.6 (C)
8	Upper strut, neutral axis	3.6 (R)	0.52 (R)

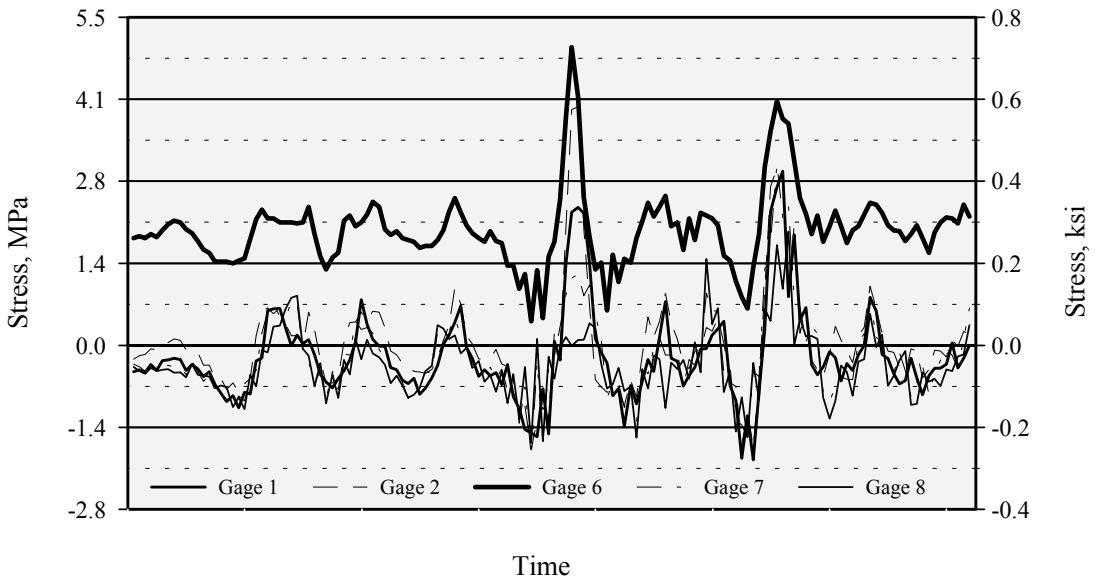

Figure C-34: Stress histories for Gage Group 3A, Truck Pass 1 (test truck in left lane).

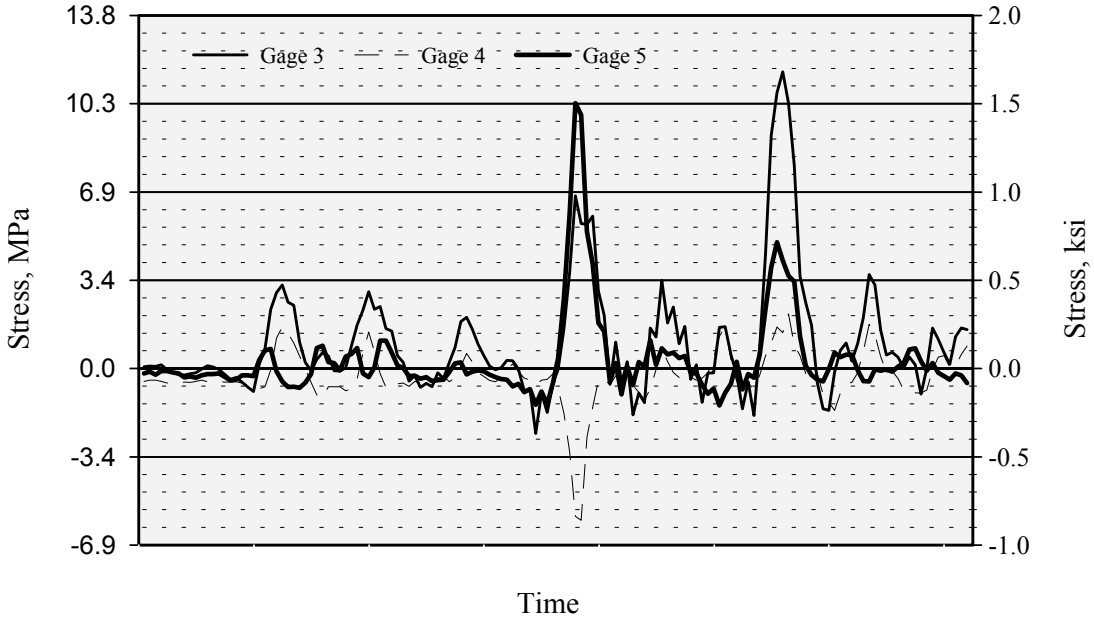

Figure C-35: Stress histories for Gage Group 3B, Truck Pass 1 (test truck in left lane).

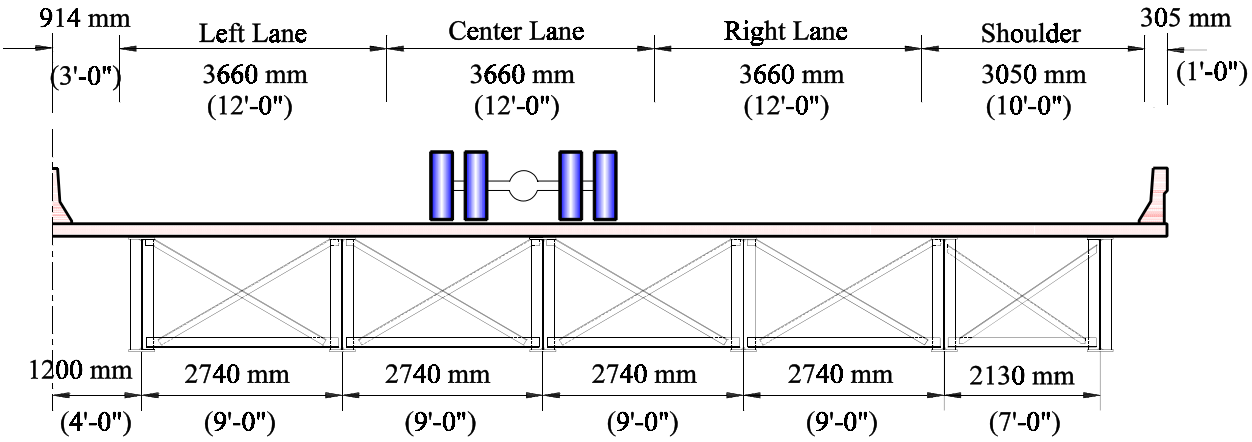

Figure C-36: Truck position for Gage Group 3, Truck Pass 2 (test truck centered in center lane).

Table C-15: Maximum measured stress ranges for Gage Group 3, Truck Pass 2 (test truck in center lane).

Gage Number	Location	Max. Stress Range, MPa	Max. Stress Range, ksi
1	Bottom flange, Girder No. 2	2.5 (T)	0.36 (T)
2	Bottom flange, Girder No. 3	5.1 (R)	0.74 (R)
3	Lower strut, neutral axis	2.1 (T)	0.31 (T)
4	Diagonal, neutral axis	3.3 (T)	0.48 (T)
5	Diagonal, neutral axis	5.7 (C)	0.82 (C)
6	Lower strut, top	5.9 (T)	0.86 (T)
7	Lower strut, bottom	4.1 (T)	0.60 (T)
8	Upper strut, neutral axis	1.0 (T)	0.15 (T)

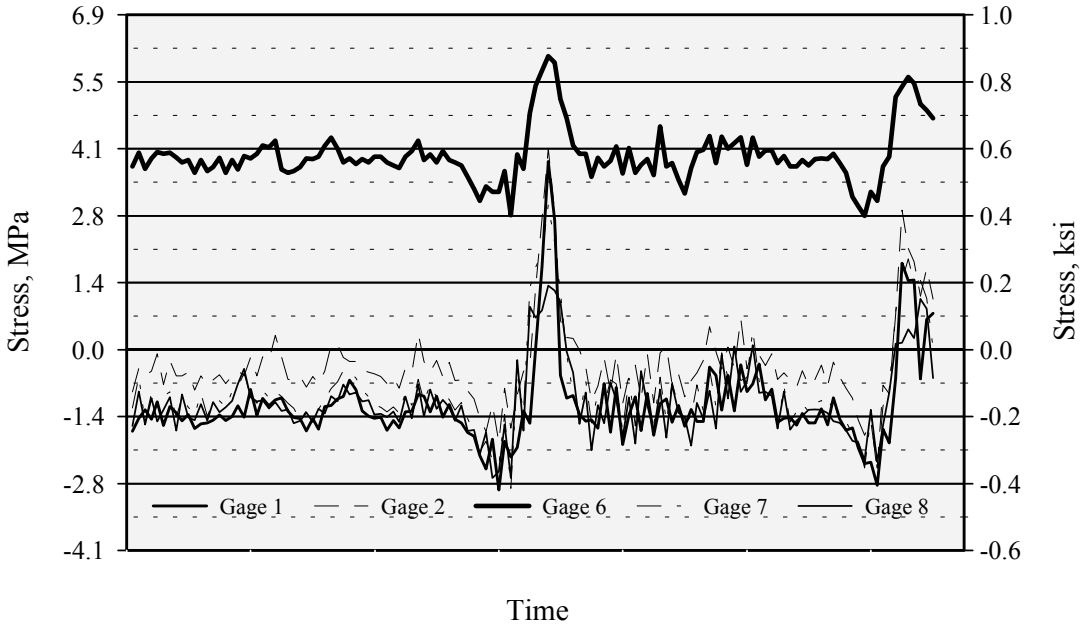

Figure C-37: Stress histories for Gage Group 3A, Truck Pass 2 (test truck centered in center lane).

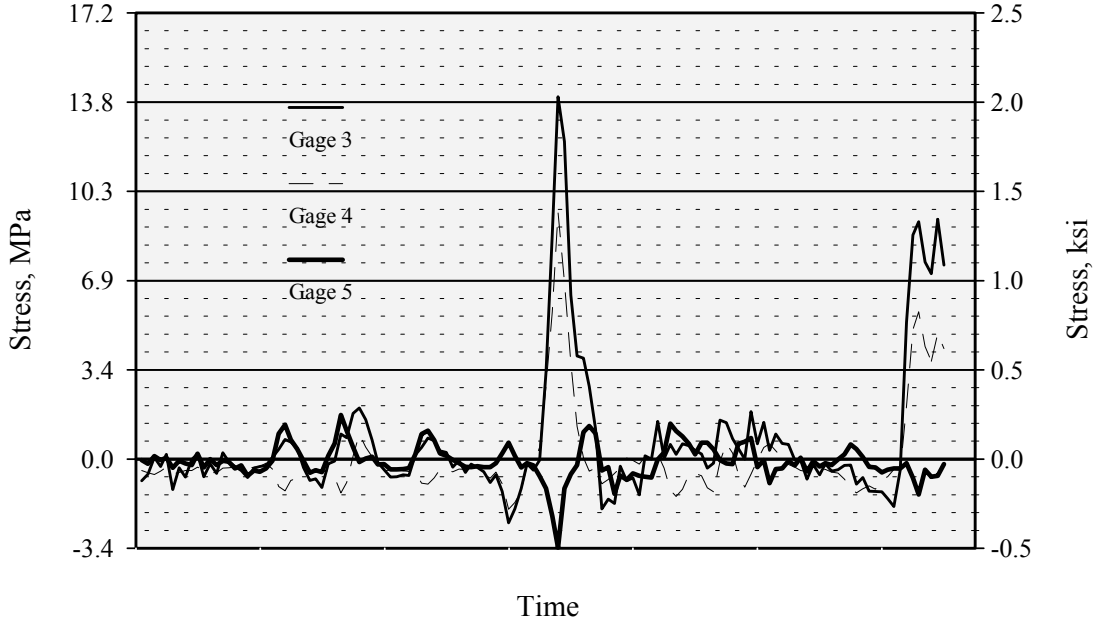

Figure C-38: Stress histories for Gage Group 3B, Truck Pass 2 (test truck centered in center lane).

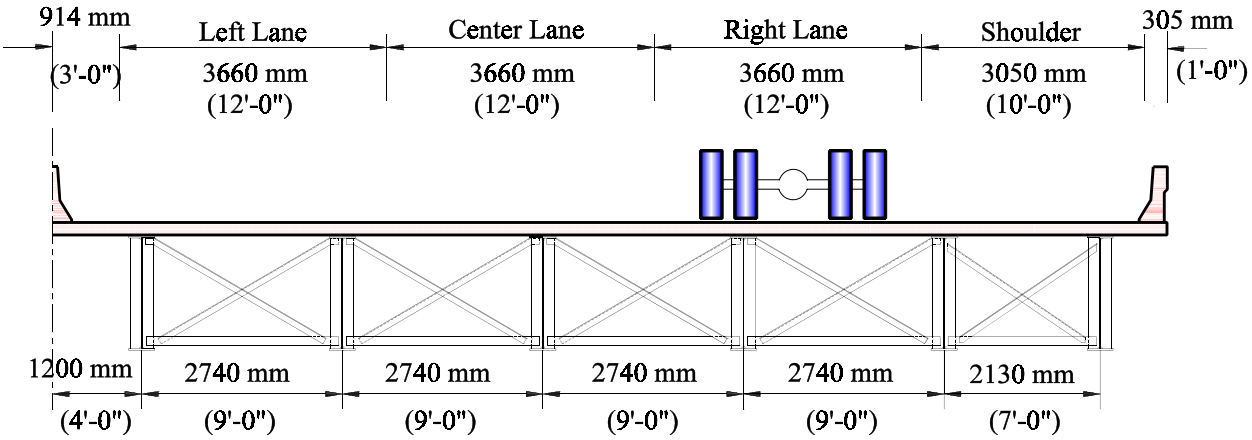

Figure C-39: Truck position for Gage Group 3, Truck Pass 3 (test truck centered in right lane).

Table C-16: Maximum measured stress ranges for Gage Group 3, Truck Pass 3 (test truck centered in right lane).

Gage Number	Location	Max. Stress Range, MPa	Max. Stress Range, ksi
1	Bottom flange, Girder No. 3	4.8 (T)	0.7 (T)
2	Bottom flange, Girder No. 2	5.8 (T)	0.8 (T)
3	Lower strut, Bay B	14 (C)	2.1 (C)
4	Diagonal, Bay B	8.1 (T)	1.2 (T)
5	Diagonal, Bay B	12 (C)	1.7 (C)
6	Bottom flange, Girder No. 1	5.0 (T)	0.7 (T)
7	Bottom flange, Girder No. 4	4.9 (T)	0.7 (T)
8	Bottom flange, Girder No. 5	3.6 (T)	0.5 (T)

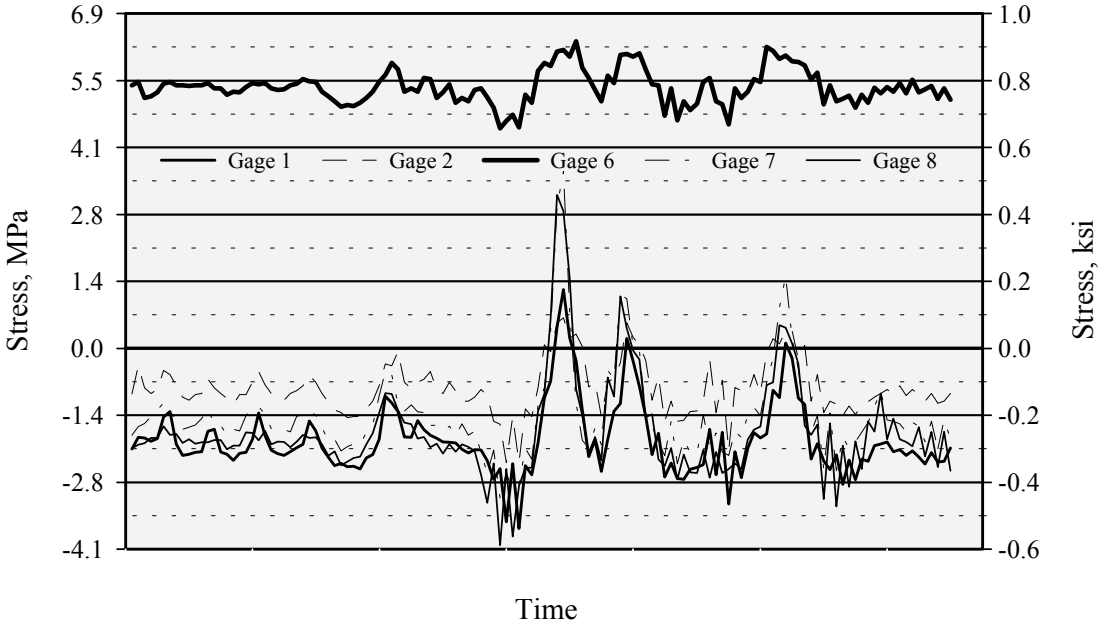

Figure C-40: Stress histories for Gage Group 3A, Truck Pass 3 (test truck centered in right lane).

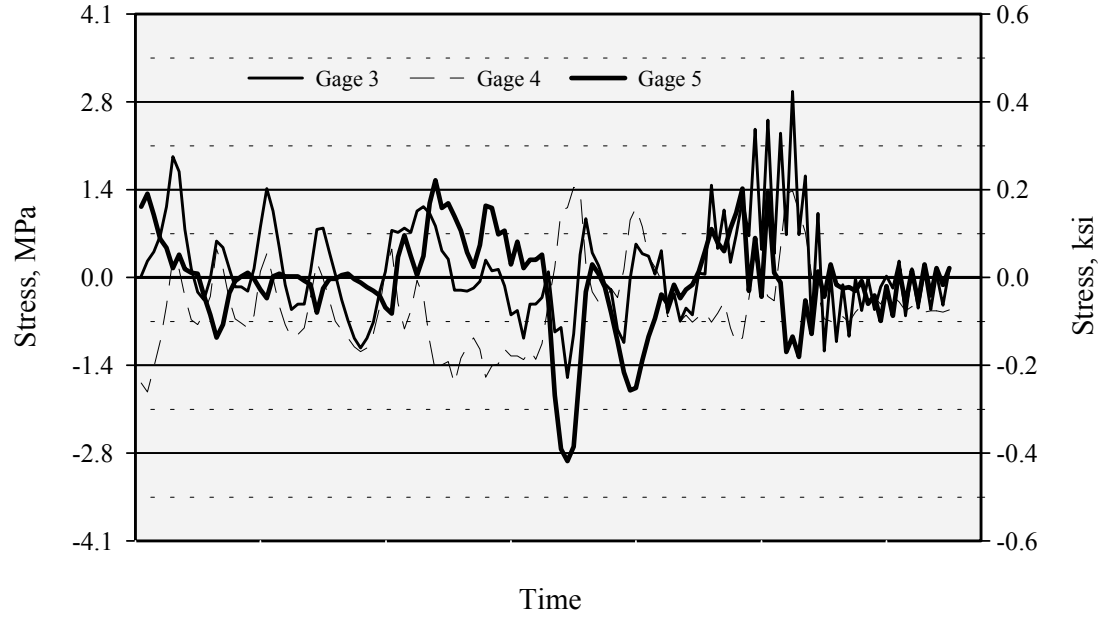

Figure C-41: Stress histories for Gage Group 3B, Truck Pass 3 (test truck centered in right lane).

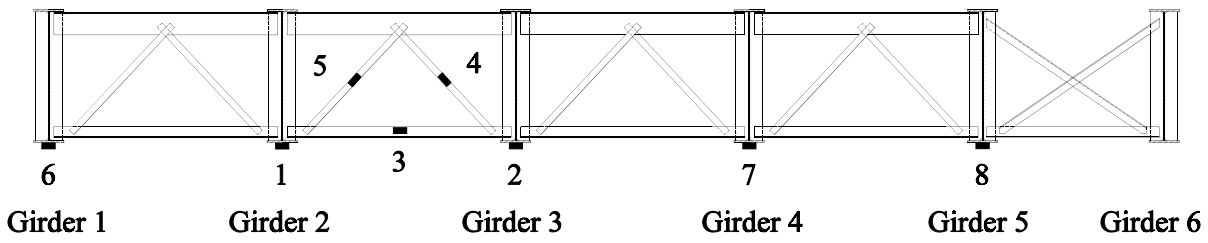

Figure C-42: Strain gage locations for Gage Group 4.

Table C-17: Gage locations for Gage Group 4.

Gage Number	Position
1	Bottom flange, centerline of girder
2	Bottom flange, centerline of girder
3	Lower strut, Neutral axis
4	Diagonal, Neutral axis
5	Diagonal, Neutral axis
6	Bottom flange, centerline of girder
7	Bottom flange, centerline of girder
8	Bottom flange, centerline of girder

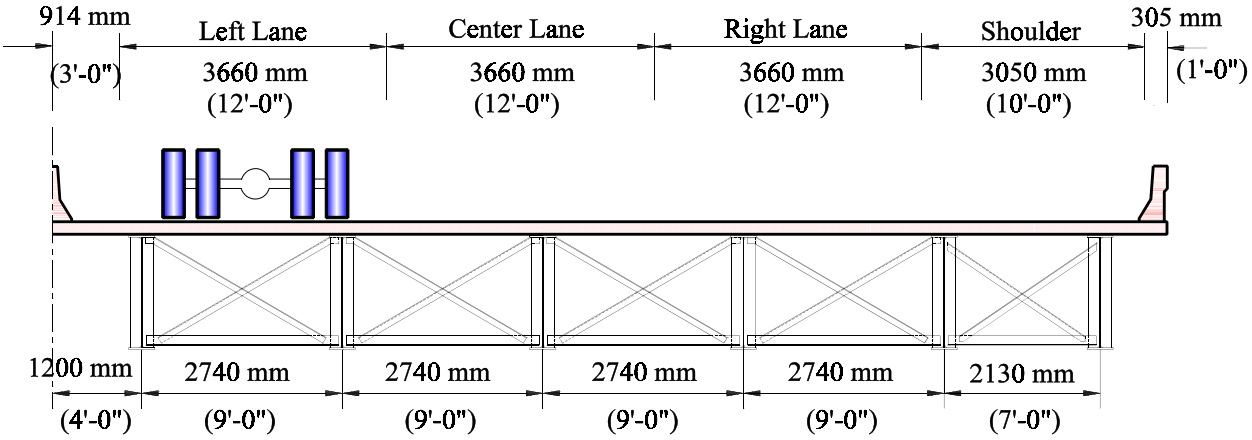

Figure C-43: Truck position for Gage Group 4, Truck Pass 1 (test truck centered in left lane).

Table C-18: Maximum measured stress ranges for Gage Group 4, Truck Pass 1 (test truck in left lane).

Gage Number	Location	Max. Stress Range, MPa	Max. Stress Range, ksi
1	Bottom flange, Girder No. 2	3.0 (T)	0.4 (T)
2	Bottom flange, Girder No. 3	4.2 (T)	0.6 (T)
3	Lower strut, neutral axis	3.2 (T)	0.5 (T)
4	Diagonal, neutral axis	5.2 (T)	0.8 (T)
5	Diagonal, neutral axis	57 (C)	8.2 (C)
6	Lower strut, top	3.3 (T)	0.5 (T)
7	Lower strut, bottom	8.6 (T)	1.2 (T)
8	Upper strut, neutral axis	---	---

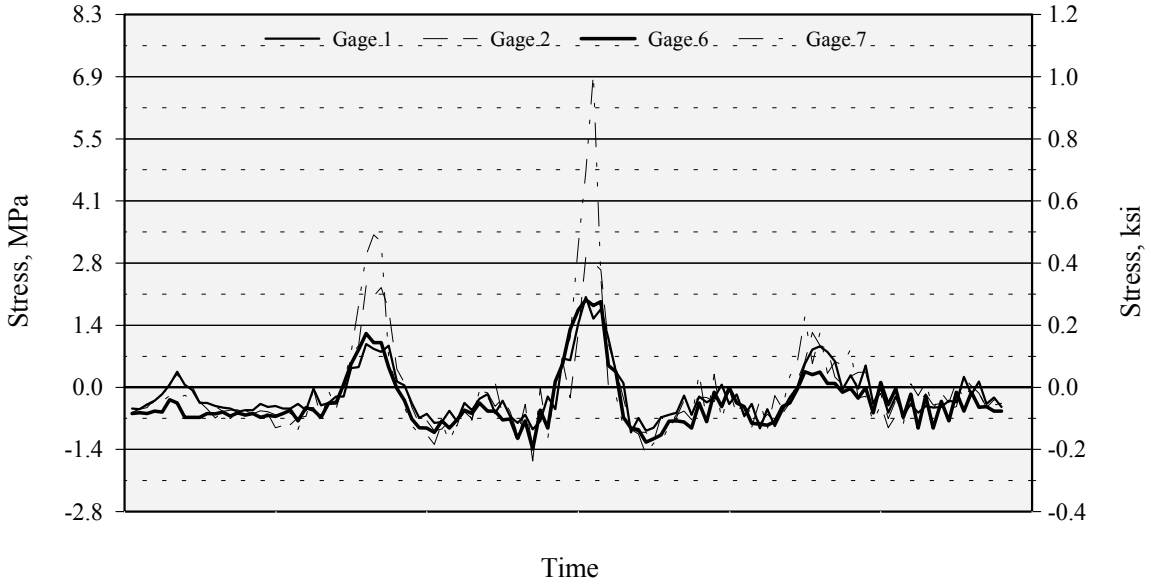

Figure C-44: Stress histories for Gage Group 4A, Truck Pass 1 (test truck centered in left lane).

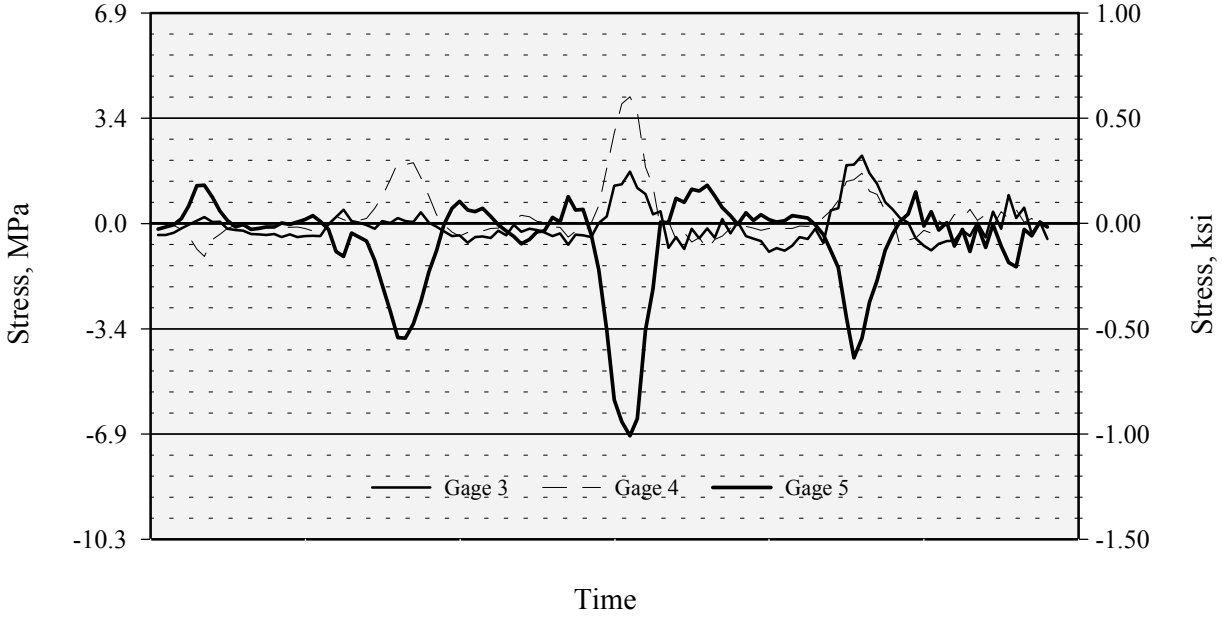

Figure C-45: Stress histories for Gage Group 4B, Truck Pass 1 (test truck centered in left lane).

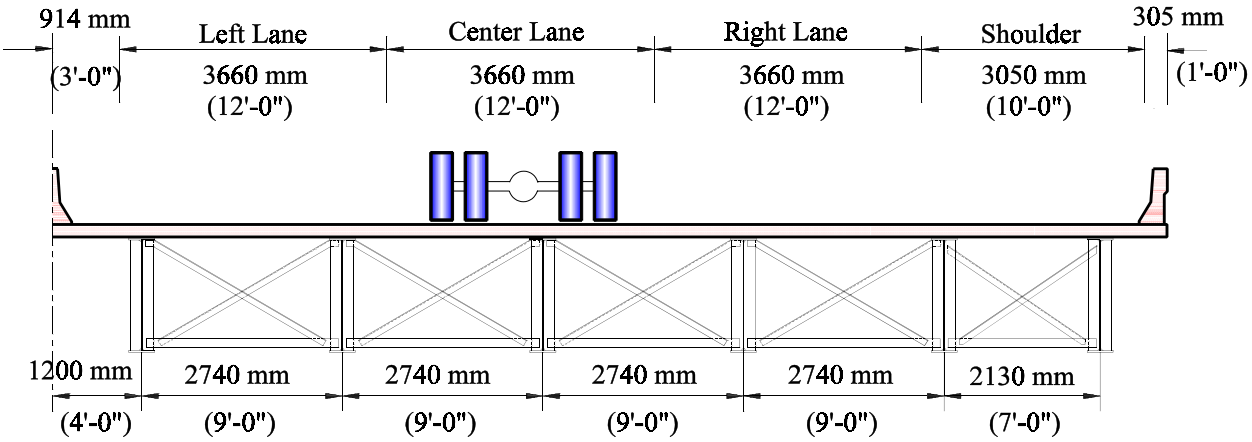

Figure C-46: Truck position for Gage Group 4, Truck Pass 2 (test truck centered in left lane).

Table C-19: Maximum measured stress ranges for Gage Group 4, Truck Pass 2 (test truck in center lane).

Gage Number	Location	Max. Stress Range, MPa	Max. Stress Range, ksi
1	Bottom flange, Girder No. 3	6.8 (T)	1.0 (T)
2	Bottom flange, Girder No. 2	6.6 (T)	0.9 (T)
3	Lower strut, Bay B	17 (T)	24 (T)
4	Diagonal, Bay B	11 (T)	1.7 (T)
5	Diagonal, Bay B	5.1 (C)	0.7 (C)
6	Bottom flange, Girder No. 1	6.1 (T)	0.9 (T)
7	Bottom flange, Girder No. 4	5.9 (T)	0.8 (T)
8	Bottom flange, Girder No. 5	4.0 (T)	0.6 (T)

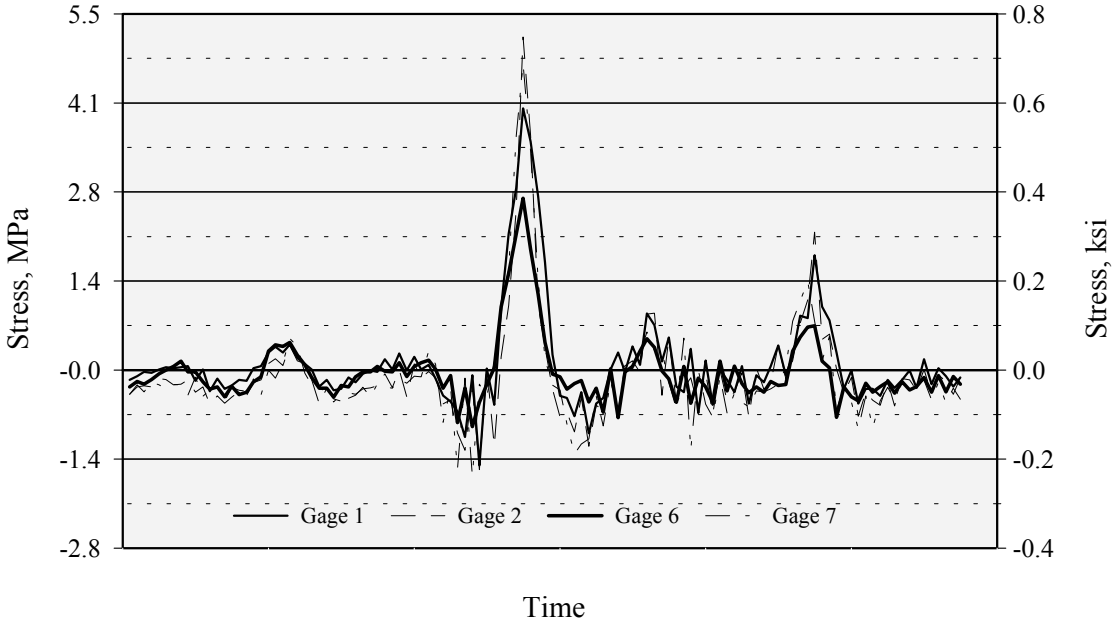

Figure C-47: Stress histories for Gage Group 4A, Truck Pass 2 (test truck centered in center lane).

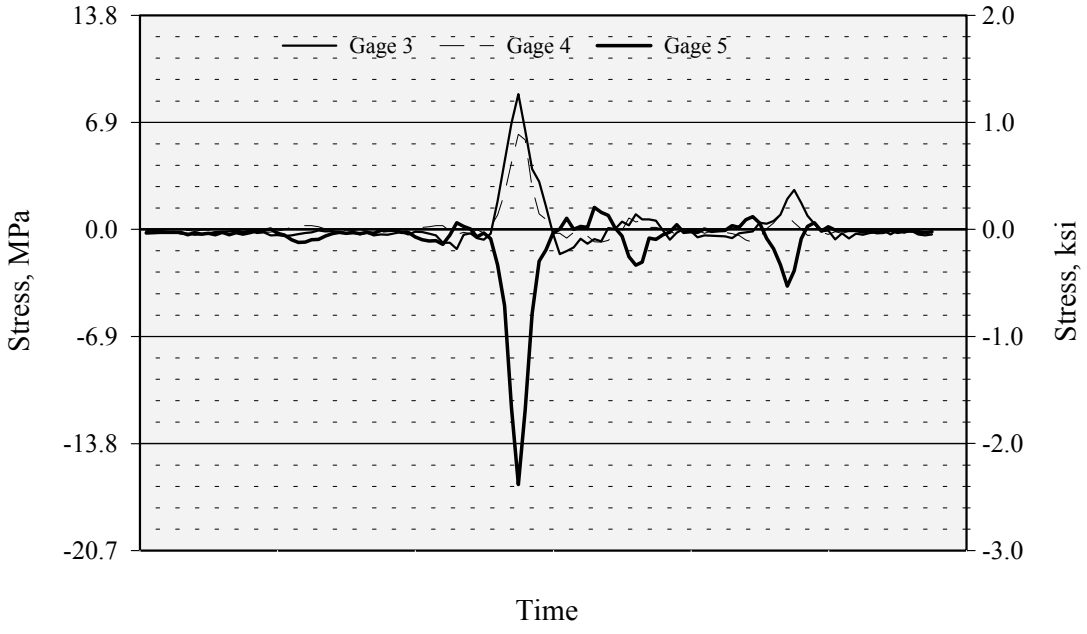

Figure C-48: Stress histories for Gage Group 4B, Truck Pass 2 (test truck centered in center lane).

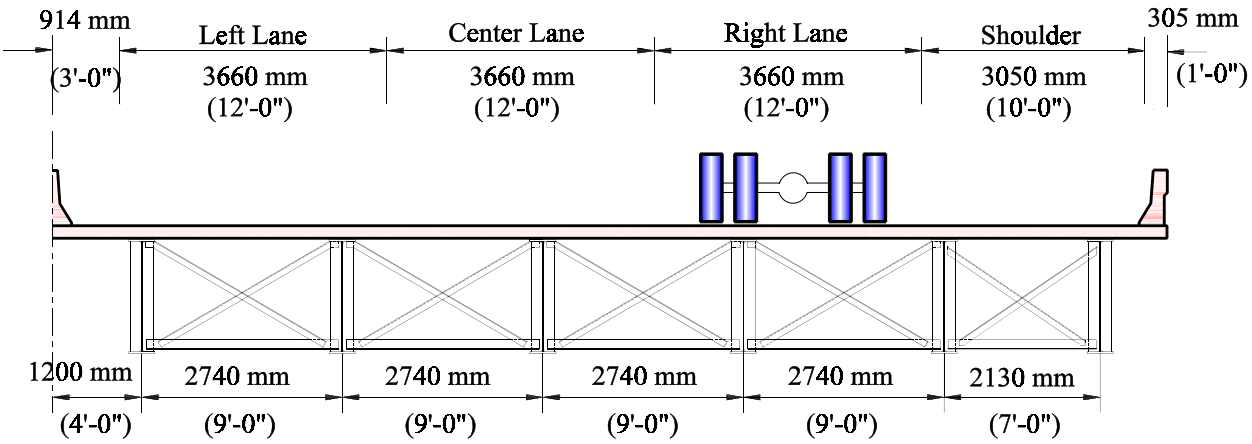

Figure C-49: Truck position for Gage Group 4, Truck Pass 3 (test truck centered in right lane).

Table C-20: Maximum measured stress ranges for Gage Group 4, Truck Pass 3 (test truck in left lane).

Gage Number	Location	Max. Stress Range, MPa	Max. Stress Range, ksi
1	Bottom flange, Girder No. 2	3.0 (T)	0.4 (T)
2	Bottom flange, Girder No. 3	4.2 (T)	0.6 (T)
3	Lower strut, neutral axis	3.2 (T)	0.5 (T)
4	Diagonal, neutral axis	5.2 (T)	0.8 (T)
5	Diagonal, neutral axis	8.2 (C)	1.2 (C)
6	Lower strut, top	3.3 (T)	0.5 (T)
7	Lower strut, bottom	59 (T)	8.6 (T)
8	Upper strut, neutral axis	---	---

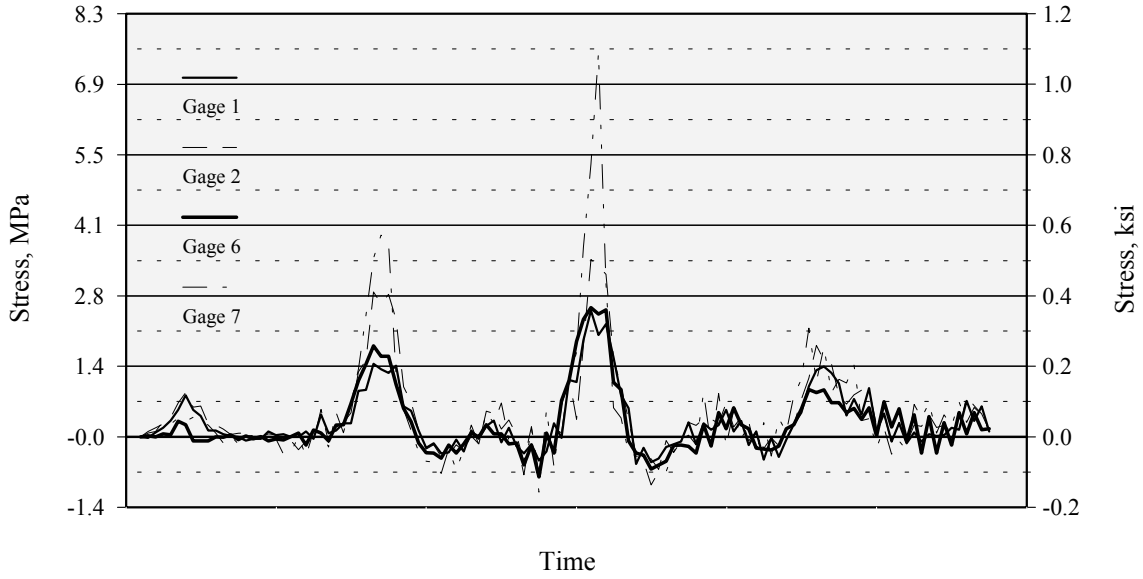

Figure C-50: Stress histories for Gage Group 4A, Truck Pass 3 (test truck centered in right lane).

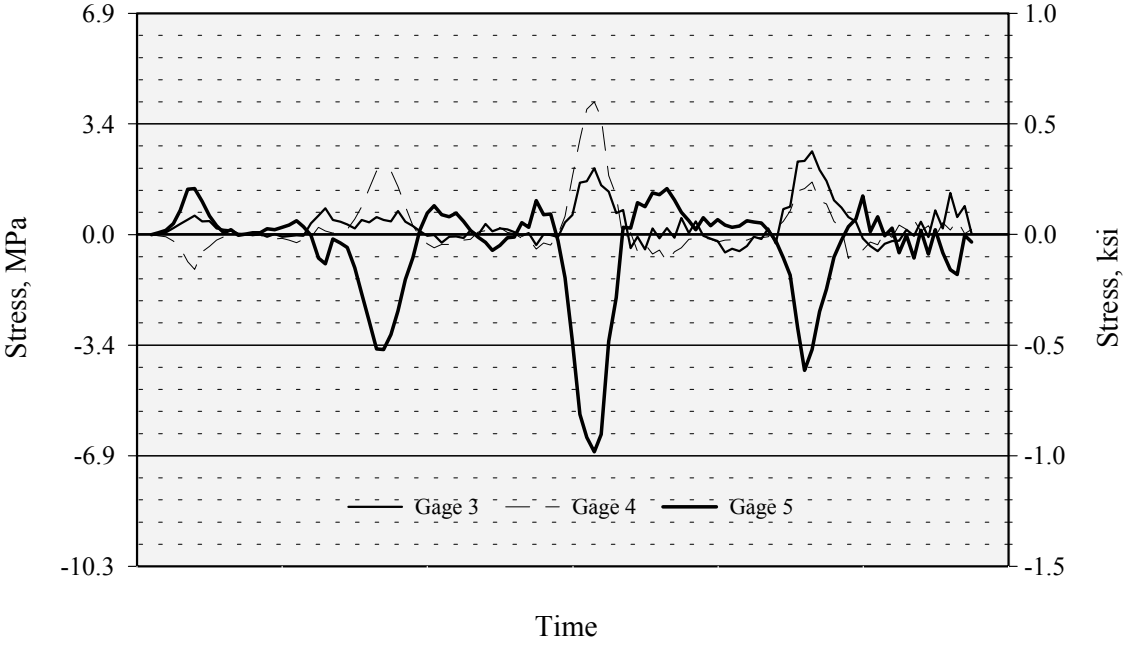

Figure C-51: Stress histories for Gage Group 4B, Truck Pass 3 (test truck centered in right lane).

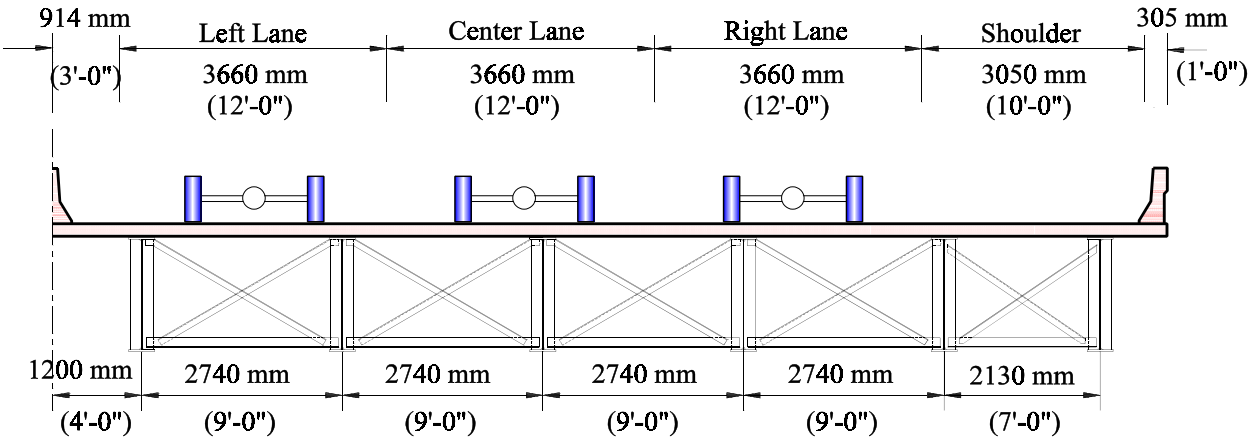

Figure C-52: Truck position for Gage Group 4, Truck Pass 4 (group of approximately 20 passenger cars).

Table C-21: Maximum measured stress ranges for Gage Group 4, Truck Pass 4 (group of approximately 20 passenger cars).

Gage Number	Location	Max. Stress Range, MPa	Max. Stress Range, ksi
1	Bottom flange, Girder No. 2	1.9 (T)	0.3 (T)
2	Bottom flange, Girder No. 3	2.8 (T)	0.4 (T)
3	Lower strut, neutral axis	3.2 (T)	0.5 (T)
4	Diagonal, neutral axis	2.5 (T)	0.4 (T)
5	Diagonal, neutral axis	3.9 (C)	5.6 (C)
6	Lower strut, top	1.3 (T)	0.2 (T)
7	Lower strut, bottom	2.6 (T)	0.4 (T)
8	Upper strut, neutral axis	---	---

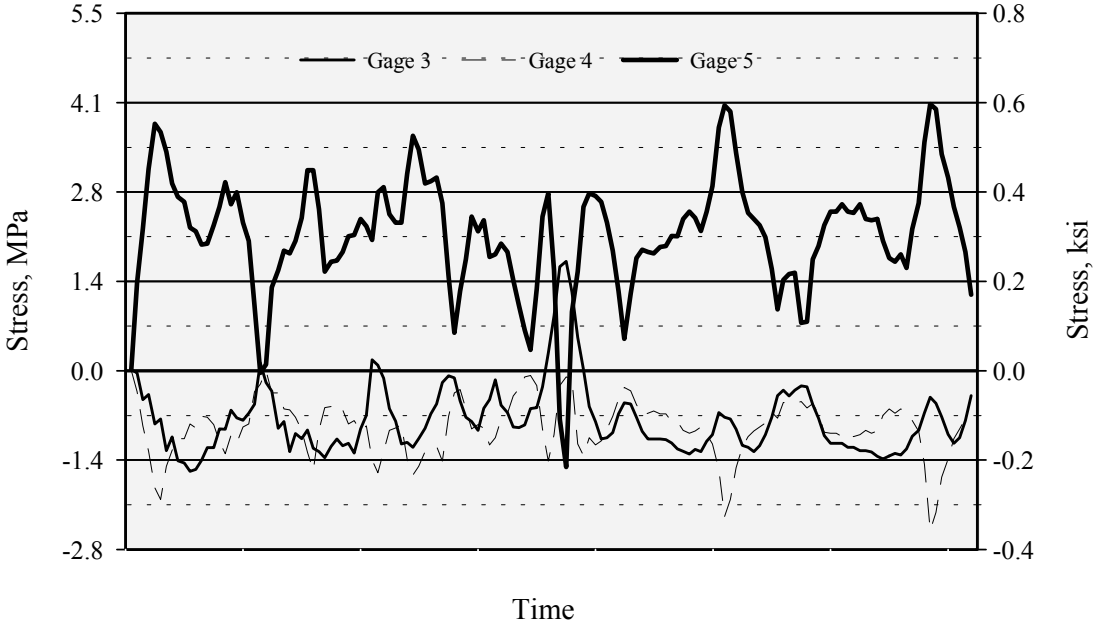

Figure C-53: Stress histories for Gage Group 4B, Truck Pass 4 (group of approximately 20 passenger cars).

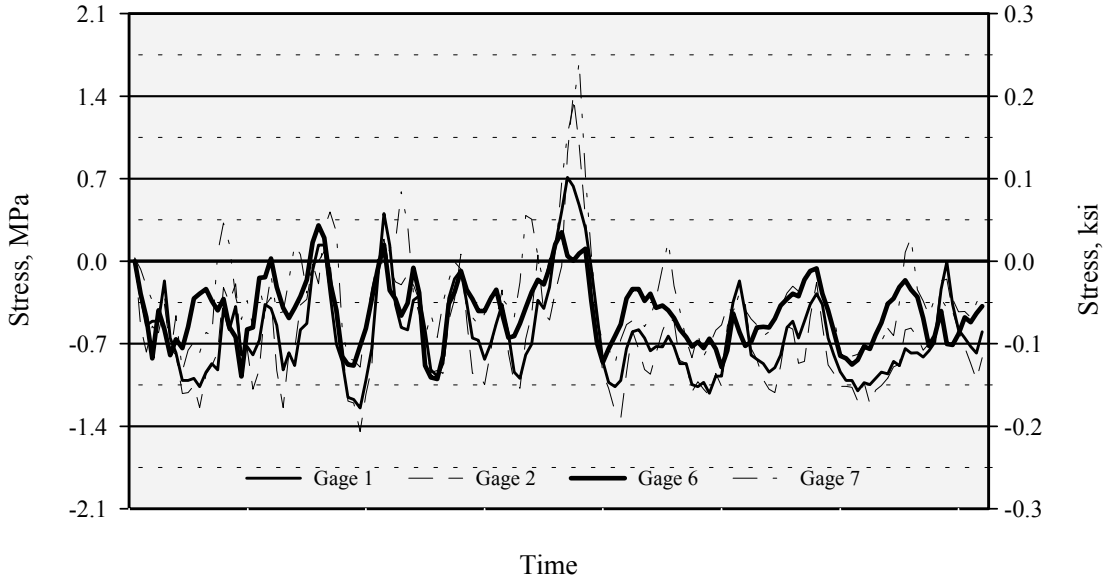

Figure C-54: Stress histories for Gage Group 4A, Truck Pass 4 (group of approximately 20 passenger cars).

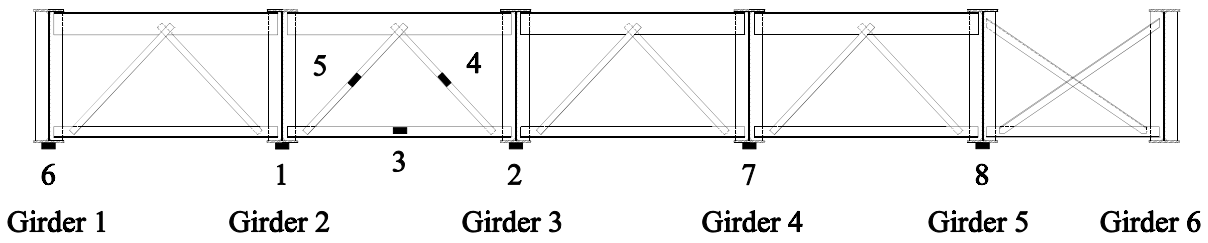

Figure C-55: Strain gage locations for Gage Group 5.

Table C-22: Gage locations for Gage Group 5.

Gage Number	Position
1	Bottom flange, centerline of girder
2	Bottom flange, centerline of girder
3	Lower strut, Neutral axis
4	Diagonal, Neutral axis
5	Diagonal, Neutral axis
6	Bottom flange, centerline of girder
7	Bottom flange, centerline of girder
8	Bottom flange, centerline of girder

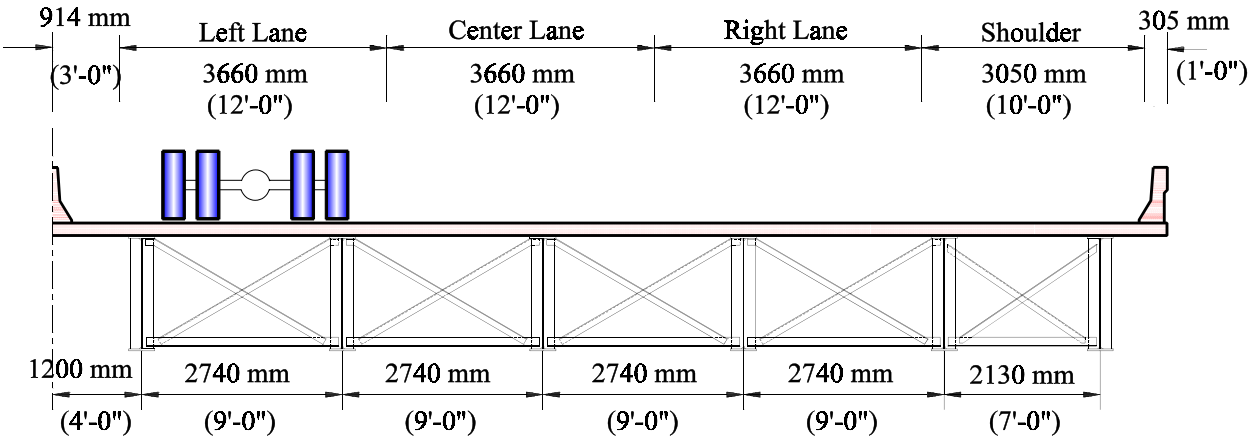

Figure C-56: Truck position for Gage Group 5, Truck Pass 1 (test truck centered in left lane).

Table C-23: Maximum measured stress ranges for Gage Group 5, Truck Pass 1 (test truck in left lane).

Gage Number	Location	Max. Stress Range, MPa	Max. Stress Range, ksi
1	Bottom flange, Girder No. 2	2.1 (C)	0.3 (C)
2	Bottom flange, Girder No. 3	4.8 (T)	0.7 (T)
3	Lower strut, neutral axis	12 (T)	1.7 (T)
4	Diagonal, neutral axis	4.9 (C)	0.7 (T)
5	Diagonal, neutral axis	5.8 (T)	0.8 (T)
6	Lower strut, top	8.5 (T)	1.2 (T)
7	Lower strut, bottom	1.3 (T)	0.2 (T)
8	Upper strut, neutral axis	1.0 (T)	0.1 (T)

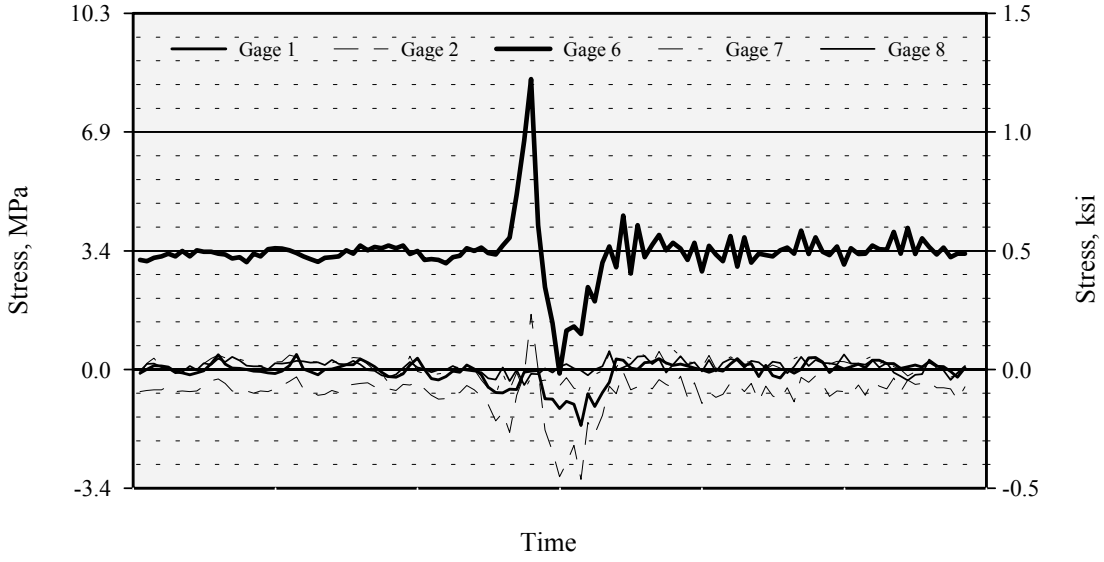

Figure C-57: Stress histories for Gage Group 5A, Truck Pass 1 (test truck centered in left lane).

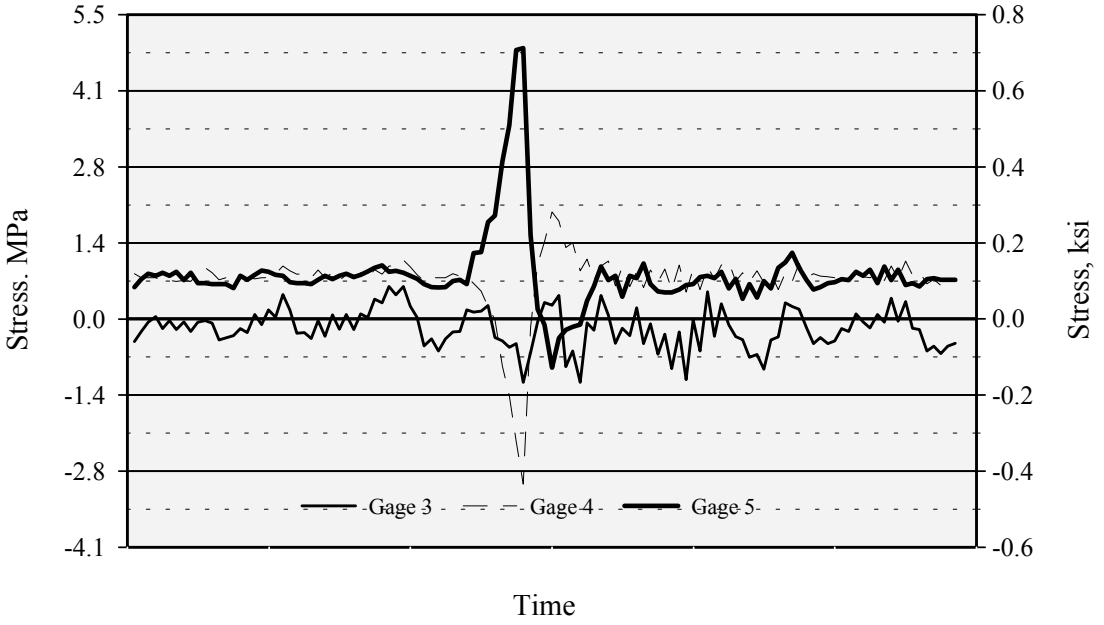

Figure C-58: Stress histories for Gage Group 5B, Truck Pass 1 (test truck in left lane).

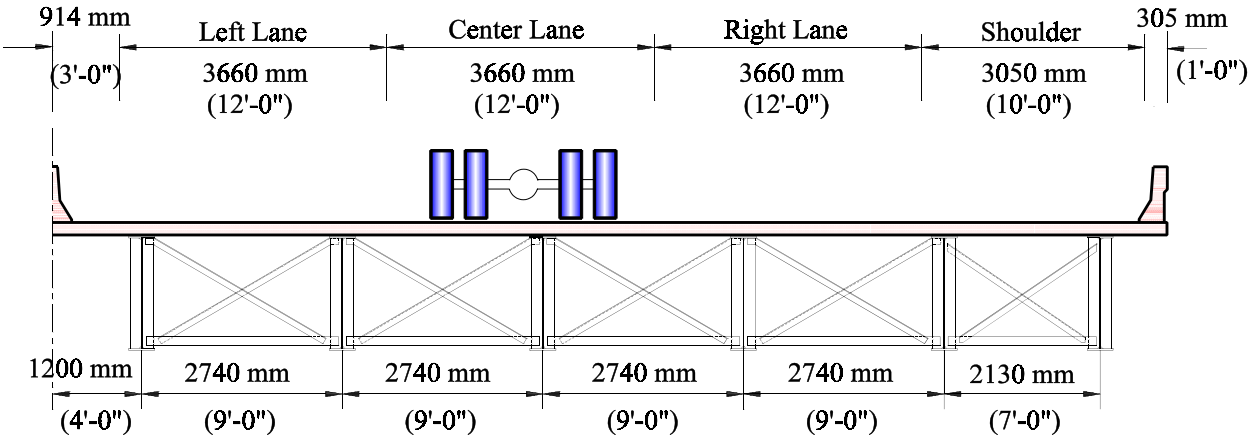

Figure C-59: Truck position for Gage Group 5, Truck Pass 2 (test truck centered in right lane).

Table C-24: Maximum measured stress ranges for Gage Group 5, Truck Pass 2 (test truck centered in center lane).

Gage Number	Location	Max. Stress Range, MPa	Max. Stress Range, ksi
1	Bottom flange, Girder No. 3	3.3 (C)	0.5 (C)
2	Bottom flange, Girder No. 2	4.7 (C)	0.7 (C)
3	Lower strut, Bay B	16 (C)	2.3 (C)
4	Diagonal, Bay B	3.8 (C)	0.6 (C)
5	Diagonal, Bay B	6.9 (C)	1.0 (C)
6	Bottom flange, Girder No. 1	8.9 (C)	1.3 (C)
7	Bottom flange, Girder No. 4	3.0 (C)	0.4 (C)
8	Bottom flange, Girder No. 5	15 (C)	2.2 (C)

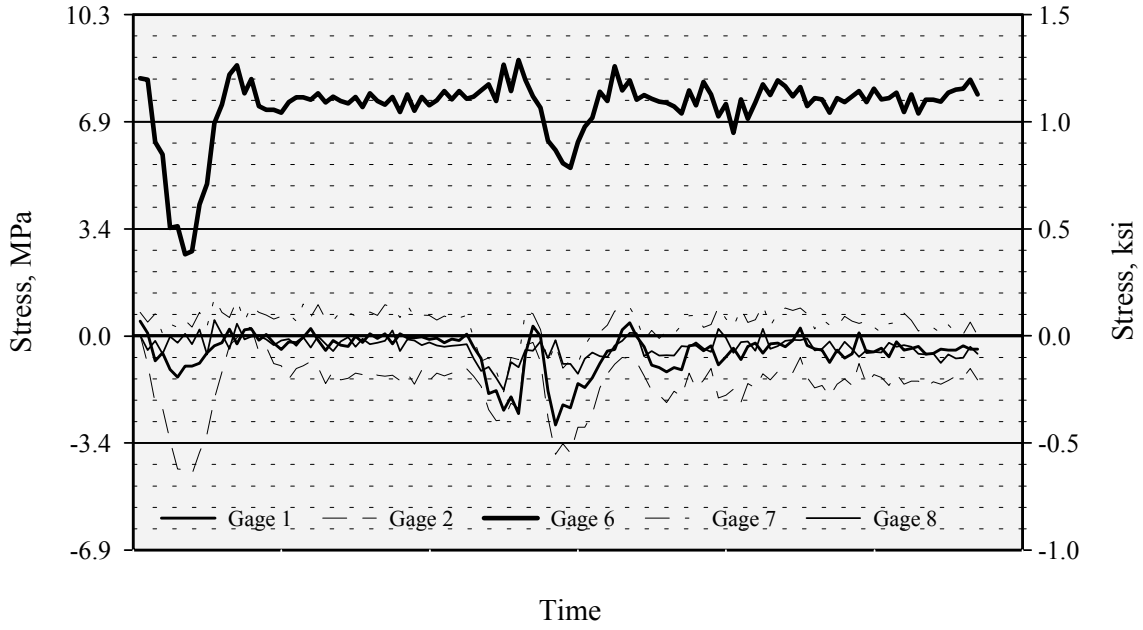

Figure C-60: Stress histories for Gage Group 5A, Truck Pass 2 (test truck centered in center lane).

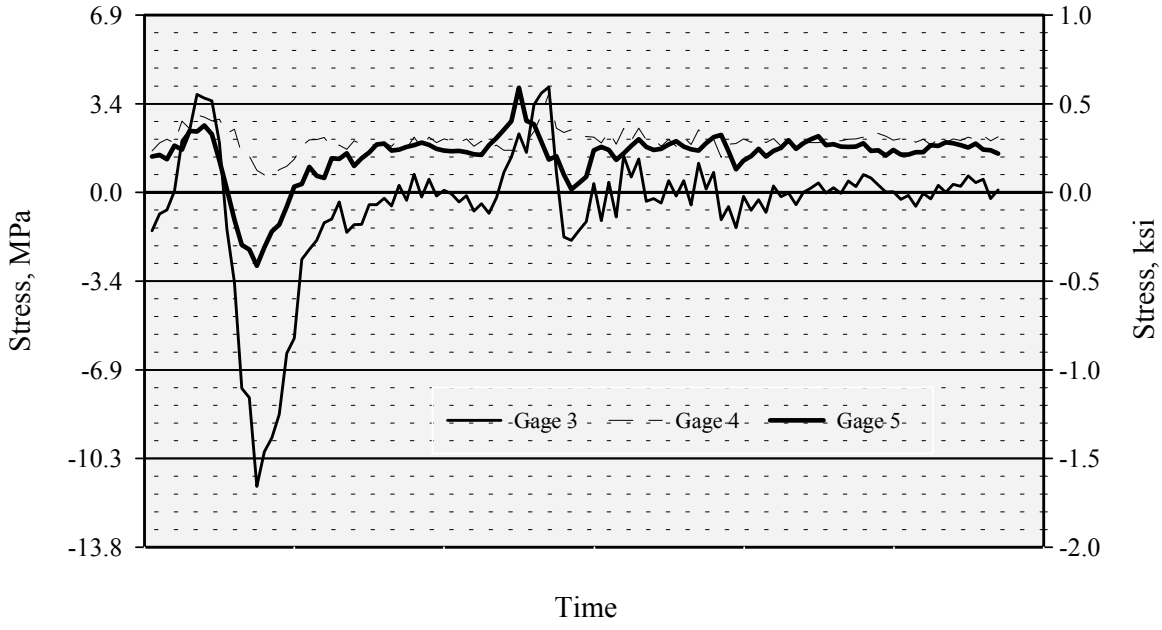

Figure C-61: Stress histories for Gage Group 5B, Truck Pass 2 (test truck centered in center lane).

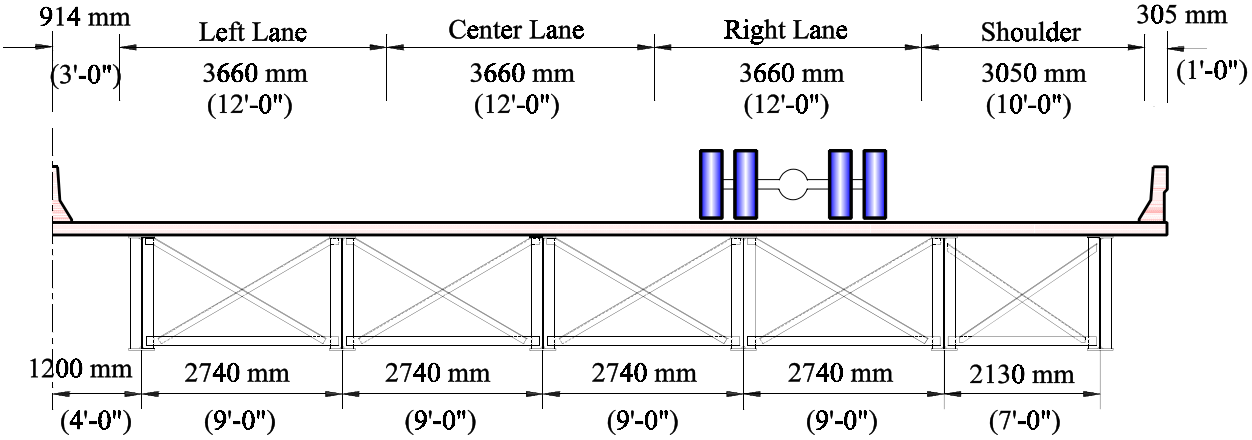

Figure C-62: Truck position for Gage Group 5, Truck Pass 3 (test truck centered in right lane).

Table C-25: Maximum measured stress ranges for Gage Group 5, Truck Pass 3 (test truck centered in right lane).

Gage Number	Location	Max. Stress Range, MPa	Max. Stress Range, ksi
1	Bottom flange, Girder No. 2	2.3 (T)	0.3 (T)
2	Bottom flange, Girder No. 3	3.2 (T)	0.5 (T)
3	Lower strut, neutral axis	3.2 (T)	4.7 (T)
4	Diagonal, neutral axis	3.9 (T)	0.6 (T)
5	Diagonal, neutral axis	3.5 (T)	0.5 (T)
6	Lower strut, top	11.4 (T)	1.7 (T)
7	Lower strut, bottom	3.4 (T)	0.5 (T)
8	Upper strut, neutral axis	3.0 (T)	0.4 (T)

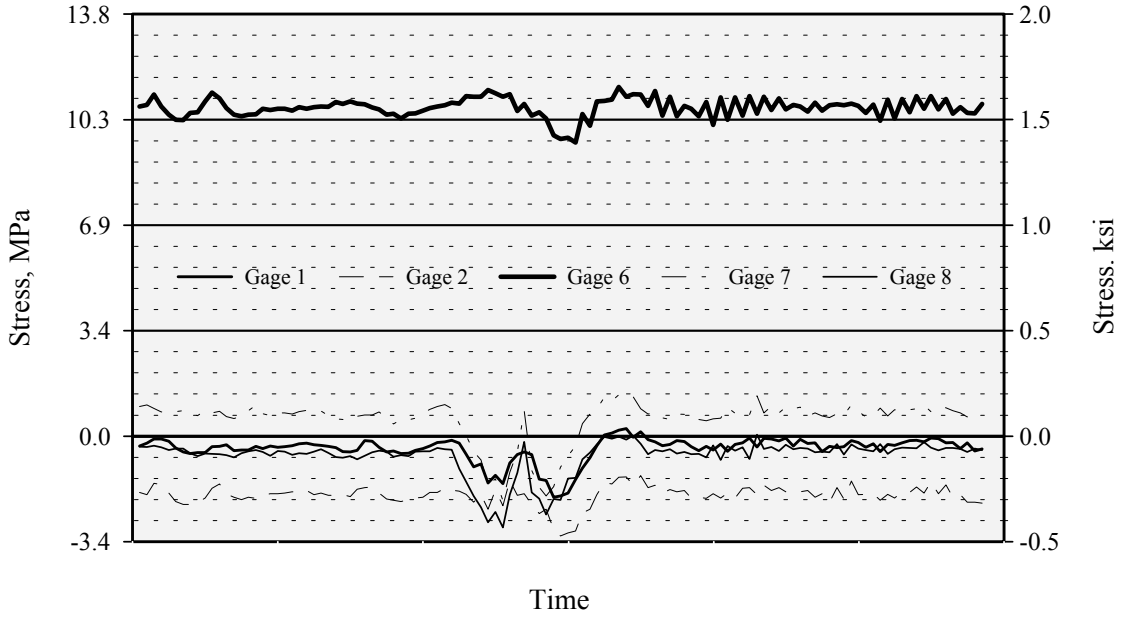

Figure C-63: Stress histories for Gage Group 5A, Truck Pass 3 (test truck centered in right lane).

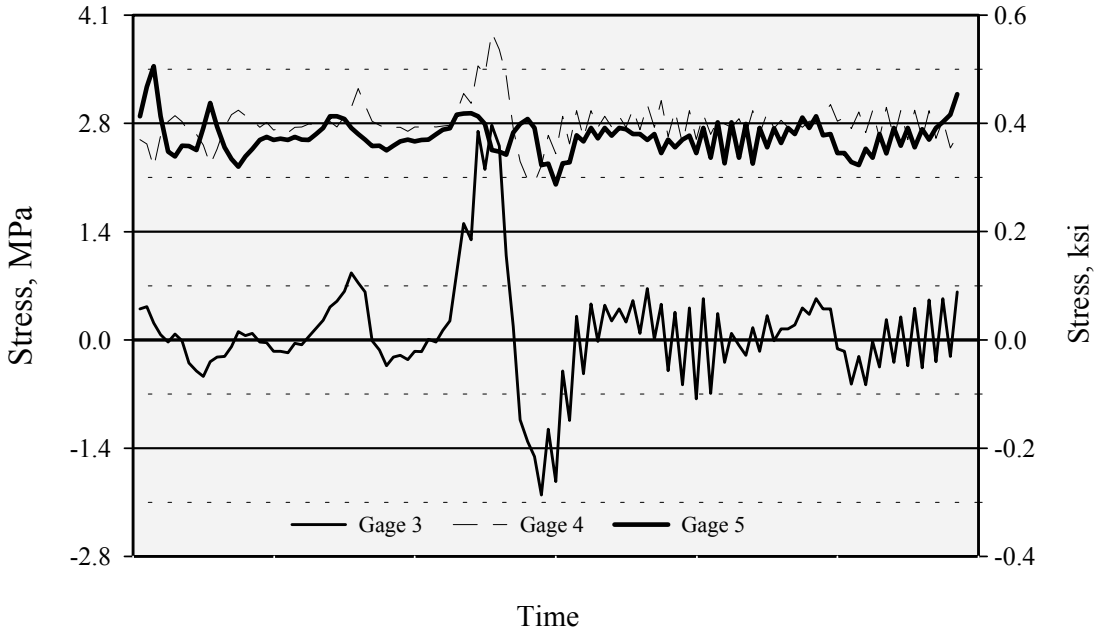

Figure C-64: Stress histories for Gage Group 5B, Truck Pass 3 (test truck centered in right lane).

APPENDIX - D

STRESS HISTORIES

for

COLETO CREEK BRIDGE
U.S. Highway 59
Victoria County

Test Date
December 15, 1993

Table D-1: Summary of recorded test truck passages, Coleto Creek Bridge.

Filename	Gage Group	Truck Pass/Position	Truck Position	Number of Scans
COLGP1P1	1	1	Truck in Position 1 (static)	N.A.
COLGP1P2	1	2	Truck in Position 2 (static)	N.A.
COLGP1P3	1	3	Truck in Position 3 (static)	N.A.
COLGP1P4	1	4	Truck in Position 4 (static)	N.A.
COLGP1P0	1	0	No traffic or truck on structure	
COLGP2P1	2	1	Truck in Position 1 (static)	
COLGP2P2	2	2	Truck in Position 2 (static)	
COLGP2P3	2	3	Truck in Position 3 (static)	
COLGP2P4	2	4	Truck in Position 4 (static)	
COLGP2P0	2	0	No traffic or truck on structure	
COLGP2P5	2	5	Test truck at 50 mph (between Pos. 1 &	
COLGP2P6	2	6	Test truck at 50 mph (Pos. 2)	
COLGP3P1	3	1	Truck in Position 1 (static)	
COLGP3P2	3	2	Truck in Position 2 (static)	
COLGP3P3	3	3	Truck in Position 3 (static)	
COLGP3P4	3	4	Truck in Position 4 (static)	
COLGP3P5	3	5	Test truck at 15 mph (Pos. 2)	
COLGP3P0	3	0	No traffic or truck on structure	
COLGP3P6	3	6	Test truck at 45 mph (between Pos. 2 &	
COLGP3P7	3	7	Test truck at 55 mph (between Pos. 2 &	
COLGP4P1	4	1	Truck in Position 1 (static)	
COLGP4P2	4	2	Truck in Position 2 (static)	
COLGP4P3	4	3	Truck in Position 3 (static)	
COLGP4P4	4	4	Truck in Position 4 (static)	
COLGP4P0	4	0	No traffic or truck on structure	
COLGP4P5	4	5	Test truck at 25 mph (Pos. 2)	

Table D-1: Summary of recorded test truck passages, Coleto Creek Bridge (cont.).

Filename	Gage Group	Truck Pass/Position	Truck Position	Number of Scans
COLGP5P1	5	1	Truck in Position 1 (static)	N.A.
COLGP5P2	5	2	Truck in Position 2 (static)	N.A.
COLGP5P3	5	3	Truck in Position 3 (static)	N.A.
COLGP5P4	5	4	Truck in Position 4 (static)	N.A.
COLGP5P5	5	5	Truck in Position 1 (static) midspan	N.A.
COLGP5P6	5	6	Truck in Position 2 (static) midspan	
COLGP5P7	5	7	Truck in Position 1 (static) midspan	
COLGP5P8	5	8	No traffic or truck on structure	
COLGP5P9	5	9	Test truck at 37 mph (Pos. 1) with traffic	

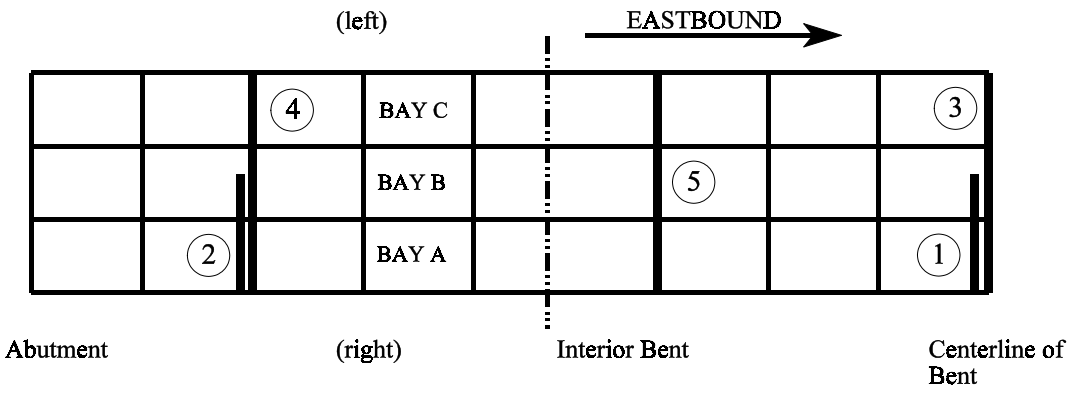

Figure D-1: Gage group locations for Coleto Creek Bridge.

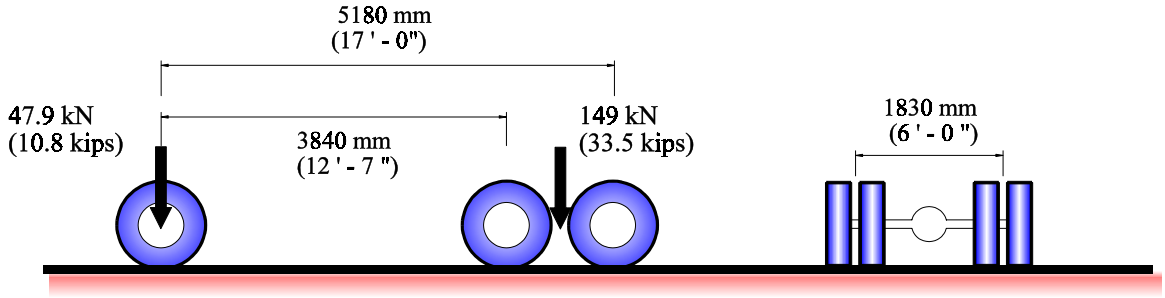

Figure D-2: Test truck axial weight and configuration, Coleto Creek Bridge.

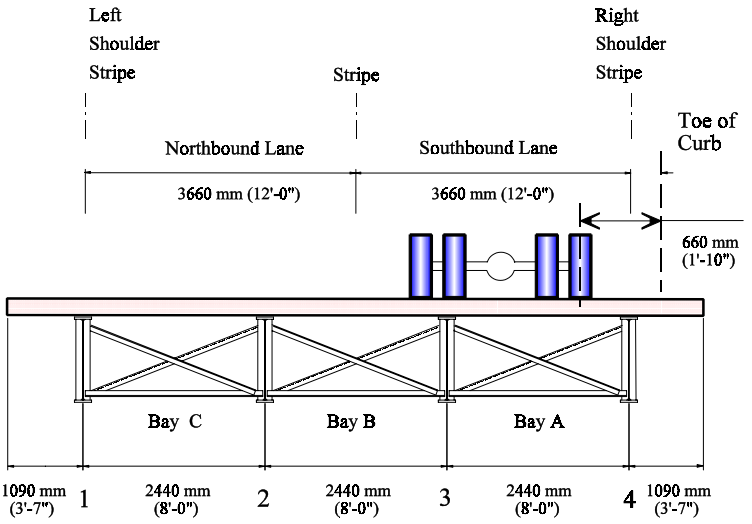

Figure D-3: Location for test truck at Position No. 1.

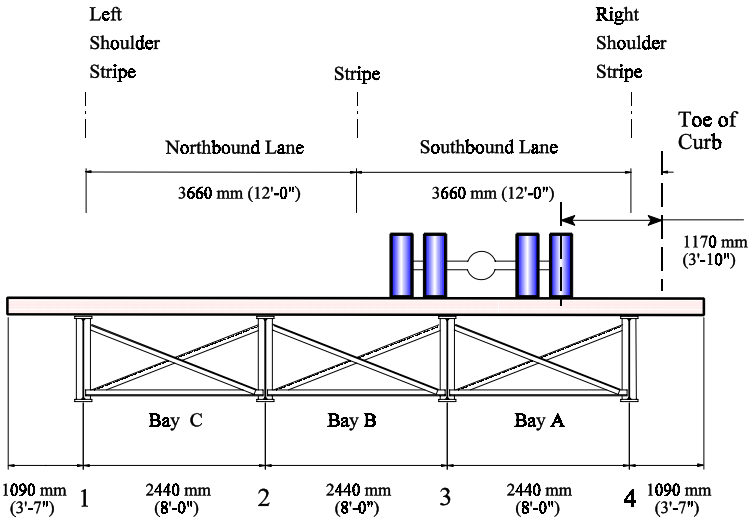

Figure D-4: Location for test truck at Position No. 2.

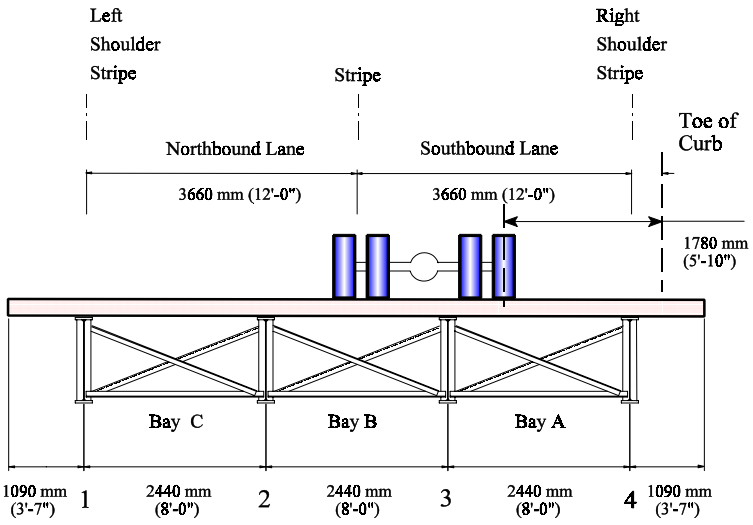

Figure D-5: Location for test truck, Position No. 3.

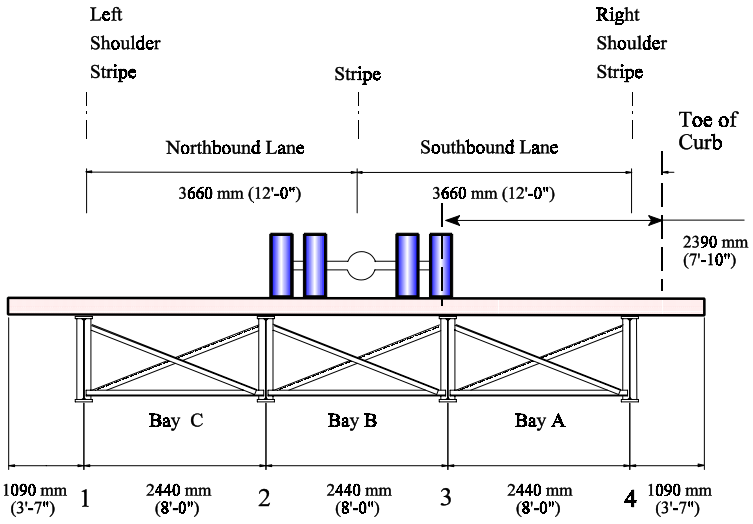

Figure D-6: Location for test truck, Position No. 4.

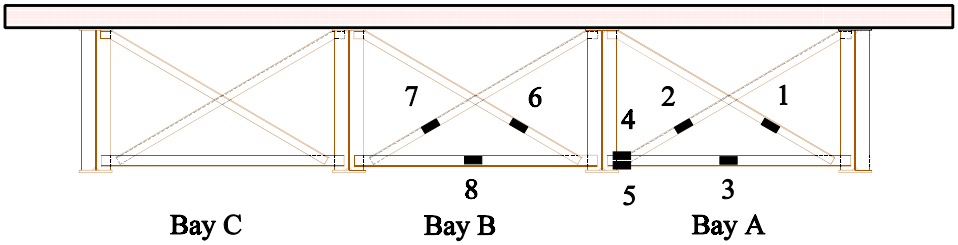

Figure D-7: Gage Group 1, midspan diaphragm location (cross frame members).

Table D-2: Static load stress values for Gage Group 1.

Truck Position	Gage Number							
	1	2	3	4	5	6	7	8
1	-0.1	2.4	1.1	3.1	1.2	4.2	-7.9	-3.8
	-0.02	0.35	0.17	0.44	0.18	0.61	-1.15	-0.55
2	-3.8	11.2	6.3	13.5	9.4	9.7	-7.8	3.7
	-0.55	1.63	0.91	1.96	1.36	1.41	-1.13	0.53
3	-6.8	18.2	10.0	21.6	15.7	13.5	-6.0	10.4
	-0.98	2.64	1.45	3.13	2.28	1.96	-0.88	1.51
4	-8.9	21.6	12.1	26.1	18.7	13.7	-1.7	15.8
	-1.29	3.13	1.75	3.79	2.72	1.99	-0.25	2.30

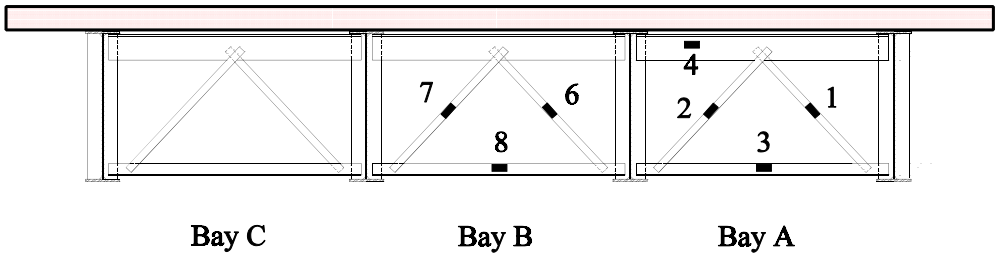

Figure D-8: Gage Group No. 2, Type A diaphragm members (positive moment region).

Table D-3: Static load stress values for Gage Group 2.

Truck Position	Gage Number							
	1	2	3	4	5	6	7	8
1	-1.32	-4.71	2.55	0.24	3.89	4.89	-2.59	-6.19
	-0.19	-0.68	0.37	0.03	0.56	0.71	-0.38	-0.90
2	-7.79	0.27	8.67	2.40	19.32	8.42	-8.02	2.67
	-1.13	-0.04	1.26	0.35	2.80	1.22	-1.16	0.39
3	-12.79	-4.30	12.29	3.44	30.65	8.36	-13.78	11.10
	-1.86	-0.62	1.78	0.50	4.45	1.21	-2.00	1.61
4	-12.13	12.72	10.97	2.72	33.39	3.86	-15.53	19.98
	-1.76	-1.85	-1.59	0.39	4.85	0.56	-2.25	2.90

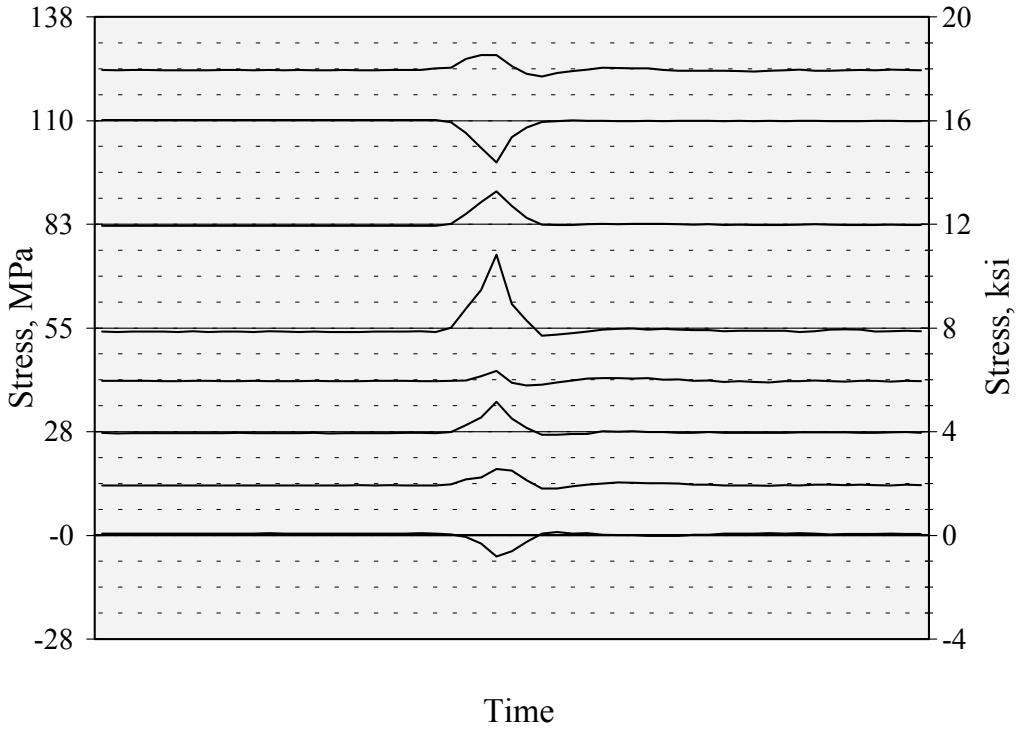

Figure D-9: Stress histories for Gage Group 2, Truck Pass 2.

Table D-4: Maximum measured stress ranges and direction for Gage Group 2, Truck Pass 2 (test truck centered in passing lane).

Number	Location	Max. Stress Range, MPa	Max. Stress Range, ksi
1	Bottom flange, Girder No. 1	7.9 (C)	1.0 (T)
2	Bottom flange, Girder No. 2	5.5 (T)	0.8 (C)
3	Bottom flange, Girder No. 3	9.0 (T)	1.3 (T)
4	Bottom flange, Girder No. 4	4.1 (T)	0.6 (T)
5	Bottom flange, Girder No. 5	21 (T)	3.1 (T)
6	Web, Girder No. 2	9.0 (C)	1.3 (T)
7	Web, Girder No. 3	11 (C)	1.6 (T)
8	Web, Girder No. 4	5.5 (T)	0.8 (C)

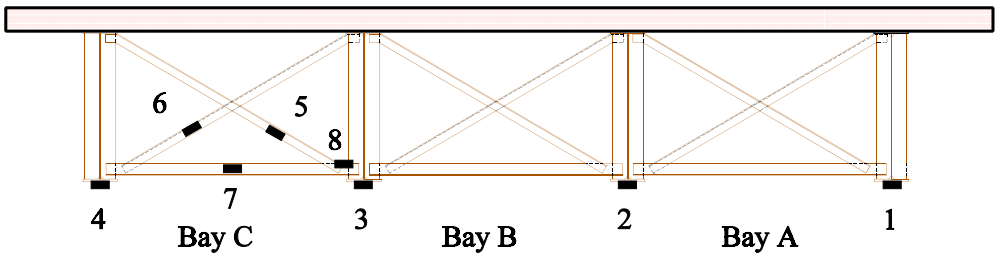

Figure D-10: Gage Group No. 3, Bay C, midspan diaphragm line. (cross frame members).

Table D-5: Static load stress values for Gage Group 3.

Truck Position	Gage Number							
	1	2	3	4	5	6	7	8
1	24.4	15.3	6.1	-1.1	-20.2	3.4	-4.8	4.0
	3.55	2.22	0.88	-0.15	-2.94	0.49	-0.70	0.58
2	21.2	14.7	7.2	1.2	-16.8	1.0	-2.0	1.2
	3.08	2.14	1.05	0.18	-2.43	0.14	-0.29	0.17
3	18.0	14.2	8.4	3.1	-11.1	-1.3	0.7	-1.5
	2.61	2.06	1.23	0.46	-1.61	-0.18	0.11	-0.21
4	14.7	13.3	9.4	5.7	-1.9	-4.3	4.5	-5.3
	2.14	1.93	1.36	0.83	-0.27	-0.62	0.65	-0.80

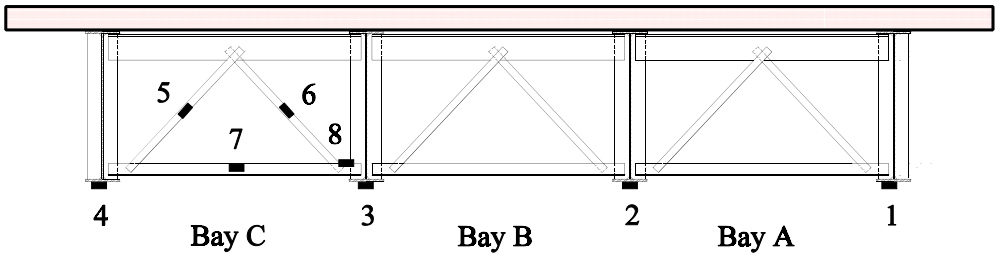

Figure D-11: Gage Group No. 4 (positive moment region).

Table D-6: Static load stress values for Gage Group 4.

Truck Position	Gage Number							
	1	2	3	4	5	6	7	8
1	32.8	22.7	-7.8	-7.4	0.8	7.1	-5.6	6.9
	4.76	3.30	-1.13	-1.07	0.12	1.04	-0.81	1.00
2	28.6	22.2	-3.3	-3.9	0.9	9.0	-2.9	3.3
	4.15	3.23	-0.48	-0.57	0.13	1.30	-0.42	0.48
3	23.9	21.5	1.0	-0.7	0.6	10.5	0.9	0.1
	3.47	3.13	0.14	-0.10	0.09	1.53	0.14	0.01
4	16.8	20.0	8.1	4.9	-0.8	13.2	5.8	-5.7
	2.43	2.91	1.17	0.71	-0.11	1.91	0.84	-0.83

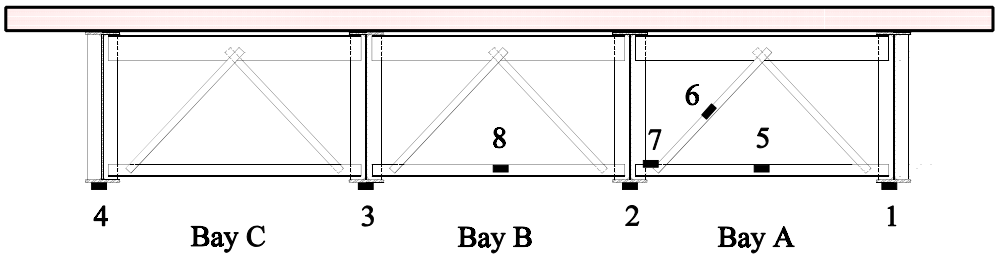

Figure D-12: Gage Group No. 5 Type A diaphragm line (positive moment region).

Table D-7: Static load stress values for Gage Group 5 (test truck positioned above diaphragm line).

Truck Position	Gage Number							
	1	2	3	4	5	6	7	8
1	7.3	3.8	-0.7	-2.3	2.8	-2.1	4.4	-3.8
	1.05	0.55	-0.11	-0.34	0.41	-0.30	0.65	-0.56
2	5.5	4.5	0.5	-1.7	6.7	2.6	13.5	1.9
	0.80	0.65	0.07	-0.24	0.97	0.38	1.97	0.28
3	4.1	4.8	1.9	-1.1	8.0	8.2	20.3	7.7
	0.60	0.70	0.27	-0.16	1.15	1.19	2.94	1.12
4	2.3	4.9	3.6	-0.4	7.6	10.5	23.1	13.3
	0.33	0.71	0.53	-0.06	1.10	1.53	3.35	1.90

Table D-8: Static load stress values for Gage Group 5
(test truck positioned at midspan).

Truck Position	Gage Number							
	1	2	3	4	5	6	7	8
1	-7.6	-5.0	-2.5	0.6	-0.6	0.6	0.2	0.6
	-1.10	-0.72	-0.36	0.09	-0.08	0.08	0.03	0.08
2	-6.2	-4.7	-2.3	0.4	-0.2	1.0	0.9	0.8
	-0.90	-0.68	-0.33	0.05	-0.03	0.14	0.13	0.12
3	-6.9	-4.4	-1.5	1.2	-0.1	0.9	1.1	0.9
	-1.00	-0.64	-0.22	0.17	-0.01	0.14	0.16	0.10

APPENDIX - E

REPAIR GUIDELINES

for

FATIGUE DAMAGE

E.1 INTRODUCTION

A review of typical connection details used in the design and construction of steel highway bridges in the state of Texas and inspection records for various bridges indicated that most of the fatigue cracking experienced in the State has been due to secondary stresses. Secondary stresses are those stress that occur from load conditions not typically considered in the design of the bridge. As discussed in Chapter One, these stresses are the result of the three-dimensional deformation of the bridge. The most common location of fatigue cracks from secondary stresses is in the web plate at the ends of unstiffened connection plate details. Fatigue cracking due to primary stresses, those stresses explicitly accounted for in design, is minimal.

While properly designed and maintained bridge components will not require a need for repair or retrofit procedures, certain factors may lead to the necessity for the repairs. For example, the design of the structure may have taken place prior the introduction of the current fatigue design provisions (1973). Or a detail was used whose fatigue strength, at the time of design, was not considered or known. This is particularly true with bridge details that have been found susceptible to distortion-induced stresses. Poor fabrication techniques resulted in defect sizes larger than those allowed by the current welding codes and implied by the AASHTO fatigue design provisions. Initial design assumptions or considerations may have changed, such as an increase in loading or fixity of joints due to poor maintenance. The requirement to increase the load carrying capacity of a bridge may require strengthening of fatigue sensitive details.

Provided that the detail has been properly classified and both the stress condition and load frequency correctly calculated, fatigue cracking should not occur. Shown in Fig. E-1 are the current AASHTO fatigue design curves. Few, if any, AASHTO Category C type details or higher have cracked in service due to primary stresses. Most of the reported fatigue damage due to primary stresses has been at Category E and EN type details. Similar to the experiences in Texas, the majority of fatigue damage that has been detected in the United States can be attributed to distortion, primarily at unstiffened web gap at the ends of diaphragm or floorbeam connection plates.

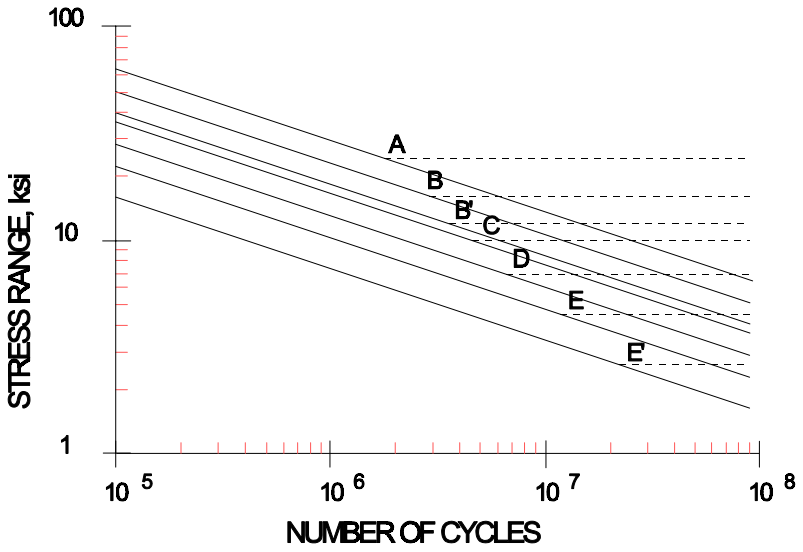

Figure E-1: AASHTO Fatigue Design Curves.

Prior to the development of any repair procedures, the source of the fatigue cracking must be determined. The cause of the cracking will determine which type of repair procedure is available. Without properly identifying the cause of the cracking, the probability of the repair procedure succeeding is reduced. The applicability and success of a given repair procedure will depend on several factors as outlined:

- type of stress causing the cracking,
- remaining service life of the bridge,
- frequency and thoroughness of the inspection program,
- anticipated quality of the repairs, and
- traffic controls available during repairs.

The retrofit procedures for fatigue damage caused by primary or load-induced stresses are different from those procedures used to retrofit cracking resulting from secondary or distortion-induced stresses. A structure whose replacement is anticipated may allow for a less extensive retrofit procedure than a structure which requires an additional fifty years of service life. Any corrective measure that cannot be inspected with any reliability will require a higher

confidence in its success.

E.2 METHODS OF REPAIR

E.2.1 Welding

For most repairs, welding is the easiest type of repair. However, one must be confident in the fracture toughness of the existing base metal. Structures built prior to the establishment of the AASHTO Fracture Control Plan and the use of Charpy toughness testing may result in increased susceptibility to brittle fracture. Preference should be given to fillet welds over groove welds. Fillet welds are the easiest type of weld to produce, an important consideration for field welding.

Welded repairs may require closure of the bridge to traffic or at least the lane or lanes of traffic immediately above the repair. Fillet welding the end of a diaphragm connection plate to the flange to control distortion induced fatigue is a good application. Welded repairs will require certified welders and inspectors.

E.2.2 Bolting

Most fatigue repairs are bolted due to the possible problems with welded repairs. Properly installed bolted connections have a fatigue strength defined by AASHTO Category B. However, thorough inspection during installation is required to guarantee the bolt preload and an oil-free faying surface necessary for slip-critical conditions. Some bolted repair procedures can become quite extensive and, thus, expensive. Bolted repairs can be used to repair fractured cross sections as a result of extensive fatigue damage. Bolts details can add redundancy to the structure.

E.2.3 Weld Toe Grinding

Weld toe grinding can be used to remove shallow fatigue cracks and to extend the fatigue life of undamaged details. Grinding the weld toe reduces the geometrical stress concentration, thus improving the fatigue strength. In addition, the small shrinkage crack that is usually present in the weld toe is removed. This is the initiation site for the fatigue crack. A pencil or rotary burr grinder can be used. Rotation of the grinding element must be in the direction of the applied stress. Abrupt changes in surface profiles must be avoided.

Grinding should not expose the root of a weld or a previously embedded weld flaw. Fatigue cracks can develop from the weld root. Flaws brought to the surface by grinding have a higher propagation rate than those embedded within the weld.

E.2.4 Peening

Peening the toe of a fillet weld can improve the fatigue life of an existing detail. Similar to grinding, the increased fatigue strength is a result in the reduction of the geometrical stress concentration. Peening also superimposes a compressive residual stress on the tensile residual stress resulting from the welding. Peening has been used to repair shallow fatigue cracks (less than 5 mm (3/16 in)), but accurate crack depth estimations are required as well as continued inspection.

E.3 LOCATING AND DRILLING CRACK TIP HOLES

In placing drilling holes, the primary concern is that the crack tip is removed from the web plate. Therefore, proper location of the crack tip is essential prior to the drilling. This should be done by blast-cleaning the surrounding area to remove all paint and foreign matter. Crack growth may be more extensive than that revealed through the paint film. Grinding to remove the paint should not be used since this process plastically deforms the surface of the plate

and may prevent proper location of the crack tip. Dye penetrant should be used and the crack tip clearly identified.

Proper location of the crack tip is essential. If the crack is not properly located and the hole is drilled behind the crack tip, an additional stress concentration is provided by the hole, increasing the propagation rate. It has been suggested that the crack tip be located on the inside circumference of the hole to ensure that the crack intersects the hole. However, it is recommended that the center of the hole be positioned at the crack tip to reduce the overall length of the finished crack and minimize section loss.

Research has indicated that crack reinitiation from the hole is prevented by satisfying the relationship:

$$\frac{\Delta K}{\sqrt{\rho}} \leq 1.5\sqrt{F_y} \qquad \left(\frac{\Delta K}{\sqrt{\rho}} \geq 4\sqrt{F_y} \right) \tag{E-1}$$

where ΔK is the stress intensity range or:

$$\Delta K = S_r\sqrt{\pi a_r} \tag{E-2}$$

with S_r equal to the stress range and a_r equal to one-half the crack length.

Equation (E-1) can be put into a more usable form by letting L be equal to the total length of the retrofitted crack (perpendicular to the stress field) or $2a$ and letting φ be equal to the hole diameter or 2ρ. By making the proper substitutions and rearranging to solve for the required hole diameter:

$$\varphi \geq \frac{S_r^2 L}{35F_y} \qquad \left(\geq \frac{S_r^2 L}{5F_y} \right) \tag{E-3}$$

Strain measurements of in-service bridges have indicated that the stress range seldom exceeds 41

MPa (6.0 ksi). Therefore, for plates having yield stress of 250 MPa (36 ksi), a diameter between 19 mm (3/4 in) and 25 mm (1.0 in) is usually sufficient. It may be more practical to specify hole diameters of 21 mm (13/16 in) and 27 mm (1-1/16 in) since drill bits of these sizes are used for high-strength bolts and are commonly on hand.

Larger diameter holes should be avoided to minimize the web cross section loss. However, when multiple crack tips need to be drilled in the same area, it may be more practical to cut one large hole than to drill a number of smaller diameter holes. The relationship given in Eq. (1) above does not take into account superposition of stress concentrations of adjacent holes.

Another factor not considered in the development of the equation for the drilled hole diameter is the method of hole preparation and degree of finish given to the hole. The hole finish is more important than simply satisfying the equation. If burrs or rough edges remain after the drilling operation, crack initiation may occur due to the stress risers. All drilled holes should be ground and surfaced to a polished finish. Dye penetrant inspection should be performed upon completion to insure that the hole circumference is free of defects and that the crack tip has been properly located.

Adjacent holes should be aligned to minimize the area removed from the cross section of the web plate, as shown schematically in Fig. E-2. This may require drilling the holes off center from the crack tip. If two adjacent holes overlap or leave a narrow ligament, the holes should be combined into a single oblong-shaped hole.

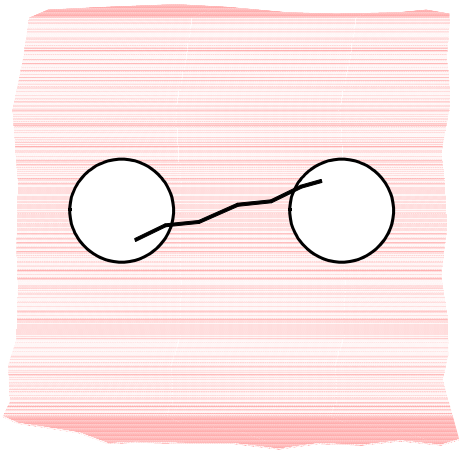

Figure E-2: Drilled hole positioning to reduce section loss.

If an uneven crack surface forms along the toe of the web-to-flange fillet weld, the entire crack should be removed when adjacent to a tension flange. A crack could develop perpendicular to this surface and propagate into the flange. In addition to drilling holes at the crack tips, a slot should be made with the edge of a rotary grinder along the toe of the fillet weld (see Fig. E-3) such that the entire crack surface is removed from both the flange and the web plate (the flange being more critical of the two). Specified procedures for retrofitting the fatigue cracks along the web-to-flange fillet weld should include the following steps:

- Accurately locate, drill, and grind holes at both ends of the web-to-flange crack.
- Inspect both holes with dye-penetrant to insure that the crack tips have been removed.
- Remove the portion of the web plate and web-to-flange containing the crack with the edge of a rotary grinder
- Inspect lower ground surface for cracks and exposed weld flaws. Remove by hole drilling and/or burr grinding as necessary.
- Prior to painting, caulk gap. Do not over-caulk to avoid limiting future inspection of the region.

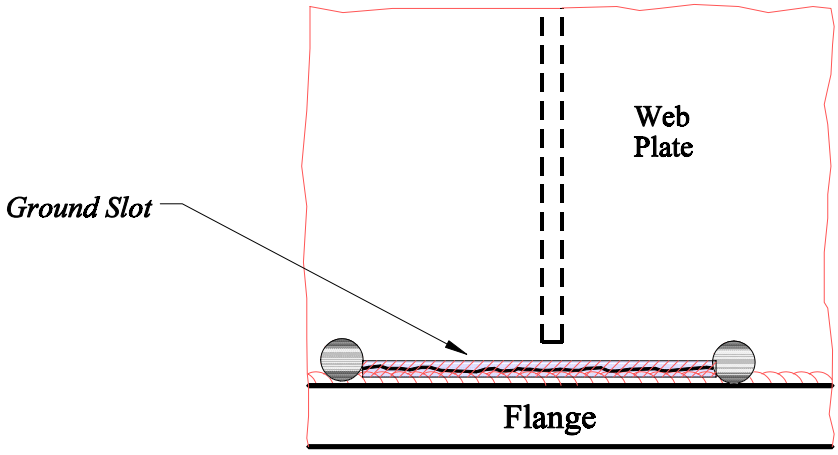

Figure E-3: Removal of web-to-flange fillet weld crack.

Provided that the length of the slot (including the holes) is no greater than 250 mm (10 in), no additional work is required. However, if the length exceeds 250 mm (10 in), a bolted splice between the flange and web plate should be used.

E.4 REPAIR OF CONNECTION DETAILS

E.4.1 Longitudinal Stiffener Terminations

The stress concentration at the end of longitudinal stiffeners may cause fatigue cracks to develop. A pair of drilled holes can be used to remove the fatigue damage and prevent any further crack growth. The holes should be sized accordingly (see Eq. (E-3)) and drilled close to the stiffener in order to minimize the section loss in the web plate.

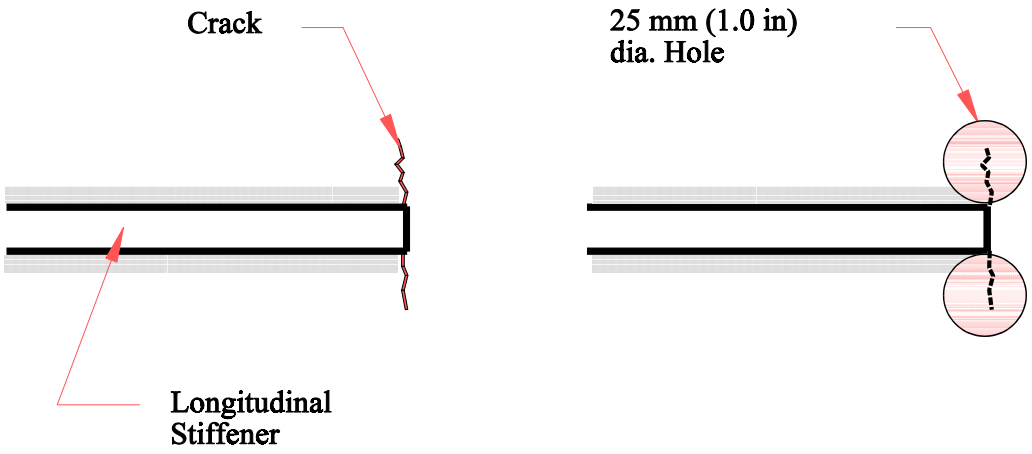

Figure E-4: Crack and drilled holes at end of longitudinal stiffeners.

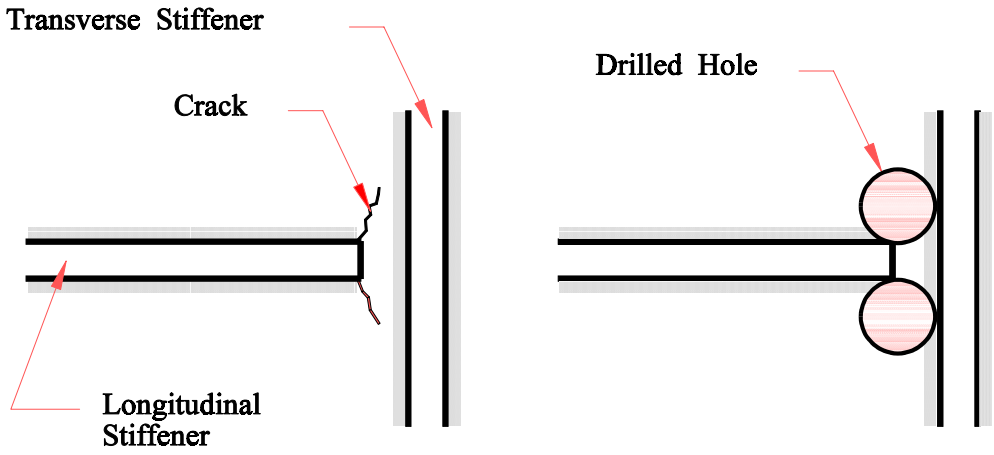

Figure E-5: Crack and drilled hole locations for longitudinal stiffener termination at transverse stiffener.

If a crack is detected on only one side of the stiffener plate (top or bottom), a pair of holes is still required since crack growth will eventually occur on the other side due to the increased stress. If a fatigue life assessment indicates that the longitudinal stiffener is susceptible to fatigue damage but no cracking has yet to be detected, holes can be drilled to intercept future crack growth.

Where longitudinal stiffeners have been interrupted by transverse stiffeners or connection plates, the repair scheme shown in Fig. E-5 can be used. An important consideration for this detail is that the drilled holes be able to intercept any cracks propagating up or down the toe of the vertical fillet weld.

E.4.2 Cover Plate Terminations

Cover plate terminations that have fatigue cracking will require a bolted splice in order to restore the cross section back to its original capacity (see Fig. E-6). A double splice plate places the high-strength bolts in double shear, thereby improving the fatigue behavior. Splice plates should be sized assuming a cracked cross section at least to the original neutral axis. A hole should be drilled through the web, directly above the cover plate termination to intercept any

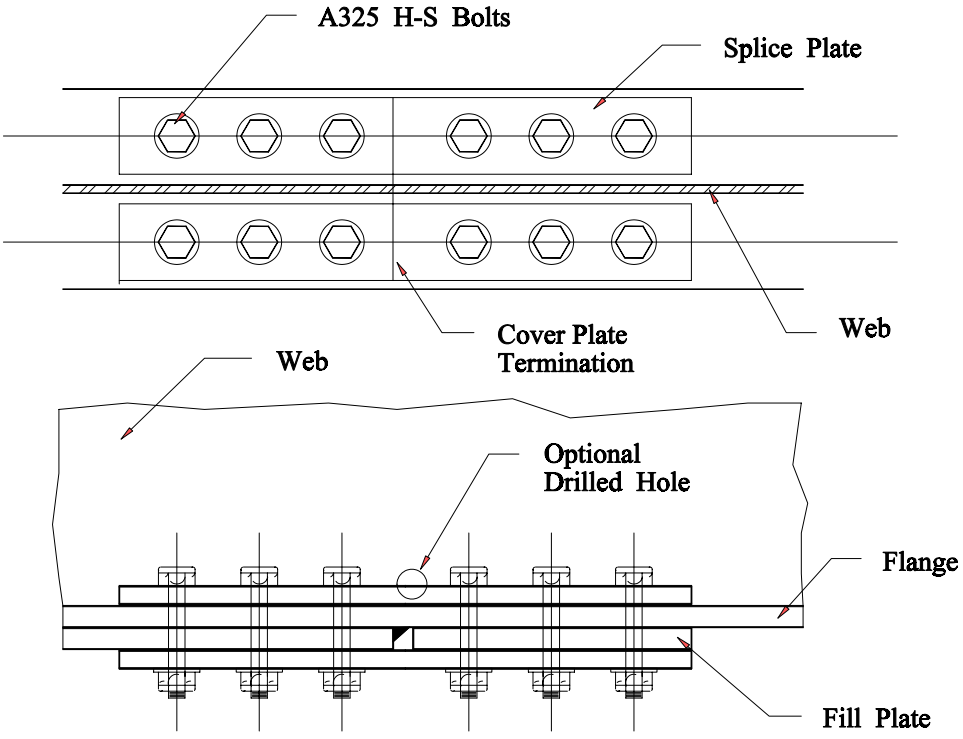

Figure E-6: Bolted splice detail for cracked coverplate termination.

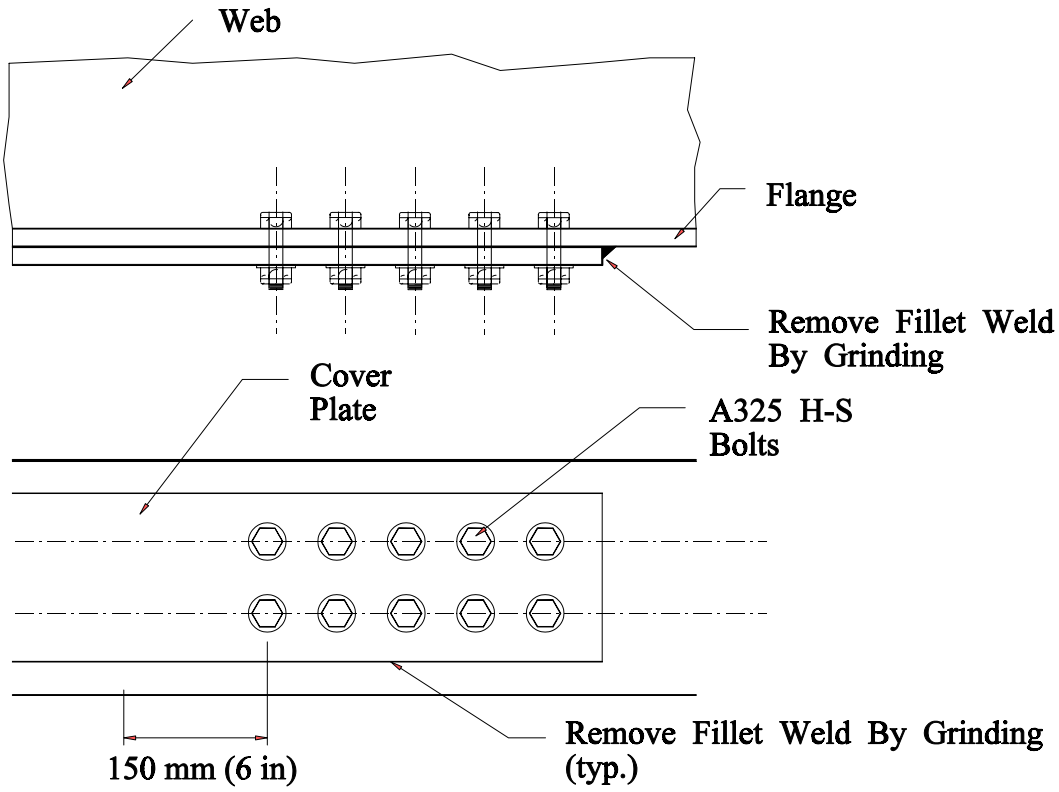

Figure E-7: Bolted retrofit for uncracked coverplate termination.

future crack growth. Allow adequate tolerances around the plate edges for future inspections.

It has been suggested that uncracked cover plate terminations can be improved by the detail shown in Fig. E-7. The existing fillet weld is removed by grinding and the end bolted with high-strength bolts. Effect on the fatigue behavior of any cutting oil in between the plates is unknown. This detail does not work for cracked terminations.

The fatigue strength of uncracked cover plate terminations can be improved by weld toe grinding or peening provided that the cracking is detected early and the crack depth is limited.

E.4.3 Lateral Gusset Plates

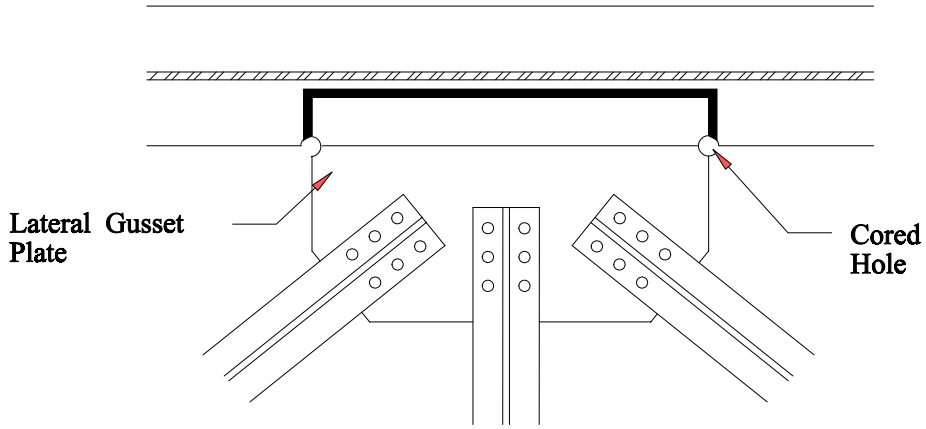

Figure E-8: Cored holes located at cracked lateral gussets welded to flanges.

If cracks have not been detected at the terminations of the longitudinal fillet welds but a fatigue assessment indicated that the fatigue life has been exhausted, peening of the weld can improve the fatigue life.

A more costly option would be to remove the gusset plate by grinding out the weld and reattaching by bolting. The flange plate should be thoroughly inspected for cracks after grinding. The gusset plate should be positioned to avoid covering the ground area to aid in future inspections.

If cracks have developed but are still relatively small, the damaged areas can be cored out and the stress concentration reduced, as illustrated in Fig. E-8. This procedure can also be used at truss gusset plates.

Fatigue damaged gusset plates welded to web plates require repair procedures similar to those used for longitudinal stiffener terminations.

E.4.4 Web Penetrations

Cracking that occurs at the sealing weld of web penetrating flanges can be arrested by hole drilling (see Fig. E-9). Cracking may occur from the lack-of-fusion plane between the web plate and flange or in the weld toe due to the stress concentration (the flange acts as a large, thick attachment with respect to the web plate). The drilled holes are usually sufficient by themselves.

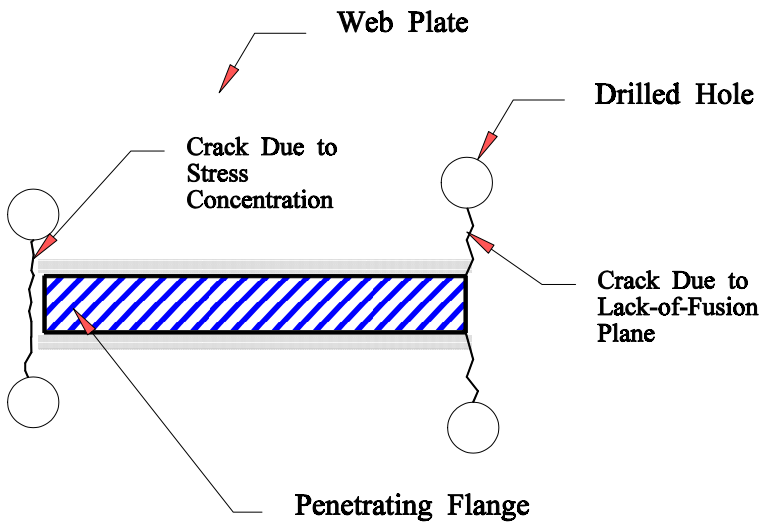

Figure E-9: Drilled hole locations at cracked web penetration.

E.4.5 Coped Beams

Cracks that develop at re-entrant corners of coped flanges can be repaired by drilling a hole at the crack tip and installing a high-strength bolt. The preload in the bolt imposes a compressive stress around the hole circumference which helps suppress further crack growth.

This type of repair is successful when the distortion level is relatively low, such as with diaphragms. When the distortion level is relatively high, such as the case with floorbeams, a doubler plate bolted to the web is required. The increased bending stiffness provided by the doubler plate reduces the bending stresses driving the fatigue cracking. Prior to the doubler plate installation, the existing fatigue crack must be arrested by hole drilling.

E.4.6 Lack-of-fusion Planes

Lack-of-fusion planes located in elements designed as non-load carrying may develop fatigue cracks when oriented perpendicular to the applied stress. Hole drilling will arrest this type of cracking. Shown in Fig. E-10 is a repair procedure for a lack-of-fusion plane occurring in a longitudinal stiffener.

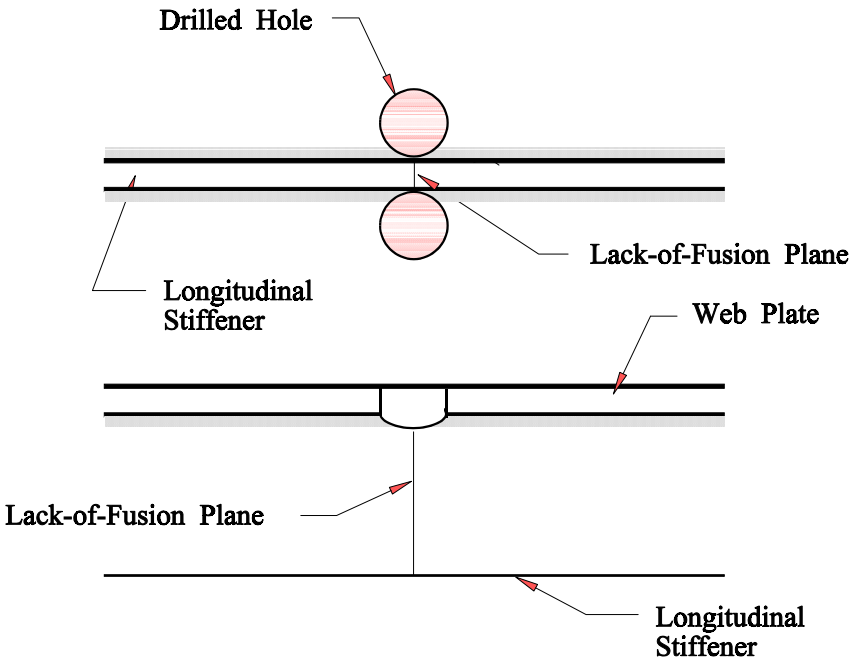

Figure E-10: Drilled hole positions for longitudinal stiffener lack-of-fusion plane.

When the longitudinal stiffener is interrupted by a transverse stiffener or connection plate, a lack-of-fusion plane may exist. The crack will develop off the root of the weld eventually follow the toe of the vertical weld. Therefore, the drilled hole must be properly located.

Lack-of-fusion planes in backing bar are a problem. Again, drilled hole can be used to arrest any fatigue cracks. If the reduction of area due to the drilled holes cannot be tolerated, the lack-of-fusion plane and backing bar can be ground out as shown in Fig. E-11. However, this is difficult and expensive to perform due to the limited access. Lack-of-fusion plane can also occur at the intersection between lateral gusset plates and transverse stiffeners or connection plates. The placement of the drilled holes isolate any developing fatigue cracks.

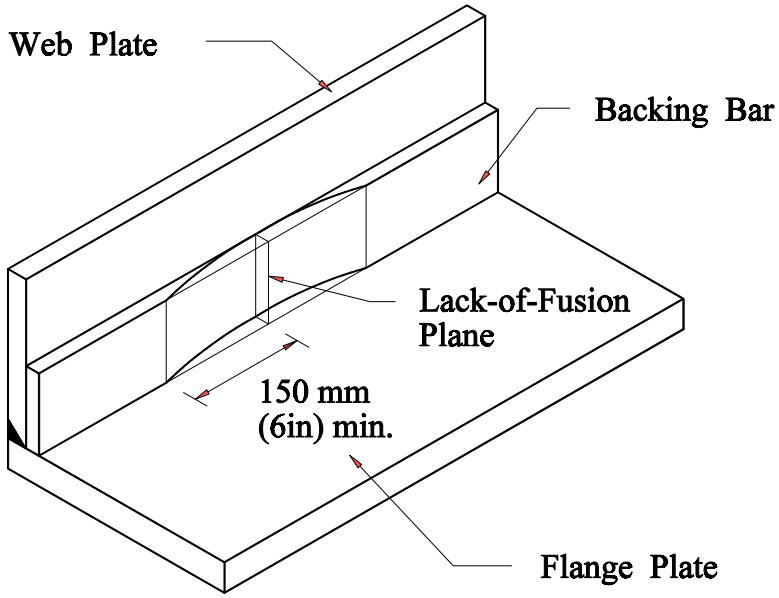

Figure E-11: Removal of backing bar lack-of-fusion plane by grinding.

E.4.7 Removal of Tack Welds

Tack welds that are located in tension zones and determined to be fatigue sensitive should be removed by grinding. Tack welds can be detrimental to the fatigue life of the structure due to their relatively small size which can result in low fracture toughness because of the quenching effect. After the tack weld is remove, the ground surface should be inspected by dye penetrant to insure that the shrinkage crack that usually forms around the toe of the weld is removed.

E.4.8 Rivet Hole Cracks

Riveted members that develop fatigue cracks may require replacement if the cracking is extensive. Isolated cases of cracking can be repaired by the installation of high-strength bolts. While the fatigue strength of rivets is classified as AASHTO Category D, built-up riveted members are classified as Category C due to the internal redundancy provided that the rivets are tight.

Prying action may cause the extreme rivet (or bolt) to fatigue crack in simple shear connections. Leaving the hole open will increase the rotational flexibility of the connection and reduce the prying action on the remaining rivets. Shear capacity requirements on the net section must be checked.

E.4.9 Unstiffened Web Gaps

As previously mentioned fatigue damage is common at unstiffened web gaps at the ends of connection plates. Prior to any permanent repair solution, holes should be drilled at the crack tips to stabilize the cracks against further crack growth or fracture. Initially, the cracks are driven by the distortion stresses. But as the cracks increase in size and possibly change direction, they are increasingly influenced by the primary or in-plane stresses. Once the crack tip holes have been drilled, several options exist, as outlined below:

- Rely on increased flexibility of drilled holes.
- Remove source of distortion, e.g., diaphragms.
- Increase web gap length.
- Welded rigid attachment.
- bolted rigid attachment.

Increased Flexibility

For certain situations, drilled holes alone may provide enough flexibility in the web gap to reduce the distortion stresses to an acceptable level. However, it is difficult to predict when this will happen. It may be necessary to saw-cut the cracks to insure flexibility. Often, the cracks form a shear lock that prevents free moment of the web plate. This option is viable if frequent inspection is available. When little or no follow-up inspection is available, one of the other options discussion next will be necessary.

Diaphragm Removal

Another option is to permanently remove the diaphragms from the bridge, as indicated by the results of the current study. By removing the diaphragms, the driving force behind the cracking is also remove. The option of diaphragm removal must be made on a case by case basis, though the parametric study has helped generalize the contributions of diaphragms and to determine when the diapgragms can be removed. Note that temporary diaphragms may be needed if the bridge is redecked since the top compression flange would be unsupported.

Increased Web Gap Length

Another possible solution to distortion-induced web cracking is to remove a portion of the connection plate in order increase its flexibility and reduced the web gap bending stresses. The problem with this approach is that the increased flexibility increases the deformations in the

web gap, resulting in bending stresses of similar magnitudes. It is difficult to predict when this type of repair will work given all the parameters involved, many of which are unknown.

This type of repair is successful when the distortion level does not increase as the stiffness of the connection decreases with increasing web gap length. Note that if a stiffener exists on the other side of the web plate, it too must be removed. Figure E-12 is a close-up view of the web gap with the end of the connection plate removed and the weld ground smooth. The procedure for this type of repair is given as:

- Drill 38 mm (1-1/2 in) diameter hole through connection. Position as close to web plate as possible.
- Flame-cut end of connection plate using drilled hole as terminus. Vertical cut should not be any closer than 6 mm (1/4 in) from the web to prevent gouging of the plate.
- Grind remaining weld metal and plate flush with web plate.
- Transition drilled hole to web plate by grinding.
- Smooth drilled hole to remove burrs.
- Inspect web plate and hole for defects using dye-penetrant.

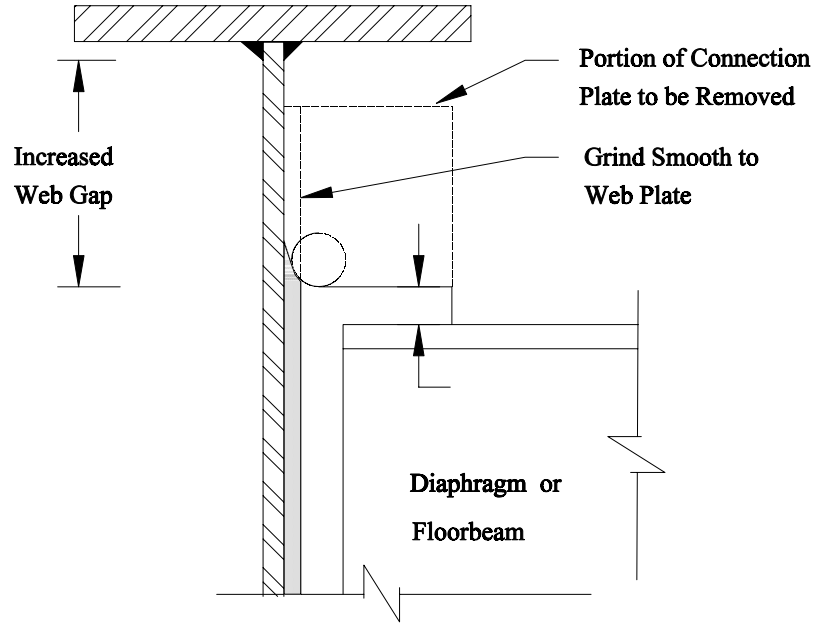

Figure E-12: Schema of increased web gap by connection plate removal.

A problem with this type of repair is that once it is performed, several other repair options are no longer possible. If it were found through observation or strain gaging that the distortion level was not significantly reduced, the next alternative would be a rigid attachment. However, this type of repair is now difficult to make since the end of the connection plate has been removed. If the connection plate also serves as a web stiffener, web crippling may be a problem and must be checked.

Another problem with this repair is that the increased web gap flexibility deceases the effectiveness of the diaphragm to distribute load between adjacent girders. The end result of this repair may be similar to diaphragm removal, though more involved and costly.

Welded Attachments

Rigid attachment of the connection plate to the flange provides a positive means of eliminating the distortion in the web gap. A cut-short connection plate can be rigidly attached to the flange be using an extension plate (see Fig. E-13). The end of the extension plate is fillet welded to the flange. The extension plate can be either welded or bolted to the connection plate depending on what type of cross frame, diaphragm, or floor beam connection exists. Fillet welds on the flange are preferred over groove welds. Larger weld defects are possible with groove welds and require additional NDT inspection.

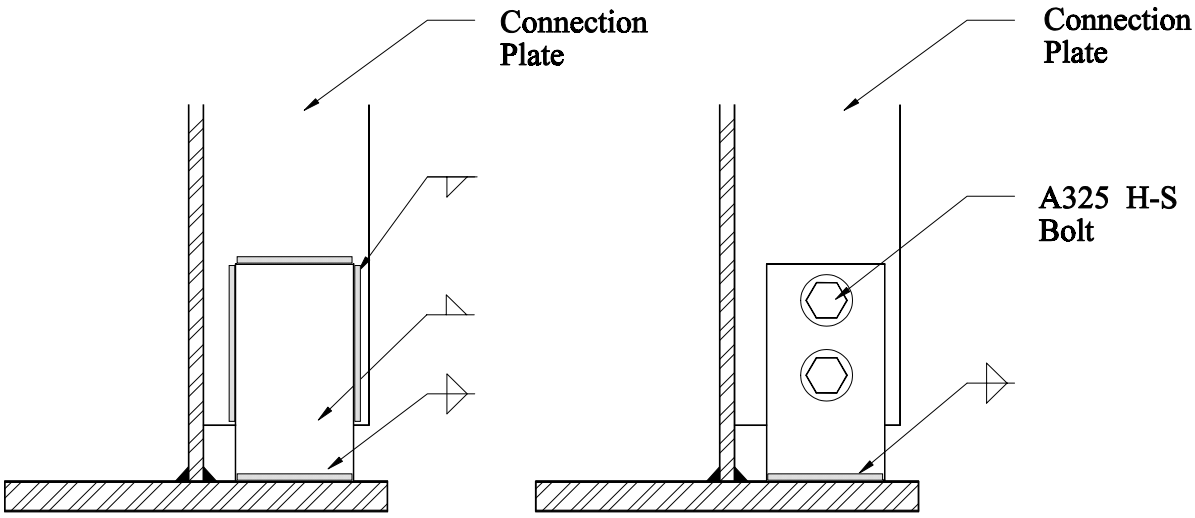

Figure E-13: Welded and bolted extension tabs for welded attachment of cut-short connection plate detail.

If the gap between the end of the connection plate and flange is from 12 to 38 mm (1/2 to 1-1/2 in) a spacer block can be used. The width of the block (dimension parallel with the direction of the bending stress) should not exceed 38 mm (1-1/2 in) to insure that the fillet welds on the flange are AASHTO Category C.

A tight-fit connection plate can be fillet welded to the flange. However, since it is difficult to remove all paint and debris from between the end of the connection plate and flange, weld quality may be poor. To insure a quality weld on the tension flange, the end of the tight-fit connection plate can be cut back. The top surface of the flange should be blast-clean prior to welded to avoid any contamination of the weld metal.

When specifying a welded repair procedure, the criteria given in Fig. E-14 must be considered. The fillet weld between the end of the connection plate and flange must not be undersized. This weld resists the out-of-plane force.

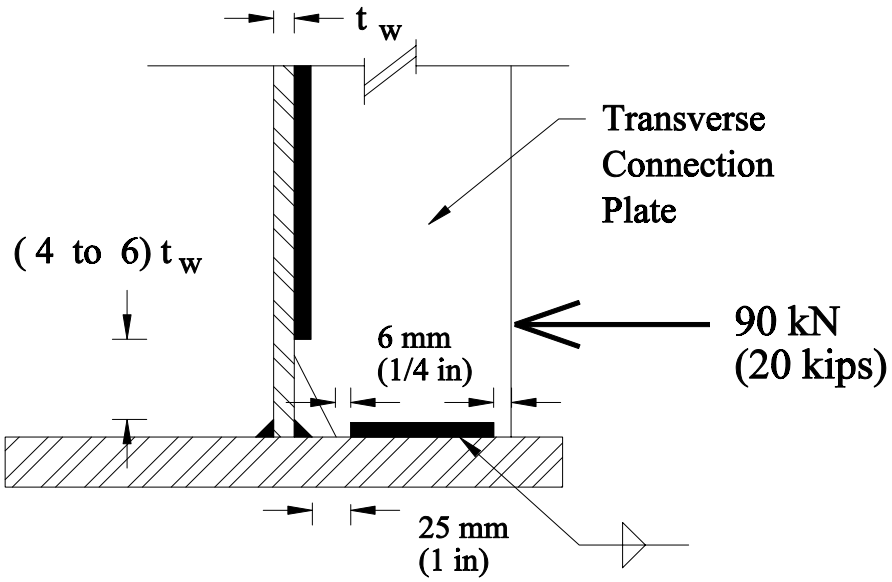

Figure 14: Design criteria for welded attachment of connection plate.

On straight, non-skewed bridges, a typical design force of approximately 90 kN (20 kips) can be used. As the skew increases, this force will increase. On highly skewed bridges, the results given in Chapter Seven should be used. Weld intersections between the transverse flange

weld and the longitudinal web-to-flange weld should be avoided. Weld wrap-arounds should be avoided.

Bolted Attachments

A structural tee or angle, as shown in Fig. E-15, can be used to provide a rigid attachment. Note the staggered hole pattern to prevent any rocking action about a single bolt gauge line. The heaviest section that is available and fits within the constraints of the detail should be used.

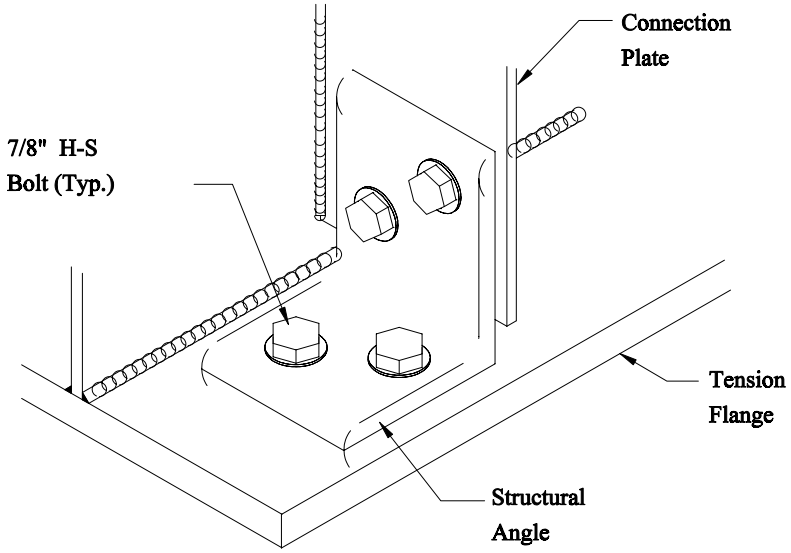

Figure 15: Bolted structural angle with staggered bolt pattern.

When web gap cracking occurs in the negative moment of bending, as is most often the case, a bolted connection become difficult since the flange is usually embedded in the concrete deck. As an alternative to removing a portion of the concrete deck, is has been suggested that

tapped hole be used. The flange must be sufficiently thick enough to allow a depth enough tap.

Concern with this type of repair is that the strength of the steel in the flange is not similar to that of the nut commonly used with high-strength bolts. Therefore, the proper bolt preload may not exist.

In situations where a significant haunch of the concrete slab occurs over the flange, access for bolt tightening can be achieved by cutting through the haunch above the connection. Once the bolted repair is installed and tightened, the void is grouted solid.

A bolted connection plate detail can be used if the gap between the end of the connection and flange is between 12 mm (1/2 in) and about 38 mm (1-1/2 in). Base plates with thicknesses less than 12 mm (1/2 in) do not provide enough stiffness. Base plates larger that 38 mm (1-1/2 in) may be difficult to work with and bolt into place. This type of connection avoids a transverse weld on the tension flange, as shown in Fig. E-16. Note that while the bolted detail provides an AASHTO fatigue category of B on the flange, the existing vertical weld on the web plate still classifies the detail as Category C.

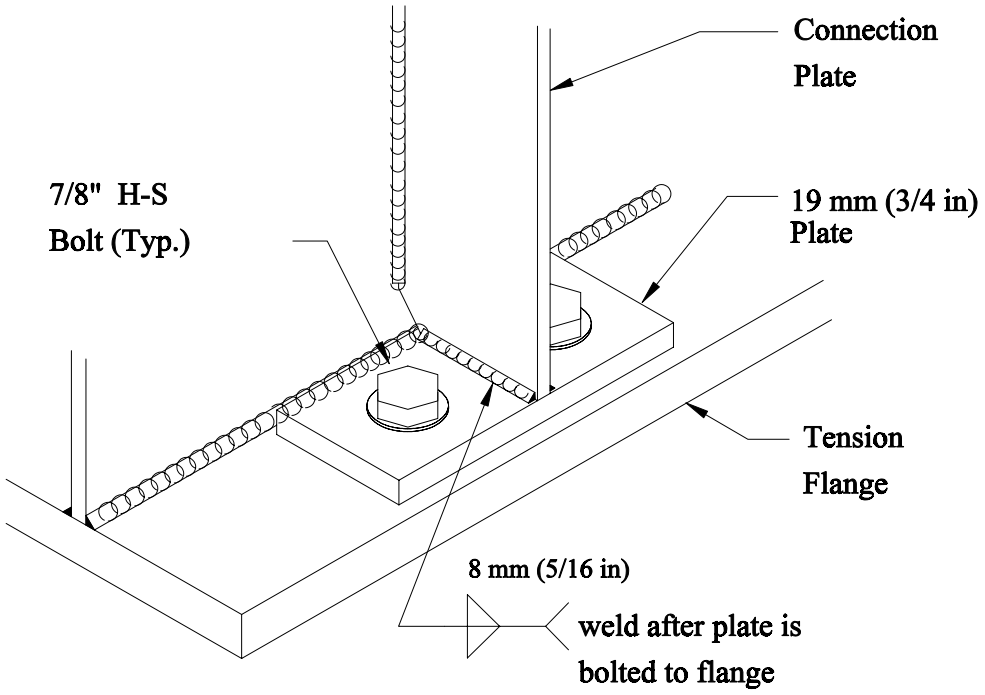

Figure E-16: Bolted base plate detail.

When the bolted base plate is used, a correct installation procedure must be used. The fillet weld between the base plate and connection must not be undersized since it will transfer the out-of-plane distortion force to the flange. The high-strength bolts must be properly torqued and the plate contact surfaces clean and free of oil. Use an assembly sequence where the bolting is performed first, then the weld is made. This prevent overstressing the weld when the bolts are tightened.

If only one gage line of bolts is used on the flange and a large distance exists between the flange and connection plate bolts, enough rotation or rocking about the gage line may occur so that distortion stresses are still significant. The repair connection should be detailed to provide as much rigidity as possible.

If a bolted connection is required to the bottom flange of a trapezoidal box, a rolled section cannot be used. The connecting element must be fabricated out of plate material, as

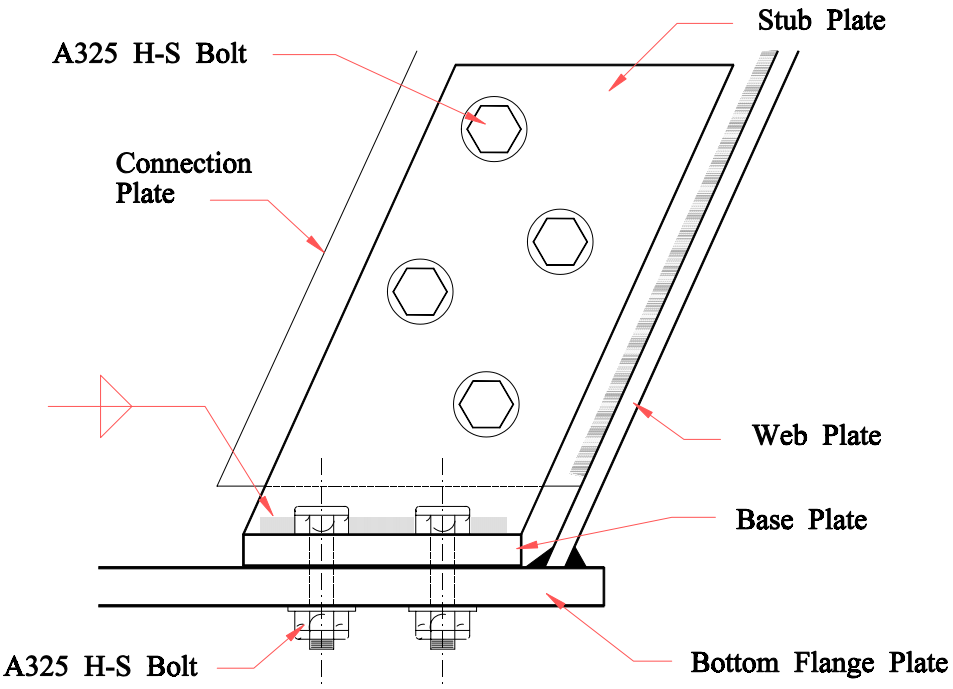

Figure E-17: Fabricated stub plate for trapezoidal boxes.

illustrated in Fig. E-17. The fillet weld between the stub and base plate may be made in the field to allow for proper fit-up.

In the negative moment region of bending, providing a rigid attachment to the top flange is made difficult by the presence of the concrete deck. Similar to the repair procedure for I-shaped girders, a taped high-strength stud can be used to connection a strap plate to the flange plate (see Fig. E-18). Note that the fill plate is used to connect the strap plate to the top strut of the cross frame diaphragm.

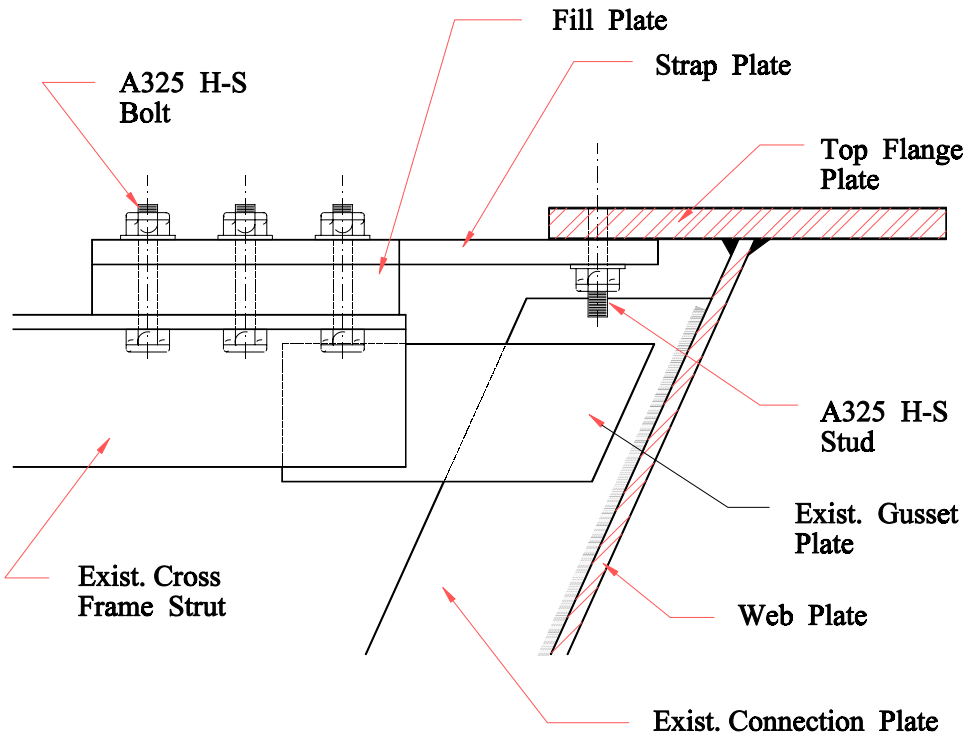

Figure E-18: Bolted attachment in negative moment regions of trapezoidal box members.

Unstiffened web gaps at intersections of gusset plates and connection plates may exist. In order to reduce the distortion in the web gaps, the lateral gusset plate must be rigidly attached to the connection plate. This can be accomplished by using bolted structural angles, as shown in Fig. E-19.

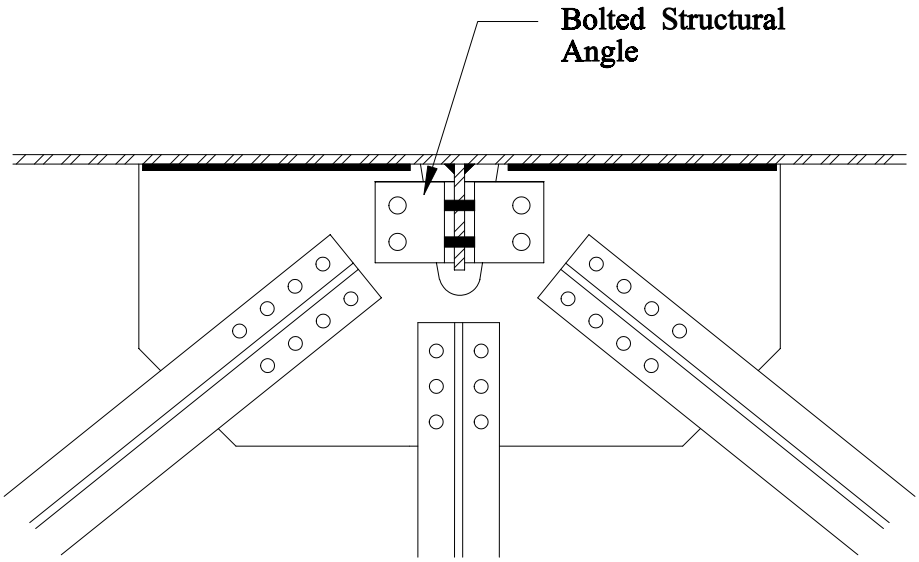

Figure E-19: Bolted repair at intersection of gusset plate and connection plate detail.